INTERNATIONAL DOCTORAL
SCHOOL OF THE USC

Néstor Alberto
Tafur Angulo

PhD Thesis

Improvement of chemical enhanced oil recovery methods

Santiago de Compostela, 2023

Doctoral Programme in Chemical and Environmental Engineering

DOCTORAL THESIS

IMPROVEMENT OF CHEMICAL ENHANCED OIL RECOVERY METHODS

Néstor Tafur Angulo

INTERNATIONAL PhD SCHOOL OF THE UNIVERSITY OF SANTIAGO DE COMPOSTELA

PhD PROGRAMME IN CHEMICAL AND ENVIRONMENTAL ENGINEERING

SANTIAGO DE COMPOSTELA

2023

USC
UNIVERSIDADE
DE SANTIAGO
DE COMPOSTELA

DECLARACIÓN DEL AUTOR DE LA TESIS

D. Néstor Tafur Angulo
Título de la tesis: Improvement of chemical enhanced oil recovery methods

Presento mi tesis, siguiendo el procedimiento adecuado al Reglamento y declaro que:

1) La tesis abarca los resultados de la elaboración de mi trabajo.
2) De ser el caso, en la tesis se hace referencia a las colaboraciones que tuvo este trabajo.
3) Confirmo que la tesis no incurre en ningún tipo de plagio de otros autores ni de trabajos presentados por mí para la obtención de otros títulos.
4) La tesis es la versión definitiva presentada para su defensa y coincide la versión impresa con la presentada en formato electrónico.

Y me comprometo a presentar el Compromiso Documental de Supervisión en el caso que el original no esté depositado en la Escuela.

En Santiago de Compostela, a 28 de Julio de 2023.

Fdo. Néstor Tafur Angulo

USC UNIVERSIDADE DE SANTIAGO DE COMPOSTELA

USC
UNIVERSIDADE
DE SANTIAGO
DE COMPOSTELA

AUTORIZACIÓN DE LOS DIRECTORES/TUTORA DE LA TESIS

Improvement of chemical enhanced oil recovery methods

Dª. Ana María Soto Campos y D. Alberto Pérez Muñuzuri

INFORMAN:

Que la presente tesis, se corresponde con el trabajo realizado por D. Néstor Tafur Angulo, bajo nuestra dirección/tutorización, y autorizamos su presentación, considerando que reúne los requisitos exigidos en el Reglamento de Estudios de Doctorado de la USC y que, como directores de esta, no incurre en las causas de abstención establecidas en la Ley 40/2015.

De acuerdo con lo indicado en el Reglamento de Estudios de Doctorado, declaran también que la presente tesis doctoral es idónea para ser defendida en base a la modalidad de compendio de publicaciones, en los que la participación del doctorando fue decisiva para su elaboración y las publicaciones se ajustan al Plan de Investigación.

En Santiago de Compostela, a 28 de Julio de 2023

Ana María Soto Campos

Alberto Pérez Muñuzuri

USC
UNIVERSIDADE
DE SANTIAGO
DE COMPOSTELA

Acknowledgements

Even though the first months of this wonderful project coincided with the beginning of the pandemic, over these three and a half years, I had the privilege of experiencing a rewarding and enriching period in my academic and personal life. For that, first and foremost, I give thanks to God for the gift of health and for accompanying and guiding me every step of the way throughout this project.

Secondly, I would like to express my gratitude to my supervisors, Dra. Ana Soto Campos and Dr. Alberto Pérez Muñuziri, for their guidance, the time they dedicated to this research, their thought-provoking discussions, and their unwavering support, both academically and personally.

I am thankful to the University of Santiago de Compostela and its Centre for Cross-disciplinary Research in Environmental Technologies (CRETUS) for allowing me to be a part of them, first in the Nonlinear Physics Group, who warmly welcomed me during the first year and provided me guidance and support, especially Darío Escala, as well as Danny, Alberto, and David. Then, I am grateful to the Group of Phase Equilibria and Separation Processes for receiving me with open arms for the second part of my thesis. I would like to offer my thanks to my lab-mates Cristina Gallego, Paula Souto, and Akram Al-Asadi, and especially to Alba Somoza and Carlos Pena for their support and technical-theoretical discussions. Finally, I wish to extend my gratitude to professors Alberto Arce, Eva Rodil, Oscar Rodriguez, and Hector Rodriguez for their consistently kind guidance.

I am profoundly grateful to the members of the Smart Water Group, at the University of Stavanger. Special thanks to my supervisors during my research stay, Skule Strand and Tina Puntervold, for their enthusiasm and advice. My gratitude also goes to Aleksandr Mamonov and Ashraful Khan for actively providing feedback during my investigation. All of them made me feel at home.

Lastly, but of utmost importance, my deepest gratitude goes to my wife, María José, my son Santiago, and my parents, Néstor and Magaly, for their unconditional love, patience, and unwavering prayer support throughout these years.

Thank you all.

Néstor Tafur Angulo

USC
UNIVERSIDADE DE SANTIAGO DE COMPOSTELA

USC
UNIVERSIDADE
DE SANTIAGO
DE COMPOSTELA

Abstract

Ecological transition is indispensable, but it requires time. In the meantime, oil will continue to be a vital source of materials and energy, and a key pillar of our quality of life. After the application of traditional methods of recovery, a significant volume of oil remains in reservoirs. Increasing the efficiency of current enhanced oil recovery (EOR) methods is essential to maximise oil recovery without investments into new infrastructure. The main objective of this thesis is to increase the oil recovery potential of some EOR techniques by using novel chemical formulations that can be applied to reservoirs that have not yet reached their potentiality.

The improvement of the macroscopic sweep efficiency of a hydrodynamically unstable displacement was analysed via fundamental numerical simulations. The study explored a promising technique to control viscous fingering using a chemical reaction at the interface of two fluids. Theoretically, recovery of the displaced fluid of up to 90% could be achieved, with a specific injection protocol, reaction velocity, and fluid properties. In field applications, finding such a reaction is a difficult task that greatly limits the possibilities of the method.

The improvement of microscopic displacement efficiency in carbonate cores was evaluated by developing formulations to reduce interfacial tension (IFT) and alter rock wettability. Phase behaviour of several binary blends was extensively analysed by means of activity maps. The selected mixtures were: dioctyl sulfosuccinate sodium (AOT) with polyoxyethylene(8) octyl ether carboxylic acid (LF2) surfactant, or with 1-dodecyl-3-methylimidazolium bromide ([C_{12}mim]Br) or 1-decyl-3-methylimidazolium chloride ([C_{10}mim]Cl) surface-active ionic liquids (SAILs). All the blends formed Winsor III microemulsions. AOT/LF2 exhibited salt sensitivity and was unstable at high temperature and salinity, while AOT/SAILs formed more stable Winsor III microemulsions with greater surface activity. However, AOT/SAIL blends were intolerant to the brine's divalent ions. A ternary blend of AOT/[C_{12}mim]Br/LF2 was designed and showed great potential for EOR in limestone cores at room temperature, the main mechanism of the extraction being IFT reduction. In the same line of research, a blend of a petroleum surfactant (RECOLAS103) and the SAIL cocosalkylpentaethoximethyl ammonium methylsulfate (C1EG), was also evaluated for EOR applications. It demonstrated higher potential than the previously studied blends, especially at high temperature. Reservoir simulations supported these findings.

The possibilities of improving microscopic displacement efficiency were also evaluated through the mechanism of rock wettability alteration. The efficacy of SAIL ([C_{12}mim]Br, [C_{12}Py]Cl and [C_{16}Py]Cl) formulations in enhancing the wettability modification properties of smart water (SmW), was assessed at 90 °C in intermediate-wet carbonate (chalk) cores. Based on the outcomes

USC
DE SANTIAGO
DE COMPOSTELA

of spontaneous imbibition tests, [C_{12}mim]Br doubled the additional oil recovery achieved with SmW, and was slightly better than [C_{12}Py]Cl. Core flooding with SmW and [C_{12}mim]Br through the same type of cores confirmed the improved performance with respect to SmW alone.

Keywords: Enhanced oil recovery, viscous fingering, wettability alteration, phase behaviour, surfactant, ionic liquid, smart water.

USC
UNIVERSIDADE DE SANTIAGO DE COMPOSTELA

Contents

1. Objectives 1
2. Introduction 5
2.1. Fundamentals 8
2.1.1. Basic concepts 8
2.1.2. Oil recovery stages 13
2.1.3. Factors involved in oil recovery efficiencies 14
2.1.3.1. Volumetric sweep efficiency 15
2.1.3.2. Displacement efficiency 17
2.2. Surfactant – Polymer flooding 20
2.2.1. Polymer flooding 20
2.2.1.1. Polymers 20
2.2.1.2. Polymers in EOR 21
2.2.2. Surfactant flooding 22
2.2.2.1. Surfactants 22
2.2.2.2. Surface-active ionic liquids 25
2.2.2.3. Surfactants in EOR 26
2.2.2.4. Micelles and microemulsions in EOR 26
2.3. EOR evaluation tests 29
2.3.1. Laboratory 29
2.3.1.1. Phase behaviour studies 29
2.3.1.2. Dynamic IFT 31
2.3.1.3. Core flooding tests 32
2.3.1.4. Dynamic adsorption 34
2.3.1.5. Spontaneous imbibition 34
2.3.2. Simulation 35
3. Publications 39
3.1. Highly viscous fluid displaced by a chemically controlled reactive interface 41
3.2. Evaluation of surfactant blends for enhanced oil recovery through activity maps 59
3.3. Improvement of a Surfactant Blend for Enhanced Oil Recovery in Carbonate Reservoirs by Means of an Ionic Liquid 85
3.4. Assessment of a Surface-active ionic liquid formulation for EOR applications: experimental and simulation studies 101

USC UNIVERSIDADE DE SANTIAGO DE COMPOSTELA

3.5. Evaluation of Surface-Active Ionic Liquids in Smart Water for Enhanced Oil Recovery in Carbonate Rocks 121

4. General discussion 135
5. Conclusions 151
List of symbols 155
References 161

APPENDICES:

Appendix A: Journal articles in which this thesis is based 169
Appendix B: "Resumo" (Summary, in Galician) 177
Appendix C: Copyright 189

USC
UNIVERSIDADE DE SANTIAGO DE COMPOSTELA

1. OBJECTIVES



USC
UNIVERSIDADE
DE SANTIAGO
DE COMPOSTELA

USC
UNIVERSIDADE
DE SANTIAGO
DE COMPOSTELA

The global challenge of climate change has led to a strong focus on renewable sources of matter and energy. However, the transition to these sources is a complex process that requires time, research, investment, and infrastructure development. In the meantime, until hydrocarbons can be replaced, oil will continue to be a vital source for powering industries, transportation, and everyday life.

While the global demand for materials and energy continues to rise, driven by economic and population growth, and the world strives to mitigate the impacts of climate change, optimising oil recovery from already developed hydrocarbon fields is becoming increasingly necessary. Traditional oil recovery methods fall short in extracting the maximum amount of oil from reservoirs, leaving significant reserves untapped. Enhance Oil Recovery (EOR) techniques can maximise oil recovery, reducing the need for new oil fields and wells, and providing additional time for the development of renewable-based technologies. Nevertheless, many of these methods are still far from being efficient in certain types of reservoirs and conditions.

The main objective of this thesis is to increase the oil recovery potential of some EOR techniques by using novel chemical formulations that can be applied to reservoirs that have not yet reached their potentiality. Namely, three chemical EOR methods are considered: the use of chemical reactions to control unstable displacement, surfactants to reduce water-oil interfacial tension (IFT) and smart water for wettability alteration. In all cases, to propose optimal formulations, the investigation first focus on fundamental studies to fully understand the behaviour of the selected chemical agents. Then, based on those fundamental findings, the research shifts to the evaluation of the most promising formulations under different conditions, with a view to proposing them for industrial applications. To accomplish the general goal, several specific objectives are proposed.

The first specific objective focuses on systematically analysing the possibilities of controlling the hydrodynamic instability (known as viscous fingering) encountered when a low viscosity fluid displaces a high viscosity one. The phenomenon is studied by numerical simulations, modelling different conditions and injection protocols to reduce the instability via chemical reactions between the two fluids at the interface. Such control has the potential to improve the displacement efficiency in oil recovery processes. This study led to the following publication: "Highly viscous fluid displaced by a chemically controlled reactive interface", *Chaos*, 31, 2021, 023135.

Another fundamental study aimed to accomplish the second specific objective of the thesis is presented. Activity maps for different formulations with surface-active properties are developed to identify the best performance conditions for each one. The phase behaviour of three binary

USC DE SANTIAGO DE COMPOSTELA

surfactant blends, as a function of salinity, blend ratios and temperature of the system, is studied. To formulate the blends, the surfactant dioctyl sulfosuccinate sodium (AOT) is mixed with the polyoxyethylene(8) octyl ether carboxylic acid (commercially called Akypo LF2) surfactant, or with 1-dodecyl-3-methylimidazolium bromide ([C_{12}mim]Br) or 1-decyl-3-methylimidazolium chloride ([C_{10}mim]Cl) surface-active ionic liquids (SAILs). This study led to the following publication: "Evaluation of surfactant blends for enhanced oil recovery through activity maps", *Journal of Molecular Liquids*, 364, 2022, 119984.

Building on the knowledge gained from this previous study, the third specific objective focuses on designing and evaluating an optimal chemical formulation based on SAILs for EOR applications. The phase behaviour, stability, water-oil IFT reduction, adsorption on rock surfaces and capacity to recover oil, are tested. The objective is set out in the publication: "Improvement of a Surfactant Blend for Enhanced Oil Recovery in Carbonate Reservoirs by Means of an Ionic Liquid", *International Journal of Molecular Sciences* 24, 2023, 726.

The fourth specific objective, developed in collaboration with the Spanish petrochemical CEPSA, is the evaluation of a promising blend constituted by a SAIL and a petroleum alkyl aryl sulfonate, to determine its real potential for use in the oil industry. The blend, composed of the SAIL cocosalkylpentaethoximethyl ammonium methylsulfate (C1EG) and a sodium alkyl (C_{10}-C_{13}) benzene sulfonate, is assessed experimentally and through numerical simulations to improve the understanding and performance of the blend during the oil displacing test under different conditions. The objective is set out in the publication: "Assessment of a Surface-active ionic liquid formulation for EOR applications: experimental and simulation studies", *Geoenergy Science and Engineering*, 224, 2023, 211619.

Finally, the last objective of the thesis aims to increase the potential for oil recovery of the smart water (specially modified seawater) EOR technique. Different SAILs are evaluated to improve the wettability alteration capacity of the smart water to change the state of carbonate rocks from intermediate-wet towards more water-wet conditions, thus improving oil recovery. To accomplish this goal, a short stay was carried out at the University of Stavanger. This study led to the following publication: "Evaluation of Surface-Active Ionic Liquids in Smart Water for Enhanced Oil Recovery in Carbonate Rocks", *Energy & Fuels,* 37, 2023, 11730.

USC
UNIVERSIDADE DE SANTIAGO DE COMPOSTELA

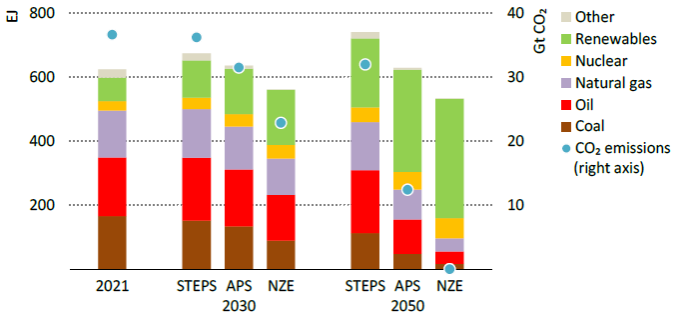
2. INTRODUCTION



USC
UNIVERSIDADE
DE SANTIAGO
DE COMPOSTELA

USC
UNIVERSIDADE
DE SANTIAGO
DE COMPOSTELA

Although oil and gas have made an invaluable contribution to the development of the world for the last century, in recent years the need to replace them with cleaner and renewable energy has been growing. Many investigations have shown the contribution of hydrocarbon combustion to carbon dioxide (CO_2) emissions and climate change. However, the means of production, distribution, and storage of renewable energy sources with net zero or low CO_2 emissions are not yet well-defined or optimised to fully satisfy the energy demand worldwide. The delay in adequately preparing renewable energy technologies could create an imbalanced market if hydrocarbon production begins to decrease in the next few years whilst the population and living standards keep increasing. The World Energy Outlook-2022 issued by the International Energy Agency (IEA)[1] forecasts the energy supply from different sources to meet global demands. Hydrocarbons still represent a key source by 2050 in both more realistic predicted scenarios: the STEPS (Stated Policies Scenario) and APS (Announced Pledges Scenario) (Figure 2.1).



Units: EJ = Exajoule; Gt CO_2 = Gigatonnes of carbon dioxide

Figure 2.1. Forecast of total energy supply by source and CO_2 emissions by scenario (STEPS = Stated Policies Scenario; APS = Announced Pledges Scenario; NZE = Net Zero Emissions) (Figure reproduced from [1], available under open CC BY 4.0 license).

As shown in Table 2.1, between 2021 and 2050, demand for oil in the aviation/shipping and industry/petrochemical sectors grows or shrinks slightly in the STEPS and APS scenarios, respectively. Oil used as petrochemical feedstock is transformed into various chemical products, such as plastics, packaging, detergents, tires, digital devices, medical equipment, fertilizers, and clothing, among many others. Additionally, products derived from oil are used extensively in renewable energy systems, including solar panels, thermal insulation, wind turbine blades, electric vehicle parts, and batteries. These factors imply that demand for oil in the chemical sector will grow significantly in the future [1].

These forecasts suggest that a transition from hydrocarbons to renewable materials and energy must be organised and planned by the agents involved, to avoid the risks of premature oil supply reduction. Deceleration of investments in the discovery of new oil reserves could lead to energy

USC DE COMPOSTELA

and material shortages. In order to handle this problem, advanced methods should be applied to recover more oil than initially estimated during the production life of the reservoirs. In some cases, thanks to the application of these technologies, oil production from mature fields can be undertaken more economically than that corresponding to new discoveries of unconventional resources or offshore fields [2,3].

Table 2.1. World oil demand by forecast scenario. (STEPS = Stated Policies Scenario; APS = Announced Pledges Scenario; NZE = Net Zero Emissions by 2050 Scenario) (Table reproduced from [1], available under open CC BY 4.0 license).

			STEPS		APS		NZE	
	2010	2021	2030	2050	2030	2050	2030	2050
Road transport	36.5	40.5	41.9	39.0	37.8	17.3	27.5	1.3
Aviation and shipping	9.9	9.9	14.0	18.1	12.8	9.5	10.0	2.0
Industry and petrochemicals	17.2	20.5	23.7	25.5	21.5	18.1	20.1	13.4
Buildings and power	12.4	11.4	9.3	7.0	8.3	3.7	6.5	0.6
Other sectors	11.2	12.2	13.6	12.5	12.6	8.6	11.1	5.6
World oil demand	87.2	94.5	102.4	102.1	93.0	57.2	75.3	22.8

2.1. FUNDAMENTALS

2.1.1 Basic Concepts

Reservoir. Crude oil and gas trapped underground accumulate in structural and stratigraphic formations, mainly in sedimentary basins [4,5]. Compartments of these formations hydraulically isolated from others are known as reservoirs. Reservoirs in sedimentary formations are characterised by porous and permeable rocks formed mainly by siliciclastic detritus (sandstone) or carbonate material (limestone and dolomite). Statistical studies suggest that around 60 % of oil reserves are contained in carbonate reservoirs [6].

Porosity. The porosity of a reservoir represents a measure of the fluid storage capacity of the rock. Sedimentary rock reservoirs are formed of sand grains (sandstone reservoirs) and carbonate particles (carbonate reservoirs). Due to the high irregularity in the shape of grains and particles, empty space (or pore space) is left between them during the lithification process, which then is filled with fluids. Hence, the porosity of a reservoir is the fraction of the bulk volume of the reservoir occupied by the fluids [7]. Mathematically, porosity can be expressed as:

$$\emptyset = \frac{V_b - V_{grain}}{V_b} = \frac{V_p}{V_b} = \frac{V_f}{V_b} \qquad \text{(Eq. 2.1)}$$

where:

ϕ= Porosity

V_b=Bulk volume of the reservoir

USC UNIVERSIDADE DE SANTIAGO DE COMPOSTELA

V_{grain}=grain volume of the reservoir

V_p= pore volume of the reservoir

V_f= volume of fluids contained in the reservoir

During reservoir formation some pore space remains isolated. Therefore, porosity is divided into absolute porosity (total pore volume to bulk volume ratio) and effective porosity (interconnected pore volume to bulk volume ratio). Since reservoir fluids only flow through the interconnected pores, the term reservoir porosity normally means effective porosity [5,8].

Permeability. Permeability is a measure of the ability of a porous rock to allow fluids to flow through its interconnected pores under a pressure gradient. That means permeability is affected by the effective porosity. Consequently, reservoir permeability is controlled by the size, shape and sorting (size distribution) of the sediment grains, their packing and the subsequent diagenesis (chemical alteration), compaction and cementation (mineral deposition) around those grains [5,7]. Reservoir permeability influences the rate and direction of the fluids flow through the reservoir [9]. The widely used mathematical expression to quantify permeability is called Darcy's Law:

$$\upsilon = \frac{q}{A_C} = \frac{-k}{\mu}\frac{dP}{dL} \qquad \text{(Eq. 2.2)}$$

where:

υ= apparent fluid flowing velocity, cm/s

q= flow rate through the porous rock, cm^3/s

A_c= cross-sectional area of the rock across which flow occurs, cm^2

k= permeability of the porous rock, Darcy (D)

μ= viscosity of the flowing fluid, centipoises (cP)

dP/dL= pressure drop in the flow direction, atm/cm

Relative Permeability. Permeability of reservoirs is termed absolute permeability (k_a) when the rock is saturated by a single fluid. If two or more fluids are presented in the reservoir at the same time, permeability is named effective permeability of each fluid. Thereby, K_o, K_w and K_g are the effective permeabilities of oil, water and gas respectively. Effective permeabilities are dependent on the rock wettability and the individual fluid saturations in the reservoir. Theoretically, the effective permeability of a fluid can range from zero to k_a. However, along its flow in the reservoir, each fluid perturbs or limits the free flow of the others through the pore space. Thus, the sum of the effective permeabilities K_o, K_w and K_g is less than k_a [7,9].

USC UNIVERSIDADE DE SANTIAGO DE COMPOSTELA

The relative permeability of each reservoir fluid is the effective permeability to absolute permeability ratio:

$$k_{ri} = \frac{k_i}{k_a} \qquad \text{(Eq. 2.3)}$$

where:

k_{ri}= relative permeability of any reservoir fluid

k_i= effective permeability of any reservoir fluid

k_a= absolute permeability of the reservoir

i= reservoir fluids (oil, water or gas)

An example of relative permeabilities of oil and water as a function of water saturation is shown in Figure 2.2.

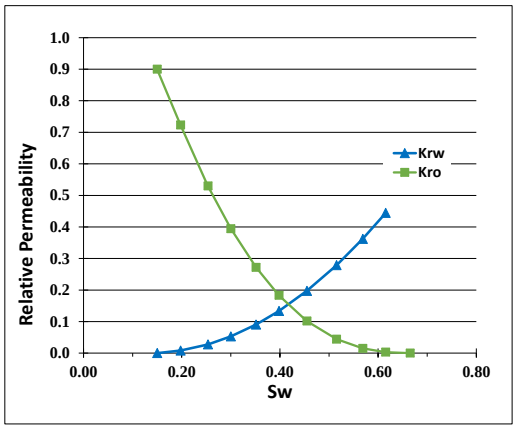


Figure 2.2. Example of relative permeability curves for oil (K_{ro}) and water (K_{rw}) as a function of water saturation (S_w) .

Fluid Saturation. Fluid saturation refers to the fraction of the pore space within a rock occupied by water or hydrocarbons. Saturation is expressed as:

$$S_i = \frac{V_i}{V_p} \qquad \text{(Eq. 2.4)}$$

where:

S_i= saturation of any reservoir fluid in the rock

V_i= volume of any reservoir fluid in the rock

V_p= pore volume of the reservoir

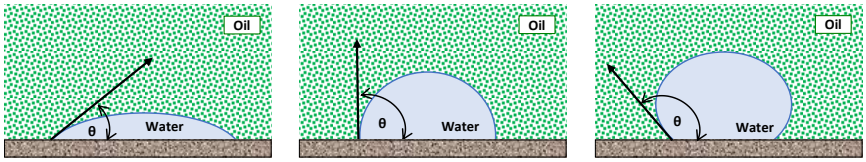
i= reservoir fluids (oil, water or gas)

The saturation of each fluid ranges from 0 to 1, and the sum of the three fluid saturations in a reservoir is the unity [4].

USC UNIVERSIDADE DE SANTIAGO DE COMPOSTELA

Wettability. Rock wettability greatly influences the fluid saturation and the relative permeabilities in reservoirs. Rock wettability is the inherent affinity or preference of a rock surface for a particular fluid (e.g., oil, water, or gas) in contact with it. This property determines the tendency of one fluid among other immiscible fluids to wet (spread or adhere) on the rock surface. The fluid with the strongest affinity to the rock surface is called the wetting fluid, and the other the non-wetting. Wetting fluid covers the rock surface and occupies the smaller pores, while the non-wetting fluid is mainly distributed in the centre of the larger pores. The wetting fluid can spontaneously imbibe a permeable rock (expelling a large amount of the non-wetting fluid) much more readily than the non-wetting fluid.

The adhering tendency of fluids can be measured by the contact angle they form on a surface. Thus it is possible to identify different types of wettability in reservoirs. Figure 2.3 shows a representation of surfaces with water-wet, oil-wet, and intermediate-wet states according to the formed contact angles. Wettability of any reservoir ranges from strongly water-wet to strongly oil-wet [7,9,10]. Evaluation of wettability can also be carried out through different well-known techniques such as the Amott index, spontaneous imbibition test, USBM (U.S. Bureau of Mines) index, and fluid displacement energy test [7].



a) θ < 90° Water-wet b) θ ~ 90° Intermediate-wet c) θ > 90° Oil-wet

Figure 2.3. Contact angle (θ) according to wetting state of surfaces (a) water-wet, (b) intermediate-wet, and (c) oil-wet.

Rock wettability is influenced by various factors, including the mineralogy and chemistry of the rock, as well as the composition of the fluids in contact with the rock. Wettability can also be altered by changes in temperature and the presence of chemical additives.

Interfacial Tension (IFT). IFT is a measure of the attractive forces between the molecules of two immiscible fluids at the interface formed when both fluids are in contact. Molecules inside a particular fluid attract each other in all directions. At the interface, there is an imbalance since there are no similar molecules past that point. The molecules at the interface experience a net inward force due to the attractive forces with the molecules of the same fluid, and a net outward force due to the attractive forces with the molecules of the other fluid. This results in the formation of a liquid film with a minimum surface area pulling it into a sphere shape, corresponding to the equilibrium state [7].

USC UNIVERSIDADE DE SANTIAGO

Capillary Pressure. Capillary pressure refers to the pressure difference between two immiscible fluids (one wetting and another non-wetting) over the curved interface at equilibrium, in a narrow capillary or pore space. It can be expressed as:

$$P_c = P_{nw} - P_w \quad \text{(Eq. 2.5)}$$

where:

P_c= capillary pressure (mN/m^2)

P_{nw} = pressure of the non-wetting fluid (mN/m^2)

P_w= pressure of the wetting fluid (mN/m^2)

In a reservoir, capillary pressure is caused by the IFT between the two fluids, the size of the pores (radii) and the curvature of the interface. This phenomenon is the result of the rock wettability: at the interface between the fluids the pressure in the non-wetting fluid is higher than that of the wetting fluid, so in consequence the interface curves [9]. Thus, capillary pressure can be expressed as a function of IFT, pore size, and wettability as following:

$$P_c = \frac{2\sigma cos\theta}{r_c} \quad \text{(Eq. 2.6)}$$

where:

P_c= capillary pressure (mN/m^2)

σ= IFT between two immiscible fluids (mN/m)

θ= contact angle (°)

r_c= pore or capillary radius (m)

In the context of porous media, capillary pressure plays a significant role in determining the movement of fluids through the pore spaces. It affects the fluid saturations and consequently the relative permeability of different fluids in the reservoir, which in turn influences their flow behaviour. A typical behaviour of capillary pressures as a function of water saturation for water-wet reservoir rocks is shown in Figure 2.4. The figure presents two different P_c curves: the drainage and the imbibition. Drainage is the process of displacing the wetting phase (e.g., water) by the non-wetting phase (oil). This process establishes the initial conditions of water (S_{wc}) and oil saturation when reservoirs are discovered. Imbibition refers to the displacement of the non-wetting phase (e.g., oil) by the wetting phase (water). This process might represent the final conditions of water and oil saturation when reservoir reaches the residual oil saturation (S_{orw}) after a water flooding process. Threshold pressure (Pd point) is the capillary pressure at 100%

USC UNIVERSIDADE DE SANTIAGO DE COMPOSTELA

wetting phase saturation required to force the non-wetting phase into the pores filled by the wetting phase [9].

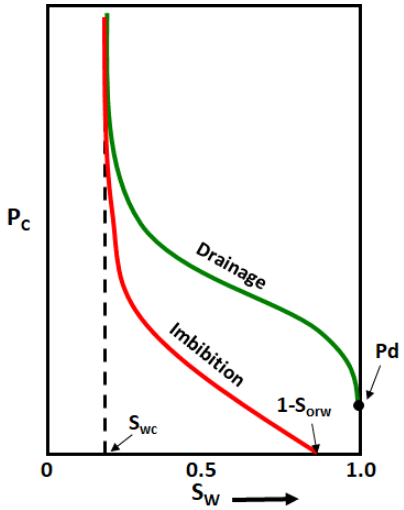


Figure 2.4. Typical capillary pressure (P_c) curves for a water-wet reservoir rock as a function of water saturation (S_w) (Figure reproduced from [9]. Permission to publish by Elsevier).

2.1.2 Oil Recovery Stages

Crude oil recovery from underground reservoirs can be classified based on the methods used to extract oil: primary, secondary, and tertiary or enhanced oil recovery (EOR) [10].

Primary oil recovery is the initial stage of oil production in which the natural energy present in the reservoir is used for extraction. This method, also known as "natural depletion", relies on the natural driving mechanisms which control the flow, pushing the fluids through reservoirs toward the producer wells. This primary energy source comes mainly from the rock and fluid expansion driven, and can also be affected by solution gas, aquifer influx, gas cap, or gravity drainage [10]. In some reservoir conditions, primary recovery is the most efficient and cost-effective method of oil extraction, as it requires minimal equipment and additional energy. However, it typically only recovers a portion of the oil in the reservoir, leaving significant amounts behind. Therefore, further methods are often used to extract additional oil from the reservoir.

Secondary oil recovery is the stage of oil production where additional methods are used to extract oil that remains in the reservoir after primary recovery, as the driving forces behind natural depletion are reduced. Secondary recovery techniques involve the addition of external energy into the reservoir through injection wells followed by extraction of oil from production wells [11]. These methods typically involve injection of water or gas into the reservoirs or their associated aquifer or gas caps. That helps to maintain pressure of the reservoir during production

USC DE SANTIAGO DE COMPOSTELA

or to immiscibly displace the remaining oil, pushing it towards production wells. The most common secondary recovery method is water flooding, since gas injection is less efficient [2,4,10].

Despite the amount of oil recovered after the natural depletion and secondary recovery stages, a significant portion of the residual oil still remains in the reservoirs, from around 35 to 50% of the original oil in place (OOIP). The term ***Tertiary Oil Recovery (or EOR)*** refers to application of techniques to extract additional oil after secondary recovery methods have become ineffective. Since tertiary recovery techniques can be also developed as the first production stage or right after primary recovery (when primary or secondary recovery techniques are not applied due to low recovery potential), the term EOR has become more accepted in recent decades. Even so, most EOR methods are implemented after water injection [10,11]. EOR involves any technique to alter the existing crude oil-brine-rock (COBR) equilibrium present in reservoirs, thus promoting favourable interactions to increase the oil recovery [2,12]. These techniques mainly include the injection of miscible gas, liquid chemicals, and thermal energy [13]. Figure 2.5 shows a resume of the main EOR techniques.

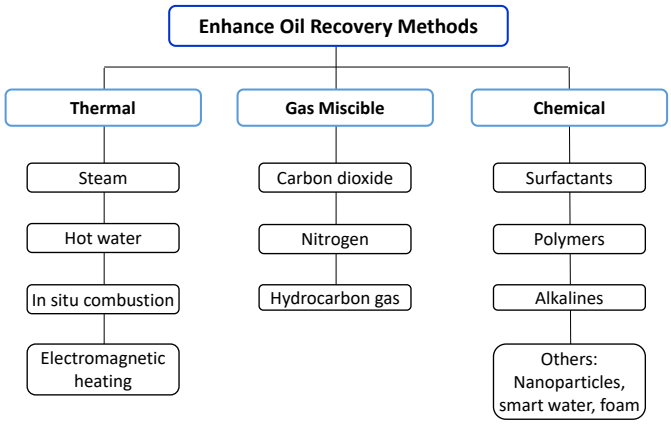


Figure 2.5. Main EOR methods.

2.1.3 Factors involved in oil recovery efficiencies

EOR methods can modify chemical and physical interactions of the original COBR equilibrium to mobilise the residual oil and increase final recovery. After water flooding, the residual oil is the amount of oil remaining in swept or bypassed areas of the reservoir. This oil, left behind the waterfront as isolated portions (bypassed), as trapped droplets in the reservoir pores (by capillary forces), or in the form of film (adhered by wettability) on the rock surface, is not distributed evenly. EOR techniques must mobilise the oil droplets in a displacement front, forming an oil bank more easily driven towards production wells [10,14].

The displacement of residual oil by applying EOR methods can be achieved through chemical and/or physical processes which are usually divided into two scales: macroscopic and microscopic. The macroscopic scale refers to mobility control between the EOR and reservoir fluids, reservoir heterogeneity, and gravity forces. The microscopic scale refers to the interaction of injected fluids with the reservoir rock and residual oil. Therefore, the use of EOR is focused on [11]:

- Increasing sweep efficiency of oil from injection wells to production wells by:
  - Reducing the mobility ratio between displacing and displaced fluids in the reservoir.
- Altering the surface and interfacial forces in the reservoir by:
  - Decreasing capillary forces effects.
  - Modifying reservoir wettability towards a more water-wet state.

The combination of these targets is expressed in the term total efficiency (E), or recovery factor (RF), which is the combination of the two macroscopic and microscopic efficiencies:

$$E = E_{Vol} \cdot E_D \qquad \text{(Eq. 2.7)}$$

where E_{Vol} refers to volumetric sweep efficiency (macroscopic efficiency) and E_D to displacement efficiency (microscopic efficiency). For EOR, E must be higher than for water flooding.

2.1.3.1. Volumetric Sweep Efficiency

Also known as macroscopic efficiency, it is provided on a macroscopic scale of the whole reservoir. It is related to how efficiently a displacing fluid sweeps the volume of a reservoir, reducing bypassing. The E_{vol} is also estimated for water flooding and normally presents lower values than those estimated for EOR methods. E_{vol} represents an average of swept and unswept fractions of the reservoir, and it is often referred to as the product of areal and vertical sweep efficiencies (Eq. 2.8) [10].

$$E_{Vol} = E_A \cdot E_V \qquad \text{(Eq. 2.8)}$$

Where E_A is the areal sweep efficiency and E_V the vertical sweep efficiency. The E_A is the fraction of the well's pattern area that has been flooded by displacing fluid. This efficiency is mainly a function of: areal heterogeneity, mobility ratio, well pattern type, and injected fluid volume.

The E_V is defined as the fraction of the vertical section of the well pattern swept by injected fluid. The E_V depends on the following factors: vertical heterogeneity, mobility ratio, gravity segregation degree, injected fluid volume. Figure 2.6 shows a scheme of E_A and E_V sweep efficiencies.

USC UNIVERSIDADE DE SANTIAGO DE COMPOSTELA

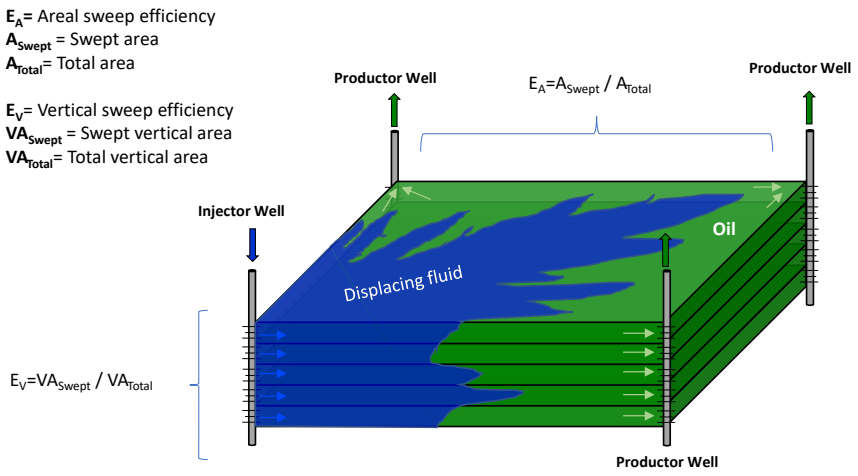


Figure 2.6. Scheme of macroscopic areal and vertical sweep efficiencies for a well pattern.

The geological heterogeneity of the reservoir is the most influential parameter in macroscopic efficiency, since the presence of discontinuities and fractures in the rock often distorts the stability of injected fluid front in EOR projects. Heterogeneity in reservoirs is determined mainly by the spatial distribution of permeability and porosity [3]. Thus, two heterogeneities can be differentiated: areal and vertical. Areal heterogeneity depends on areal variations of rock properties and boundary conditions, as well as stratigraphic and structural discontinuities. Regarding vertical heterogeneity, a reservoir can present many layers with very different rock properties resulting in higher degree of heterogeneity in the vertical direction. This can result in the early breakthrough of injected fluids in production wells, reducing the effectiveness of the mechanism. Layers and channels in areal directions with higher permeability cutting through the reservoir are a large disadvantage for the applications of secondary and EOR methods. These zones, also called thief zones, become the preferential flow paths for the injected fluids, bypassing oil zones with lower permeability [3].

The impact of geological heterogeneity is accentuated when the injected fluid has a significantly lower viscosity than the displaced oil. Therefore, the successful of EOR projects is highly linked to the Mobility Ratio (M), which is defined as the ratio of the displacing fluid to the displaced oil mobilities, as:

$$M = \frac{\lambda_{displacing}}{\lambda_{Displaced}} \qquad \text{(Eq. 2.9)}$$

The mobility (λ_i) of any fluid through the reservoir is estimated by the ratio of relative permeability (K_{ri}) to viscosity (μ_i) of the fluid:

$$\lambda_i = \frac{K_{ri}}{\mu_i} \qquad \text{(Eq. 2.10)}$$

USC UNIVERSIDADE DE SANTIAGO DE COMPOSTELA

Viscosity often being the most influential factor in M. According to Eq. 2.9, a displacement is considered favourable when $M \leq 1$ while it is unfavourable when $M > 1$ [15]. Thus, mobility control is achieved once the mobility of the displacing fluid is equal or less than the minimum displaced oil mobility (λ_o) at reservoir and flow conditions [2]. When λ_o is lower than the injected water mobility λ_w, control of M can be achieved using chemicals to reduce the K_{rw} or increase its μ_w, as well as injection of thermal energy to reduce the viscosity of the oil μ_o.

Unfavourable mobility ratios can consequently lead to viscous fingering effects, lowering macroscopic efficiency. Viscous fingering is a hydrodynamic instability which occurs between fluids with different viscosities when they are in contact with each other. This phenomenon, also known as Saffman-Taylor instability, is triggered when a less viscous fluid is injected into a more viscous fluid, whereon the interface between the two fluids becomes unstable and begins to develop finger-like protrusions which penetrate the displaced fluid. These "fingers" grow and branch out, creating a fractal-like pattern [16]. The extent of instability at the interface is related to the differences between the fluid viscosities, and therefore to the magnitude of M. Higher values of M will result in greater instability. If $M \leq 1$, little penetration of the displacing fluid into the displaced oil is observed, resulting in a uniform front. Figure 2.7 presents the relationship between M and stability conditions of the interface [10].

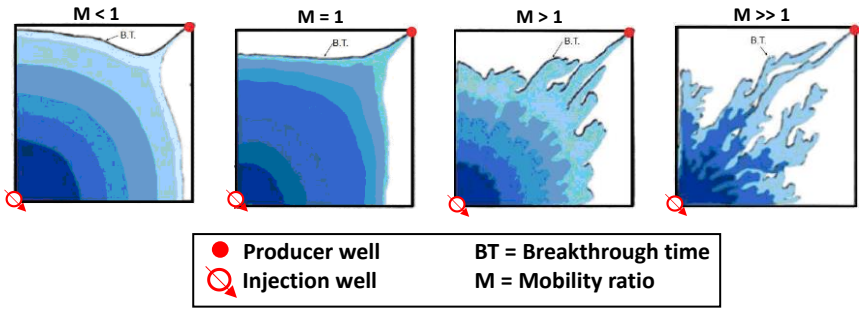


Figure 2.7. Schematic of Viscous fingering pattern as a function of mobility ratio M

As shown, the efficiency E_A is highly dependent on M. Viscous fingering instabilities begin at $M > 1$, and fingers are more prominent as M increases. The highest flow velocity is located along the straight line between the inlet and the outlet points, which is the area of least resistance to flow. That translates into an earlier breakthrough of the fluids at higher M through this path.

2.1.3.2. Displacement Efficiency

Displacement efficiency, E_D, also known as microscopic efficiency, refers to the mobilisation of the trapped oil at pore scale. E_D is a measure of the remaining oil located specifically in flooded zones, after water flooding or EOR process [10]. Mathematically, it is stated as:

USC UNIVERSIDADE DE SANTIAGO

$$E_D = \frac{S_{oi} - S_{or}}{S_{oi}} \quad \text{(Eq. 2.11)}$$

where, S_{oi} is the initial oil saturation and S_{or} the residual oil saturation in the swept zone.

The trapping mechanism of oil in the form of droplets within porous media is closely related to the pore structure of the media, IFT and rock wettability [10].

At the pore scale, oil phase trapping and fluid mobilisation in reservoir rocks are dominated by viscous and capillary forces. Viscous forces in porous media are reflected in the differential pressure magnitude across the media during the flow of a fluid. Capillary forces are the result of capillary pressure, IFT and rock wettability conditions of the reservoir. The relationship of viscous to capillary forces can be expressed with the dimensionless capillary number N_C [2,10,17]:

$$N_C = \frac{\mu \cdot \upsilon}{\sigma \cdot cos\theta} \quad \text{(Eq. 2.12)}$$

where μ is the dynamic viscosity, υ the pore flow velocity of the displacing phase, σ is the IFT and θ the contact angle between oil and aqueous phases. The wetting state of the porous media is reflected in N_C by the contact angle θ.

For values of $Nc < 10^{-5}$, fluid flow in porous media is governed by capillary forces, making viscous forces negligible, and capillary trapping of oil droplets takes place. After water flooding, *Nc* values can range from 10^{-7} to 10^{-6}, and high volumes of oil remain in reservoirs. Oil recovery is not a function of *Nc* at any $Nc < 10^{-6}$ condition (any change of *Nc* below 10^{-6} will not increase recovery). To further mobilise the oil trapped due to capillary forces, *Nc* must be increased. In general, there is a *Nc* value above which the capillary trapped oil droplets start to be mobilised reducing the S_{or}. This value, the critical capillary number (Nc_c), is in the range of 10^{-5} to 10^{-4}. That magnitude depends on the wetting state and type of reservoir rock [2,10,18].

For a strong water-wet reservoir (where $\cos\theta \approx 1$), *Nc* can be increased by increasing velocity and viscosity of the displacing fluid, or by lowering the IFT between oil and aqueous phase. In an oil field displacement, viscosity and velocity of the displacing fluid are closely related to the injection pressure which is limited by the reservoir rock properties and fracture pressure of the reservoir. Thus, increasing displacing fluid viscosity will require a reduction of its injection velocity, in order to keep the injection pressure within acceptable operational range. Conventionally, for water or other displacing fluids with viscosities similar to a light oil (10^{-3} Pa·s), the injection velocity is 1 ft/D, which is around 3.5×10^{-6} m/s. Normally, IFT values found between oil and brine at reservoir conditions range from 20-30 mN/m. Using the Eq. 2.12, *Nc* results in the order of 10^{-7}. Since it is not recommended to create a high-pressure gradient with high injection velocity and high viscosity fluids, the options to increase *Nc* are narrowed to reducing the IFT. According to above

estimations, lowering the IFT less than 0.1 mN/m allows for *Nc* values higher than Nc_c. Values of IFT in the range of 10^{-3} mN/m can lead to very high values of *Nc*, on the order of 10^{-2}, thus minimising capillary trapping [2,3,19]. Theoretically, increasing *Nc* to 10^{-2} can drop S_{or} to zero [20]. In real conditions, total desaturation (S_{or} equal to zero) will not be achieved due to some oil droplets remaining trapped in the smallest pores. Therefore, a maximum *Nc* exists, termed Nc_{max}, above which S_{or} will not be further decreased. The relationship between *Nc* and S_{or} can be observed in the capillary desaturation curve (CDC), which presents the semi-log relation of S_{or} as a function of *Nc*. Figure 2.8 presents that relation in a CDC for wetting and non-wetting phases. The profile of the CDC and the values of Nc_c and the Nc_{max} are related to several parameters such as the wettability, type, and pore size of the porous media [2,18,19].

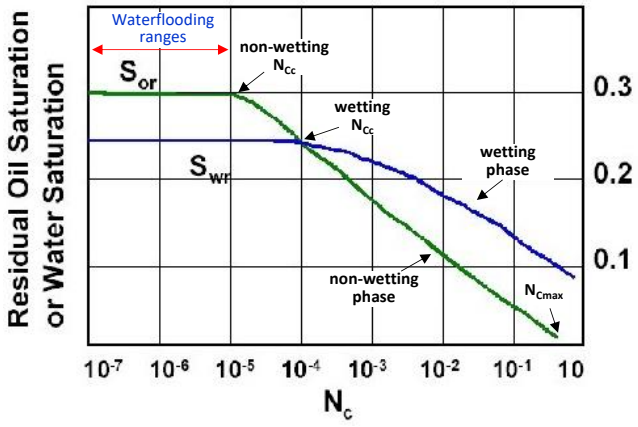


Figure 2.8. Example of capillary desaturation curve (CDC)

In an EOR project, the ideal success is to approach *E* of around 1.0 by increasing both the E_{vol} and E_D efficiencies, through the injection of a displacing fluid with low IFT and viscosity high enough to uniformly sweep the whole reservoir. The injection of a first chemical slug to reduce the IFT or modify the wetting state of the rock, followed by a second chemical flooding with a higher viscosity displacing fluid to improve the sweep of the reservoir is considered a successful option [2,10]. Reduction of IFT to low or ultralow values, ranging from 10^{-2} to 10^{-3} mN/m, can be achieved with the use of surface-active agents (surfactants for short) at certain specifications and conditions, or with the injection of alkalis to promote the formation of soaps in situ. To increase the viscosity of the injected fluid, a water-soluble polymer is added to the aqueous injected fluid. In cases where the displacing fluid is a gas, some surfactants are used to form foams to reduce the gas relative permeability and favour mobility [10,21]. The contact angle θ, which also influences final *Nc* values, can be modified altering the rock wettability towards a more water-wet state. This can be achieved by injecting some surfactants, seawater or modified seawater (named smart water) specifically designed for that purpose [22–24].

USC UNIVERSIDADE DE SANTIAGO

2.2. SURFACTANT – POLYMER FLOODING

Surfactants and polymers in EOR projects can be applied in different ways, such as injecting a slug of surfactant before the polymer flood, injecting both surfactant and polymer as a single slug, or alternating injection of the chemicals in a polymer-surfactant-polymer mode to control surfactant mobility [25].

2.2.1. Polymer Flooding

According to Eq. 2.9 and 2.10, the control of the mobility can be carried out modifying relative permeabilities or viscosities of displaced and displacing fluids, changing one or several parameters at the same time. One of these ways is the addition of polymer to the displacing fluid to increase the apparent viscosity. Low concentrations of water-soluble polymers (ranging from 300 to 3000 ppm) with high molecular weight can drastically increase the viscosity of the injected water. As discussed in section 2.1.3, increasing the displacing fluid viscosity improves the mobility, *M,* which has a large impact on E_{vol}, but little influence on E_D [10,14].

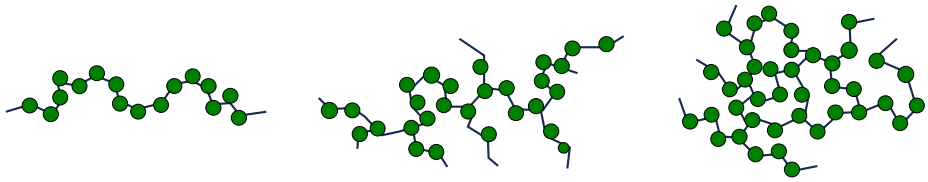
2.2.1.1. Polymers

A polymer is a large molecule, or macromolecule, consisting of many repeating subunits called monomers, which are connected by covalent bonds. The number of the repeating subunits is called degree of polymerisation. The process of joining monomers together to form polymers is called polymerisation. Polymers can present mainly three molecule structures: linear, branched and cross-linked chains (Figure 2.9). A polymer with only one type of monomer is known as a homopolymer, while a polymer synthesised with two types of monomers is called copolymer. Copolymers are composed of various monomers that can be distributed in different ways, such as randomly, in blocks, or by inserting one monomer along the chain of the other monomer type. Polymers can be natural or synthetic, and they can have a wide range of properties depending on their chemical structure and the type of monomers used. The ionic nature of the monomers determines the arrangement of the polymers in solution, which depends on the interactions of the chains with each other and with the solvent. The arrangement can be mainly in random coils, expanded or helix dispositions [26,27].

The molecular weight (M_w) of polymers, which can vary significantly, is a critical parameter because it greatly impacts several properties and the performance of polymer solutions. For example, higher M_w polymers tend to have higher melting and boiling points, greater mechanical strength, and higher viscosity compared to lower M_w polymers. Some synthetic polymers can exhibit a mixture of molecules with variable degrees of polymerisation. This property is named polydispersity. The polydispersity gives polymers a molecular weight distribution (M_{wD}) instead

USC UNIVERSIDADE DE SANTIAGO

of a single M_w. The M_{wD} is a range of values that represents the distribution of M_w in a polymer sample. Owing to that, an average M_w is commonly estimated. The M_{wD} depends on the procedure used for polymerisation and on the fractionation method [26,27].



a) Linear chain b) Branched chain c) cross-linked chain

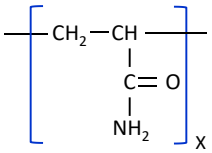
Figure 2.9. Molecular structure of polymer chain: (a) linear chain, (b) branched chain and (c) cross-linked polymer.

2.2.1.2. Polymers in EOR

Two types of water-soluble polymers are generally used in EOR projects for mobility control purposes: polyacrylamides (synthetic polymers) and polysaccharides (biopolymers). However, polyacrylamide is the most widely used due to its significantly higher viscoelasticity. Polymerising acrylamide monomers, producing polyacrylamide (PAM), can produce macromolecules with M_w on the order of 0.5 – 30 million Da. However, in EOR processes, M_w goes from 1 to 10 million Da.

Due to the ionic character of PAM, it is adsorbed on some mineral surfaces such as those contained in reservoirs, mainly on sandstone rocks. To reduce this adsorption, PAM is partially hydrolysed through its reaction with sodium or potassium hydroxide or with sodium carbonate, turning some amide groups ($CONH_2$) to carboxyl groups (COO^-). This process forms the partially hydrolysed polyacrylamide (HPAM) copolymer, which can be also produced by copolymerisation. Figure 2.10 presents the structures of PAM and HPAM. The subscripts X and Y represent the polymerisation degree of each monomer in a polymer molecule.

(a)



(b)

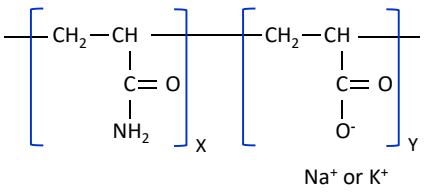


Figure 2.10. Molecular structure of synthetic polymers (a) PAM and (b) HPAM.

USC UNIVERSIDADE DE SANTIAGO DE COMPOSTELA

The mole fraction of amide changed by hydrolysis is known as the hydrolysis degree of HPAM. It commercially ranges from 15 to 35%. The hydrolysis process introduces negative charges to PAM, which reduces its adsorption on negative charged surfaces and modifies the rheological properties of the polymer solution. However, even PAM with no hydrolysis treatment has a small percentage of hydrolysed groups (about 2-4%), so for use with positive charged surfaces (like carbonate reservoirs) it requires further processing [2,10].

2.2.2. Surfactant Flooding

This flooding is based on the injection of a surfactant (or blend of surfactants) formulation able to reduce the IFT between the trapped oil and the aqueous phase to low values, below 10^{-2} mN/m. However, according to the fundamentals shown in section 2.1.3, ultra low values (below 10^{-3} mN/m) are much more promising to reach higher *Nc* values and significant reduction of S_{or}.

Surfactants can be injected into the reservoir as part of a water flooding or polymer flooding process to improve oil recovery. The effectiveness of surfactants in EOR depends on a number of factors, including the type and concentration of surfactant, reservoir temperature, adsorption of the surfactant on the rock surface, and composition of reservoir fluids, among others. The selection of the appropriate surfactant and formulation design are crucial for achieving the desired EOR outcome.

2.2.2.1. Surfactants

Surface-active agents are commonly organic amphiphilic molecules, meaning they have both hydrophilic (water-affinity) and hydrophobic (water-repelling) properties. Most surfactants contain a polar hydrophilic head group and a non-polar hydrophobic tail. The hydrophilic section is usually water soluble while the hydrophobic section is oil soluble, which make surfactants soluble in both polar and non-polar solvents. This characteristic allows them to form a monolayer at the interface between two immiscible phases, such as oil and water. The hydrophobic tail of the surfactant is oriented towards the oil and its hydrophilic head oriented towards the water. The driving force for surfactant adsorption at the phase boundary is the reduction of the free energy of that interface (free energy per unit area refers to the amount of work needed to expand the interface). This reduces the IFT between both phases. Typically, the hydrophobic segment consists of a lengthy hydrocarbon chain, although it can also be comprised of a siloxane or fluorocarbon chain, or a short polymer chain. Additionally, the hydrophobic section may be either linear or branched. The hydrophilic part consists of moieties which can be sulfonates, sulphates,

USC UNIVERSIDADE DE SANTIAGO DE COMPOSTELA

carboxylates, alcohols, polyethylene chains, quaternary ammonium salts, etc. [2,10,13,26,28]. Figure 2.11 shows a representation of a surfactant molecule.

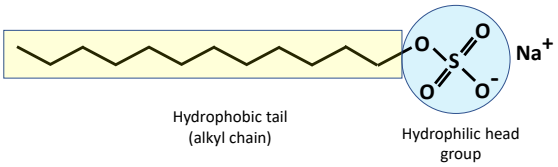


Figure 2.11. Scheme of a surfactant molecule (Sodium Dodecyl Sulfate, SDS).

The length of the tail, the position of the head group, and the extent of the tail branching, determine the physicochemical behaviour of the surfactant in aqueous solutions and in the non-polar phase.

Surfactants can be classified based on the ionic nature of the hydrophilic head group in aqueous solutions, as anionic, cationic, nonionic and zwitterionic.

Anionic surfactants have a negatively charged hydrophilic head group. The negative charge of most anionic surfactants is given by a sulphate (SO_4^-), sulfonate (SO_3^-), phosphate (PO_4^-), or a carboxylate (COO^-) group. Carboxylates can act as carboxylic acids and their ionic state depends on the pH of the system. Anionic surfactants have widely predominated in surfactant EOR applications due to their low adsorption in sandstone rocks (which present negatively charged surfaces) and that most of these techniques have been used on sandstone reservoirs. Furthermore, they are able to reach very low IFTs with the oil phase and can be produced economically [28].

Cationic surfactants have a positively charged hydrophilic section which is often a quaternary ammonium group. These surfactants are less used for EOR purposes due to their strong electrostatic interactions with negatively charged minerals, like clays on sandstone rocks, which cause high adsorption. However this type of surfactant can be useful in carbonate reservoirs, to alter the wettability of oil-wet rocks towards more water-wet [28].

Nonionic surfactants do not have a charged group in their chemical structure since they do not ionise in water, unlike anionic or cationic surfactants. They are typically composed of a hydrophobic tail (often an alkyl chain) and a hydrophilic head, which can be made up of various non-dissociable functional groups such as polyethylene oxide (PEO), polypropylene oxide (PPO), or glycerol. Even though these surfactants do not have a strong polar head group, they can be solubilised in water due to their ionic nature endowed by the hydrogen bonds and van der Waals forces. Those surfactants do not reach as low IFTs as anionic surfactants. Nonetheless, they are

USC
DE SANTIAGO
DE COMPOSTELA

less sensitive to changes in pH and high salinity than anionic or cationic surfactants, which makes them more stable under a wider range of reservoir conditions. Thus, they are mainly used as co-surfactants with other surfactants to create surfactant blend systems that can be tailored to specific reservoir conditions. The use of mixed surfactant systems can increase the efficiency of oil recovery and reduce the amount of surfactant required [2,26,28].

Zwitterionic surfactants are a unique type of surfactants that contain two hydrophilic head groups with different charges. Thus, they can be anionic-cationic, anionic-nonionic or cationic-nonionic surfactants. The positive charge is mostly encountered in an ammonium group, while the negative charge varies, frequently being a carboxylate group. Zwitterionic surfactants are highly effective at reducing surface tension, as they can interact with both positively and negatively charged surfaces. They are also highly stable in a wide range of conditions, including high and low pH environments, high temperatures, and high salt concentrations. However, their manufacture can be costly [2,26,28].

Figure 2.12 shows a summary of the main families of surfactants tested in EOR laboratory or field studies, classified by their ionic character [13,29].

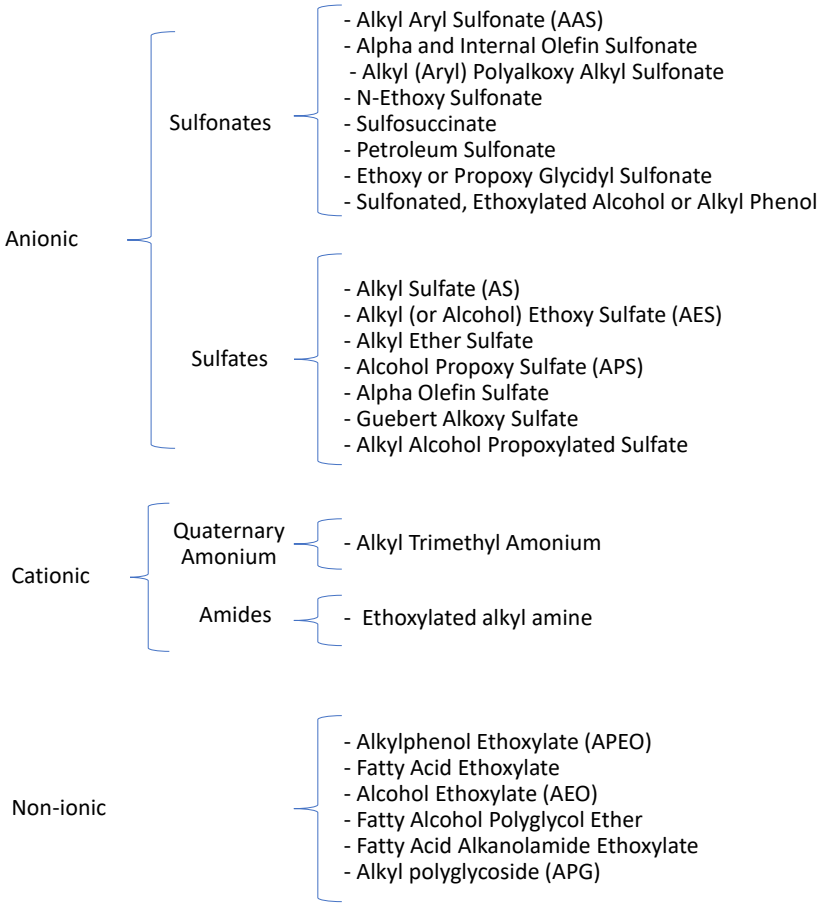


Figure 2.12. Main surfactant families by ionic nature type.

2.2.2.2. Surface-Active Ionic Liquids

Ionic liquids (ILs) are salts with melting or glass transition temperatures below 100 °C. The cation, in most cases, has an organic nature with different substituents or R groups associated (see Figure 2.13). Commonly, the substituents on the cation are alkyl chains, however, they can also be several other functional groups such as methoxy, alkenyl, fluoroalkyl, etc. [30,31]. The anion can be inorganic or organic. Common cations and anions of ILs are shown in Figures 2.13 and 2.14, respectively. Among these salts, room-temperature ILs attract more interest in industrial applications. The selection of an organic ion with a delocalized charge or with a bulky asymmetric substituent promotes poor coordination between ions and decreases melting temperatures.

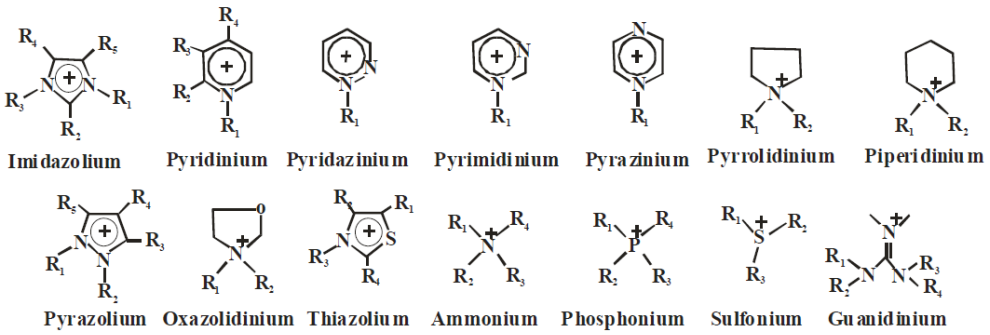


Figure 2.13. Most typical cations found in ILs.

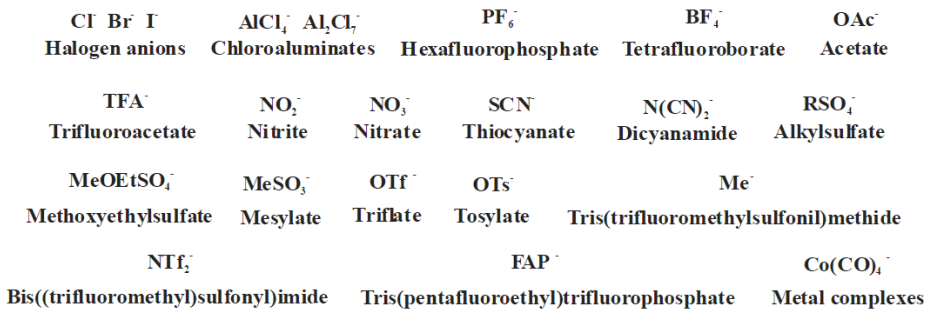


Figure 2.14. Most typical anions found in ILs.

ILs exhibit unique properties such as low volatility, high thermal stability, negligible vapor pressure, and the ability to dissolve a wide range of materials [30,32]. Their most interesting feature is that, due to the high number of possible combinations of cations, anions and substituents, a large amount of ILs may be synthesised. Thus, physical, chemical or even biological properties can be tuned by selecting the suitable cation and anion. Such properties include

USC UNIVERSIDADE DE SANTIAGO DE COMPOSTELA

hydrophilicity, chemical and thermal stability, melting point, or viscosity, among many others [30,31]. Focusing on EOR applications, the possibility of tuning their hydrophilicity and surface-active character are the most interesting. The hydrophilicity of an IL can be tailored by modifying the R group. The hydrophilicity of the cation tends to decrease by increasing the alkyl chain length [30]. Moreover, its solubility is strongly related to the anion nature. For instance, imidazolium ILs with an anion of acetate [$CH_3CO_2^-$], halide [Cl^-, Br^-, I^-], nitrate [NO_3^-] or trifluoroacetate [CF_3CO_2] are completely soluble in water, while ILs with a hexafluorophosphate [PF_6^-] or bis(trifluoromethylsulfonyl)imide [$(CF_3SO_2)_2N^-$] anions are insoluble. Solubility of ILs with tetrafluoroborate [BF_4^-] or triflate [$CF_3SO_3^-$] anion depends on the cation's alkyl chain length [33].

A surface-active ionic liquid (SAIL) is a type of IL which has amphiphilic properties and a high surface activity. SAILs usually show a relatively long alkyl chain as substituent of the cation, which confers them hydrophobic character, and a cation head group as responsible for the hydrophilicity of the SAIL. Similarly to traditional surfactants, these characteristics allow SAILs to interact with both polar and nonpolar phases, which reduces the IFT between two immiscible liquids. Also, they may spontaneously form micelles. Therefore, SAILs are being studied as interesting alternatives to traditional surfactants in EOR [32].

2.2.2.3. Surfactants in EOR

Compared to laboratory studies, the number of reports on the field performance of surfactants in EOR is very limited. However, different types of surfactants have been used for EOR flooding [13]. Because the majority of surfactant EOR projects have been performed in sandstone reservoirs, anionic surfactants have become the most employed surfactant type in field applications [20,34]. Among them, sulfonate surfactants, such as petroleum sulfonates, internal olefin sulfonates, and alkyl aryl sulfonates are the most widely used. Petroleum sulfonates are the most popular since they can be easily produced, derived from the sulfonation of a portion of the crude oil in an intermediate molecular weight stream from the refinery [20,34]. Most of the sulfonate surfactants are stable at high temperatures, but their effectiveness can be hindered in high-salinity conditions due to precipitation, as they are susceptible to divalent cations [20].

The application of surfactant flooding in carbonate has been limited in comparison to sandstone reservoirs. Only a few nonionic surfactants, of the alcohol ethoxylate type, have been tested in carbonate reservoirs [13,20,35].

2.2.2.4. Micelles and Microemulsions in EOR

The balance between the hydrophilic and the hydrophobic parts of a surfactant leads to a more hydrophilic or hydrophobic character of it. Thus, the Hydrophilic-Lipophilic Balance (HLB) of a

surfactant governs its tendency to partition more in water or in oil, and consequently the tendency to form oil-in-water or water-in-oil emulsions, respectively. For instance, considering a fixed hydrophilic head group, a surfactant with a longer hydrocarbon chain tends to partition into the oil phase more readily than one with a shorter hydrocarbon chain [10].

Micelles. When a surfactant begins to be added to a solvent, its molecules are adsorbed at the solvent surface or at the interface between two immiscible fluids. By increasing surfactant concentration, molecules cover the area of the surface or interface, continuously decreasing the free energy (IFT). At certain surfactant concentrations, molecules spontaneously start to form organised aggregates called micelles. At this point, the free energy decrease sharply changes its trend as a function of surfactant concentration, stabilising or smoothly decreasing the IFT. That surfactant concentration is named Critical Micelle Concentration (CMC). Above the CMC, further additional surfactant molecules will form micelles which partition preferentially in one phase, depending on the HLB of the surfactant [2,10,21]. Figure 2.15 presents the CMC estimations of different surfactants in a typical representation of IFT measurements as a function of surfactant concentration.

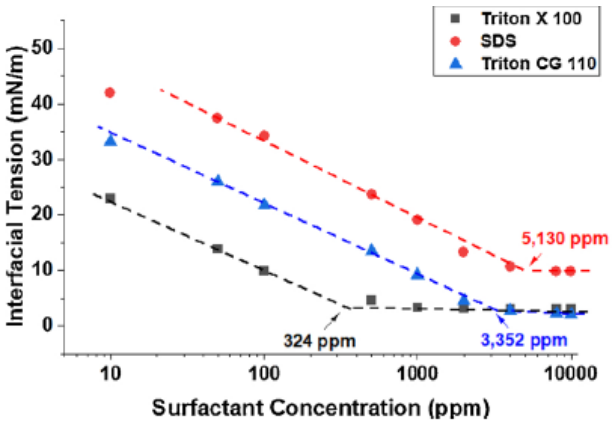


Figure 2.15. Typical plot for CMC estimation. IFT measurements as a function of three commercial surfactant concentration (Figure reproduced from [36]. Permission to publish by Elsevier).

If the surfactant partitions in the aqueous phase, micelles aggregate with the polar head group oriented outward and the hydrophobic chain inward. In that way, the alkyl chains reduce their energetically adverse interactions with the aqueous phase and the polar groups keep in contact with water. This kind of aggregation is known as direct micelle. Since the internal structure consists of hydrocarbon chain associations, such micelles can solubilise organic compounds. Analogously, when surfactant partitions in a hydrocarbon solvent, molecules form reverse micelles, orienting the polar head group inside the micelle and the hydrocarbon chain outward [2,10,21]. A schematic representation of both direct and reverse micelles is shown in Figure 2.16.

Microemulsions. As explained above, at surfactant concentrations higher than the CMC, a hydrophilic surfactant can solubilise significant amounts of oil into direct micelles under certain ideal conditions. The same process can be observed in hydrophobic surfactants, which can solubilise the water phase inside reverse micelles. A microemulsion is a system of oil, water, and amphiphile which is an optically isotropic and thermodynamically stable liquid solution. The droplets (swollen micelles) are typically in the size range of 10 to 100 nm, which is much smaller than those in an ordinary emulsion (generally known as macroemulsion). Depending on drop size, an aqueous phase microemulsion with solubilised oil can be translucent [10,21,26]. However, the higher the solubilisation the less transparent the microemulsion [37]. Microemulsions have highly dynamic internal structures and show low IFT, high stability, and high solubilisation capacity.

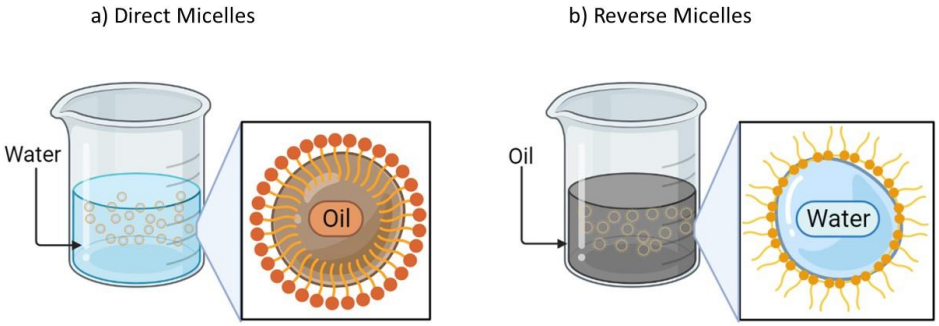


Figure 2.16. Representation of (a) direct and (b) reverse micelle structures

At equilibrium, microemulsions (constituted of water, oil and surfactant) can be classified into three main types, according to Winsor theory [38]:

1. Winsor type I or oil-in-water (O/W) microemulsion: the oil phase is dispersed in the water phase in the form of swollen direct micelles. This microemulsion can coexist with an excess upper oil phase.
2. Winsor type II or water-in-oil (W/O) microemulsions: the water phase is dispersed in the oil phase inside reverse swollen micelles. The microemulsion can be in equilibrium with a lower excess water phase.
3. Winsor type III or bicontinuous microemulsions: in this type of microemulsion, the oil and water phases are interpenetrating and form a continuous network throughout the system in a combination of swollen direct and reverse micelles. Thus, a Winsor type III microemulsion is saturated with both oil and water phases. The microemulsion can coexist in equilibrium with excess water and oil phases.

USC UNIVERSIDADE DE SANTIAGO DE COMPOSTELA

Winsor types I, II and III are also known as lower-phase, upper-phase, and middle-phase microemulsions respectively [2,39], according to the relative positions in equilibrium of the microemulsion with the excess water and oil phases in a test tube. In EOR, Winsor type III microemulsions are desired because the equilibrated interactions lead to minimum values of water-oil IFT.

2.3. EOR EVALUATION TESTS

Experimental tests at the laboratory scale and advanced numerical simulations are the required stages to evaluate and identify best potential surfactant formulations for EOR.

2.3.1. Laboratory

2.3.1.1. Phase Behaviour Studies

The formation of microemulsions and their equilibrium involve several key parameters. These include the type and concentration of surfactant and cosurfactant, the ratio of oil to water, salinity and general composition of the aqueous phase, system temperature, the nature of the oil phase, etc. Thus, microemulsions can exhibit a wide range of phase behaviours as a function of these key parameters. Phase behaviour of microemulsions is a complex phenomenon, characterised by changes in their thermodynamic properties. Alterations of variables can lead to a transition of microemulsion types (e.g., from Winsor type I to type II or vice versa) [10].

The phase behaviour of microemulsions can be represented using ternary phase diagrams which show the boundaries between the different phases. To build a ternary phase diagram for a microemulsion system, the number of existing variables must be reduced to three by combining some of them into pseudo-components, and leaving other variables fixed. Therefore, a surfactant as pseudo-component can be formed by surfactant and cosurfactant or cosolvent at a fixed ratio, water as pseudo-component usually contains electrolytes, and oil may be a mixture of oils at fixed ratio. Other properties such as temperature and pressure are commonly fixed. Figure 2.17 shows a series of ternary diagrams and test tubes for a microemulsion transition between Winsor type I (WI), type III (WIII) and type II (WII) as a function of salinity or temperature. The three pseudo-components represented in the apex of the triangular diagram are: surfactant (S), oil (O), and water (brine) (W), at fixed temperature and pressure.

A transition from Winsor type I to type II microemulsions can occur by changing one or several variables at the same time. In general, for ionic surfactants there will exist a microemulsion Winsor type I at relatively low salinity. Increasing the salinity of the brine (in the aqueous phase) makes the microemulsion less hydrophilic. Increasing the salinity can initially enhance the

solubilisation of additional oil into the aqueous phase of the still Winsor type I microemulsion. Further increments of salinity will decrease the solubility of the surfactant in the aqueous phase, forcing surfactant to be gradually expelled towards the oil phase. At high salinity, the microemulsion will have shifted to a Winsor type II microemulsion. At certain intermediate salinities, during the transition from Winsor type I to type II, it is possible to obtain a three-phase region where the third phase is the Winsor type III microemulsion. Due to its intermediate density between aqueous and oil phase densities, the microemulsion is located at the middle of the phases in the optimal test tube (Figure 2.17). The salinity at which oil and water volume solubilisation in the Winsor type III microemulsion are equal is named the optimal salinity. Analogously, for nonionic surfactants, increments of temperature produce similar effects in the phase behaviour of microemulsions [26].

As explained in section 2.2.2.4, Winsor type III microemulsions have a significant relevance to surfactant flooding since these microemulsions show the largest surface activity between oil and aqueous phases. The lowest IFT values, through microemulsion phase behaviour, may likely be found in this region or very close. Surfactants at conditions leading to Winsor type I to type II microemulsions will have higher IFT values. A representation of the existing correlation between the microemulsion phase behaviour and IFT can be seen in Figure 2.18. Commonly, for surfactant flooding, one surfactant alone may not reach ultralow IFT values at reservoir conditions, thus blending with a second surfactant becomes necessary [40].

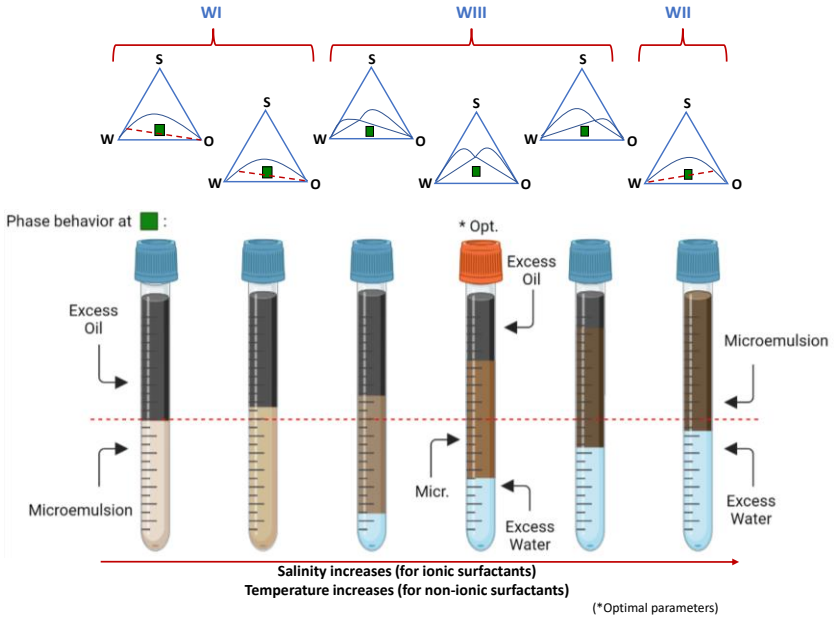


Figure 2.17. Schematic representation of ternary phase diagrams and pipettes with microemulsions obtained varying one formulation parameter.

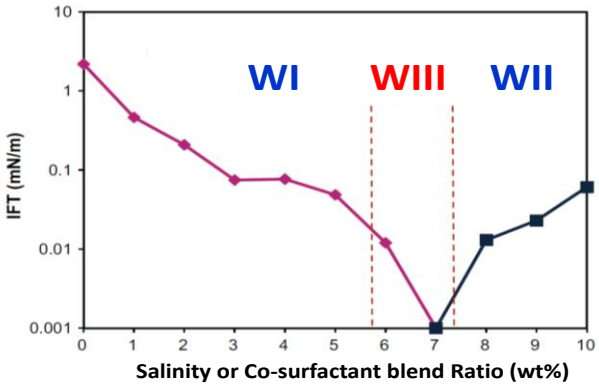


Figure 2.18. Correlation between the microemulsion phase behaviour and IFT (Figure reproduced/adapted from [41]. Permission to publish by Elsevier).

In surfactant flooding, the adsorption of surfactant on the rock surface, besides the loss of process efficiency, affects the concentration of surfactant in the aqueous phase and consequently, the IFT. Higher surfactant adsorption occurs mainly due to electrostatic interaction between the charged hydrophilic head group of the injected ionic surfactant and charged sites on rock surfaces. Other factors such as salinity, temperature and pH of the COBR system can influence the final adsorption level. Usually, the easiest factor to vary in an EOR project to avoid these problems is the type of surfactant, finding one suitable for the reservoir conditions [21].

2.3.1.2. Dynamic IFT

Water-oil IFT is a key factor in surfactant EOR. Dynamic IFT values can be measured by means of the spinning-drop method [42]. This method involves a small drop of one lower density immiscible fluid (oil phase) being suspended in a second immiscible higher density fluid (aqueous phase). The spinning-drop tensiometer consists of a horizontal capillary tube where the drop of the lighter phase is injected into the heavier phase. The tube is then rotated at high constant speed (around 3000 – 5000 rpm) to generate centrifugal forces that deform the spinning drop. Observing the deformation it is possible to estimate the IFT. As the drop spins, it elongates and thins out (Figure 2.19), causing the surface area of the interface between the two fluids to increase [43].

The surface area's evolution is due to energy changes related to the surface tension and centrifugal forces. The final elongated shape of the spinning drop, once the drop has reached the equilibrium state, is the result of contributions from both the surface tension and rotation energy. At high rotation speeds, the elongated spinning drop shape can be approximated to a cylinder and IFT can be estimated by the Vonnegut equation [42,43]:

USC UNIVERSIDADE DE SANTIAGO DE COMPOSTELA

$$\sigma = \frac{\Delta\rho \cdot \omega^2 \cdot R^3}{2}\left(\frac{1}{2} + \frac{1}{3}\frac{R}{L}\right) \quad \text{(Eq. 2.13)}$$

where:

σ= dynamic IFT

Δρ= density difference between the dense and light phases

ω= angular velocity

R= radius of the oil drop

L= Length of the oil drop

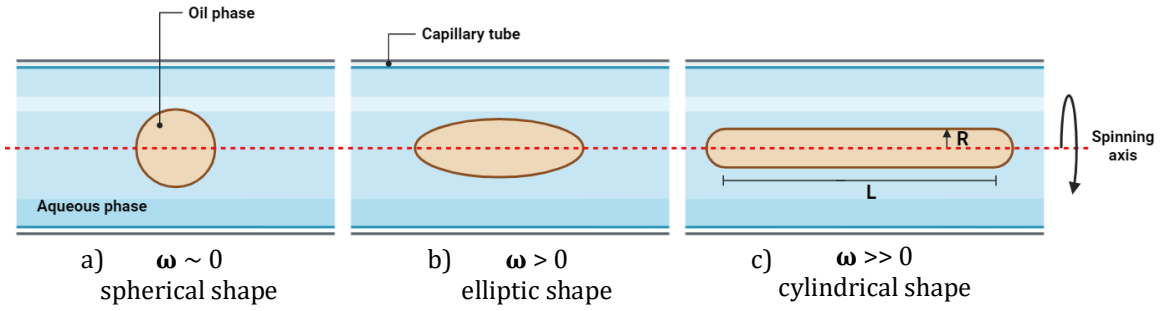


Figure 2.19. Schematic of the spinning-drop method theory. A drop of a lower density immiscible liquid is immersed in a second higher density liquid. Evolution of the drop shape as the angular velocity (ω) increases. *R*= radius and *L*=length of the approximated cylindrical shape.

At high rotation velocity, *R/L* ratio tends to zero, and the Eq. 2.13 simplifies to:

$$\sigma = \frac{\Delta\rho \cdot \omega^2 \cdot R^3}{4} \quad \text{(Eq. 2.14)}$$

Using a spinning drop tensiometer it is also possible to estimate IFT for drop shapes other than cylindrical using the Young-Laplace equation method [44].

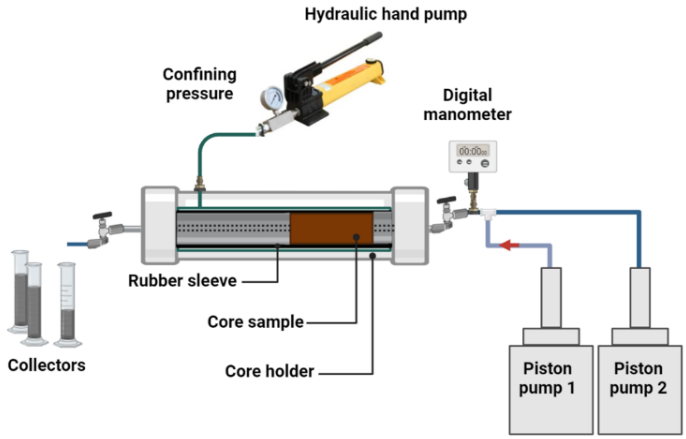
2.3.1.3. Core Flooding Tests

The core flooding test is a laboratory experiment used in the oil and gas industry to simulate fluid displacement operations. Its purpose is to evaluate the effect of injecting fluids specially designed to improve or enhance oil recovery. The technique conducts experiments on core samples, which can be taken from reservoirs or outcrop rocks. Typically, a small cylindrical core sample is placed into a core holder, and confining pressure is applied around the core to mimic burial pressure. At the start of the test, fluids inside the core can be either formation brine, oil (pure or crude), or a combination of brine and oil. In situ fluids are then flowed through the core by injecting fluids such as brine, surfactant solutions, polymers, or gas. As the fluid is injected, it displaces the trapped oil within the rock pores, mimicking the secondary or EOR process. Depending on the

test's purpose, core flooding test conditions may be ambient temperature/low pressure or high temperature/high pressure [45,46].

Throughout the displacement test, various parameters such as pressure, flow rate, and effluent composition can be measured. These measurements allow researchers to estimate the permeability and porosity of core samples, relative permeability, saturation change, and interactions between the fluid and the rock. Using those results, researchers can evaluate the effectiveness of secondary recovery or different EOR methods and optimise strategies for a given reservoir [45,46]. Figure 2.20 shows a representation of two setups for core flooding tests at different conditions.

(a)



(b)

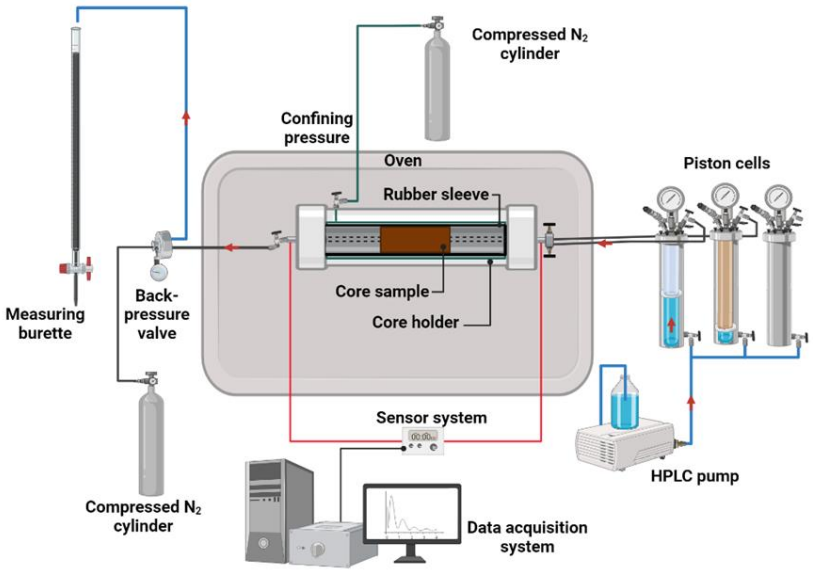


Figure 2.20. Schematic of core flooding test setups for (a) ambient temperature/low pressure and (b) high temperature/high pressure conditions.

USC UNIVERSIDADE DE SANTIAGO DE COMPOSTELA

2.3.1.4. Dynamic Adsorption

The adsorption of a surfactant on the rock surface can be evaluated as a function of injection rate and surfactant concentration, among other parameters, by batch equilibrium tests using the same set-up as in core flooding experiments. Typically, these tests are conducted in single-phase mode, that is, without an oil phase. To estimate the surfactant adsorption in core material, a surfactant solution with a known composition is injected into the core until the effluent concentration equals the injected concentration. The retained surfactant can then be determined by material balance via a surfactant concentration analysis of all effluent samples [10].

The results of the test can be used to optimise the concentration and injection rate of surfactants during EOR processes, and to improve the overall efficiency of oil recovery operations.

2.3.1.5. Spontaneous Imbibition

Spontaneous imbibition is a phenomenon in which a wetting fluid is spontaneously attracted into a porous medium (such as a rock) due to capillary forces and the natural wettability of the medium. Spontaneous imbibition tests in the oil industry are conducted in the laboratory to evaluate the ability of a porous rock to imbibe a given fluid and to study the effectiveness of different techniques or chemical formulations to improve oil recovery. In these tests, an oil saturated core sample is placed in the imbibition cell and immersed in an imbibition fluid such as brine, or a chemical formulation. The fluid will be drawn by the core and moves through it by capillary imbibition, filling the pores and displacing the oil. The displaced oil moves towards the other end of the core and is collected in a container. The imbibition fluid will be replaced periodically through one end of the cell. The imbibition rate and the saturation profile are estimated by monitoring the amount of fluid collected over time. Various parameters such as the wettability of the rock surface and the properties of the fluids can be evaluated [47]. The setup used for conducting spontaneous imbibition tests in illustrated in Figure 2.21.

Spontaneous imbibition is an important factor in oil recovery, particularly in fractured or low-permeability reservoirs where traditional recovery techniques such as water flooding may not be effective [47].

USC
UNIVERSIDADE DE SANTIAGO DE COMPOSTELA

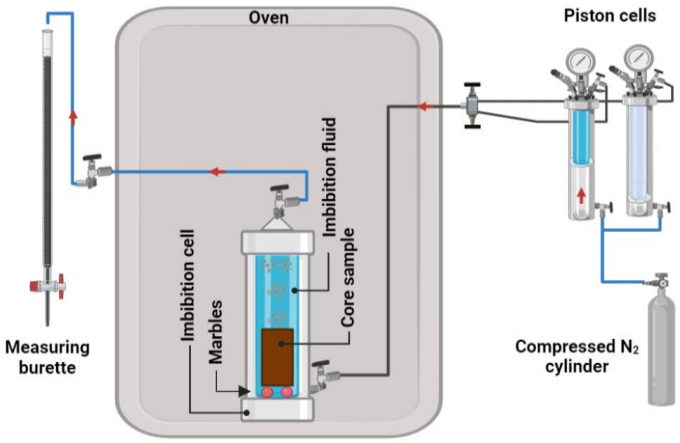


Figure 2.21. Schematic of spontaneous imbibition test setup for high temperature/high pressure conditions.

2.3.2. Simulation

Reservoir simulation is a computer-based technique used in the oil and gas industry which integrates mathematics, physics, reservoir engineering and computer programming to model the behaviour of oil, gas, and water, within an underground reservoir [8]. The aim of reservoir simulation is to understand and predict the performance of oil and gas reservoirs under different operating conditions in order to optimise production strategies. By simulating various scenarios and parameters, it is possible to take decisions with respect to reservoir management strategies, such as well drilling, production rates, and injection strategies, to maximise hydrocarbon recovery. The need to minimise costs and assess the associated risks of different development plans in hydrocarbon recovery projects, which involve investments of hundreds of millions of dollars, has boosted progress in reservoir simulation. Poorly controlled variables such as heterogeneity of rock properties, variations of fluid properties, fluid-fluid and rock-fluid interactions, and the recovery mechanism complexities contribute to this risk [8].

In plain terms, reservoir simulation models are computational representations of fluid flow through porous media based on fundamental principles such as Darcy's law (which describes the fluids flow through porous media), mass conservation law, and energy equations. These models are built using mathematical, numerical, and computer methods. Fluid flow can be modelled mathematically using sets of nonlinear partial differential equations with boundary and initial conditions. However, these equations are too complex to be solved analytically for reservoir studies. Therefore, numerical methods (usually finite differences in hydrocarbon industry) are used to discretise the nonlinear partial differential equations into non-linear algebraic equations, which can be solved by computer programs designed for this purpose [48,49]. The numerical

models are typically built on a three-dimensional grid that represents the reservoir structure. Outcomes include estimating production rates, fluid movement within the reservoir, pressure changes, and hydrocarbon recovered over time and space. Figure 2.22 shows a representation of a 3D grid to geometrically model the structure of a reservoir.

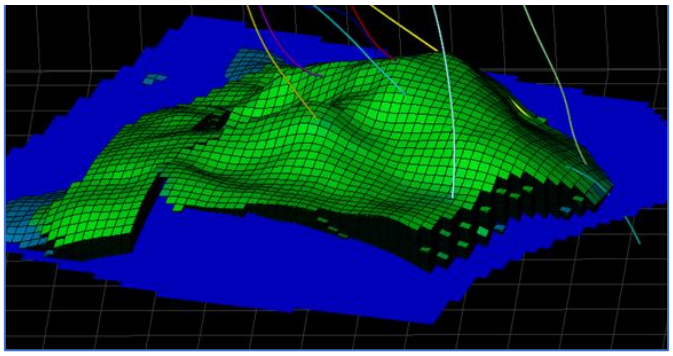


Figure 2.22. 3D modelling of a reservoir structure

As part of reservoir models, variables such as rock properties, fluid properties, fluid-fluid and rock-fluid interactions, well configuration, historical pressure and production/injection rates are incorporated. Then, these models are calibrated using the historical data to improve their accuracy and reliability.

While classical reservoir engineering handles average data for a whole reservoir without accurately taking into account variations in rock and fluid properties, numerical simulations allow robust studies with more complex calculations, dividing the reservoir into blocks and resolving thousands of fundamental equations for each block of fluid flow through porous media [48]. Reservoir simulation is used in various stages of the oil and gas field life cycle, from exploration and appraisal to production and EOR operations.

Reservoir simulation software packages are commonly used in the petroleum industry, both on field and laboratory scales, and their accuracy and reliability continue to improve with advancements in computing power and numerical methods [48]. One of the two most widely used commercial simulation packages is CMG-STARS, developed by the company Computer Modelling Group (CMG). CMG-STARS is a finite difference numerical simulator, well-known for its capacity to model both field and laboratory scales [50,51]. CMG-STARS was selected in a section of the present thesis to model laboratory chemical EOR tests, specifically for surfactant flooding.

The modelling approach of microemulsion phase behaviour at reservoir conditions is a very complex process due to the great number of variables involved in surfactant performance. CMG-STARS approximates Winsor type III microemulsion handling two liquid phases, oil and water,

USC DE COMPOSTELA

and specifying surfactant partitions between the phases. IFT values are associated to those conditions [52].

Since IFT reduction can reduce S_{or} and consequently alter the relative permeability curves, CMG-STARS models the capillary desaturation process by interpolating relative permeability curves as a function of capillary number *Nc*. *Nc* is continuously estimated during surfactant flooding [53,54]. Two extreme conditions in which these interpolations are carried out are the displacement of oil by water (high IFT with low $Nc=6.0\times10^{-8}$) and the displacement of oil by surfactant in a fully miscible process (ultralow IFT, with high $Nc=2.3\times10^{-1}$) [55]. An example of interpolated permeability curves is presented in Figure 2.23.

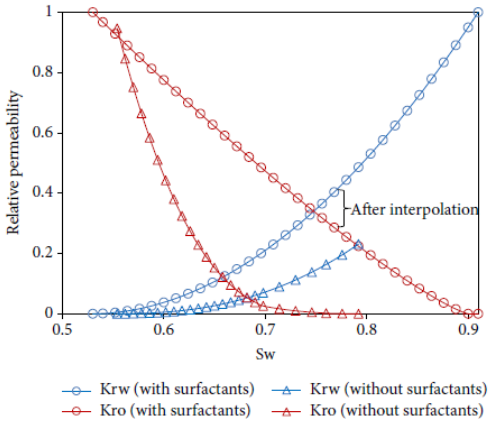


Figure 2.23. Example of interpolated relative permeability curves (Figure reproduced from [56]. Available under open CC BY 4.0 license).

USC UNIVERSIDADE DE SANTIAGO DE COMPOSTELA

USC
UNIVERSIDADE
DE SANTIAGO
DE COMPOSTELA

3. PUBLICATIONS



USC
UNIVERSIDADE
DE SANTIAGO
DE COMPOSTELA

USC
UNIVERSIDADE
DE SANTIAGO
DE COMPOSTELA

Chaos ARTICLE scitation.org/journal/cha

Highly viscous fluid displaced by a chemically controlled reactive interface

Cite as: Chaos **31**, 023135 (2021); doi: 10.1063/5.0031058
Submitted: 27 September 2020 · Accepted: 1 February 2021 ·
Published Online: 22 February 2021

View Online Export Citation CrossMark

Néstor Tafur,[1] Darío M. Escala,[1] Ana Soto,[2] and Alberto P. Muñuzuri[1,a)]

AFFILIATIONS

[1]Institute CRETUS, Group of Nonlinear Physics, Department of Physics, Universidade de Santiago de Compostela, 15782 Santiago de Compostela, Spain
[2]Institute CRETUS, Group EQUIFASE, Department of Chemical Engineering, Universidade de Santiago de Compostela, 15782 Santiago de Compostela, Spain

[a)]**Author to whom correspondence should be addressed:** alberto.perez.munuzuri@usc.es

ABSTRACT

Displacement of a viscous fluid by a less viscous one is a challenging problem that usually involves the formation of interfacial digitations propagating into each one of the fluids, mixing them and preventing their normal displacement. We propose in this manuscript a protocol that is implemented via numerical simulation of the corresponding equations to improve the efficiency of the displacement. We consider a chemically active interface between the two chemically active fluids that produce a large viscosity interface that facilitates the process. All the relevant parameters of the mechanism are numerically analyzed aiming to optimize the efficiency of the method.

Published under license by AIP Publishing. https://doi.org/10.1063/5.0031058

Forced motion of highly viscous fluids is a complicated problem with many industrial applications due to the instabilities at the interface that play against it. When in a horizontal displacement a fluid with less viscosity is arranged to push another with higher viscosity, it is highly likely that the first one induces deformations of the interface formed between both fluids creating fingerlike forms (fingers), which implies that the less viscous fluid penetrates the higher viscosity fluid. This situation is a hydrodynamic instability called viscous fingering and, in several areas, it is an unwanted phenomenon that is aimed to suppress or minimize. Our scope in this manuscript is to minimize this phenomenon by controlling the interfacial instability by means of a chemical reaction. The chemical reaction acts on the viscosity at the interface producing a much higher viscous ring that behaves as an actual stopper facilitating the displacing process. We propose a methodology, and the different parameters of the system are analyzed and their role on the efficiency of the displacement is revealed.

I. INTRODUCTION

Hydrodynamic instabilities are generated at the interface between two fluids with two different viscosities when the lower viscosity fluid tries to displace the other fluid with larger viscosity, causing a phenomenon called the Saffman–Taylor instability, or viscous fingering (Saffman and Taylor, 1958). This system has been extensively studied both experimentally and numerically (Saffman, 1986; Homsy, 1987; and De Wit, 2003). Size and shape of the fingers, velocity of growing, forces involved in the displacement, etc., have been analyzed and characterized (Benham and Olson, 1963 and Perkins and Hoffman, 1965). Other studies deal with the existence of a porous media and the effect in the instability (Peters and Cavalero, 1990), considering miscible and immiscible displacements.

The oil industry is one of the most interested in this problem as it directly affects their production strategies. Here, the behavior of viscous fingering through homogeneous and heterogeneous porous media has been analyzed (Araktingi and Orr, 1993 and Sharma *et al.*, 2011). Some authors considered a three-component flow in order to improve the displacement (Blunt and Christie, 1994), and others considered a compositional displacement regarding oil composition (Blunt *et al.*, 1994). This research helped develop more efficient enhanced oil recovery (EOR) processes in the industry.

Thus, the next step for practical applications is to control the fingering mechanism. Several approaches have been done in this sense trying to control or manipulate the instability by means of interfacial chemical reactions. Nagatsu *et al.* (2007) considered experimentally the coupling between reaction and hydrodynamics in a Hele–Shaw cell resulting in changes in the displacing fluid

USC UNIVERSIDADE DE SANTIAGO DE COMPOSTELA

viscosity and how this was reflected in the finger configuration. This study was continued in forthcoming contributions (Nagatsu *et al.*, 2010; 2011). De Wit (2020) proposed a theoretical model to account for the chemically induced changes in the viscosity considering a simple A + B → C reaction. Taking advantage of clock reactions (Kovacs *et al.*, 2005), other authors (Escala *et al.*, 2019) have triggered fingering phenomena in a stable configuration by rapidly increasing the interface viscosity.

Despite the large number of research related to fingering and the attempts to manipulate its patterns, there are few studies that try to control, or even suppress, this phenomenon through experimental protocols in reactive systems that could help attenuate the instability and offer efficient results for fluids displacement.

By means of mathematical modeling and numerical simulations, this manuscript aims to systematically analyze the different conditions and configurations that improve the displacement efficiency of a larger viscosity fluid displaced by another with lower viscosity through a chemical reaction at the interface between both fluids. The chemical reaction generated when fluid A (displacing fluid) and fluid B (displaced fluid) are mixed produces a front of product C at the contact zone that we consider to have larger viscosity, and, thus, would be able to control the hydrodynamic instabilities (Fernandez and Homsy, 2003 and Nagatsu *et al.*, 2007; 2009; 2011). The focus of this manuscript is to analyze the physical properties of the flow and how the reacting interface controls the instabilities. In that sense, an interesting parameter in our simulations will be the chemical reaction rate that controls the Damköhler number and, thus, the ratio between the characteristic chemical times and the hydrodynamical one. The efficiency of this displacement is estimated by measuring the amount of fluid B displaced or recovered. The term recovery will be used in this study to refer to the total percentage of the displaced fluid that has been swept until a time when the product C (or the reactant A for non-reactive cases) reaches the limits of the reactor (breakthrough time).

The manuscript is organized as follows. After the introduction, a description of the model used is presented, including the equations considered. This section is followed by the description of the results obtained with our simulations including the protocol proposed. Here, the different parameters of the system are systematically evaluated and their influence in the flow dynamics reported aiming to achieve the optimum situation in terms of the amount of displaced fluid recovery. The final section of the manuscript presents the discussion of our results and conclusion.

II. MODEL SYSTEM

In the numerical simulations, we consider an isothermal radial displacement of the fluids in a Hele–Shaw reactor. The Hele–Shaw cell has been used in experimental studies of fluids flowing through porous media by several researchers. It consists of two horizontal glass plates separated by a constant thin gap, which is much smaller than the radius R, or any of the two other spatial dimensions L_y or L_x. Typically, the gap is in the order of 0.5 mm or less while L_x and L_y are usually larger than 10 cm (Wooding, 1969; Nagatsu and Ueda, 2001; and De Wit, 2020). The cell is filled with fluids from the center (through a small orifice in one of the plates) or from the edges, depending on the direction of the fluid displacement configured (linear or radial). In our numerical study, we set the configuration of the Hele–Shaw cell to model a radial flow in a circular reactor, injecting the fluid from an inlet point located at the center of the circle (Li and Rivière, 2016; Brau *et al.*, 2017; and Escala *et al.* 2019). We established the inlet point as a circular orifice of radius r = 0.2 cm, the reactor radius to R = 10 cm, and the gap h = 0.25 mm. The reactor is opened to the atmospheric pressure following the experimental conditions in previous experiments (Vishnudas and Chaudhuri, 2017; Escala *et al.*, 2019; Mishra *et al.*, 2010; Gérard and De Wit, 2009; and Escala and Munuzuri, 2021). The system considers Newtonian aqueous fluids, miscible and with equal densities for all the involved species so that buoyancy effects in this process are negligible.

Two fluids are initially considered, the displaced fluid that is initially in the reactor and the displacing one that is injected during the simulation from the center of the reactor. These two miscible fluids react at the interface producing an additional compound, named C. Considering an incompressible 2D radial displacement, the dynamics of a reactive and isothermal interface in porous media is given by the following set of reaction–diffusion–convection (RDC) equations based on Darcy's law:

$$\vec{\nabla} \cdot \vec{u} = 0, \tag{1}$$

$$\vec{\nabla} p = -\frac{\mu(\mathrm{A}, \mathrm{B}, \mathrm{C})}{\kappa} \vec{u}, \tag{2}$$

$$\varphi \frac{\partial \mathrm{A}}{\partial t} + \vec{u} \cdot \vec{\nabla} A = \varphi D_{\mathrm{A}} \nabla^2 \mathrm{A} \; - k_1 \mathrm{A}\,\mathrm{B}, \tag{3}$$

$$\varphi \frac{\partial \mathrm{B}}{\partial t} + \vec{u} \cdot \vec{\nabla} \mathrm{B} = \varphi D_{\mathrm{B}} \nabla^2 \mathrm{B} - k_1 \mathrm{A}\,\mathrm{B}, \tag{4}$$

$$\varphi \frac{\partial \mathrm{C}}{\partial t} + \vec{u} \cdot \vec{\nabla} \mathrm{C} = \varphi D_{\mathrm{C}} \nabla^2 \mathrm{C} + k_1 \mathrm{A}\,\mathrm{B}. \tag{5}$$

Considering that the displacing solution is entirely composed of the specie A, the displaced solution is entirely composed of specie B, and the product C emerges when both liquids react at the interface; then, A = A(*x,y,t*), B = B(*x,y,t*), C = C(*x,y,t*), represent the spatial concentrations of the species A, B, and product C, respectively, at any time and location. $\phi = 1$ is the porosity of the system and it is set constant for a Hele–Shaw cell (Gérard and De Wit, 2009 and De Wit, 2016; 2020). D_A, D_B, and D_C are the diffusion coefficients of species A, B, and C, respectively. κ is the permeability of the system, and it is calculated as $h^2/12$ (Gérard and De Wit, 2009; Homsy, 1987; and De Wit 2020).

We consider that both, displacing and displaced solutions, meet at the interface and mix via diffusion and chemically interact via the simple chemical model presented in reaction R1,

$$\mathrm{R1}: \mathrm{A} \; + \mathrm{B} \xrightarrow{k_1} \mathrm{C}, \tag{6}$$

where the product C is generated at the mixing zone when A and B make contact. k_1 is the reaction rate constant assuming a mass action velocity law.

The viscosity of the system $\mu = \mu(\mathrm{A}, \mathrm{B}, \mathrm{C})$ is assumed to be affected by the concentration of species A, B, and C, by the following

USC UNIVERSIDADE DE SANTIAGO DE COMPOSTELA

Published under license by AIP Publishing.

relation (De Wit, 2020):

$$\mu(A, B, C) = \mu_a e^{(R_b B + R_c C)/A_0}, \quad (7)$$

where $\mu_a = \mu(A_0,0,0)$, represents the viscosity of the displacing solution when $A = A_0$. The parameters R_B and R_C are the log mobility ratios defined as $R_B = \ln(\mu_B/\mu_A)$ and $R_C = \ln(\mu_C/\mu_A)$. R_B compares the viscosity between displacing and displaced solutions, and R_C compares the viscosity of the product C and the displacing solution. In the present work, both parameters are considered positive and $\mu_A < \mu_B < \mu_C$; thus, the initial scenario is always hydrodynamically unstable and the product C locally increases the viscosity in the mixing zone (Gérard and De Wit, 2009 and De Wit, 2016; 2020). The values of the other parameters are kept constant for all the simulations used with this model and are shown in the Appendix.

Simulations were performed using the computational fluid dynamic (CFD) software suite Ansys Fluent® 20.1 (ANSYS, Inc., 2020). The numerical domain (S) is a quarter of a circular region of radius R = 10 cm discretized using a mapped mesh of radial elements as indicated in the supplementary material [see Fig. S1(a)]. The inlet flow velocity at the central boundary is calculated as

$$-\vec{n} \cdot \vec{u} = v_0(Q), \quad (8)$$

where Q is the volumetric flow rate and $v_0 = Q/2\pi rh$. The injection orifice is a quarter of a circle of radius 0.2 cm located at the lower left corner of the domain. The injected fluid is considered to overflow at R = 10 cm; this outflow boundary considers atmospheric pressure, with P = 0 Pa as the outflow condition. In order to extrapolate the results to a full circular medium, the lower and left side of the boundary conditions are set equal to zero normal velocity and zero normal gradients for all the variables at these boundaries (symmetry conditions in ANSYS Inc., 2020, package). Both the pressure and species fields are discretized using second order upwind schemes. Simulations are performed using a coupled pressure solver and the SIMPLE algorithm with a variable time step setting. Time and space are in real units.

The initial conditions are set using the following stepwise function:

$$A(x, y, 0) = \begin{cases} A_0(1 + \xi\, N(x, y)), & (x, y) \le R_i, \\ 0, & (x, y) > R_i, \end{cases} \quad (9)$$

$$B(x, y, 0) = \begin{cases} 0, & (x, y) \le R_i, \\ B_0(1 + \xi\, N(x, y)), & (x, y) > R_i, \end{cases} \quad (10)$$

$$C(x, y, 0) = 0, \quad \forall (x, y), \quad (11)$$

where A_0 and B_0 are the initial concentration of species A and B, respectively. For simplicity, both values are always set equal to 1 mol/l. $N(x,y)$ is a normally distributed noise function of amplitude $\xi = 0.01$. For stability reasons, all simulations consider that both fluids are initially located inside the domain and make contact at a circular region with an initial radius $R_i = 0.5$ cm from the injection point [see Fig. S1(b) in the supplementary material]. The mesh size was chosen after performing a mesh independence study and the results are reported in the supplementary material (see Fig. S2).

The volumes of the three fluids are calculated by the following equations:

$$V_A = \frac{V_T}{A_0} \frac{\int\int_S A(x, y, t) dS}{\int\int_S dS}, \quad (12)$$

$$V_B = \frac{V_T}{B_0} \frac{\int\int_S B(x, y, t) dS}{\int\int_S dS}, \quad (13)$$

$$V_C = V_T - V_A - V_B, \quad (14)$$

where V_A, V_B, and V_C are the total volumes of the fluids A, B, and C inside the reactor, respectively, and depend on the concentrations A and B during the process. V_T is the total volume of the cell, which is a fixed value estimated with the total area of the cell times the gap,

$$V_T = \text{Area}_{\text{Cell}} \times h = 78.50\,\text{cm}^2 \times 0.025\,\text{cm} = 1.960\,\text{cm}^3. \quad (15)$$

Thus, initially (at t = 0 s), $V_C = 0$ cm^3 and $V_T = V_A + V_B$. Once the injection has started (t > 0 s), $V_C > 0$ cm^3 and $V_T = V_A + V_B + V_C$. The volumes of A and B were calculated as the average value of the normalized concentration fields over the entire computational domain (S), multiplied by the total volume of the cell.

The following protocol is used along the simulations. The circular medium is filled with fluid B with initial concentration B_0. The less viscous fluid A, with an initial concentration A_0, is placed into the system at the center of the cell forming an interface with an initial radius $R_i = 0.5$ cm (initial time t = 0 s). Then, fluid A begins to be injected with a rate Q_1. Fluid A pushes the more viscous fluid B and fingering occurs at the interface due to the chosen viscosities' configuration. The two reactants mix along the contact zone by diffusion and convection, giving rise to the product C after the reaction takes place. Once the interface has reached a given average radius r_{ring} (calculated as explained in the supplementary material), the injection is stopped for a given period of time (closing time, t_c). The purpose of this period is to allow chemical species to mix by diffusion and react freely until the total rate of C production becomes independent on time, which allows us to infer that at this point the interface is more stable, generating a type of well-defined ring at the central part of the interface with larger viscosity than fluid B, and, thus, capable of displacing it. The intention of this part of the process is to establish a well-defined initial configuration that it is almost independent on the history to reach it in order to start the final pumping stage. (This will become more evident below in the Results section.)

After the closing time t_c, the last part of the protocol begins and the fluid A starts to be injected again with a flow rate Q_2, displacing the product C and, in turn, the fluid C displaces the fluid B. The injection is stopped once the fluid C or fluid A reaches the outer limit of the cell.

The average radius of the interface, r_{ring}, is defined as the distance from the injection point to the mean location of the fingers (calculated averaging tips and bases for all the fingers) following Perkins and Hoffman (1965). Figure S3 in the supplementary material illustrates the method to calculate it.

We consider a standard case to compare with the rest of the simulations; the origin of this set of parameters will become apparent in Sec. III. This standard case is defined by the parameters $r_{ring} = 1$ cm, $t_c = 5000$ s, and $Q_2 = 1$ ml/min. From this base case, a parametric sweep study is carried out in order to improve the recovery of the displaced solution. The control parameters in our

USC UNIVERSIDADE DE SANTIAGO DE COMPOSTELA

Published under license by AIP Publishing.

simulation are the flow rate Q_2, the closing time t_c, and the interface radius r_{ring}. A statistical analysis is made with 20 repetitions of each simulated case. Results are presented as the average of these simulations with their standard deviations as an error bar.

The aim of these simulations is to optimize and increase the amount of displaced fluid to be recovered. For that, we define the recovery percentage of fluid B (%Rec) by

$$\%Rec = \left[1 - \left(\frac{V_{Bf}}{V_{Bi}}\right)\right] \times 100, \tag{16}$$

where V_{Bi} is the volume of fluid B at initial time t = 0 s ($V_{Bi} = 1.957$ cm^3 for all cases) and V_{Bf} is its volume at the end of the experiment. Note that the experiment is considered to finish once the fluid A or the reaction product C reaches the outer boundary of the cell.

III. RESULTS

The protocol proposed in this manuscript is divided in three different steps as it was mentioned above. First, an injection period (with a flow rate Q_1) is needed to establish the interface at some distance from the injection inlet. It is followed by a closing period. During this time, the system is allowed to rest and only diffusion helps create an interface where the reaction takes place. Finally, a second injection period is considered with a different flow rate Q_2.

The first injection period lasts till the average interface radius reaches $r_{ring} = 1$ cm (calculated as explained in the supplementary material). This process is done considering two scenarios: first, with a displacing fluid rate Q_1=1 ml/min (Péclet number $Pe = 1.06 \times 10^4$) for 3 s and, second, with a flow rate $Q_1 = 10$ ml/min ($Pe = 1.06 \times 10^5$) for 0.3 s. In both cases, the total amount of displacing fluid A injected into the reactor is the same; just the rate of injection is different and, thus, the Péclet number (defined as the ratio of the convection rate and the diffusion rate—Landau and Lifshitz, 1987; Petitjeans *et al.*, 1999; and Nagatsu and Ueda, 2001). Both cases ($Q_1 = 1$ ml/min and $Q_1 = 10$ ml/min) are simulated to determine the influence of the Péclet number on the interface development (ring) during the closing time. In both cases, the mixing A + B takes place by convection and, in a smaller proportion, by diffusion. The difference between the two cases lies in the level of instability generated at the interface, which is detected through the volume of product C (V_C) generated in each case. During this stage, low flow rates (lower Péclet number) allow the reaction for larger times and, thus, larger amounts of C are produced at the interface.

When the injection is closed, the Péclet number reaches the lowest value and the convective processes disappear. During the following closing period, the chemical reaction and product C generation continue to take place at the interface. The results of the simulations show that the conditions how the first injection period is carried out (rates and time of injection) do not strongly influence the development of the ring during the closing period, provided that the closing time (t_c) is long enough to disperse the instabilities. Figure 1(a) shows the generation of product C during the closing period in the two scenarios considered, $Q_1 = 1$ ml/min and $Q_1 = 10$ ml/min. At $t_c = 0$ s, different volumes of product C (V_C) can be noted due to the different instability levels in the two scenarios during the first injection period. Once injection is stopped, the rate of fluid C production becomes larger in the $Q_1 = 10$ ml/min case than the $Q_1 = 1$ ml/min one. This is due to the larger fingers at the interface in the more unstable case, $Q_1 = 10$ ml/min, which increases the contact area between the reactants A and B, promoting transversal diffusion and chemical reaction. Eventually, V_C becomes equal in both cases, independently on the initial injection protocol followed, given that the closing time is large enough. We consider a closing time $t_c = 5000$ s large enough to suppress the differences in the instability levels. All values of V_C shown integrate the total values of V_C observed at any location in the integration domain. Figure 1(b) shows the rate of production of C (V_C/t_C) vs closing time t_c [corresponding with the first temporal derivative of Fig. 1(a)]. The first observation here is that the behavior in both configurations becomes equivalent after some transient. Second, once this transient is reached (about 2500 s), the production of product C for both cases considered asymptotically approaches a constant value (not shown in the figure). Thus, for any given injection rate, Q_1, there is a corresponding closing time that allows us to reach the same configuration.

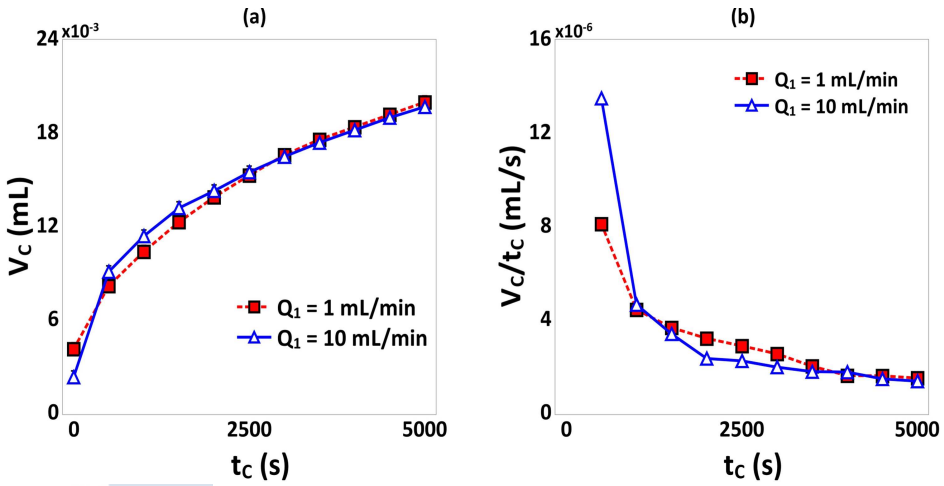


FIG. 1. Effect of the closing time (t_C). (a) Temporal evolution of product C generation, total volume on C produced (V_C) during the closing period and after the first injection period and (b) evolution of the rate of production of C or first temporal derivative of (a) (V_C/t_C) during the closing time. Two injection rates are considered, $Q_1 = 1$ ml/min and $Q_1 = 10$ ml/min during the first injection period. (Model parameters: $r_{ring} = 1$ cm, $R_C = 5$, $R_B = 2$, $D_A = D_B = D_C = 1 \times 10^{-9}$ m^2/s, and $k_1 = 10$ l/s mol).

USC UNIVERSIDADE DE SANTIAGO DE COMPOSTELA

Published under license by AIP Publishing.

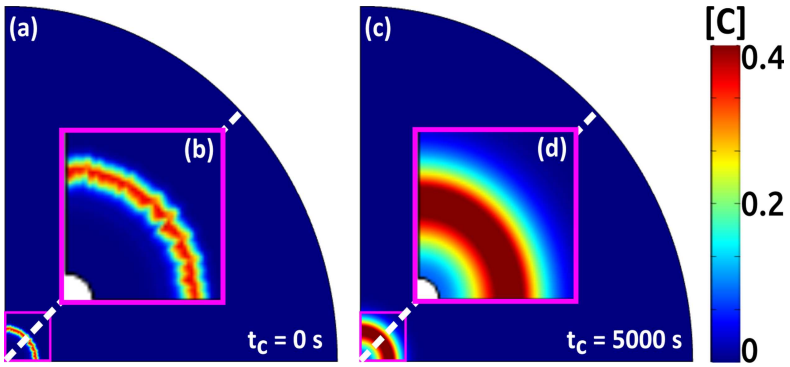


FIG. 2. Temporal evolution of the spatial distribution of the product C concentration (M) in the cell: (a) right after the first injection period and (c) at the end of the closing time. (b) and (d) show the details of the interfacial area zoomed out. Rest of the parameters: $r_{ring} = 1$ cm, $R_C = 5$, $R_B = 2$, $D_A = D_B = D_C = 1 \times 10^{-9}$ m^2/s, $k_1 = 10$ L/s·mol, and $Q_1 = 1$ ml/min, at (2a, 2b) $t_c = 0$ s and (2c, 2d) $t_c = 5000$ s.

According to this behavior, the closing time $t_C = 5000$ s would ensure approximately the same conditions for a wide variety of initial rates Q_1 at the end of the closing period. In this context, a rate of $Q_1 = 1$ ml/min is set for all the simulations for simplicity (as we already mentioned above when defining the base case, $Q_1 = 1$ ml/min, $r_{ring} = 1$ cm, and $t_c = 5000$ s).

Figure 2 displays the evolution of the concentration of product C during the closing period. Figure 2(a) corresponds with the initial situation, right after the first injection period (with an injection flow rate of $Q_1 = 1$ ml/min), and Fig. 2(c) the final configuration at $t_c = 5000$ s. Figures 2(b) and 2(d) show expanded views of the interface presented in Figs. 2(a) and 2(c), respectively, where the formation of a well-defined ring around $r_{ring} = 1$ cm is observed.

Note that during the closing time, the reactants continue mixing by diffusion and reacting. Volume of fluid C increases during this time across the interface making this product zone thicker and better defined as time goes on. That behavior is quantitatively observed in Fig. 3. Figures 3(a) and 3(b) show the evolution of the profiles for C in the first (first injection period) and second (closing period) stages of the protocol followed (the profiles are taken along the orange lines in Fig. 2). Here, the concentration of product C is plotted vs the radial distance. During the first injection period [Fig. 3(a)], the concentration of product C increases rapidly as the injection continues and the contact area between the reactants increases, promoting the chemical reaction between them. During the closing period [Fig. 3(b)], changes in the concentration take place at a slower pace than in Fig. 3(a) as the contact area remains in the same location approximately and species A and B in that area are being consumed. During the closing period, the profile of product C becomes wider but remains at the approximately same location [see Fig. 2(d)].

Figures 3(c) and 3(d) present the viscosity of the fluid C along the radial direction in the two stages considered (first injection time and closing period, respectively). Figure 3(c) shows the evolution of the viscosity profile that clearly marks the evolution of the interface where the reaction is taking place. Only in Fig. 3(d) the viscosity profile reaches its optimum configuration showing a wide enough ring with large viscosity. This ring will be used below to improve the displacement of fluid B.

After the closing period, the injection of fluid A is restarted at a fixed rate $Q_2 = 1$ ml/min during the so-called second injection period. The injection rate is kept constant until the end of the experiment when the product C reaches the outer boundary of the reactor. The end of the experiment is determined both by visual inspection [Fig. 4(a)] and analyzing the evolution of the C product production. A sudden drop in the production of C marks the exit of C product from the reactor [see Fig. 4(b)]. An additional set of figures showing the spatiotemporal evolution of the fingering pattern, the distribution of the fluid C concentrations, and the different viscosity profiles for this model are included in Fig. S4 of the supplementary material. The case shown in these figures will be used as a reference to compare all other configurations considered along the manuscript and we label it as the base case or standard case.

Figure 5(a) shows, for the standard case, the evolution of the percentage of recovery with time. The blue continuous line with triangles shows the variation of the percentage of recovery for the non-reactive case (same conditions as in the reactive case but $k_1 = 0$). It is clear that the reactive case (dashed line) improves the percentage of recovery and facilitates the displacement of the more viscous solution. In order to compare both experiments, the time has been normalized by the time to finish the experiment or time at which the displacing solution (fluid A) or C product (interface) reaches the outer boundary as discussed previously. Figure 5(b) shows the fingering patterns for the non-reactive case for comparison with the reactive standard case shown in Fig. 4(a).

It is clear from the previous results that the effect of a highly viscous interface produced by a reaction between the displacing and displaced fluids enhances the displacement mechanism. In the following, we analyze the effect of the different parameters in the model in order to optimize the percentage of recovery of the displacing fluid.

A. Flow rate Q_2—second injection period

The Péclet number describes the ratio between convection rates over diffusion rates. It is well-known that large Péclet numbers are more prone to destabilize the interface. Diffusion coefficients are not likely to be changed under experimental conditions; thus, the only parameter controlling the Péclet number is the injection velocity. Figure 6 shows the effect of varying the second injection flow rate, Q_2. Two cases are considered: $Q_2 = 10$ ml/min [triangles in Fig. 6(a)] and $Q_2 = 0.5$ ml/min [open circles in Fig. 6(a)], and the results are compared with the standard case with $Q_2 = 1$ ml/min [full squares in Fig. 6(a)]. In Fig. 6(a), we present the percentage

USC UNIVERSIDADE DE SANTIAGO DE COMPOSTELA

Published under license by AIP Publishing.

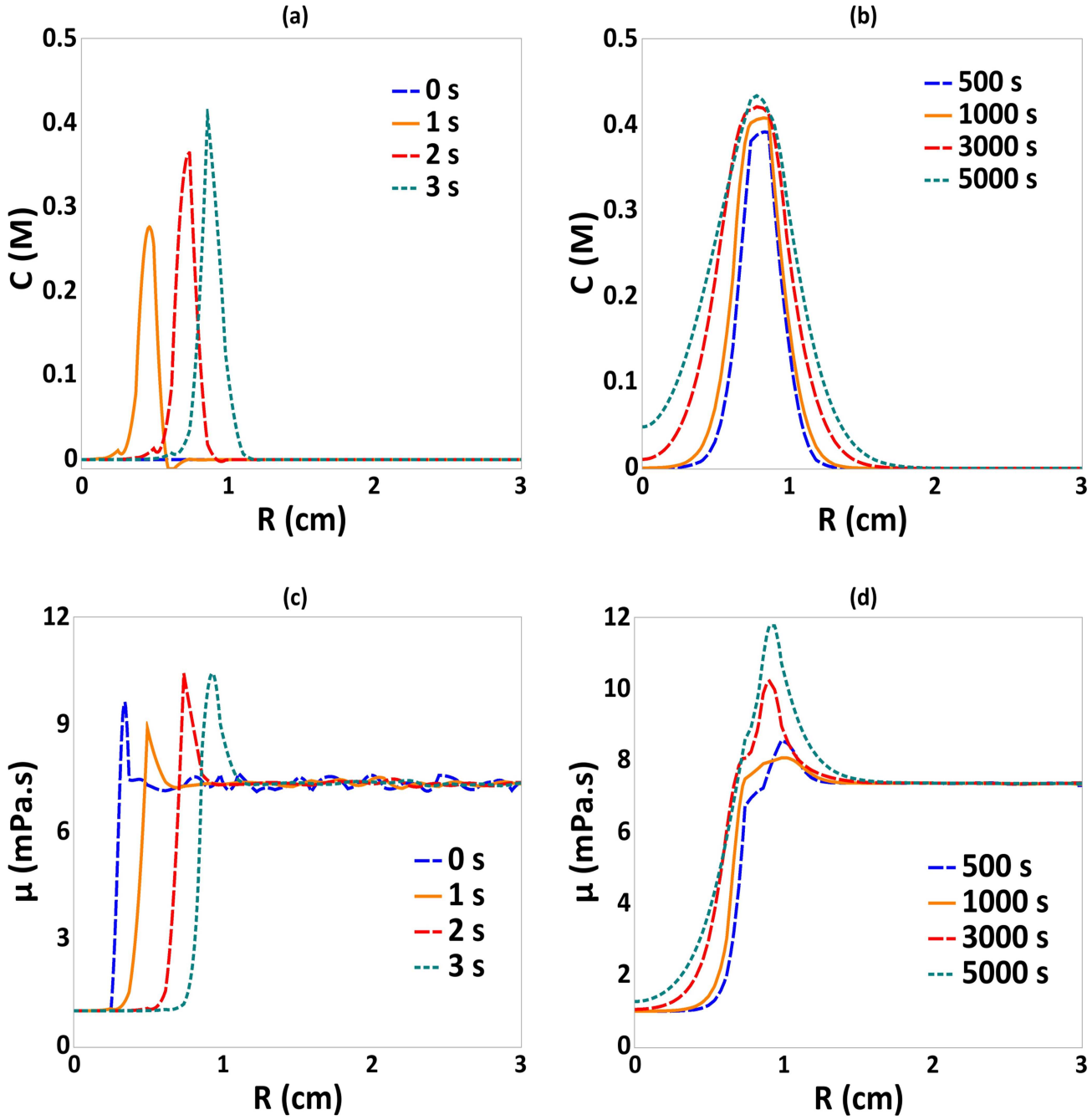


FIG. 3. Radial profile of product C during (a) the first period of injection and (b) the closing time period. The radial viscosity, μ (Pa s) profiles are shown in (c) during the first period of injection and (d) during the closing period. In all figures, the profiles are shown for different moments of time and are taken along the orange line in Fig. 2. Model parameters: $r_{ring} = 1$ cm, $R_C = 5$, $R_B = 2$, $D_A = D_B = D_C = 1 \times 10^{-9}$ m^2/s, $k_1 = 10$ L/s mol, and $Q_1 = 1$ ml/min.

of recovered fluid B vs time for the three cases considered. Time is rescaled by the final experimental time that it is given by the time the fluid A or compound C reaches the outer boundary. The reduction of the efficiency for $Q_2 = 10$ ml/min is around 4% comparing with the standard case ($Q_2 = 1$ ml/min). For $Q_2 = 0.5$ ml/min, the variation of the efficiency is non-existent at the end of each experiment. Figure 6(b) shows the fingering patterns for the rate $Q_2 = 10$ ml/min at the end of the experiment.

USC UNIVERSIDADE DE SANTIAGO DE COMPOSTELA

Published under license by AIP Publishing.

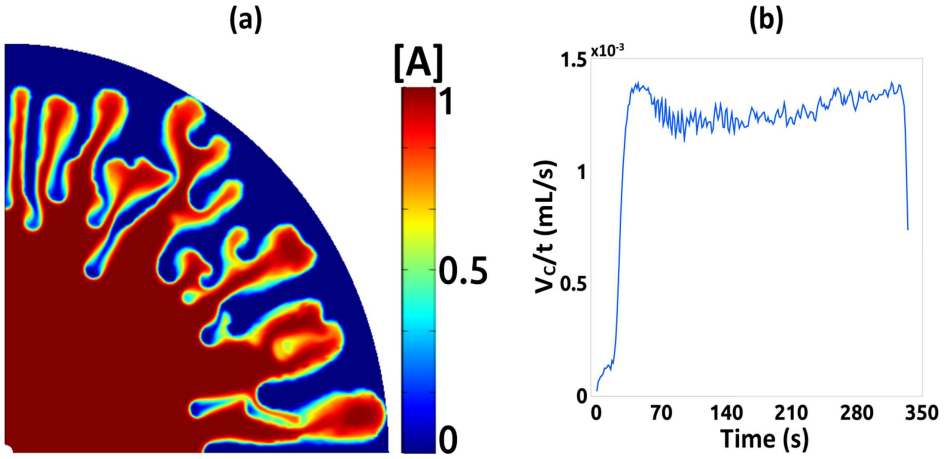


FIG. 4. (a) Final viscous fingering patterns observed at the end of the simulation of the second injection period (when the fluid A or product C reaches the outer boundary at $t = 336$ s) for the base case. Color-coded is the concentration (in M) of the displacing fluid A in the reactor. (b) Temporal evolution of the production of the product C (V_C/t_C) during the second injection period for the base case (model parameters: $r_{ring} = 1$ cm, $t_c = 5000$ s, $R_C = 5$, $R_B = 2$, $D_A = D_B = D_C = 1 \times 10^{-9}$ m^2/s, $k_1 = 10$ L/s mol, $Q_1 = 1$ ml/min, and $Q_2 = 1$ ml/min)

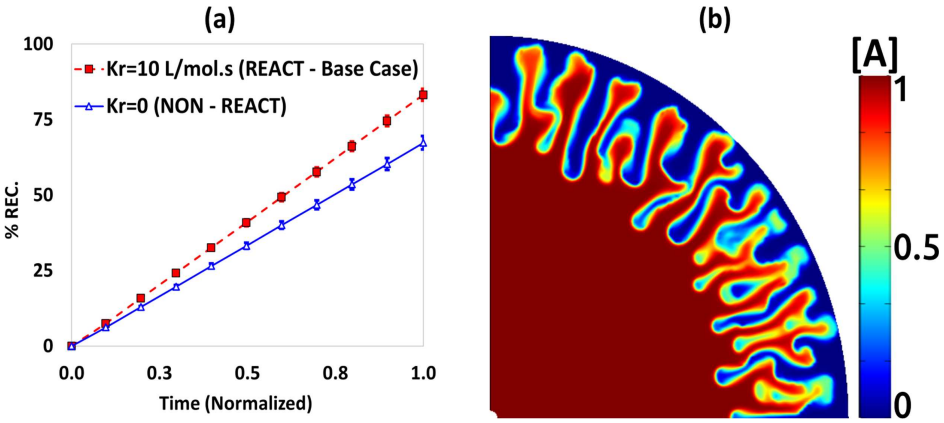


FIG. 5. (a) Temporal evolution of the percentage of recovery (%REC) as a function of the normalized time for the reactive (base case) and non-reactive cases. (b) Viscous fingering patterns of fluid A concentration (M) for the non-reactive system at breakthrough time (model parameters: $R_C = 5$, $R_B = 2$, $D_A = D_B = D_C = 1 \times 10^{-9}$ m^2/s, $Q_1 = 1$ ml/min, and $Q_2 = 1$ ml/min).

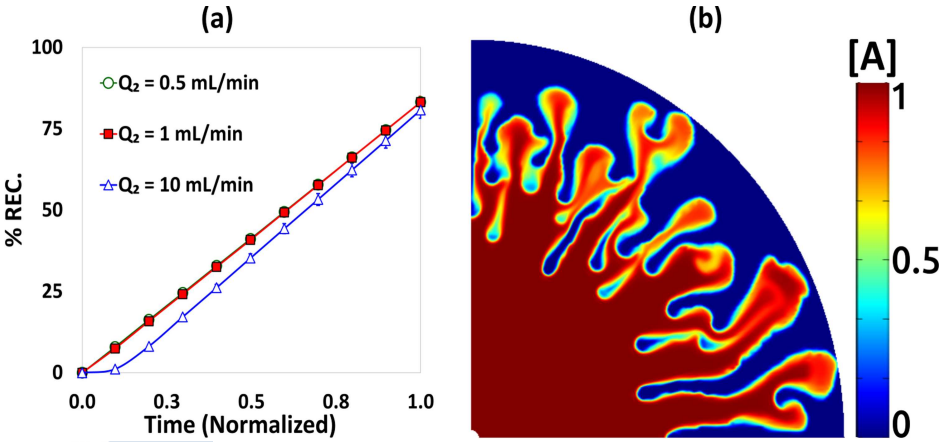


FIG. 6. (a) Temporal evolution of the percentage of recovery (%REC) during the whole process for different values of the second injection rate (Q_2). (b) Viscous fingering pattern of fluid A at the end of the experiment ($t = 31.8$ s), the injection rate was $Q_2 = 10$ ml/min (model parameters for both figures: $r_{ring} = 1$ cm, $t_c = 5000$ s, $R_C = 5$, $R_B = 2$, $D_A = D_B = D_C = 1 \times 10^{-9}$ m^2/s, $k_1 = 10$ L/s mol, and $Q_1 = 1$ ml/min).

USC UNIVERSIDADE DE SANTIAGO DE COMPOSTELA

Published under license by AIP Publishing.

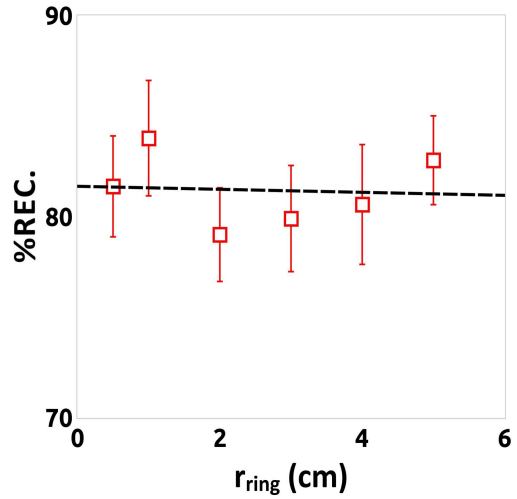


FIG. 7. Percentage of displaced fluid, B recovered (%REC) vs the initial average radius of the interfacial ring (r_{ring}) (model parameters: $t_c = 5000$ s, $R_C = 5$, $R_B = 2$, $D_A = D_B = D_C = 1 \times 10^{-9}$ m^2/s, $k_1 = 10$ L/s mol, $Q_1 = 1$ ml/min, and $Q_2 = 1$ ml/min).

B. Ring radius (r_{ring})

In this subsection, we check the role played, if it exists, by the initial location of the interface at the end of the second injection period. This is the role of the average radius of the interface area r_{ring} at the end of the first injection period. The position where the well-defined interfacial ring will be formed during the closing period is controlled by the injected volume of the displacing fluid, A, during the first injection period. The final recovery or percentage of displaced fluid recovered is plotted vs the radius of the interfacial ring r_{ring} in Fig. 7. Note that the efficiency of the process remains almost unchanged independently on the value of r_{ring}.

C. Closing time (t_c)

Closing time, t_c, is the period of time between the two injection periods; the flow rate is zero and, thus, no solution A is pumped into the cell. This parameter helps improve the efficiency of the process. In fact, this time becomes more important as the contact area between the two fluids (A and B) becomes larger, something that it is controlled by the initial interfacial radius r_{ring}. The larger r_{ring}, the larger the contact area between both fluids is. Note that a smaller value of r_{ring} makes the interfacial region to stabilize in a relatively short time, while larger values of r_{ring} make the mixing zone larger, and more time is needed to fully develop this interfacial ring. The response of the recovery as a combined function of these two parameters (t_c and r_{ring}) is shown in Fig. 8(a). Here, we observe a general tendency to slightly increase the recovery with larger values of t_c and r_{ring}. At $r_{ring} = 1$ cm, the closing time does not have much impact; however, its influence starts to be noticed from $r_{ring} = 3$ cm improving the sweep efficiency when t_c is increased. The straight dashed horizontal line in the graph ($t_c = 0$ s) represents the process when there is no closing time (the protocol only has one continuous period of injection), that means that no well-formed ring is created during the displacement. That line gives a good reference when choosing the closing period as well as the total volume of fluid A injected (that determines the initial value of r_{ring}). Figure 8(b) displays an example of the fingering patterns observed for $r_{ring} = 5$ cm and $t_c = 20\,000$ s. Note that the wavelength and characteristics of the fingers are completely different from those in the previous simulations [see Figs. 4(a), 5(b), and 6(b)]; this differentiated morphology improves the efficiency of the recovery method. The spatiotemporal evolution of this displacement, the profile of the product C concentrations, and viscosities for this case ($r_{ring} = 5$ cm and $t_c = 20\,000$ s) are presented in Fig. S5 in the supplementary material.

D. Mobility ratio (R_C)

The model parameter R_C or log mobility ratio describes the logarithm of the ratio between the viscosity of the product C and that of the displacing fluid A, $R_C = \ln(\mu_C/\mu_A)$. In the previous results reported along this manuscript, its value was kept equal to $R_C = 5$; thus, the viscosity ratio between the product C and the displacing fluid A (μ_C/μ_A) is 148:1. There are several ways to control this parameter experimentally. It can be considered that the viscosity of the displaced solution, B, cannot be altered and that the displacing solution is given by the problem itself (typically water with some

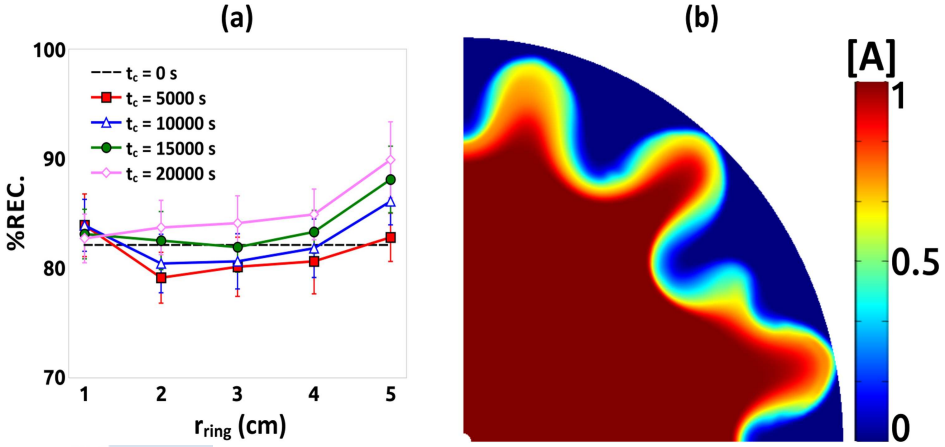


FIG. 8. (a) Variation of the percentage of fluid B recovery (%REC) as a function of the initial average interfacial ring radius, r_{ring}, and the closing time, t_c. (b) Viscous fingering patterns of fluid A (in M) for an initial interfacial radius $r_{ring} = 5$ cm and a closing time $t_c = 20\,000$ s at the end of the experiment ($t = 220$ s) (model parameters for both figures: $R_C = 5$, $R_B = 2$, $D_A = D_B = D_C = 1 \times 10^{-9}$ m^2/s, $k_1 = 10$ L/s mol, $Q_1 = 1$ ml/min, and $Q_2 = 1$ ml/min).

USC UNIVERSIDADE DE SANTIAGO DE COMPOSTELA

Published under license by AIP Publishing.

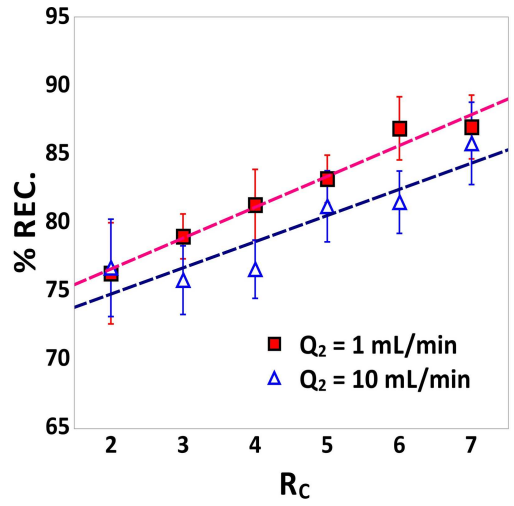


FIG. 9. Percentage of the displaced solution recovered (%REC) vs the log mobility ratio (R_C) at the end of each experiment for two different values of the injection flow rate $Q_2 = 10$ ml/min (blue line) and $Q_2 = 1$ ml/min (red line in the figure). R_C is basically controlled by the viscosity of the product C (model parameters: $r_{ring} = 1$ cm, $t_c = 5000$ s, R_C and Q_2, for $R_B = 2$, $D_A = D_B = D_C = 1 \times 10^{-9}$ m^2/s, $k_1 = 10$ L/s mol, and $Q_1 = 1$ ml/min).

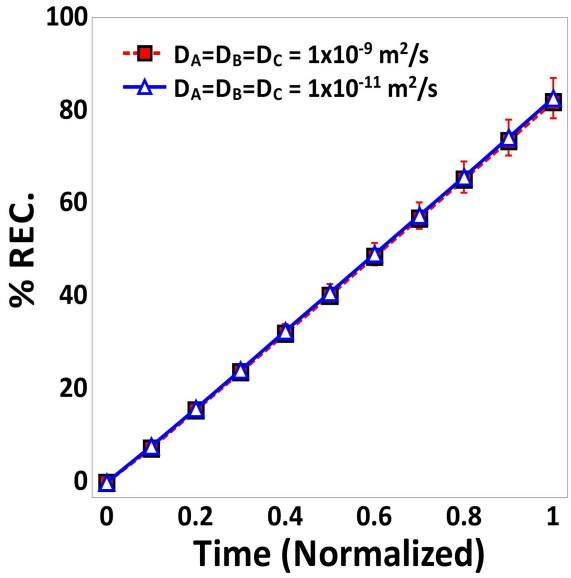


FIG. 10. Temporal evolution of the percentage of displaced fluid recovery as a function of the diffusion coefficients $D_A = D_B = D_C$, for two cases $D_A = D_B = D_C = 1 \times 10^{-9}$ m^2/s (aqueous solutions marked with triangles) and $D_A = D_B = D_C = 1 \times 10^{-11}$ m^2/s (polymeric solutions marked with squares) (rest of the parameters: $r_{ring} = 1$ cm, $t_c = 5000$ s, $R_B = 2$, $R_C = 5$, $k_1 = 10$ L/s mol, Q_1 and $Q_2 = 1$ ml/min).

substances in the solution). But the viscosity of the product C can be changed depending on the reaction that it is considered to happen at the interface area between solutions A and B.

Figure 9 presents the percentage of the total recovery at the end of each experiment as a function of the viscosity of the interfacial product for two different values of the second injection period flow rate, $Q_2 = 10$ ml/min (blue line) and $Q_2 = 1$ ml/min (red line in the figure). In general, increasing the viscosity of the product C significantly improves the percentage of the displaced solution recovered.

Comparing the two curves in Fig. 9 for the different values of Q_2, one can note that increasing the flow rate does not improve the efficiency of the method as the system becomes more unstable and, thus, more difficult to control.

E. Diffusion coefficients (D_C)

The other mechanism playing a role in the method developed here is the diffusion as it is the responsible of the mixing of the two solutions. We have considered two aqueous solutions with relatively high diffusion coefficients so that they can easily mix. Reducing the diffusion coefficients D_A, D_B, and D_C is equivalent to increase the Péclet number; mass transport will then depend more on the convective mechanism rather than in the diffusion, and this should be reflected at the interface that will turn more unstable producing thinner fingers.

So far, the present approach has been focused on the behavior of aqueous solutions, with relatively high diffusion coefficients, where the mixture among the chemical species can occur without much difficulty. When the diffusion coefficients D_A, D_B, and D_C are reduced to similar values as those for polymers (around 1×10^{-11} m^2/s) and keeping the same values for Q_1 and Q_2, the total effect results in an increase of the Péclet number, mass transport will depend more on the convection mechanism than on the diffusion, and this should be reflected at the interface that will turn more unstable with thinner fingers.

Figure 10 presents the evolution of the percentage of recovery for two different sets of values for the diffusion coefficients; D_A, D_B, and $D_C = 1 \times 10^{-9}$ m^2/s (squares in the figure) and D_A, D_B, and $D_C = 1 \times 10^{-11}$ m^2/s (triangles in the figure). The latest values correspond with those of a polymeric solution. Note that both curves coincide independently on whether the solutions are purely aqueous or polymeric. In order to understand this behavior, we need to note the rest of the parameters used in our design. In particular, the large value of the Damköhler number demonstrates that the characteristic chemical reaction times are much larger than the diffusive mass transport and this allows us to keep the displacement mechanism, overlapping the expected convection effects.

F. Energy consumption

An interesting parameter to analyze, specifically considering industrial applications, is the energy needed to complete each of the processes considered. In the system we are working with, the inflow is kept constant at the expense of maintaining the appropriate pressure at the injection location. Thus, the energy used is going to be related with the summation of all the pressure values at the injection site. In general, the energy of the process is estimated by

USC UNIVERSIDADE DE SANTIAGO DE COMPOSTELA

Published under license by AIP Publishing.

$$E = \int_{t=0}^{t_f} P_0(t) \cdot Q(t) \cdot dt, \tag{17}$$

where $P_0(t)$ is a variable that contains all the successive values of the pressure at the entrance of the reactor along the experiment that are directly being calculated by the program used for simulations. $Q(t)$ is the injection rate. For simplicity, we consider in the following only the energy consumption during the latest stage of the protocol (second injection period). Note that the energy consumed during the two previous stages (first injection period and closing period) is constant for all the cases considered in this subsection.

Figure 11 presents the results calculated for the simulations presented above. Figure 11(a) shows the variation of the pressure at the injection location vs time for several values of the log mobility ratio (R_C) that in our case is controlled by the viscosity of the product C. As expected, the level of pressure at the origin is much larger during the first moments of injection and monotonically decreases to much lower values in all the cases considered. The values presented are averages over 20 simulations as explained in the Methods section. Figure 11(b) uses the values of Fig. 11(a) to calculate the energy consumed to keep working the experiment vs time. The total energy consumed in each simulation is plotted in Fig. 11(c) for the six values of R_C considered. Note that as the viscosity of C is increased (R_C is increased) the consumption of energy is also increased. Rising the viscosity of C from $R_C = 2$ up to $R_C = 7$ implies a total increment of the consumption of energy of 30%. These results agree with those presented in Fig. 9 where the efficiency of the method is plotted for several values of R_C. Also, as it is expected, greater efforts to displace a more viscous interface will require larger energy consumption.

IV. CONCLUSIONS

Displacing highly viscous solutions by injecting a less viscous fluid is a complicated problem that has been approached from different perspectives along the time as it is a key mechanism for many industrial applications. In this manuscript, we exploit the possibilities of introducing an interfacial reaction that locally rises the viscosity improving the total volume of the viscous solution displaced. In fact, experimental evidence pointed to this possibility (Fernandez and Homsy, 2003; Nagatsu *et al.*, 2007; 2009; 2011; and Escala and Munuzuri, 2021). Here, we consider a simple kinetic reaction and we couple it with the corresponding Navier–Stokes equations to produce a realistic mathematical model of the phenomenon. The reaction only takes place at the interface of the two colliding fluids, the diffusion mechanism allows some mixing of both fluids and, as a result, an interface is generated where the reaction can take place and produce the substance C that, by construction, has a larger viscosity than the two previous solutions. This methodology results in displacing the more viscous fluid with a recovery percentage larger than in the non-reactive situation.

Along this manuscript we investigated the role played by all the critical parameters trying to optimize the efficiency of the process. The protocol developed consists of three steps. A first injection period where the less viscous fluid is injected into the reactor previously filled with the B fluid. The second step is a period of time characterized by a zero-injection flow rate. The last step is another injection period with a different flow rate. We first focused our research on the morphology of the initial interface before the second injection period. In order to optimize the efficiency, we noted that for this topology, the value of the initial average interfacial ring as well as the duration of the closing period was critical. Larger initial interfacial radius as well as larger closing periods allowed the formation of a thick stable highly viscous interfacial ring that optimizes the efficiency of the method. Not only the ring size nor the closing time but also the level of instability due to the first injection period should be considered. Larger injection rates during the first period (Q_1) induce a more intense instability at the interface (larger number of finger tips at the interface and the increased contact area between both fluids) and thus may require longer closing times in order to smooth it. This means that the first injection period can usually be compensated by the appropriate closing time that helps

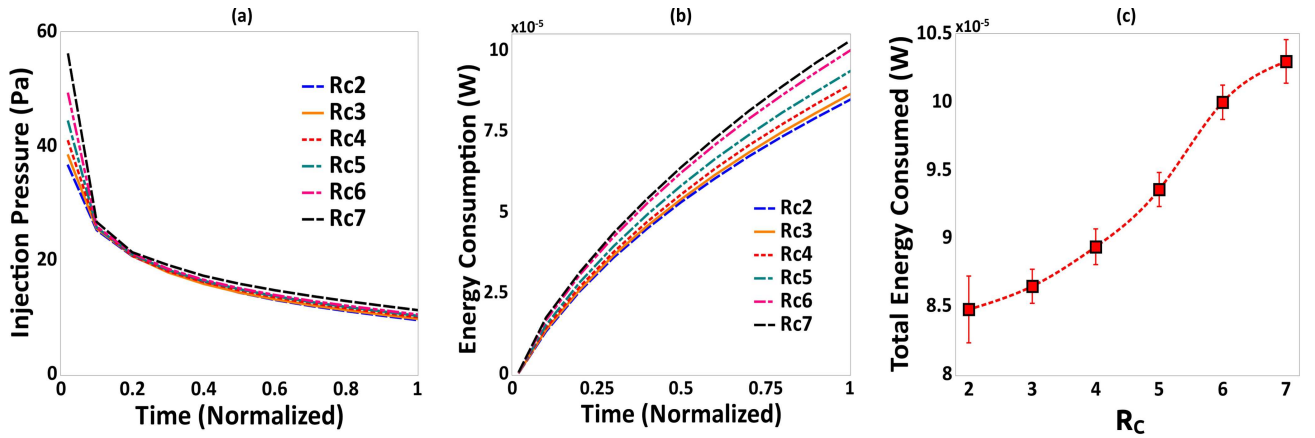


FIG. 11. Energy consumption. (a) Variation of the pressure at the injection location vs time till the end of the experiment for several values of the log mobility ratio (R_C). (b) Variation of the energy spent to keep the experiment going vs time for the same values of R_C. (c) Total energy required per experiment vs R_C (dashed line is just a guide for the eyes) (model parameters: $r_{ring} = 1$ cm, $t_c = 5000$ s, $R_B = 2$, $k_1 = 10$ l/s mol, $D_A = D_B = D_C = 1 \times 10^{-9}$ m^2/s, Q_1 and $Q_2 = 1$ ml/min).

USC UNIVERSIDADE DE SANTIAGO DE COMPOSTELA

Published under license by AIP Publishing.

produce a robust stable interfacial ring. The conditions considered in our simulations tended to suppress all these effects so that the second injection period always started with a well-defined highly viscous ring.

The rest of the parameters considered in the manuscript are the viscosity of the product C solution, the second injection rate (Q_2), and the diffusion coefficients of the fluids involved. Just the viscosity of C reported a strong influence on the efficiency of the method. The two other parameters, the second injection rate (Q_2) and the diffusion coefficients, only introduced small variations in the efficiency. When the viscosity ratio of the ring, given by the mobility R_C, decreases (its viscosity decreases regarding to the displacing fluid), its sweeping properties decrease noticeably. On the other hand, when this viscosity ratio increases, the efficiency of the method increases.

The results presented here show that this methodology has a very promising potential in order to significantly improve the efficiency of the interfacial reaction-based recovery methods. In fact, all the relevant parameters have been analyzed and the efficiency optimized. This mathematical result opens the possibility to experimentally exploit in depth the method with the perspective of industrial applications.

SUPPLEMENTARY MATERIAL

See the supplementary material for details on the accuracy of the numerical method used for simulations.

ACKNOWLEDGMENTS

We gratefully acknowledge financial support by the Spanish Ministerio de Economía y Competitividad and European Regional Development Fund under Contract No. RTI2018-097063-B-I00 AEI/FEDER, UE, and by Xunta de Galicia under Research Grant No. 2018-PG082. The authors are part of the CRETUS Strategic Partnership (No. AGRUP2015/02). All these programs are co-funded by FEDER (UE).

The authors report no conflict of interest.

APPENDIX: SIMULATION PARAMETERS

Table I presents a list of all the parameters that are kept constant along all the simulations presented in the manuscript.

TABLE I. Parameters used during the simulations.

Parameter	Value	Unit
Reaction rate constant (k_1)	10	l/s mol
Viscosity fluid A (μ_a)	1	mPa s
Density fluids A, B, C (Rho)	1000	kg/m^3
Initial concentration fluid A (A_0)	1	M
Initial concentration fluid B (B_0)	1	M
Initial concentration fluid C (C_0)	0	M
Molar mass fluids A, B, C	0.032	kg/mol
System temperature	293.15	K

DATA AVAILABILITY

The data that support the findings of this study are available from the corresponding author upon reasonable request.

REFERENCES

ANSYS, Inc., ANSYS Fluent User's Guide, Release 20.1 (2020).
Araktingi, U. and Orr, F., "Viscous fingering in heterogeneous porous media," SPE Adv. Technol. Series **1**(I), 71–80 (1993).
Benham, A. and Olson, R., "A model study of viscous fingering," Soc. Pet. Eng. J. **3**, 136–144 (1963).
Blunt, M. and Christie, M., "Theory of viscous fingering in two phase, three component flow," SPE Adv. Technol. Ser. **2**(2), 22613 (1994).
Blunt, M. J., Barker, J. W., Rubin, B., Mansfield, M., Culverwell, I. D., and Christie, M. A., "Predictive theory for viscous fingering in compositional displacement," SPE Reservoir Eng. **9**, 73–80 (1994).
Brau, F., Schuszter, G., and De Wit, A., "Flow control of A + B → C fronts by radial injection," Phys. Rev. Lett. **118**, 134101 (2017).
De Wit, A., *Fingering of Chemical Fronts* (Université Libre de Bruxelles, 2003).
De Wit, A., "Chemo-hydrodynamic patterns in porous media," Philos. Trans. R. Soc. A **374**, 20150419 (2016).
De Wit, A., "Chemo-hydrodynamic patterns and instabilities," Annu. Rev. Fluid Mech. **52**, 531–555 (2020).
Escala, D. M., De Wit, A., Carballido-Landeira, J., and Muñuzuri, A. P., "Viscous fingering induced by a pH-sensitive clock reaction," Langmuir **35**, 4182–4188 (2019).
Escala, D. M. and Muñuzuri, A. P., "Constructing or deconstructing a fluid instability: A bottom-up approach" Sci. Rep. (submitted) (2021).
Fernandez, J. and Homsy, G. M., "Viscous fingering with chemical reaction: Effect of in-situ production of surfactants," J. Fluid Mech. **480**, 267–281 (2003).
Gérard, T. and De Wit, A., "Miscible viscous fingering induced by a simple A+ B→ C chemical reaction," Phys. Rev. E **79**(1), 016308 (2009).
Homsy, G., "Viscous fingering in porous media," Annu. Rev. Fluid Mech. **19**, 271–311 (1987).
Kovacs, K., McIlwaine, R., Gannon, K., Taylor, A. F., and Scott, S. K., "Complex behavior in the formaldehyde-sulfite reaction," J. Phys. Chem. A **109**, 283–288 (2005).
Landau, L. D. and Lifshitz, E. M., *Fluid Mechanics. Course of Theoretical Physics*, 2nd ed. (Pergamon Press, 1987), Vol. 6.
Li, J. and Rivière, B., "Numerical modeling of miscible viscous fingering instabilities by high-order methods," Transp. Porous Media **113**, 607–628 (2016).
Mishra, M., Trevelyan, P. M. J., Almarcha, C., and De Wit, A., "Influence of double diffusive effects on miscible viscous fingering," Phys. Rev. Lett **105**, 204501 (2010).
Nagatsu, Y. and Ueda, T., "Effects of reactant concentrations on reactive miscible viscous fingering, Fluid mechanics and transport phenomena," AIChE J. **47**(8), 1711–1720 (2001).
Nagatsu, Y., Matsuda, K., Kato, Y., and Tada, Y., "Experimental study on miscible viscous fingering involving viscosity changes induced by variations in chemical species concentrations due to chemical reactions," J. Fluid Mech. **571**, 475–493 (2007).
Nagatsu, Y., Kondo, Y., Kato, Y., and Tada, Y., "Effects of moderate Damköhler number on miscible viscous fingering involving viscosity decrease due to a chemical reaction," J. Fluid Mech. **625**, 97–124 (2009).
Nagatsu, Y., Iguchi, C., Matsuda, K., Kato, Y., and Tada, Y., "Miscible viscous fingering involving viscosity changes of the displacing fluid by chemical reactions," J. Phys. Fluids **22**, 024101 (2010).
Nagatsu, Y., Kondo, Y., Kato, Y., and Tada, Y., "Miscible viscous fingering involving viscosity increase by a chemical reaction with moderate Damköhler number," J. Phys. Fluids **23**, 014109 (2011).
Perkins, T. and Hoffman, R., "Mechanics of viscous fingering in miscible systems," Soc. Pet. Eng. **5**, 301 (1965).

USC UNIVERSIDADE DE SANTIAGO DE COMPOSTELA

Published under license by AIP Publishing.

Peters, E. J. and Cavalero, S. R., "The fractal nature of viscous fingering in porous media," in *Annual Technical Conference and Exhibition of the Society of Petroleum Engineers* (SPE, 1990), pp. 225–230.

Petitjeans, P., Chen, C., Meiburg, E., and Maxworthy, T., "Miscible quarter five-spot displacements in a Hele-Shaw cell and the role of flow-induced dispersion," Phys. Fluids **11**(7), 1705 (1999).

Saffman, P. G. and Taylor, G. I., "The penetration of a fluid into a porous medium or Hele-Shaw cell containing a more viscous liquid," Proc. R. Soc. London A **245**, 312 (1958).

Saffman, P. G., "Viscous fingering in Hele-Shaw cells," J. Fluid Mech. **173**, 73 (1986).

Sharma, J., Inwood, S. B., and Kovscek, A. R., "Experiments and analysis of multi-scale viscous fingering during forced imbibition," in *Society of Petroleum Engineers. Annual Technical Conference and Exhibition* (SPE, 2011), p. 143946.

Vishnudas, R. and Chaudhuri, A., "A comprehensive numerical study of immiscible and miscible viscous fingers during chemical enhanced oil recovery," Fuel **194**, 480–490 (2017).

Wooding, R., "Growth of fingers at an unstable diffusing interface in a porous medium or Hele-Shaw cell," J. Fluid Mech. **39**(3), 477–495 (1969).

USC UNIVERSIDADE DE SANTIAGO DE COMPOSTELA

Published under license by AIP Publishing.

Supporting Information for Publication (SI)

Highly viscous fluid displaced by a chemically controlled reactive interface

Néstor Tafur[1], Darío M. Escala[1], Ana Soto[2] and Alberto P. Muñuzuri[1,a)]

[1] Institute CRETUS. Group of Nonlinear Physics. Dept. of Physics. Universidade de Santiago de Compostela. 15782 Santiago de Compostela, Spain

[2] Institute CRETUS. Group EQUIFASE. Dept. of Chemical Engineering. Universidade de Santiago de Compostela. 15782 Santiago de Compostela, Spain

[a)] Author to whom correspondence should be addressed: alberto.perez.munuzuri@usc.es

1. Meshing

The numerical domain consists of a quarter of circle of radius R = 10 cm discretized using a mapped mesh of radial elements (see Fig. S1a). The displacing solution enters the domain through a velocity inlet located at the inner circle of radius r = 2 mm. The velocity is calculated from the flow rate Q as indicated in the manuscript. A pressure outlet is set as the outflow boundary condition. The remaining boundaries are set as symmetry conditions. Both fluids are initially located inside the domain and make contact in the circular region of radius R_i = 0.5 cm (Fig. S1b).

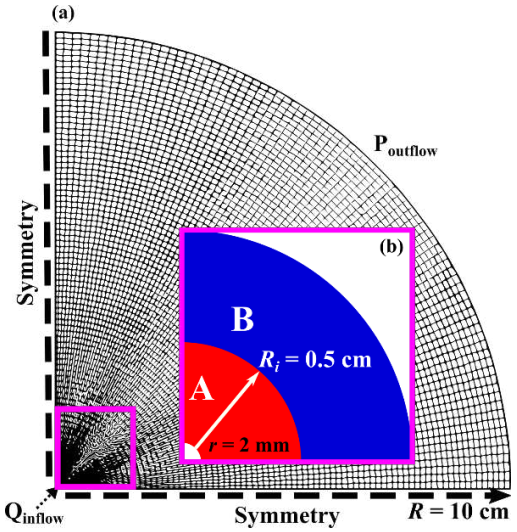


FIG. S1. (a) Schematic of the simulation domain. (b) Detailed diagram of the Initial condition configuration.

USC UNIVERSIDADE DE SANTIAGO DE COMPOSTELA

2. Mesh Independence Study

The system is simulated making use of a radial mesh to model the radial displacement. The study of mesh resolution sensitivity has been carried out to identify the optimal grid resolution which must show the independence of the final recovery with the cells' size, and also should have a good balance with the computational time. The mesh resolution with 6400 number of elements was selected for the present research. The optimal mesh resolution for this model was defined through a parameterization of the number of elements, from a grid of 100 to 10000 number of elements. The control property for that parameterization was the recovery percentage of fluid B as a function of the mesh resolution. For each grid resolution, three simulations were run with three different seeds. The difference among these three results is lower than 5%. The Fig. S2 presents the average of the three final recoveries per resolution.

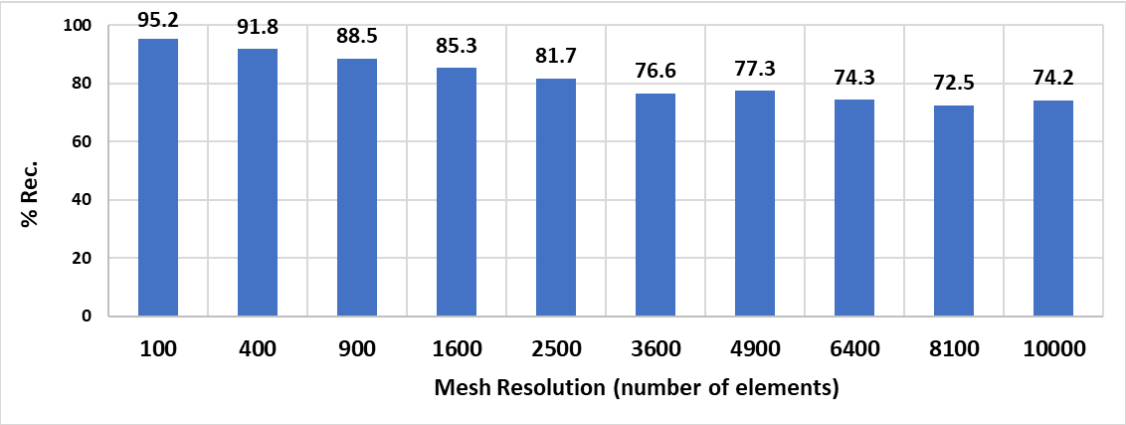


FIG. S2. Final recovery response as a function of the mesh resolution

3. Average Radius of the Ring (r_{ring})

The average radius of the ring (r_{ring}) is a parameter used to characterize the location of the large viscosity interfacial ring as it was introduced in Section II of the main manuscript. A simple method to estimate it was introduced by Perkins and Hoffman (1965) while calculating the length of the finger region. The method consists in determining all the locations of the bases and tips of the fingers and, thus, naming r_{base} as the average distance to the center from all the finger bases and r_{tips} as the average distance to the center from all the finger tips. Since the process is simulated as a miscible system, the threshold to define the limits of the tips and the bases of the fingers is set at 0.8 M of fluid A concentration. The magnitude r_{ring} is given by

$$r_{ring} = \frac{r_{base} + r_{tips}}{2}$$

USC UNIVERSIDADE DE SANTIAGO DE COMPOSTELA

and provides an estimate of the location if the interfacial ring. Fig. S3.1 exemplifies the method to calculate this magnitude for a particular simulation.

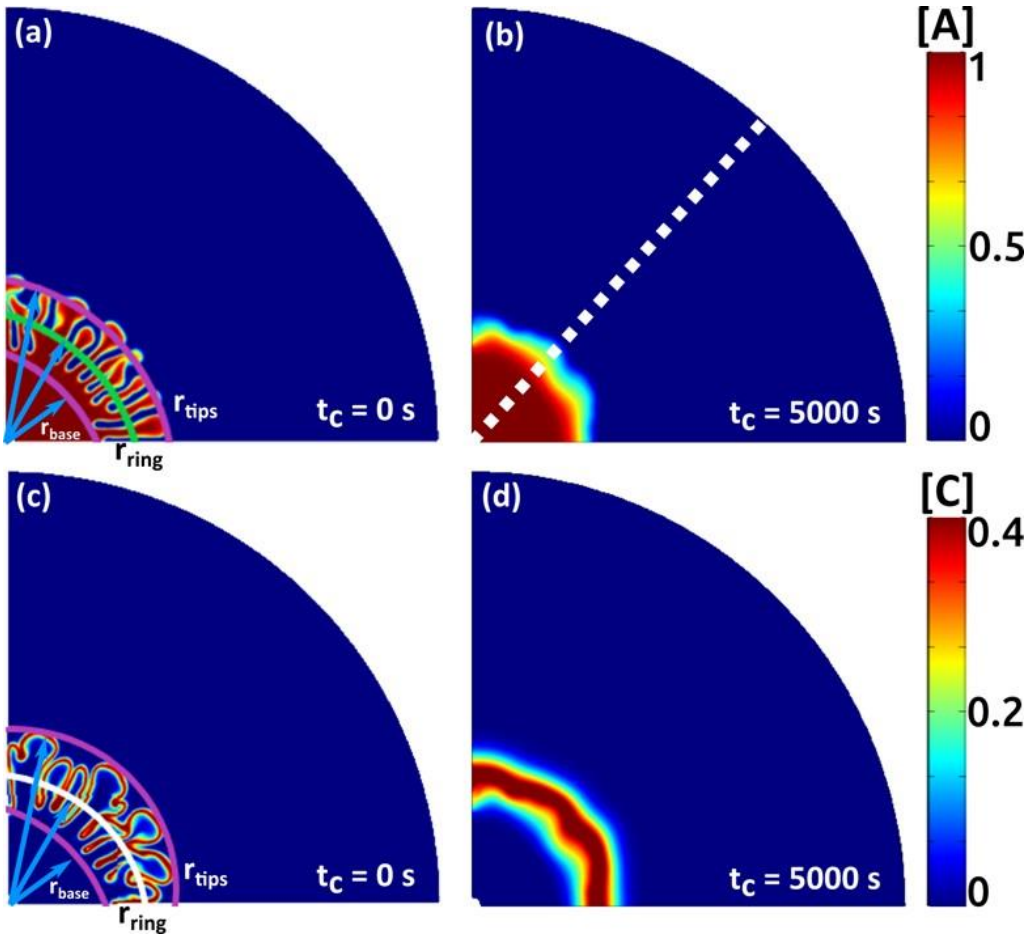


FIG. S3. Definition of the magnitude r_{ring} for a particular simulation. r_{base} is the average distance to the center from all the finger bases and r_{tips} is the average distance to the center from all the finger tips. The magnitude r_{ring} is given by the average of these two magnitudes and approximately provides the radial location of the interfacial ring. The upper row shows the values of concentrations for the fluid A at (a) t=0 s (i.e., the beginning of the closing period) and (b) t=5000 s (final instants of the closing period) for the Base Case. The lower row presents the concentration map for the C product at (a) t=0s and (b) t=5000 s.

4. Spatio-Temporal Evolution of the Standard Case

Fig. S4.1 presents the fingering pattern development during the second period of injection for the Base Case. It is the temporal evolution of the pattern shown in Fig. 4 for the normalized times: 0, 0.25, 0.5, and 0.75.

USC
UNIVERSIDADE DE SANTIAGO DE COMPOSTELA

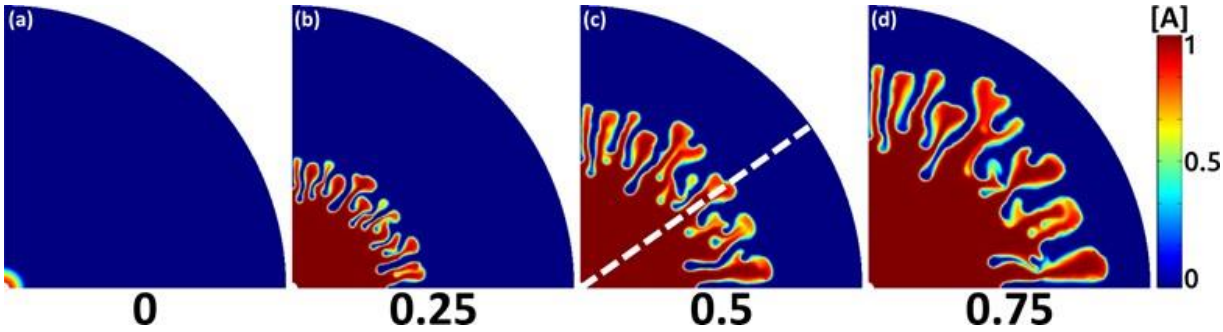


FIG. S4.1. Evolution of the fingering pattern during the second period of injection for the Base Case. Color-coded is the concentration (in M) of the displacing fluid A in the reactor for the Base Case. Four pictures are plotted corresponding with the normalized times (a) 0, (b) 0.25, (c) 0.5, and (d) 0.75. (Model parameters: r_{ring} = 1 cm, tc= 5000s, R_C=5, R_B=2, D_A=D_B=D_C=1x10^{-9} m^2/s, k_1=10 L/s·mol, Q_1=1 mL/min, and Q_2=1 mL/min.).

Fig. S4.2 presents the radial distribution of the fluid C concentrations (Fig. S4.2a) at different times, and the viscosity profiles (Fig. S4.2b) during the second period of injection for the Base Case for the normalized times: 0, 0.25, 0.5, 0.75 and 1.

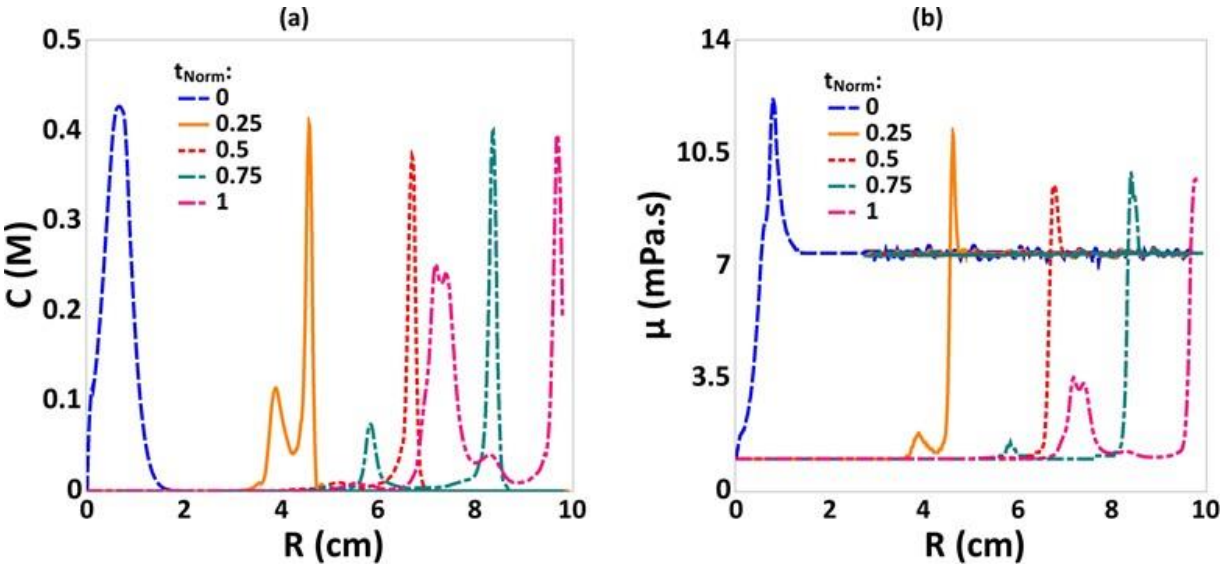


FIG. S4.2. Temporal variation of the radial distribution of (a) the product C concentration (M), and (b) the fluid C viscosity (Pa s) during the second period of injection in the reactor for the Base Case, at normalized times 0, 0.25, 0.5, 0.75, and 1. The profiles are recorded along the white dashed line in Fig. S4.1. (Model parameters: r_{ring} = 1 cm, tc= 5000s, R_C=5, R_B=2, D_A=D_B=D_C=1x10^{-9} m^2/s, k_1=10 L/s·mol, Q_1=1 mL/min and Q_2=1 mL/min.).

5. Temporal Evolution of The Fingering Instability for r_{ring} =5 cm and t_c=20000 s.

Fig. S5.1 presents the fingering pattern during the second period of injection when r_{ring} is located at 5 cm and the closing time is extended until 20000 s. This corresponds with the temporal evolution of the pattern shown in Fig. 8 for the normalized times: 0, 0.25, 0.5, and 0.75.

USC
UNIVERSIDADE DE SANTIAGO DE COMPOSTELA

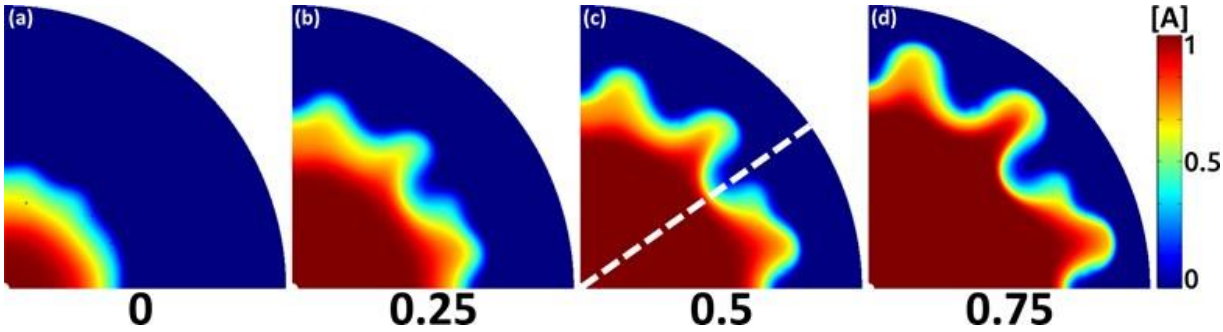


FIG. S5.1. Evolution of the fingering pattern during the second period of injection for the extended closing time tc=20000 s and a r_{ring} located at 5 cm from the inlet point. Color-coded represents the concentration (in M) of the displacing fluid A, at normalized time: (a) 0, (b) 0.25, (c) 0.5, and (d) 0.75. (Model parameters: R_C=5, R_B=2, D_A=D_B=D_C=1x10^{-9} m^2/s, k_1=10 L/s·mol, Q_1=1 mL/min, and Q_2=1 mL/min.).

Fig. S5.2 presents the radial distribution of the fluid C concentrations (Fig. S5.2a), and the viscosities profiles (Fig. S5.2b) during the second period of injection for the tc=20000 s and a r_{ring} = 5 cm case, for normalized times: 0, 0.25, 0.5, 0.75 and 1.

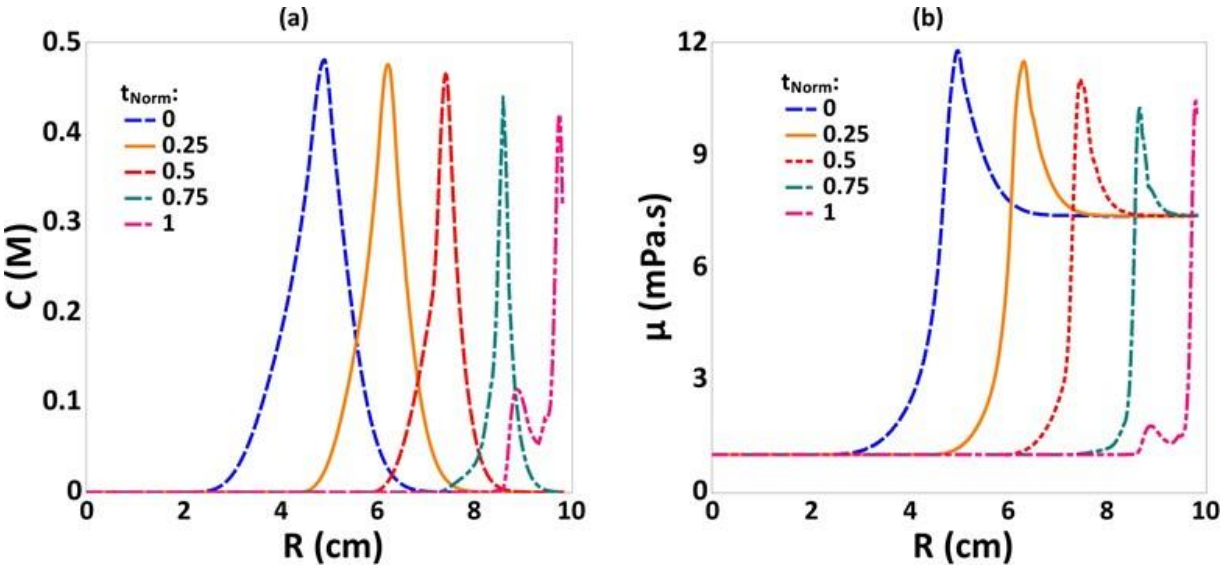


FIG. S5.2. Radial profile of (a) the product C concentration (M), and (b) the fluid C viscosity (Pa s) during the second period of injection for the extended closing time tc=20000 s and a r_{ring} located at 5 cm, at normalized times 0, 0.25, 0.5, 0.75, and 1. The profiles are recorded along the white dashed line in Fig. S5.1. (Model parameters: R_C=5, R_B=2, D_A=D_B=D_C=1x10^{-9} m^2/s, k_1=10 L/s·mol, Q_1=1 mL/min and Q_2=1 mL/min.).

USC
UNIVERSIDADE DE SANTIAGO DE COMPOSTELA

USC
UNIVERSIDADE
DE SANTIAGO
DE COMPOSTELA

Journal of Molecular Liquids 364 (2022) 119984

Contents lists available at ScienceDirect

Journal of Molecular Liquids

journal homepage: www.elsevier.com/locate/molliq

Evaluation of surfactant blends for enhanced oil recovery through activity maps

Nestor Tafur, Alba Somoza, Ana Soto *

CRETUS, Department of Chemical Engineering, Universidade de Santiago de Compostela, E-15782, Santiago de Compostela, Spain

ARTICLE INFO

Article history:
Received 28 April 2022
Revised 4 July 2022
Accepted 29 July 2022
Available online 2 August 2022

Keywords:
Anionic
Cationic
Ionic liquid
Microemulsion
Winsor III

ABSTRACT

Better use of already exploited oil reservoirs using Enhanced Oil Recovery techniques is becoming essential. The use of surfactant blends is a common approach when individual surfactants are not effective. However, defining the optimum conditions for application becomes very challenging due to the number of variables involved in specific cases. In this work, blends of dioctyl sulfosuccinate sodium salt with Akypo LF2 and two surfactant ionic liquids (1-decyl-3-methylimidazolium chloride and 1-dodecyl-3-methylimidazolium bromide) were evaluated for oil recovery. Activity maps, representations of the phase behavior of the surfactants as a function of blend ratio, salinity and temperature, were found to be useful tools to describe conditions leading to Winsor type III systems. Among the blends studied, mixtures with Akypo LF2 were found of interest for application at low temperatures, showing interfacial tensions close to 0.01 mN/m in a wide range of salinity concentrations. In the case of blends with ionic liquids, even though they led to more promising solubilization parameters, the high sensitivity of these mixtures to blend ratio changes discourages, in principle, their use for practical applications.

© 2022 The Authors. Published by Elsevier B.V. This is an open access article under the CC BY-NC-ND license (http://creativecommons.org/licenses/by-nc-nd/4.0/).

1. Introduction

Considering the investment and other associated risks involved in discovering and developing new oil fields, hydrocarbon exploration has decreased in recent years, whilst oil reserves around the world are being depleted [1,2]. In this context, oil companies must turn to their existing oil fields and maximize the oil recovery from already exploited reservoirs. As water flooding alone is insufficient to displace all the oil in place, due to viscous and capillary trapping forces, the application of Enhanced Oil Recovery (EOR) techniques is needed to extract as much oil as possible. For this reason, these methods will probably become more relevant than in the previous decades, with an increasing imperative on their being employed wherever economically feasible. One of the main chemical EOR methods is surfactant flooding. A surfactant is a substance which lowers the surface tension of the medium in which it is dissolved, and/or the interfacial tension with other phases [3]. Anionic, cationic and non-ionic surfactants have been proposed for EOR. Recently, aqueous mixtures of two oppositely charged surfactants, so-called catanionic surfactant mixtures, have been shown promising for the application [4].

The oil droplets (residual oil), which remain trapped in the pores of the reservoir after water flooding cannot be displaced under normal oil–water interfacial tension (IFT), around 10–30 mN/m, because of the strong capillary forces. To start the mobilization of oil droplets and decrease the residual oil saturation to very low values, IFT must first be reduced to around 10^{-2} to 10^{-3} mN/m during surfactant flooding [5–9]. Such ultralow values of IFT correspond to Winsor Type III systems, according to the Winsor classification [10], where a surfactant solubilizes equal volumes of oil and water to form a middle microemulsion in equilibrium with excess oil (upper) and excess water (lower) phases. This behavior is preferred to Winsor Type I, with an aqueous microemulsion in equilibrium with an excess oil phase, or Winsor Type II where the biphasic system corresponds to an oily microemulsion in equilibrium with an excess water phase. The fragile equilibrium of optimal Winsor III microemulsions can be easily broken with changes in water salinity, temperature, surfactant concentration, etc., causing a shift to Winsor Type I or II [11].

The presence of a salinity gradient in the reservoir makes it difficult to keep the surfactant formulation in optimal conditions (ultra-low IFT) along its path from the injection well to the production wells. This is a typical problem found when water flooding is not carried out with the formation brine. A gradient appears between the injected and formation water salinities because of the mixing that occurs in the process, and the existence of non-

* Corresponding author.
E-mail address: ana.soto@usc.es (A. Soto).

https://doi.org/10.1016/j.molliq.2022.119984
0167-7322/© 2022 The Authors. Published by Elsevier B.V.
This is an open access article under the CC BY-NC-ND license (http://creativecommons.org/licenses/by-nc-nd/4.0/).

swept heterogeneous zones which contain immobile oil and formation brine. This salinity gradient depends on the initial water saturation, the composition and concentration of injected and formation water, pore volume, arrangement of the injector/producer wells, and volume of injected water, among other factors. Sheng [12] suggests that a 80/20 ratio for injection water/formation brine salinity should be selected to design formulations able to produce Winsor type III systems. Thus, the influence of salt concentration on microemulsion behavior is a relevant study for EOR.

The use of surfactant blends is a common approach when single surfactants are unable to meet the demanding requirements of surfactant EOR. These blends can be adjusted to obtain an optimal microemulsion (Winsor III system) at the desired salinity by changing the surfactant mix ratios. The synergy between two surfactants encourages the formation of mixed micelles, improving the performance of the formulation [13–16]. Previous studies [4,13,16–23] have shown favorable interactions in quite different systems, such as anionic-anionic, anionic-nonionic and anionic-cationic. In this line, Anton *et al.* [24] tested the combination of sodium dodecyl sulfate with tetradecyltrimethylammonium bromide looking for an optimal formulation. The desired three-phase behavior was found with water, oil and alcohol for mixtures up to 25 % of any of the surfactants. Higher concentrations led to precipitation of flat crystals. The design of alcohol-free anionic-cationic microemulsions which avoid such precipitation problems was approached in detergency studies, and the combination of a branched surfactant and surfactants with varying tail length was proposed [18,25]. Puerto *et al.* studied the use of alkoxyglycidylether sulfonates for EOR, and proposed their combination with an internal olefin sulfonate in order to avoid the cloud-point phenomenon found at elevated temperatures [20]. To address the disadvantages of the use of alkalis during surfactant flooding, Zhang *et al.* [26] proposed the use of blends of cationic, anionic, zwitterionic and nonionic surfactants to achieve ultra-low IFT. The authors demonstrated that anionic/cationic and anionic/zwitterionic blends for highly active aggregates behave like nonionic surfactants and show a high salinity tolerance. The surfactants used and their mixing ratios can be tailored to achieve optimal formulations at different salt concentrations. The possibilities of anionic/cationic blends were further studied by Li *et al.* [22]. A polyoxyethylene ether carboxylate anionic surfactant was blended with a quaternary ammonium chloride cationic surfactant and tested for a high-temperature, low-salinity, and high-hardness condition. The ethoxy number of the anionic compound and the chain length of the anionic surfactant were tuned to obtain optimal surfactant blends able to produce ultra-low IFT. In our previous work [27], blends of traditional surfactants and surface-active ionic liquids (SAILs) were tested for EOR. To that aim, the phase behavior of the mixtures with octane and a hard brine was determined at several temperatures. The combination of an internal olefin with dodecyltrimethylammonium bromide or 1-dodecyl-3-methylimidazolium bromide was proposed for the application. However, there is a lack of studies in the literature involving the phase behavior of surfactant blends at a wide range of salinities and temperatures.

The purpose of the present work therefore is to evaluate the phase behavior of different surfactant blends with water and oil at such conditions. In order to formulate the surfactant blends, the anionic branched surfactant dioctyl sulfosuccinate sodium salt (AOT) was selected. It has a relatively short but bulky double alkyl chain and a small ionic head group. This disproportion between the hydrophilic and hydrophobic parts makes it highly lipophilic [28], thus allowing a flexible tuning through blending with more hydrophilic surfactants. It was also selected because it has been shown as a component of interest in the design of microemulsions for various applications [29,30]. To design an anionic/nonionic blend, polyoxyethylene(8) octyl ether carboxylic acid (Akypo LF2) was selected. This is a triblock alkyl ethoxy carboxylate surfactant whose ionization level depends on the pH of the formula, behaving like a nonionic surfactant at acid pH, and an anionic one in an alkaline solution. It has a short lipophilic chain and a relatively long hydrophilic section. Due to its chemical structure, the ethoxy and carboxylate groups make it tolerant to high salinity and stable long-term to high temperature [23,31,32]. To design anionic/cationic blends, ionic liquids were selected as cationic components. These salts with long alkyl chains are being currently proposed as surfactants for EOR due to their promising features, such as the possibility of their functionalization [33–38]. However, their success in forming Winsor type III systems is low, and blends with traditional surfactants are required [27,39–41]. The selected surface active ionic liquids (SAILs) were 1-decyl-3-methylimidazolium chloride ($[C_{10}mim]Cl$) and 1-dodecyl-3-methylimidazolium bromide ($[C_{12}mim]Br$).

The main contribution of this paper is the proposal of activity maps to analyze the influence of salt concentration, thus considering the possible variation of this parameter from injection to production wells, and temperature, on the phase behavior of surfactant blends. Even though obtaining these maps is a time-consuming procedure, they are an extremely useful tool to determine the limits of the region with the greatest interfacial activity (three-phase zone) of a surfactant system, varying two or three formulation parameters at the same time. The information provided offers a thorough understanding of the performance of the surfactant formulation, with the aim of predicting the behavior of chemical flooding in the reservoir in the event of salinity changes, thus allowing better decisions regarding the process. To that aim, the following studies were carried out:

- Phase behavior of AOT/Akypo LF2, AOT/$[C_{10}mim]Cl$ and AOT/$[C_{12}mim]Br$ blends at 25 °C and seawater salinity (5 wt% NaCl).
- Influence of water salinity on phase behavior. The concentration was varied from 1 to 15 wt% NaCl. This allowed activity maps to be made of the studied blends at 25 °C.
- Influence of temperature on phase behavior. Determinations at two new temperatures (50 and 75 °C) were carried out covering the entire range of salinities. This allowed the analysis of the variation of the size of the Winsor III region with this variable.
- Measurements of IFT for promising blends at optimal conditions, to ensure the achievement of ultra-low IFT and the validity of the blends for EOR.

2. Materials and methods

2.1. Materials

The anionic surfactant dioctyl sulfosuccinate sodium salt (Aerosol® OT, AOT) and the salt sodium chloride (NaCl), with purity grade of ≥ 97 wt% and ≥ 99 wt% respectively, were purchased from Sigma-Aldrich. The polyoxyethylene(8) octyl ether carboxylic acid ($C_8EO_8OCH_2COOH$), commercially named Akypo LF2 (hereinafter referred as LF2 for simplicity), was kindly provided by KAO Chemicals with a purity of ≥ 98 wt%. The cationic SAIL 1-dodecyl-3-methylimidazolium bromide ($[C_{12}mim]Br$) was purchased from Iolitec with a purity of > 98 wt%, while the SAIL 1-decyl-3-methylimidazolium chloride ($[C_{10}mim]Cl$) was synthesized. To that aim, 1-methylimidazole (Aldrich, 99 wt%) was directly alkylated with 1-chlorodecane (Aldrich, 98 wt%) at 60 °C under inert atmosphere for 72 h. The product was dissolved in acetonitrile (Panreac, >99.9 wt%) and washed several times with ethyl acetate (Aldrich, >99.5 wt%) to eliminate unreacted starting materials. After washing, most of the organic solvent was removed in a rotary evaporator, followed by stirring and heating at 70 °C for 48 h under

high vacuum (<0.1 mbar) to complete the removal of any residual volatile compounds present. A purity > 99 wt% was estimated by chromatography. Fig. 1 shows the chemical structures of surfactants. N-octane was used as a model oil because it can mimic crude oil behavior in optimal salinity determinations for many surfactants [27]. It was purchased from Sigma-Aldrich with purity grade > 99 wt%.

2.2. Methods

Fig. 2 shows a schematic representation of the methodology used in this work. It involves phase behavior determinations and IFT measurements.

2.2.1. Phase behavior

The phase behavior of mixtures of water, oil (*n*-octane) and surfactant (AOT, LF2, [C_{10}mim]Cl, [C_{12}mim]Br and their blends) was visually analyzed following the so called encased-glass-pipette method [20,42]. The borosilicate glass pipettes were sealed at the tip, then once the reagents of the formulations were placed inside the pipettes (water oil ratio was ~ 1 and the concentration of surfactant in the aqueous phase 4 wt%), they were heat-sealed at the top and gently mixed for 24 h in a rotary mixer at ambient temperature. Thereafter, each pipette was enclosed in a 10 cm^3 test tube filled with silicone oil, to favor thermostatization, and placed in a dry block heater OVAN model BD200-RE at the required temperature (25, 50 or 75 °C). When no change in the interfacial surface position was noticed, equilibrium condition was assumed. A surfactant concentration higher than that usually found in formulations was used to facilitate the visualization of the interfacial surface and the estimation of solubilization parameters. This procedure is frequently used in this kind of study [20,23,27,41].

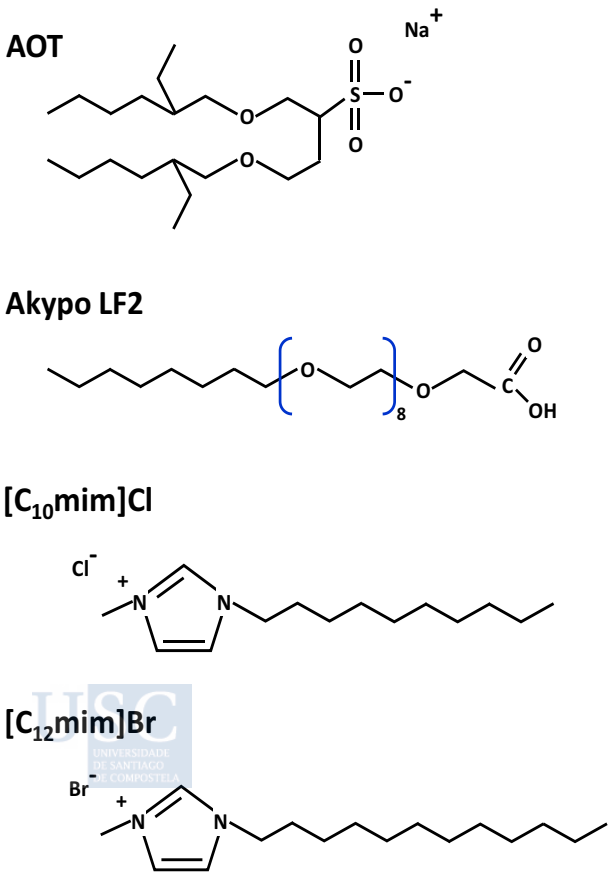


Fig. 1. Chemical structure of surfactants and ionic liquids.

Solubilization parameters were determined as the volume of oil or water solubilized in the microemulsion divided by volume of surfactant (V_o/V_S and V_W/V_S), assuming all the surfactant is present in the microemulsion phase. To attain an optimal formulation, three phases must coexist (Winsor type III system) and the solubilization parameters must be equal and of large value. According to Hugh's correlation [43] (Eq.1), this condition leads to ultra-low IFT.

$$IFT_{Huh} = c/(V_i/V_S^*)^2 \quad (1)$$

where V_i/V_S^* is the optimal solubilization parameter, and C is an empirical constant which ranges from 0.1 – 0.35 mN/m. A value of 0.3 was assigned to this constant to estimate IFT_{Huh} for the evaluated blends.

In order to find the hydrophilic or lipophilic character of the target surfactants, salinity scans were carried out for LF2 and [C_{10}mim]Cl at 25 °C. To that aim, several pipettes were prepared with different salt concentrations ranging from zero to 15 wt%, at 2 wt% intervals, in the aqueous phase. In the case of AOT and [C_{12}mim]Br, the information was taken from a previous work [27].

The blending of surfactants can be used to adjust the hydrophilic-lypophilic balance and obtain a Winsor type III system. As in the case of the salinity scan, a blend scan is one-dimensional phase behavior evaluation with changes in a formulation variable, in this case the blend ratio. Its main objective is the determination of the optimal blend ratio required to achieve a triphasic system with a middle microemulsion. The blend scans were carried out at 25 °C with AOT and LF2, [C_{10}mim]Cl or [C_{12}mim]Br. Blend ratios were prepared at 5 wt% intervals, maintaining 4 wt% as the concentration of surfactant in the formulation. When a transition from Winsor I to Winsor II was observed without triphasic systems in the middle, the step was reduced to 1 wt%. Water salinity was initially set to 5 wt% NaCl to approximate the salinity of seawater (5 wt% TDS).

With the purpose of evaluating the effect of salinity and temperature on the phase behavior, blend scans were also carried out at salinities ranging from 1 wt% NaCl to 15 wt% NaCl, and temperatures of 50 and 75 °C. The interval for the salinity changes was adapted to the needs of each system. Thus, for the very electrolyte sensitive systems, the evaluation was done with increments of 1 wt% NaCl concentration, while for less sensitive mixtures increments of 5 wt% NaCl were used.

An activity map has as its main target the visualization of the greatest activity zone, as a function of two or three formulation variables, which can offer helpful insights into the development of a surfactant flooding strategy providing the highest oil recovery [12,44]. Thus, as the present study is particularly focused on optimizing the phase behavior of the systems during a hypothetical blend injection in an EOR process, the chosen formulation variables were: blend ratio, aqueous phase salinity (mimicking the salinity gradient that could be encountered in the reservoir during chemical flooding), and temperature. Thus, the type of Winsor system was analyzed through the preparation of activity maps as a function of these three variables.

2.2.2. Interfacial tension (IFT)

If the surfactant blends were clear or translucent, dynamic IFTs were measured between *n*-octane (representing oil) and the aqueous phase at 1 wt% blend concentration using a spinning drop tensiometer (Krüss model Site 100), as in our previous reports [38,41]. For all measurements, the capillary tube of the spinning drop was filled with the aqueous phase, and a 4 μL drop of *n*-octane was left inside. Measurements were taken at a fixed rotation speed of 3000 rpm, making sure that length of the drop was 4 times greater than its diameter. Measurements were taken at 25 °C, along the three-phase region, at different blend ratios and salinities.

USC UNIVERSIDADE DE SANTIAGO DE COMPOSTELA

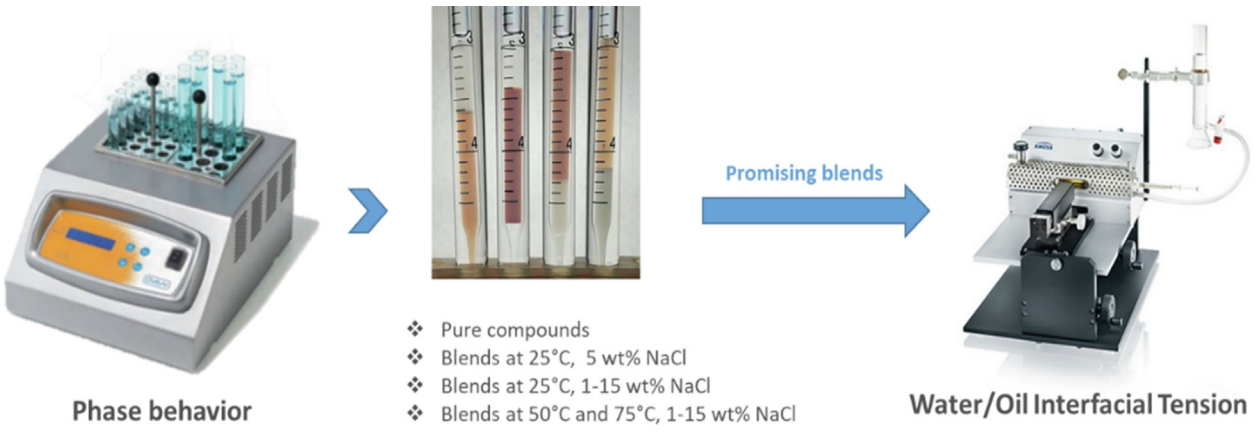


Fig. 2. Schematic representation of the methodology used in this work.

3. Results and discussion

3.1. Phase behavior

Salinity scans were carried out for LF2 and [C_{10}mim]Cl at 25 °C. Results can be seen in Figures S1 and S2 from Supporting Information (SI). Both surfactants were found to be highly hydrophilic, remaining Winsor I systems along the salinity interval evaluated. A similar behavior was previously found [27] in the case of the SAIL [C_{12}mim]Br, microemulsions of Winsor type I were found up to 15 %wt NaCl. Conversely, the pure surfactant AOT is highly lipophilic, changing from Winsor I to Winsor II at 0.21 wt% NaCl optimal salinity [27]. Therefore, fixing a salt concentration of 5 wt% NaCl in water/oil systems, AOT was mainly located at the upper phase (Winsor II), while the rest of the surfactants were found in the lower phase (Winsor I). The lipophilic character of the AOT was then used as a tuning tool to find optimal blend ratios (leading to three phase systems with equal and large solubilization parameters), in combination with more hydrophilic surfactants.

3.1.1. Blend scans at 25 °C and seawater salinity

Three surfactant systems, AOT/LF2, AOT/[C_{10}mim]Cl and AOT/[C_{12}mim]Br, were subjected to blend screening at a fixed salinity of 5 wt% NaCl and 25 °C to determine the optimal mixing ratios. Fig. 3a shows the blend scan of the AOT/LF2 mixture. Both surfactants show very different hydrophilicity. At low proportions of AOT (left side Fig. 3a), the blend behaved as hydrophilic and pipettes were in the Winsor I region. Increasing the AOT ratio made the formulation more lipophilic, and Winsor type II systems were found passing through the three-phase region. Winsor type III systems were found at ratios between 50/50 and 60/40 AOT/LF2. However, the volume of the microemulsion phase was limited. As expected, similar tendencies were found for the other two blends (Fig. 3b and 3c left) due to the hydrophilic character of the SAILs. In the case of the blend with [C_{10}mim]Cl, a change from Winsor I to Winsor III was initially observed (tests not shown) close to a composition ratio of 45/55 AOT/[C_{10}mim]Cl, which is why a narrower blend scan was carried out from 40/60 to 48/52 ratios (Fig. 3b). A narrower three-phase region than in the case of LF2 was found (between 43/57 and 45/55), however, the volume of the microemulsion was greater. Also, the dissimilar optimal salinities of AOT and [C_{12}mim]Br lead to a very narrow region of optimal salinities. In fact, a Winsor type III system was only found at 35/65 AOT/[C_{12}mim]Br ratio, the volume of the middle microemulsion being very significant (Fig. 3c left).

The capacity of solubilization of the evaluated blends was studied through the solubilization parameters (V_o/V_S and V_W/V_S). Fig. 3 right shows these relative volumes, for the three blends studied, as a function of blend ratio. As shown, the AOT/LF2 blend had the lowest optimal solubilization parameter (V_i/V_s^*, when $V_o/V_S = V_W/V_S$) of 2.5 (Fig. 3a right). Numerical data are shown in Table 1. A low value of V_i/V_s^* indicates a low capacity of the formulation to solubilize large volumes of oil and water in the middle phase. Based on Huh's equation (Eq. (1)), the IFT_{Huh} was approximately 4.8×10^{-2} mN/m at the optimal blend ratio AOT/LF2 = 53/47. The solubilization parameter plot for the mixture AOT/[C_{10}mim]Cl (Fig. 3b right) shows a higher value of the optimal solubilization parameter ($V_i/V_s^* \sim 6.6$) at a 44/56 blend ratio, giving rise to IFT_{Huh} of about 6.9×10^{-3} mN/m. The blend AOT/[C_{12}mim]Br showed the highest value of V_i/V_s^*, about 14.5 at an optimal blend ratio of 35/65 (Fig. 3c right), deriving on an ultralow IFT_{Huh} of about 1.4×10^{-3} mN/m at that optimal point, a promising value for EOR applications.

The justification for these remarkable differences in solubilization capabilities between AOT/LF2 and AOT/SAILs blends lies in the electrostatic activity between the oppositely charged head groups of the surfactants. They tend to form ion pairs, so that synergy between surfactants increases when their charges are opposite [22,45]. AOT is anionic whereas SAILs are cationic surfactants. LF2 is a weak carboxylic acid sensitive to the surrounding solution's pH. In alkaline environments it behaves as an anionic surfactant (–COO^-), while in acid solutions it acts as a nonionic surfactant (–COOH), similar to the nonionic surfactant C_8EO_8OH. In neutral conditions, it behaves more like a nonionic surfactant [32]. Thus, the anionic/nonionic blend is less synergic than the anionic/cationic ones. Electrostatic interactions between oppositely charged surfactant head groups lead to an effective reduction of the area of the combined surfactant-head groups, leading to a higher surface activity and greater capacity of solubilization [22].

Some works have evaluated the synergy between AOT and nonionic polyoxyethylene alkyl ether ($C_{10}EO_8/C_{10}EO_{10}/C_{13}EO_{10}$) [46] or [$C_n$mim]Br (n = 8, 10, 12, 14) SAILs [47,48], by means of the determination of the micellar interaction parameter (β^m). Positive values of β^m are associated with repulsion between two surfactant molecules, while negative values with attraction in the mixed micelles. Therefore, at higher negative values, the synergy between the head groups of two surfactants is also higher. Those studies [46–48] estimated lower negative values for AOT/nonionic surfactant blends (in the range of −0.902 to −6.34), and higher negative values for AOT/SAIL blends (between −17.6 and −23.1). The negative values in the first case are due to the insertion of ethylene oxide chains in nonionic surfactants reducing the repulsion between these and anionic head groups in mixed micelles. The negative values in the second case are associated to the formation of ion-pairs, leading to an increase of the aggregation number or even the formation of microstructures such as vesicles. Such syner-

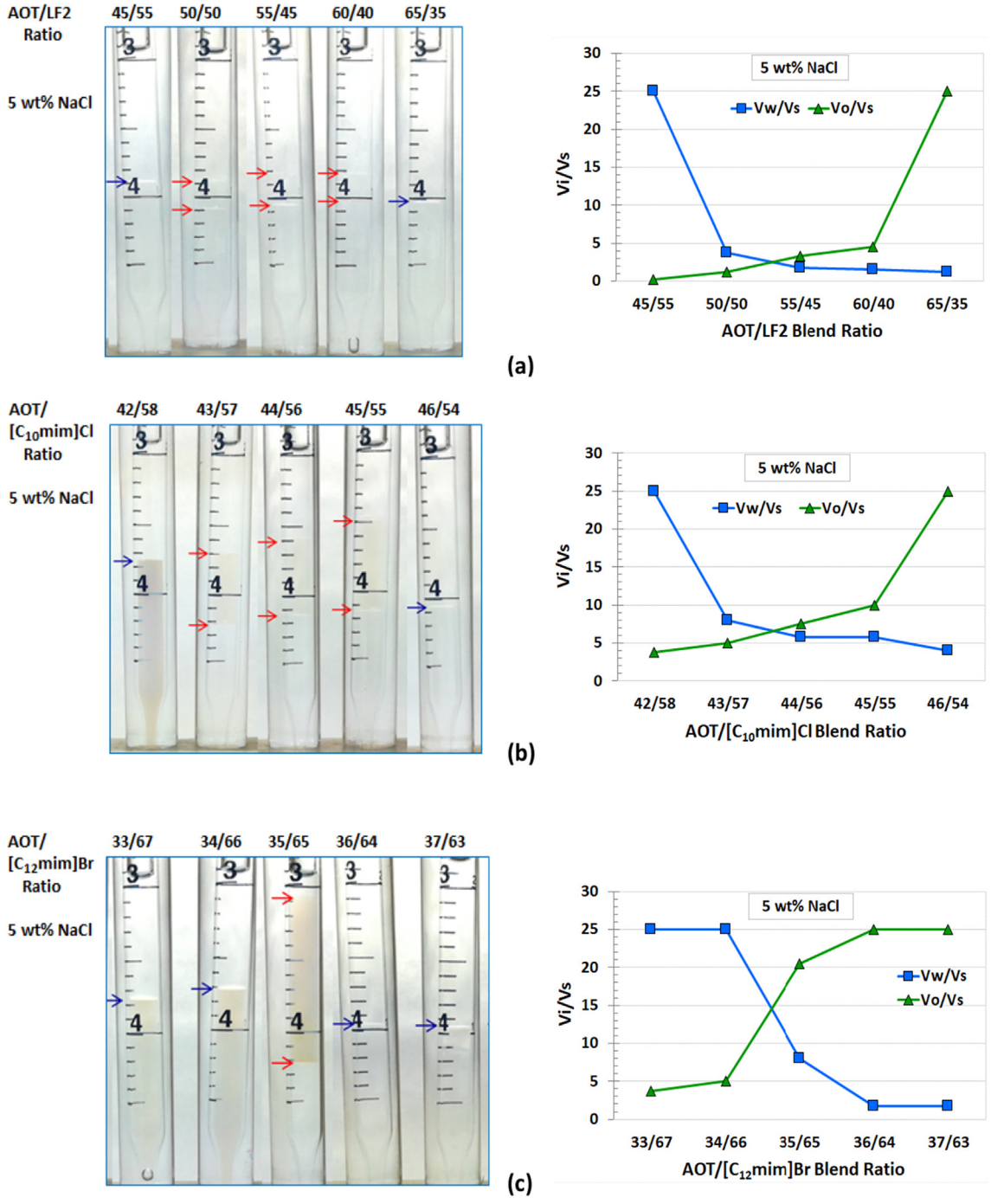


Fig. 3. Blend scans and solubilization parameters (V_i/V_s) for the studied blends at 5 wt% NaCl and 25 °C. (a) AOT/LF2, (b) AOT/[C_{10}mim]Cl, (c) AOT/[C_{12}mim]Br.

getic effects favor solubilization. When a very high synergism is found between surfactants, the surface area charge of mixed micelles is reduced practically to zero and blends can show less hydrophilic behavior or even behave like nonionic surfactants. Thus, catanionic mixtures interact more strongly with the oil, so as their concentration at the interface increases, the interaction of the surfactant mixture with the oil phase is also increased, a change which is compensated by decreasing the salinity in order to increase the interaction on the water side [24]. Then stronger interactions of the surfactant mixture with both oil and water result in a higher solubilization. In the case of AOT/SAILs, parameter β^m reduced with the increase of the alkyl chain length, and consequently micellar radius, which explains the larger solubilization capacity of AOT/[C_{12}mim]Br with respect to AOT/[C_{10}mim]Cl.

3.1.2. Effect of salinity

It is well-known that increasing the aqueous phase salinity reduces the polar interaction between water molecules and head-groups of ionic surfactants, inducing surfactants to be expelled from the aqueous phase to the oil phase, while nonionic surfactants are more insensitive to electrolyte concentration [9,49]. Aiming to analyze the influence of salt concentration on the phase behavior of the studied blends, tests were also carried out at 1, 10 and 15 wt% NaCl.

Fig. 4 shows AOT/LF2 blend scans at different salt concentrations and 25 °C. In this case, the maximum salt concentration tested was 13 wt% since higher concentrations led to the appearance of a coacervate. As shown, the effect of salinity is rather significant on this blend. The increase of salt concentration has two effects: the size of the Winsor III regions (the range of composi-

Table 1
Optimal blend ratios and corresponding solubilization parameters for AOT/LF2, AOT/[C_{10}mim]Cl and AOT/[C_{12}mim]Br blends at several salinities and temperatures and atmospheric pressure.

AOT/LF2							
25 °C							
1 wt% NaCl		5 wt% NaCl		10 wt% NaCl		13 wt% NaCl	
Mass ratio	V_i/V_S^*	Mass ratio	V_i/V_S^*	Mass ratio	V_i/V_S^*	Mass ratio	V_i/V_S^*
84/16	5.7	53/47	2.5	39/61	2.2	35/65	1.9
50 °C							
1 wt% NaCl							
Mass ratio	V_i/V_S^*						
88/12	4.25						
AOT/[C_{10}mim]Cl							
25 °C							
1 wt% NaCl		5 wt% NaCl		10 wt% NaCl		15 wt% NaCl	
Mass ratio	V_i/V_S^*	Mass ratio	V_i/V_S^*	Mass ratio	V_i/V_S^*	Mass ratio	V_i/V_S^*
45/55	8.6	44/56	6.6	43/56	6.4	43/57	8.1
50 °C							
1 wt% NaCl		5 wt% NaCl		10 wt% NaCl		15 wt% NaCl	
Mass ratio	V_i/V_S^*	Mass ratio	V_i/V_S^*	Mass ratio	V_i/V_S^*	Mass ratio	V_i/V_S^*
49/55	5.9	43/57	3.7	43/57	3.7	43/57	3.7
75 °C							
1 wt% NaCl		5 wt% NaCl		10 wt% NaCl		15 wt% NaCl	
Mass ratio	V_i/V_S^*	Mass ratio	V_i/V_S^*	Mass ratio	V_i/V_S^*	Mass ratio	V_i/V_S^*
43/57	2.8	42/58	3.2	41/59	2.5	40/60	2.2
AOT/[C_{12}mim]Br							
25 °C							
1 wt% NaCl		5 wt% NaCl		10 wt% NaCl		15 wt% NaCl	
Mass ratio	V_i/V_S^*	Mass ratio	V_i/V_S^*	Mass ratio	V_i/V_S^*	Mass ratio	V_i/V_S^*
36/64	14.8	35/65	14.5	34/66	14.0	32/68	15.3
50 °C							
1 wt% NaCl		5 wt% NaCl		10 wt% NaCl		15 wt% NaCl	
Mass ratio	V_i/V_S^*	Mass ratio	V_i/V_S^*	Mass ratio	V_i/V_S^*	Mass ratio	V_i/V_S^*
37/63	6.7	35/65	6.1	33/67	7.2	32/68	8.4
75 °C							
1 wt% NaCl		5 wt% NaCl		10 wt% NaCl		15 wt% NaCl	
Mass ratio	V_i/V_S^*	Mass ratio	V_i/V_S^*	Mass ratio	V_i/V_S^*	Mass ratio	V_i/V_S^*
37/63	5.4	35/65	3.8	32/68	3.7	31/69	3.7

tions leading to three equilibrium phases) increases, and the proportion of AOT leading to optimal formulations decreases. At 1 wt% NaCl, three-phase systems are found from 80/20 to 90/10 AOT/LF2 ratios, and in the case of 13 wt% NaCl, a middle microemulsion is found from 20/80 to 50/50 blend ratios. Moreover, at low salinity (1 wt% NaCl), the optimal AOT/LF2 ratio was estimated to be 84/16 and decreased in AOT fraction to 39/61 and 35/65 at 10 wt% and 13 wt% NaCl, respectively. The blend becomes more lipophilic when salinity concentration increases, and the concentration of AOT required to achieve the hydrophilic-lipophilic balance decreases. Regarding the optimal solubilization parameter, it decreases from 5.7 to 1.9 when NaCl concentration increases from 1 to 13 wt% (see Table 1). The behavior found for this blend is typical of anionic surfactants. This may be explained by the lower synergism between the surfactants of this blend, the interactions between negatively charged AOT head groups being more significant than those of the nonionic ethoxylated groups of LF2 with water. The addition of NaCl reduces the electrostatic interaction between water molecules and the sulfonate group of AOT making it partition to the oil phase.

Fig. 5 shows AOT/[C_{10}mim]Cl blend scans at 1, 10 and 15 wt% NaCl concentrations and 25 °C. As shown, the blend is less sensitive to salinity than the mixture with LF2. In fact, salt concentration hardly affects the size of the Winsor III region, which is very narrow at all concentrations. The salinity has also little influence on the blend optimal ratio that goes from 45/55 AOT/[C_{10}mim]Cl at 1 wt% to 43/57 at 15 wt% NaCl. Regarding optimal solubilization parameters, V_i/V_s^*=8.6 at 1 wt%, and this value decreases down to 6.6 and 6.4 at 5 and 10 wt% NaCl (Fig. 5 right) then increases up to 8.1 at the highest salt concentration. The same qualitative behavior was found in the case of the blend with the other SAIL, [C_{12}mim]Br. The salinity has a negligible influence on the size of the three-phase region and likewise on the optimal blend ratio, with optimal solubilization parameters first decreasing and then increasing with salt concentration. Fig. 6 shows that at 1 wt% NaCl, V_i/V_s^*=14.8 at 36/64 AOT/[C_{12}mim]Br, while at 10 wt% NaCl the optimal solubilization parameter is 14.0 at 34/66. The greatest solubilization capacity was found at 15 wt% NaCl, V_i/V_s^*=15.3 at 32/68 optimal ratio. Lower concentrations of SAIL were required to achieve optimal formulations with [C_{10}mim]Cl than with [C_{12}mim]Br, however in the last case solubilization parameters are higher (better synergy between surfactants) and could be of interest for EOR.

Based on the results shown in Figs. 4, 5, and 6 a more detailed screening was carried out at 25 °C to generate activity maps, a clear visual representation of phase behavior of the blends studied, as a function of surfactant ratio and salinity. The activity map corresponding to the AOT/LF2 blend is shown in Fig. 7. Due to the high sensitivity of this mixture to salinity, new pipettes were prepared at intermediate salt concentrations between those initially studied. Circles in Fig. 7 show all the tests carried out. Black circles represent pipettes with two phases (Winsor I or Winsor II) and red circles show pipettes with three phases and a middle microemulsion. The highlighted area shows promising formulations for EOR due to their Winsor type III behavior. The figure also shows blend ratios and salinity concentrations leading to optimal formulations (dashed line) associated to low IFT. The activity map (Fig. 7) clearly shows that blends with AOT concentrations higher than 65 wt% are

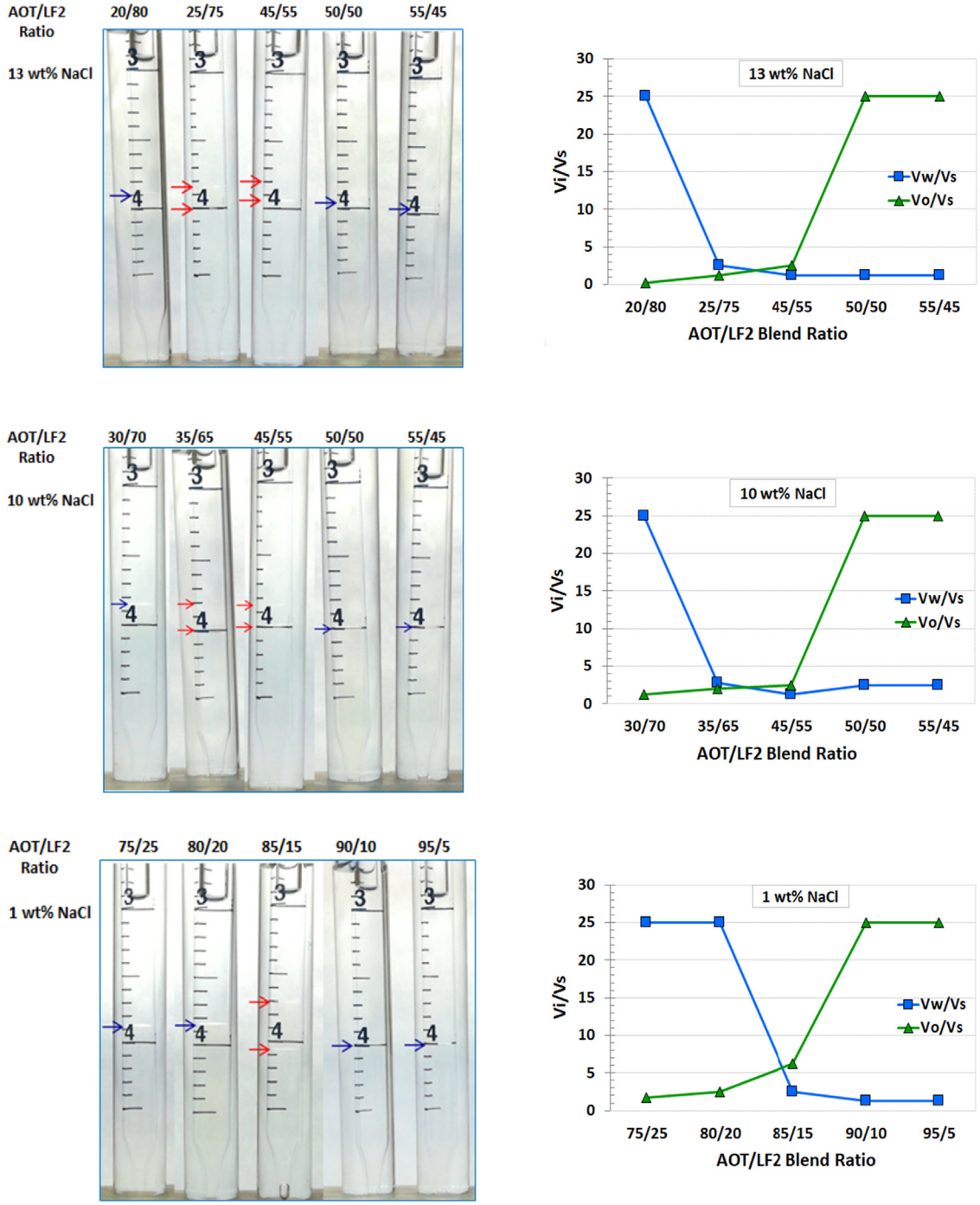


Fig. 4. Effect of salinity on blend scans and solubilization parameters (V_i/V_s) for AOT/LF2 at 25 °C.

the most sensitive to salinity, where a small difference in wt% NaCl produces a significant change in the composition of the optimal blend ratio. In this sense, the use of this blend at low salinities is discouraged, because slight variations in either salt concentration or composition of the injected blend inside the reservoir would shift the formulation away from its optimal behavior. Conversely, at the highest concentrations of salt, the slope of the line corresponding to optimal formulations is high and the Winsor III region large. Even with significant variation in salinity or blend ratio, the Winsor III system remains, although the formulation moves away from its optimal behavior. The higher sensitivity of the blend at AOT compositions >65 wt% is accounted for by the excess of anionic surfactant, which makes it behave like an ionic surfactant. The increase of salinity in the water phase diminishes water activity and affinity of the surfactant for that phase. Increasing the concentration of LF2, a change in the trend is noticed and the blend becomes more tolerant to NaCl increases. The ethoxylate block is likely the main cause of the interaction with the aqueous phase, and the presence of the inorganic salt has no significant influence, since the solubility of the surfactant in water is mainly due to the hydration of the ethoxy groups and not to electrostatic interactions [19,32].

Different behavior is observed in Fig. 8, showing activity maps for the blends of AOT with SAILs at 25 °C. These systems were clearly less sensitive to salt concentration than the blend with LF2. At the optimal blend ratios, with the dashed lines corresponding to the optimal formulations being practically vertical (especially in the blend with [C_{10}mim]Cl), an increase in NaCl concentration would keep the system as Winsor III and at the optimal formulation (or very close to it). This is of great importance,

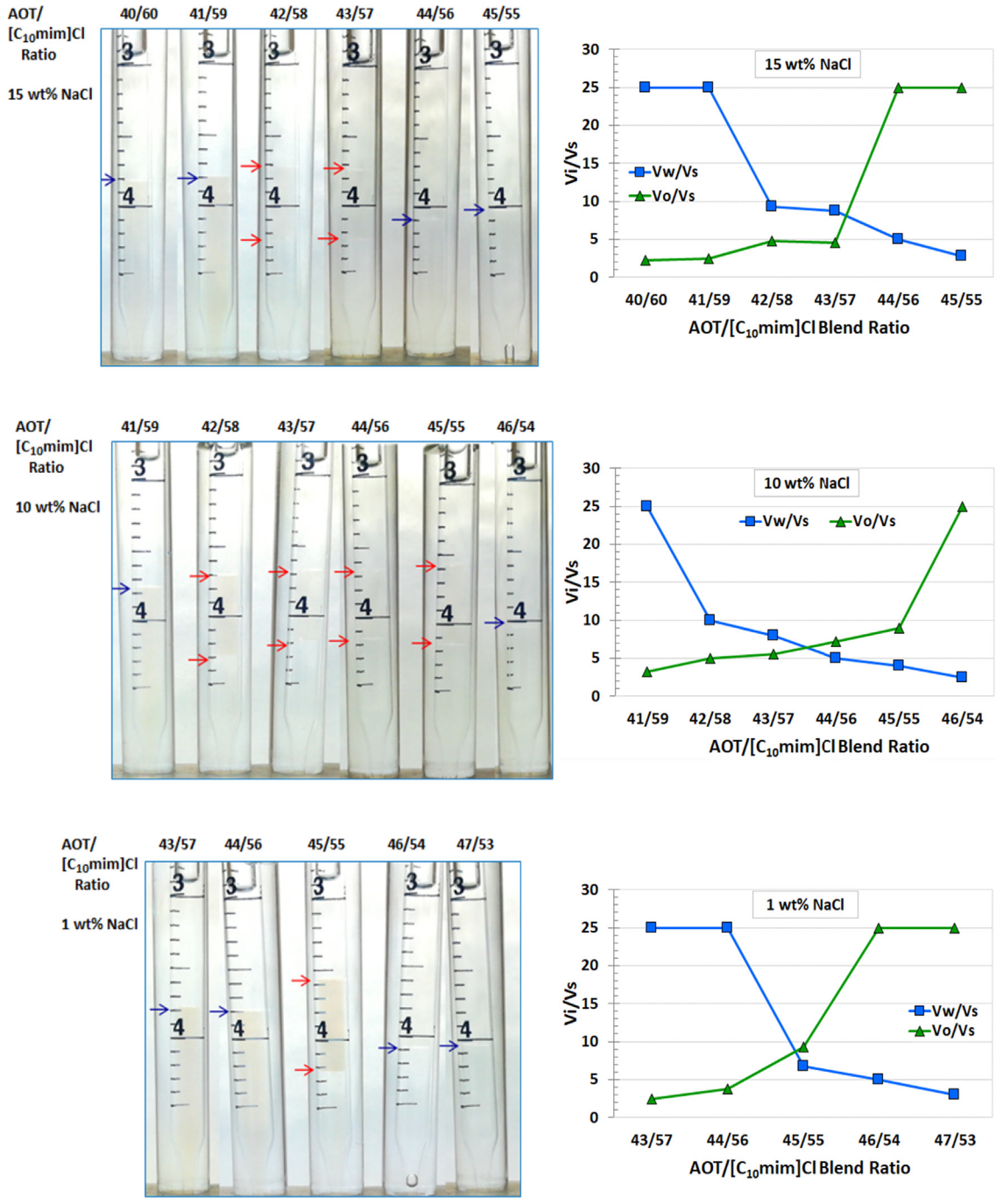


Fig. 5. Effect of salinity on blend scans and solubilization parameters (V_i/V_s) for AOT/[C_{10}mim]Cl at 25 °C.

because the injection water used in EOR frequently differs from the formation brine found in the reservoir, and salinity varies in the flooding process. The lipophilic AOT and hydrophilic SAILs were mixed seeking Winsor III behavior, however electrostatically neutral complexes are also formed due to the different charge of the components of the blend. When the synergy is high enough and the oppositely charged surfactants interact strongly, the mixed surfactants behave as nonionic and are less salinity sensitive [4,50]. On the other hand, Fig. 8 also shows that blends with SAILs are very sensitive to blend ratio. In mixtures with [C_{10}mim]Cl, and more significantly in the case of [C_{12}mim]Br, a small change in blend ratio generates distancing from the optimal region and low IFTs. This problem could be a concern in practice, due to the possible adsorption of surfactants on the rocks of the reservoir. Figure S3 in the Supporting Information allows the comparison of the activity maps of the three blends studied, and shows an advantage of the mixture with LF2 regarding variations of blend ratio, in comparison to those with SAILs.

3.1.3. Effect of temperature

The effect of the temperature on phase behavior of the studied blends was analyzed. To that end, blend scans were carried out at 50 °C and 75 °C (pipette photographs and solubilization parameters can be seen in SI, Figures S4-S13).

Fig. 9 shows the activity map for the AOT/LF2 blend including the effect of temperature. The solubilization capacity of the system was drastically affected by this variable. Even though the range of blend ratios in which Winsor III systems appear is greater at 50 °C than at 25 °C, the middle microemulsions found had low volumes, hard to estimate accurately, especially at salt concentrations above 4 wt% NaCl. In some cases, coacervates were also identified by the

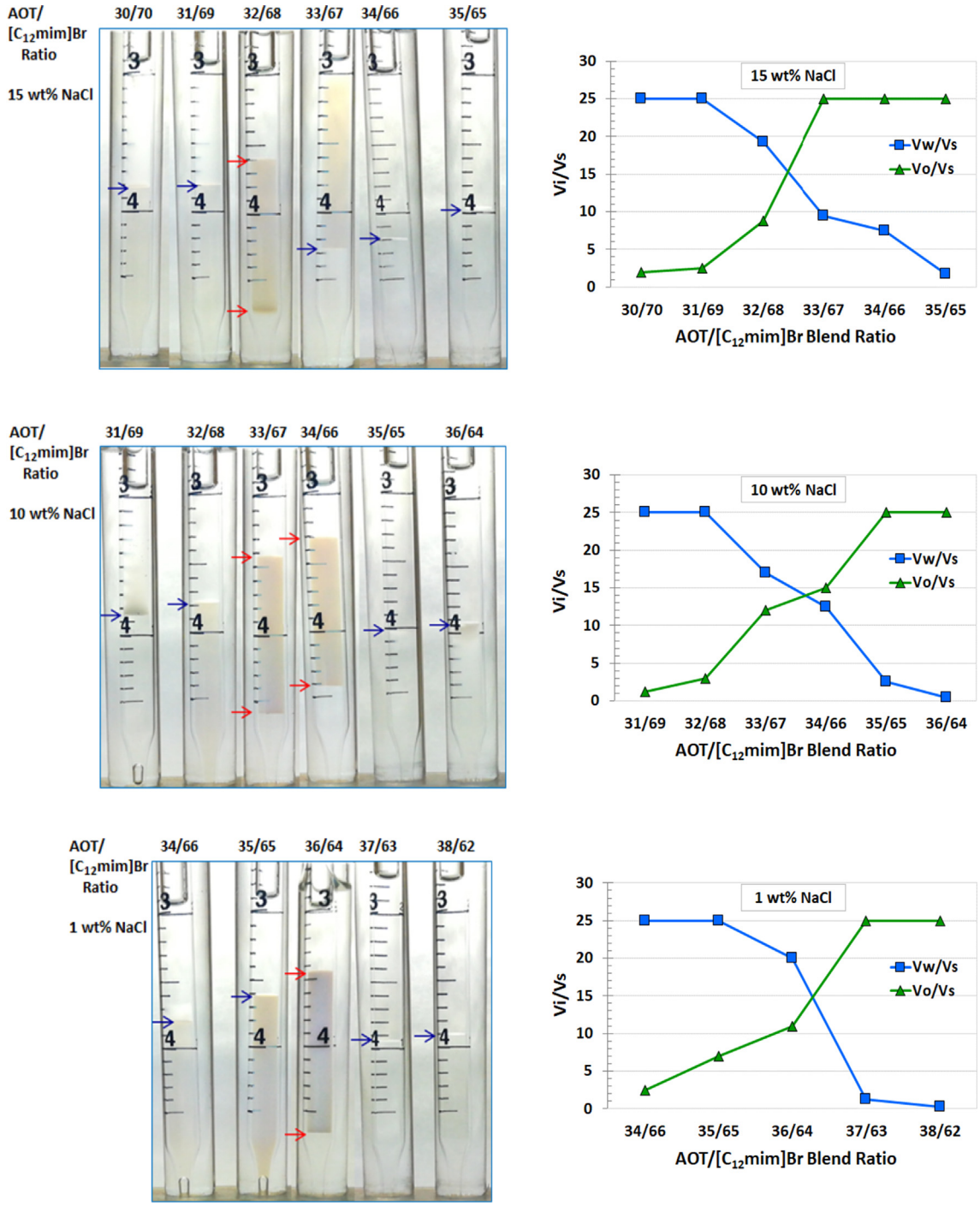


Fig. 6. Effect of salinity on blend scans and solubilization parameters (V_i/V_s) for AOT/[C_{12}mim]Br at 25 °C.

high curvature of the interface. The problem is even worse at 75 °C, reason why measurements were not carried out.

Figs. 10 and 11 show the activity maps for AOT/[C_{10}mim]Cl and AOT/[C_{12}mim]Br, respectively, including the effect of temperature. A widening of the triphasic areas with temperature was observed for the two blends. This is in agreement with results previously reported for anionic, nonionic and cationic-anionic mixtures [4,51–54].

Fig. 12 allows the visualization of the salinity and temperature effects on the optimal AOT/SAIL blend ratios. These mixtures behaved like non-ionic surfactants due to the formation of electrostatically neutral complexes. High temperature breaks hydrogen bonds between blends and water, thus decreasing the affinity of the surfactant for the aqueous phase and increasing its lipophilic character. Consequently, higher temperatures required lower proportions of AOT (very lipophilic) in the blend to achieve an optimal behavior. This effect is more apparent in the case of SAILs of shorter alkyl length and at higher salt concentrations (see Fig. 12).

3.1.4. Solubilization parameters

Optimal blend ratios and corresponding solubilization parameters for AOT/LF2, AOT/[C_{10}mim]Cl and AOT/[C_{12}mim]Br blends at several salinities and temperatures and atmospheric pressure are presented in Table 1.

As explained above, in the case of AOT/LF2 blend at 50 °C, solubilization parameters could only be estimated at 1 and 2 wt% NaCl (Figure S5 in SI). At 1 wt% NaCl, a value V_i/V_s^*= 4.25 was found at an optimal blend ratio 88/12 AOT/LF2. In comparison with results achieved at 25 °C at the same salt concentration, the optimal solubilization parameter decreased (leading to a higher IFT and lower

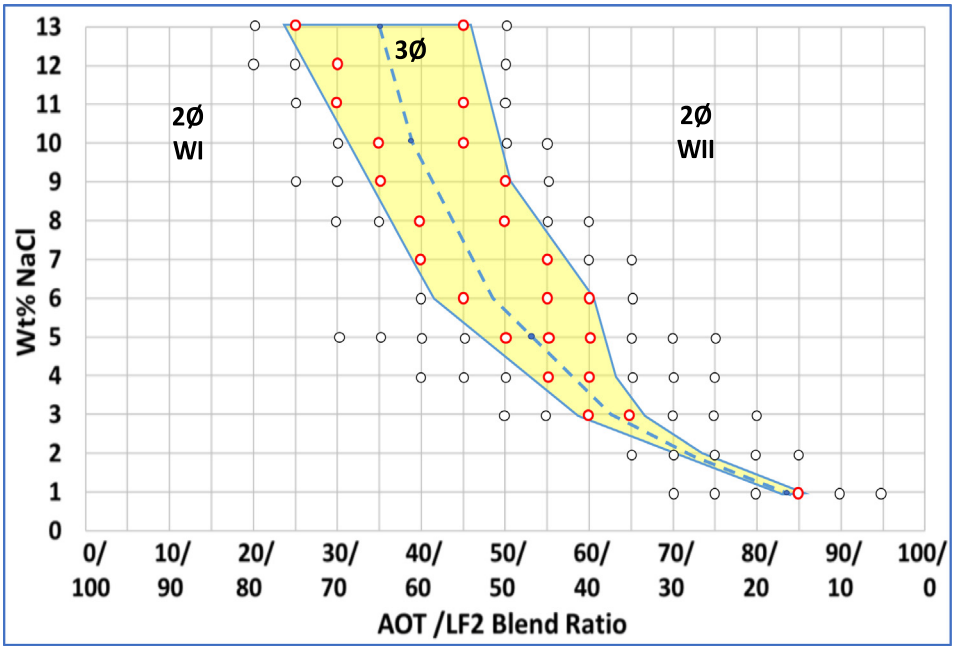


Fig. 7. Activity map for AOT/LF2 blend, as a function of salinity and blend ratio, at 25 °C. Black and red circles represent two- and three- phase systems, respectively. Blue dashed line represents optimal blend ratios.

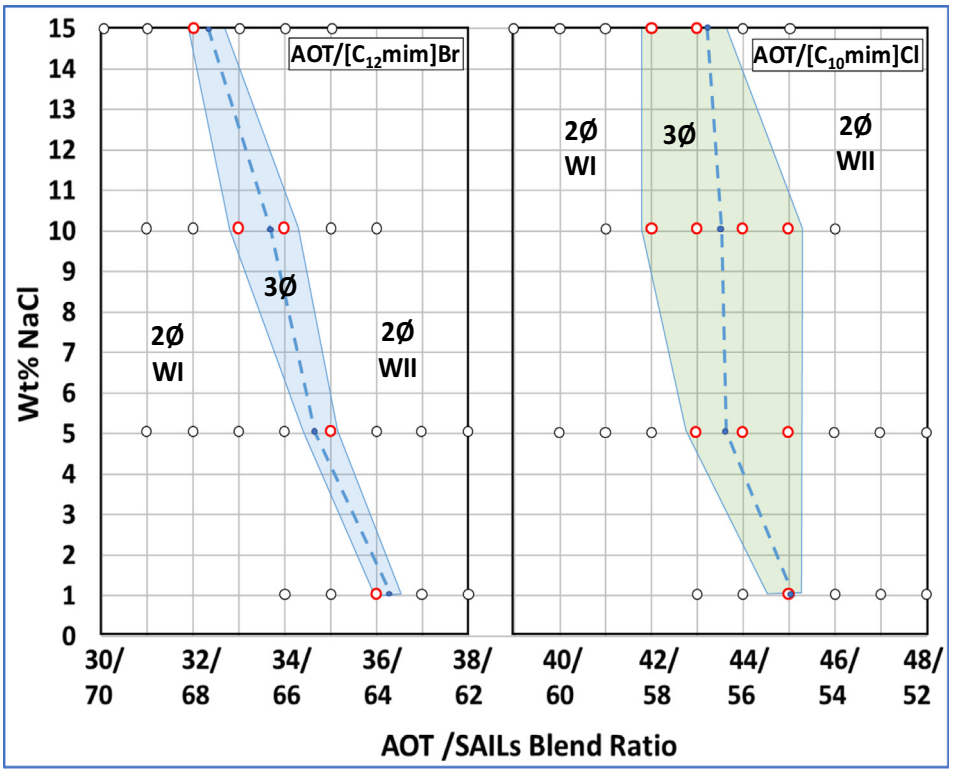


Fig. 8. Activity map for AOT/SAIL blends, as a function of salinity and blend ratio, at 25 °C. Black and red circles represent two- and three- phase systems, respectively. Blue dashed lines represent optimal blend ratios.

oil recovery), and the concentration of AOT slightly increased. Higher temperatures increase the hydrophilic character of the blend. It is worth mentioning that a previous study [32] shows the appearance of cloudy solutions when Akypo LF2 was used at 50 °C, however these problems disappear when combined with AOT. No further evaluations were carried out at higher temperatures for this blend that, among the temperatures studied, shows optimal behavior at 25 °C.

Fig. 13 allows the visualization of the salinity and temperature effects on the optimal solubilization parameters for AOT/SAIL blends. At all the studied salt concentrations, optimal solubilization parameters decrease with temperature, an effect more pronounced when the temperature increases from 25 to 50 °C and with the SAIL of longer alkyl chain length. Further studies (out of the scope of this work), based for instance on molecular simulation, are required to understand the combined effect of all the involved variables on the phase behavior of the different blends.

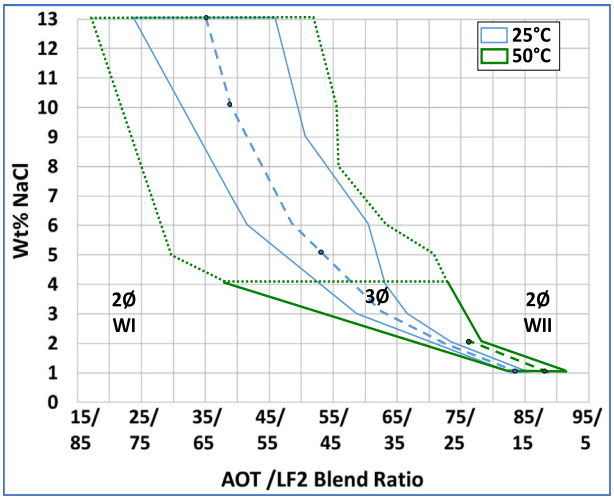


Fig. 9. Effect of temperature on the activity map of the AOT/LF2 blend.

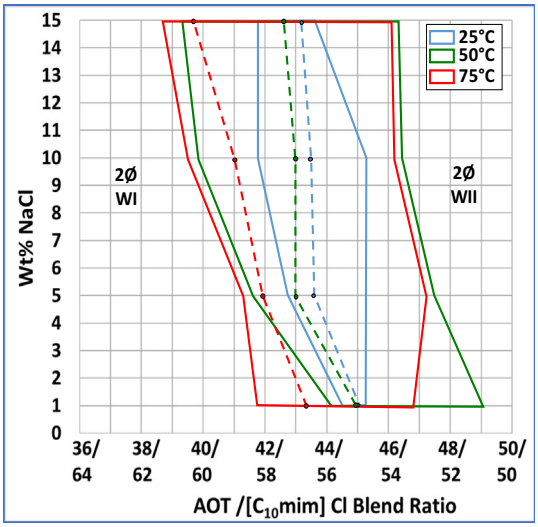


Fig. 10. Effect of temperature on the activity map of the AOT/ [C_{10}mim]Cl blend.

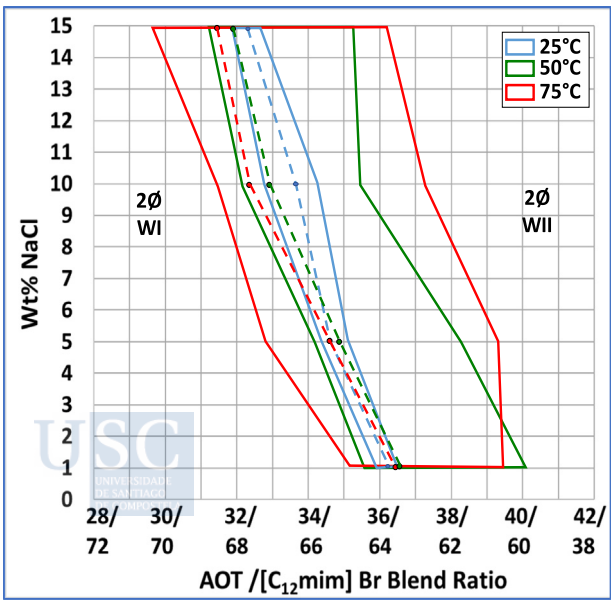


Fig. 11. Effect of temperature on the activity map of the AOT/ [C_{12}mim]Br blend.

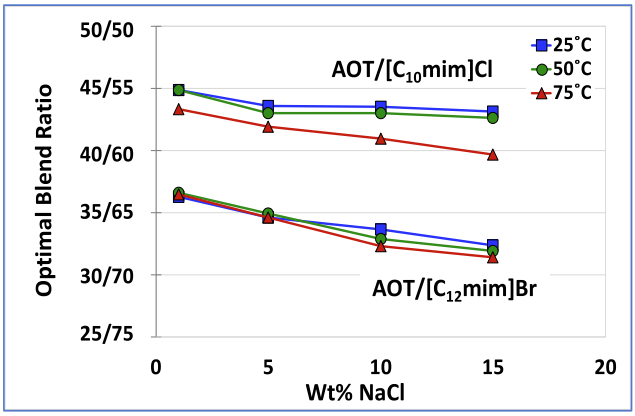


Fig. 12. Effect of salinity and temperature on the optimal blend ratio for AOT/ [C_{10}mim]Cl blend (above) and AOT/ [C_{12}mim]Br blend (below).

3.2. Interfacial tension measurements

Blends with SAILs were found to be too sensitive to blend ratios. Moreover, in absence of the oil, the injection fluids were found unstable, so they only could be injected as microemulsions. In the case of the blend AOT/LF2, a temperature of 25 °C was established as the best for the operation. For that reason, and focusing on IFT reduction as the main goal of surfactant EOR, measurements of this variable were carried out for the blend AOT/LF2 at 25 °C at optimal blend ratios. The surfactant concentration in the aqueous phase was 1 wt%. Experimental values of IFT and those calculated with Huh's equation for optimal conditions are shown in Table 2. Except in the case of 1 wt% NaCl, values of IFT estimated by the Huh's equation are over-estimated. Some experimental measurements were also carried out at blend ratios close to optimal (always in the Winsor III region). Results are shown in Fig. 14. As shown, optimal blend ratios achieved through experimental IFT measurements slightly differ from those previously obtained through solubilization parameters. Promising values of IFT, close to 0.01 mN/m in all cases, are found for the application of this blend at 25 °C.

4. Summary and conclusions

In this work, three blends (AOT/LF2, AOT/[C_{10}mim]Cl and AOT/[C_{12}mim]Br) were evaluated for EOR. Both the carboxylic acid and the SAILs can be used to balance the hydrophilic-lipophilic character of the surfactant blend, thus improving the properties of the overly lipophilic AOT for the application. In the case of the anionic (AOT) - cationic (SAILs) mixtures, the properties of the blend depend on the formation of electronically neutral complexes due to their opposite charges. Activity maps, representations of the type of phase behavior of the surfactants as a function of blend ratio, salinity and temperature, were found to be useful tools for a clear visualization of the conditions of interest for the application of blends to EOR.

4.1. AOT/LF2 blend

Among all the studied blends, AOT/LF2 was found to be the most salinity sensitive, with significant changes in both optimal blend ratio and solubilization parameters, as NaCl concentration varies.

The effect of salt was more significant in the case of blends with AOT concentrations higher than 65 wt%, at which the mixture behaved like anionic surfactants, and less significant for lower con-

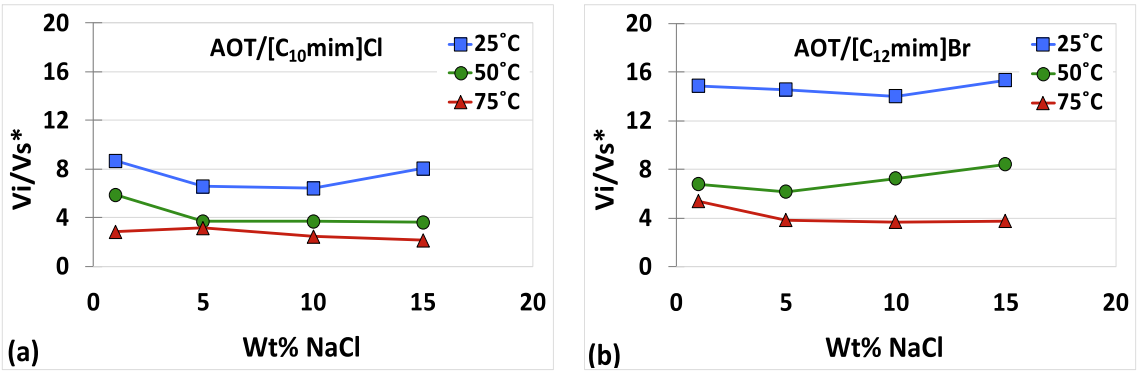


Fig. 13. Effect of salinity and temperature on the optimal solubilization parameters for (a) AOT/ [C_{10}mim]Cl blend and (b) AOT/[C_{12}mim]Br blend.

Table 2
Experimental and calculated, through Huh's equation, IFT for AOT/LF2 optimal blend ratios at 25 °C and different salinities.

Salinity (wt% NaCl)	Optimal mass ratio	Experimental IFT (mN/m)	Calculated IFT (mN/m)
1	84/16	1.51×10^{-2}	9.2×10^{-3}
5	53/47	1.21×10^{-2}	4.8×10^{-2}
10	39/61	1.23×10^{-2}	6.3×10^{-2}

centrations at which the behavior approached nonionic surfactants.

The main advantage of this blend lies in its low sensitivity to the blend ratio, allowing good performance even if there are changes in surfactant composition inside the reservoir. The increase of temperature led to middle microemulsions of low volumes and small solubilization parameters.

The application of this blend would be of interest at low temperatures. At 25 °C and the optimal blend ratios, IFTs close to 0.01 mN/m were found throughout all the range of salinities studied. Futures studies should focus on core flooding experiments to confirm the oil recovery capacity of the blend.

4.2. AOT/SAILs blends

Both AOT/SAILs performed similarly. With a behavior similar to nonionic surfactants, they were shown to be more tolerant to salinity changes. Thus, the variation of NaCl hardly affected optimal blend ratios or solubilization parameters. These last being higher, and promising, in the case of the SAIL of higher alkyl chain length.

As in the case of the blend with LF2, the increase of temperature led to wider Winsor III regions and lower solubilization parameters. However, problems of stability in the absence of oil, and the high sensitivity of these mixtures to blend ratio changes discourage, in principle, the use of these blends for practical applications.

CRediT authorship contribution statement

Nestor Tafur: experimental, analysis, first-draft writing. **Alba Somoza:** experimental orientation, editing. **Ana Soto:** conceptualization, supervision, writing, funding acquisition.

Declaration of Competing Interest

The authors declare that they have no known competing financial interests or personal relationships that could have appeared to influence the work reported in this paper.

Acknowledgements

The authors acknowledge the Ministry of Science and Innovation and State Research Agency (AEI, 10.13039/501100011033) for financial support throughout project PGC2018-097342-B-I00, including European Regional Development Fund. A. Somoza also acknowledges predoctoral financial support (grant ref. PRE2019-089101). We would also like to thank Kao Corporation S.A. for supplying the Akypo LF2 surfactant.

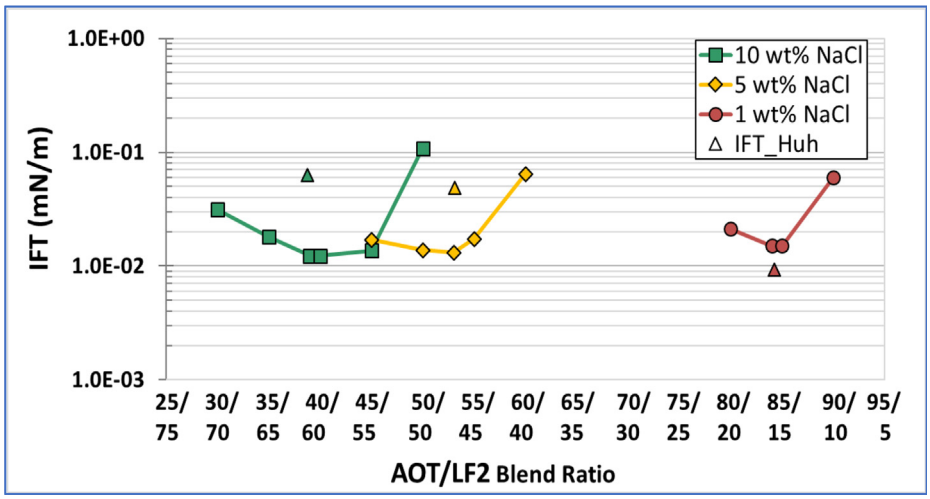


Fig. 14. IFT measurements for AOT/LF2 blend, as a function of blend ratio and salt concentration, at 25 °C.

References

[1] Y. Chen, Y. Lu, Features of O&G supply and demand and trend of E&D under the low oil price cycle, Soc. Pet. Eng. - SPE/IATMI Asia Pacific Oil Gas Conf. Exhib. 2019, APOG 2019. (2019) 1–9. https://doi.org/10.2118/196537-ms.

[2] IFP Energies Nouvelles, Exploration-production investments, Onshore and offshore drilling activities and markets, geophysics and offshore construction, 2019. https://www.ifpenergiesnouvelles.com/article/exploration-production-investments-onshore-and-offshore-drilling-activities-and-markets-geophysics-and-offshore-construction.

[3] M.J. Rosen, J.T. Kunjappu, Surfactants and interfacial phenomena, 4th ed., John Wiley & Sons, New Jersey, 2012.

[4] Y. Li, W. Zhang, K. Bailing, M. Puerto, X. Bao, S. Ou, S. Zhiqin, Y. Yiqing, L. Yanhua, G. Songyuan, C. Miller, G.J. Hirasaki, Mixtures of anionic/cationic surfactants: A new approach for enhanced oil recovery in low-salinity, high-temperature sandstone reservoir, SPE J. 21 (2016) 1164–1177, https://doi.org/10.2118/169051-pa.

[5] K. Spildo, A. Johannessen, A. Skauge, Low salinity waterflood at reduced capillarity, SPE - DOE Improv Oil Recover. Symp. Proc. 2 (2012) 1264–1276, https://doi.org/10.2118/154236-ms.

[6] J. Sheng, Enhanced oil recovery field case studies, 2nd ed., Elsevier Inc., Amsterdam, 2013.

[7] N. Ghadami, D. Arsanti, M. Faizal Sedaralit, Uncertainty assessment of chemical EOR in one of the offshore fields in Malaysia, Soc. Pet. Eng. - SPE Asia Pacific Enhanc. Oil Recover. Conf. EORC (2015. (2015)) 522–536, https://doi.org/10.2118/174614-ms.

[8] M.S. Kamal, I.A. Hussein, A.S. Sultan, Review on surfactant flooding: phase behavior, retention, IFT, and field applications, Energy and Fuels. 31 (2017) 7701–7720, https://doi.org/10.1021/acs.energyfuels.7b00353.

[9] D. Green, G.P. Willhite, Enhanced oil recovery, 2nd Ed, Society of Petroleum Engineers, Inc, Richardson, Texas, 2018.

[10] P.A. Winsor, Hydrotropy, solubilisation and related emulsification processes. Part I, Trans. Faraday Soc. 44 (1948) 376–398, https://doi.org/10.1039/tf9484400376.

[11] J.L. Salager, J.C. Morgan, R.S. Schechter, W.H. Wade, E. Vasquez, Optimum formulation of surfactant-water-oil systems for minimum interfacial tension or phase behaviour., Soc. Pet. Eng. J. 19 (1979) 107–115. https://doi.org/https://doi.org/10.2118/7054-PA.

[12] J. Sheng, Modern chemical enhanced oil recovery: Theory and practice, 2nd Ed., Elsevier Inc., Amsterdam, 2011.

[13] S. Bharadwaj, J.C. Ahluwalia, Mixed-surfactant system of dodecylbenzene sulfonate and alpha-olefin sulfonate: Micellar and volumetric studies, JAOCS, J. Am. Oil Chem. Soc. 73 (1996) 39–45, https://doi.org/10.1007/BF02523446.

[14] M.S. Bakshi, S. Sachar, N. Mahajan, I. Kaur, G. Kaur, N. Singh, P. Sehgal, H. Doe, Mixed-micelle formation by strongly interacting surfactant binary mixtures: Effect of head-group modification, Colloid Polym. Sci. 280 (2002) 990–1000, https://doi.org/10.1007/s00396-002-0717-9.

[15] I.J. Park, B.H. Lee, Mixed micellization of sodium dodecylbenzene sulfonate with polyoxyethylene lauryl ether surfactants (POLE4 and POLE23) in n-butanol aqueous solution, J. Surfactants Deterg. 15 (2012) 41–46, https://doi.org/10.1007/s11743-011-1287-y.

[16] P.M. Holland, D.N. Rubingh, Mixed surfactant systems, Fuel Sci. Technol. Int. 11 (1993) 241–242, https://doi.org/10.1080/08843759308916065.

[17] K. Holmberg, B. Jönsson, B. Kronberg, B. Lindman, Surfactants and polymers in aqueous solution., 2nd Ed, John Wiley & Sons, Ltd., Chichester, England, 2002. https://doi.org/10.1002/0470856424.

[18] T. Doan, E. Acosta, J.F. Scamehorn, D.A. Sabatini, Formulating middle-phase microemulsions using mixed anionic and cationic surfactant systems, J. Surfactants Deterg. 6 (2003) 215–224, https://doi.org/10.1007/s11743-003-0264-3.

[19] Y. Li, X. He, X. Cao, G. Zhao, X. Tian, X. Cui, Molecular behavior and synergistic effects between sodium dodecylbenzene sulfonate and Triton X-100 at oil/water interface, J. Colloid Interface Sci. 307 (2007) 215–220, https://doi.org/10.1016/j.jcis.2006.11.026.

[20] M. Puerto, G.J. Hirasaki, C.A. Miller, J.R. Barnes, Surfactant systems for EOR in high-temperature, high-salinity environments, SPE J. 17 (2012) 11–19, https://doi.org/10.2118/129675-PA.

[21] P. Ghosh, H. Sharma, K.K. Mohanty, Chemical flooding in low permeability carbonate rocks, Proc. - SPE Annu Tech. Conf. Exhib. (2017) 9–11, https://doi.org/10.2118/187274-ms.

[22] Y. Li, M. Puerto, X. Bao, W. Zhang, J. Jin, Z. Su, S. Shen, G. Hirasaki, C. Miller, Synergism and performance for systems containing binary mixtures of anionic/cationic surfactants for enhanced oil recovery, J. Surfactants Deterg. 20 (2017) 21–34, https://doi.org/10.1007/s11743-016-1892-x.

[23] J. Montes, N. Blin, A.E. Alvarez, I. Barrio, A. Panadero, R. Rodriguez, M. Coca, F. Trujillo, Novel anionic surfactant formulation for high temperature carbonate reservoirs, Soc. Pet. Eng. - SPE EOR Conf. Oil Gas West Asia (2018), https://doi.org/10.2118/190353-ms.

[24] R.E. Antón, D. Gómez, A. Graciaa, J. Lachaise, J.L. Salager, Surfactant-oil-water systems near the affinity inversion part IX: Optimum formulation and phase behavior of mixed anionic-cationic systems, J. Dispers. Sci. Technol. 14 (1993) 401–416, https://doi.org/10.1080/01932699308943413.

[25] A. Upadhyaya, E.J. Acosta, J.F. Scamehorn, D.A. Sabatini, Microemulsion phase behavior of anionic-cationic surfactant mixtures: Effect of tail branching, J. Surfactants Deterg. 9 (2006) 169–179, https://doi.org/10.1007/s11743-006-0387-6.

[26] G. Zhang, J. Yu, C. Du, R. Lee, Formulation of surfactants for very low/high salinity surfactant flooding without alkali, Proc. - SPE Int. Symp. Oilf. Chem. 1 (2015) 399–414, https://doi.org/10.2118/173738-ms.

[27] I. Rodriguez-Escontrela, M.C. Puerto, C.A. Miller, A. Soto, Ionic liquids for low-tension oil recovery processes: phase behavior tests, J. Colloid Interface Sci. 504 (2017) 404–416, https://doi.org/10.1016/j.jcis.2017.05.102.

[28] E.Y. Sheu, S.H. Chen, J.S. Huang, Structure and growth of Bis(2-ethylhexyl) sulfosuccinate micelles in aqueous solutions, J. Phys. Chem. 91 (1987) 3306–3310, https://doi.org/10.1021/j100290a049.

[29] B. Wu, B.J. Shiau, D.A. Sabatini, J.H. Harwell, D.Q. Vu, Formulating microemulsion systems for a weathered jet fuel waste using surfactant/cosurfactant mixtures, Sep. Sci. Technol. 35 (2000) 1917–1937, https://doi.org/10.1081/SS-100100627.

[30] W. Wan, J. Zhao, J.H. Harwell, B.-J. Shiau, Characterization of crude oil equivalent alkane carbon number (EACN) for surfactant flooding design, J. Dispers. Sci. Technol. 37 (2) (2016) 280–287.

[31] C. Negin, S. Ali, Q. Xie, Most common surfactants employed in chemical enhanced oil recovery, Petroleum. 3 (2017) 197–211, https://doi.org/10.1016/j.petlm.2016.11.007.

[32] P. Denk, A. El Maangar, J. Lal, D. Kleber, T. Zemb, W. Kunz, Phase diagrams and microstructures of aqueous short alkyl chain polyethylene glycol ether carboxylate and carboxylic acid triblock surfactant solutions, J. Colloid Interface Sci. 590 (2021) 375–386, https://doi.org/10.1016/j.jcis.2021.01.061.

[33] A.Z. Hezave, S. Dorostkar, S. Ayatollahi, M. Nabipour, B. Hemmateenejad, Investigating the effect of ionic liquid (1-dodecyl-3-methylimidazolium chloride ([C12mim] [Cl])) on the water/oil interfacial tension as a novel surfactant, Colloids Surfaces A Physicochem. Eng. Asp. 421 (2013) 63–71, https://doi.org/10.1016/j.colsurfa.2012.12.008.

[34] A.Z. Hezave, S. Dorostkar, S. Ayatollahi, M. Nabipour, B. Hemmateenejad, Effect of different families (imidazolium and pyridinium) of ionic liquids-based surfactants on interfacial tension of water/crude oil system, Fluid Phase Equilib. 360 (2013) 139–145, https://doi.org/10.1016/j.fluid.2013.09.025.

[35] S. Sakthivel, S. Velusamy, R.L. Gardas, J.S. Sangwai, Use of aromatic ionic liquids in the reduction of surface phenomena of crude oil-water system and their synergism with brine, Ind. Eng. Chem. Res. 54 (2015) 968–978, https://doi.org/10.1021/ie504331k.

[36] A.K. Manshad, M. Rezaei, S. Moradi, I. Nowrouzi, A.H. Mohammadi, Wettability alteration and interfacial tension (IFT) reduction in enhanced oil recovery (EOR) process by ionic liquid flooding, J. Mol. Liq. 248 (2017) 153–162, https://doi.org/10.1016/j.molliq.2017.10.009.

[37] P. Pillai, A. Kumar, A. Mandal, Mechanistic studies of enhanced oil recovery by imidazolium-based ionic liquids as novel surfactants, J. Ind. Eng. Chem. 63 (2018) 262–274, https://doi.org/10.1016/j.jiec.2018.02.024.

[38] A. Somoza, A. Arce, A. Soto, Oil recovery tests with ionic liquids: a review and evaluation of 1-decyl-3-methylimidazolium triflate, Pet. Sci. (2021), https://doi.org/10.1016/j.petsci.2021.10.025.

[39] H. Jia, X. Leng, M. Hu, Y. Song, H. Wu, P. Lian, Y. Liang, Y. Zhu, J. Liu, H. Zhou, Systematic investigation of the effects of mixed cationic/anionic surfactants on the interfacial tension of a water/model oil system and their application to enhance crude oil recovery, Colloids Surfaces A Physicochem. Eng. Asp. 529 (2017) 621–627, https://doi.org/10.1016/j.colsurfa.2017.06.055.

[40] S.K. Nandwani, M. Chakraborty, H.J. Bart, S. Gupta, Synergism, phase behaviour and characterization of ionic liquid-nonionic surfactant mixture in high salinity environment of oil reservoirs, Fuel. 229 (2018) 167–179, https://doi.org/10.1016/j.fuel.2018.05.021.

[41] A. Somoza, N. Tafur, A. Arce, A. Soto, Design and performance analysis of a formulation based on SDBS and ionic liquid for EOR in carbonate reservoirs, J. Pet. Sci. Eng. 209 (2022), https://doi.org/10.1016/j.petrol.2021.109856 109856.

[42] J.R. Barnes, J.P. Smit, J.R. Smit, P.G. Shpakoff, K.H. Raney, M.C. Puerto, Development of surfactants for chemical flooding at difficult reservoir conditions, SPE Symp. Improv. Oil Recover. 1 (2008) 435–452, https://doi.org/10.2118/113313-ms.

[43] C. Huh, Interfacial tensions and solubilizing ability of a microemulsion phase that coexists with oil and brine, J. Colloid Interface Sci. 71 (1979) 408–426, https://doi.org/10.1016/0021-9797(79)90249-2.

[44] R.C. Nelson, J.B. Lawson, D.R. Thigpen, G.L. Stegemeier, Cosurfactant-Enhanced Alkaline Flooding, Soc. Pet. Eng. AIME. (1984) 413–424, https://doi.org/10.2118/12672-ms.

[45] G. Kume, M. Gallotti, G. Nunes, Review on anionic/cationic surfactant mixtures, J. Surfactants Deterg. 11 (2008) 1–11, https://doi.org/10.1007/s11743-007-1047-1.

[46] R.K. Mahajan, D. Nandni, Micellization and phase behavior of binary mixtures of anionic and nonionic surfactants in aqueous media, Ind. Eng. Chem. Res. 51 (2012) 3338–3349, https://doi.org/10.1021/ie202463w.

[47] S. Novak, S. Morasi Piperčić, S. Makarić, I. Primožič, M. Ćurlin, Z. Štefanić, D. Domazet Jurašin, Interplay of noncovalent interactions in ionic liquid/sodium bis(2-ethylhexyl) sulfosuccinate mixtures: from lamellar to bicontinuous cubic liquid crystalline phase, J. Phys. Chem. B. 120 (2016) 12557–12567, https://doi.org/10.1021/acs.jpcb.6b10515.

[48] M.T. Garcia, I. Ribosa, J.J. González, F. Comelles, Surface activity, self-aggregation and antimicrobial activity of catanionic mixtures of surface active imidazolium- or pyridinium-based ionic liquids and sodium bis(2-

ethylhexyl) sulfosuccionate, J. Mol. Liq. 303 (2020), https://doi.org/10.1016/j.molliq.2020.112637 112637.
[49] J.L. Salager, A.M. Forgiarini, J. Bullón, How to attain ultralow interfacial tension and three-phase behavior with surfactant formulation for enhanced oil recovery: a review. Part 1. Optimum formulation for simple surfactant-oil-water ternary systems, J. Surfactants Deterg. 16 (2013) 449–472, https://doi.org/10.1007/s11743-013-1470-4.
[50] R.E. Antón, J.M. Andérez, C. Bracho, F. Vejar, J.L. Salager, Practical surfactant mixing rules based on the attainment of microemulsion-oil-water three-phase behavior systems, Adv. Polym. Sci. 218 (2008) 83–113, https://doi.org/10.1007/12_2008_163.
[51] C.L. Sassen, A. Gonzalez Casielles, T.W. de Loos, J. de Swaan Arons, The influence of pressure and temperature on the phase behaviour of the system H2O + C12+ C7E5 and relevant binary subsystems, Fluid Phase Equilib. 72 (1992) 173–187, https://doi.org/10.1016/0378-3812(92)85025-4.
[52] R.E. Antón, A. Graciaa, J. Lachaise, J.L. Salager, Surfactant-oil-water systems near the affinity inversion, Part VIII: Optimum formulation and phase behavior of mixed anionic-nonionic systems versus temperature, J. Dispers. Sci. Technol. 13 (1992) 565–579, https://doi.org/10.1080/01932699208943334.
[53] K.-H. Oh, J.R. Baran, W.H. Wade, V. Weerasooriya, Temperature insensitive microemulsion phase behavior with non-ionic surfactants, J. Dispers. Sci. Technol. 16 (2) (1995) 165–188.
[54] M.G. Aarra, H. Høiland, A. Skauge, Phase behavior and salt partitioning in two- and three-phase anionic surfactant microemulsion systems: Part I, phase behavior as a function of temperature, J. Colloid Interface Sci. 215 (1999) 201–215, https://doi.org/10.1006/jcis.1999.6228.

USC UNIVERSIDADE DE SANTIAGO DE COMPOSTELA

Journal of Molecular liquid

Evaluation of surfactant blends for Enhanced Oil Recovery through activity maps

Nestor Tafur, Alba Somoza, Ana Soto*
CRETUS. Department of Chemical Engineering, Universidade de Santiago de Compostela, E-15782, Santiago de Compostela, Spain.

SUPPLEMENTARY INFORMATION

1. Salinity scans for Akypo LF2 and [C_{10}mim]Cl.

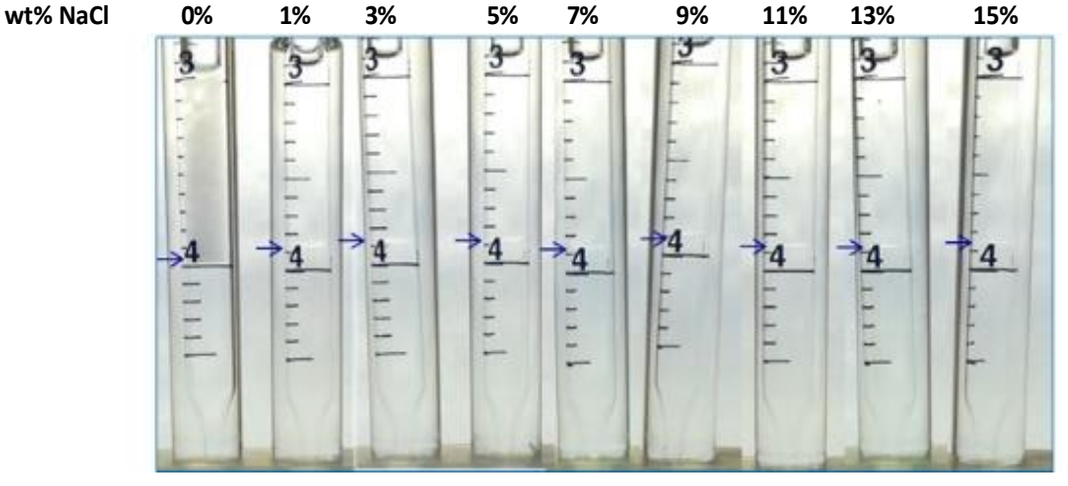


Figure S1. Salinity scan for Akypo LF2 at 25 °C.

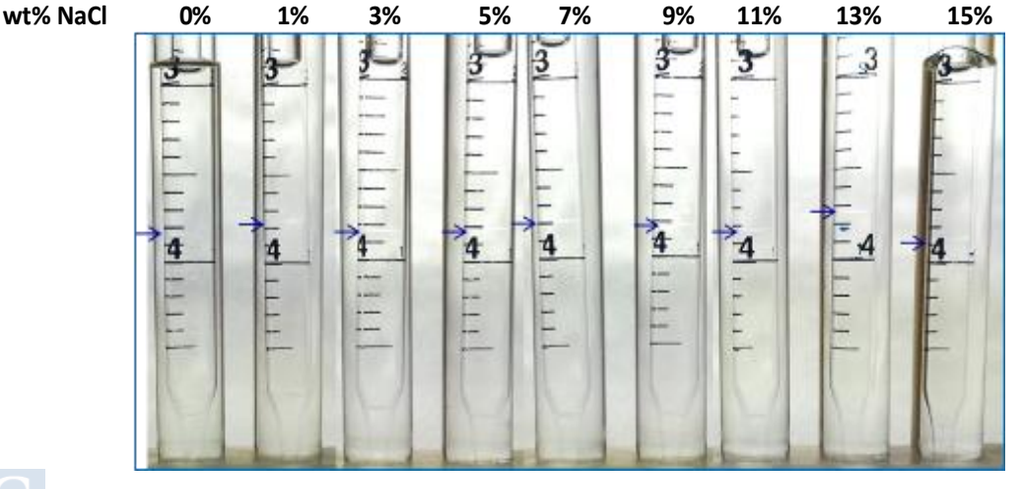


Figure S2. Salinity scan for [C_{10}mim]Cl at 25 °C.

2. Comparison of activity maps for the studied blends.

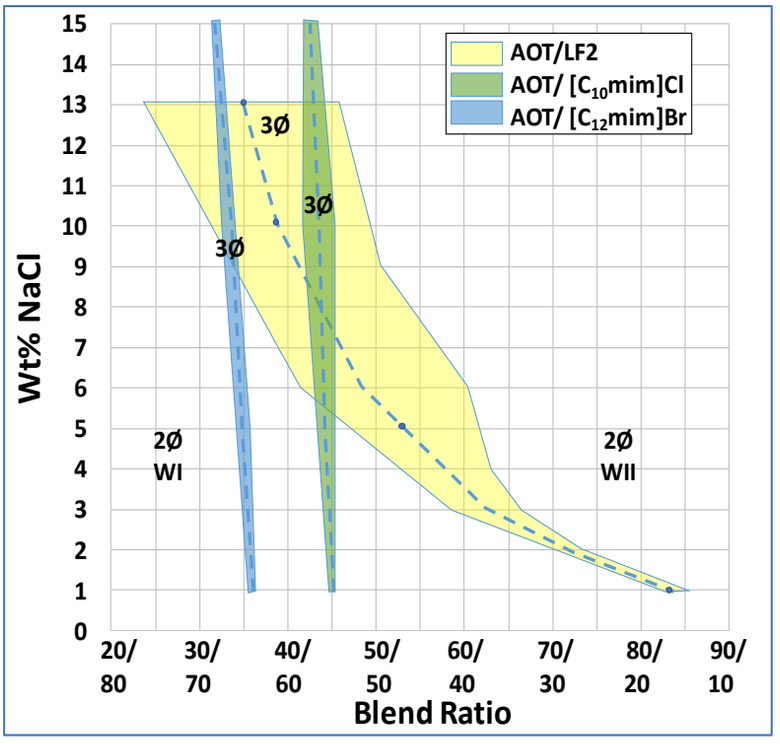


Figure S3. Activity maps for AOT/LF2 (yellow color), AOT/ [C_{10}mim]Cl (green color), and AOT/[C_{12}mim]Br (blue color) blends at 25°C. Blue dashed line represents optimal blend ratios.

USC
UNIVERSIDADE DE SANTIAGO DE COMPOSTELA

3. Blend scans and solubilization parameters for AOT/LF2, AOT/[C_{10}mim]Cl and AOT/[C_{12}mim]Br blends at different salinities and temperatures.

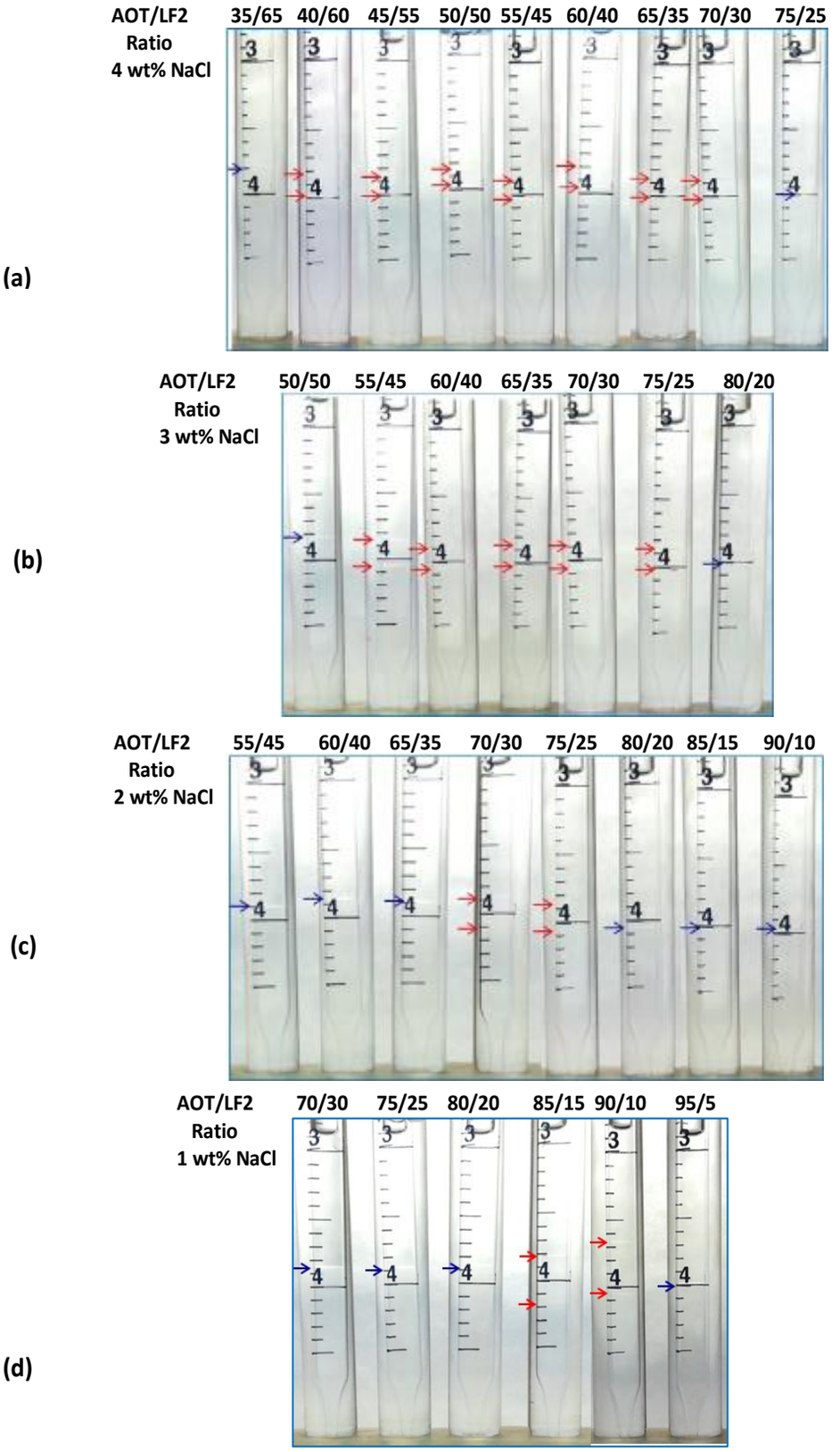
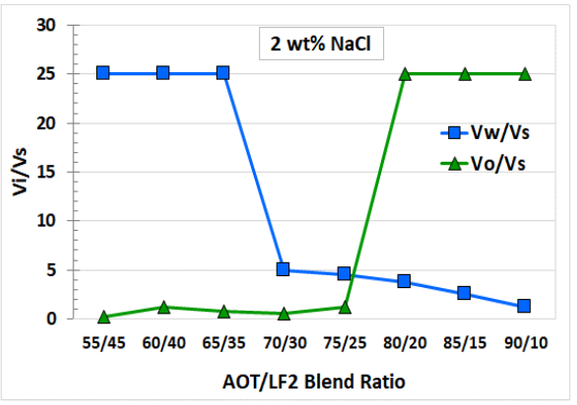


Figure S4. Blend scans for AOT/LF2 at 50°C and at salinity concentration of (a) 4 wt%, (b) 3 wt%, (c) 2 wt% and (d) 1 wt% NaCl.

USC UNIVERSIDADE DE SANTIAGO DE COMPOSTELA

(a)



(b)

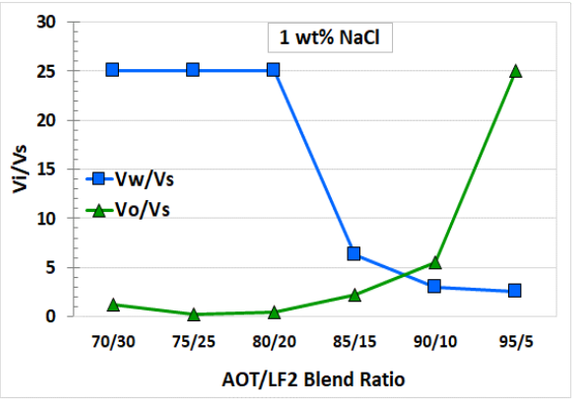


Figure S5. Solubilization parameters (V_i/V_s) for AOT/LF2 at 50°C and at salinity concentration of (a) 2 wt% and (b) 1 wt% NaCl.

USC
UNIVERSIDADE DE SANTIAGO DE COMPOSTELA

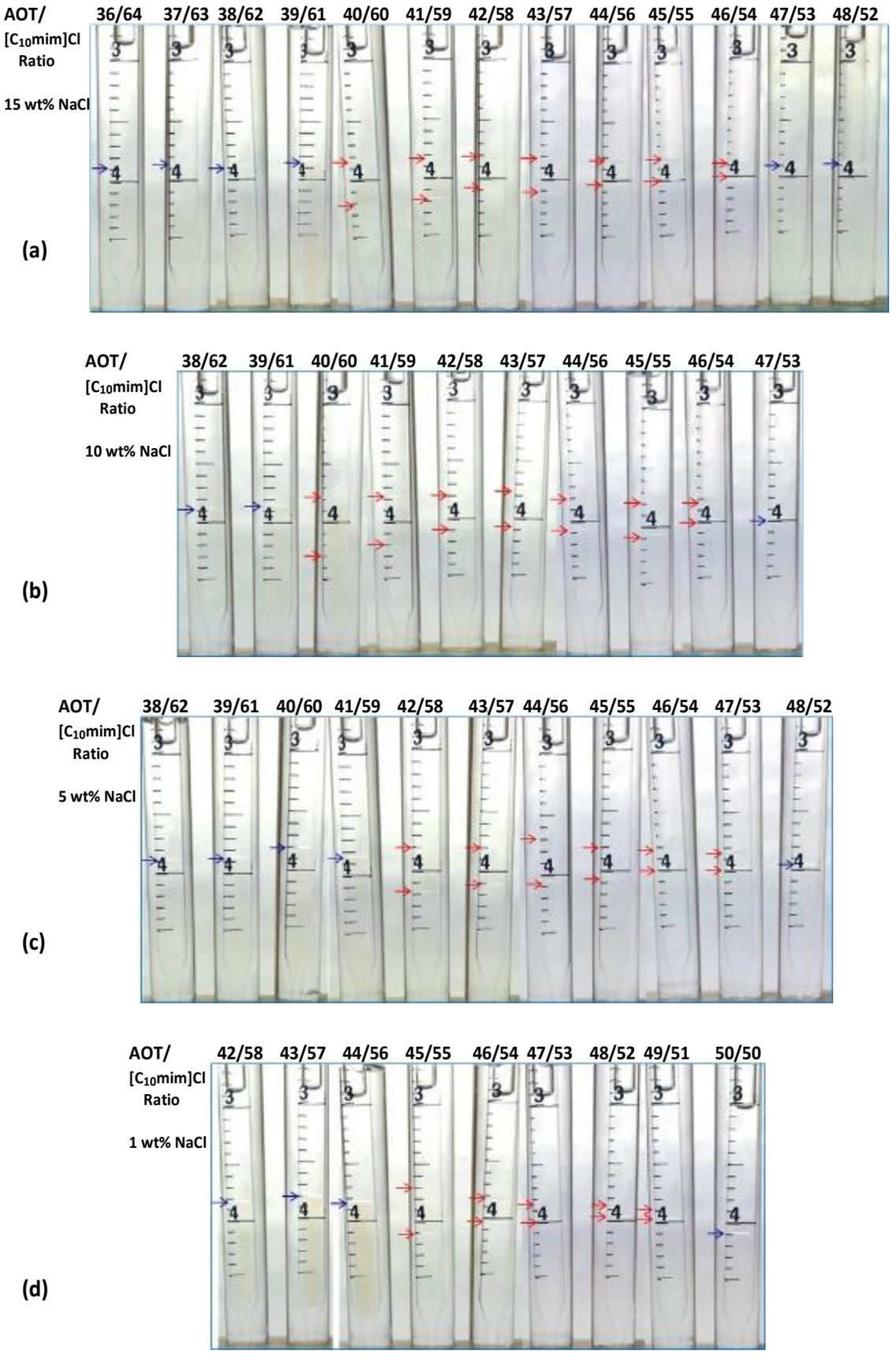
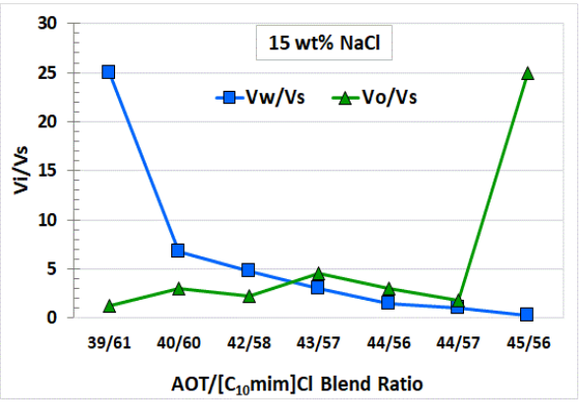


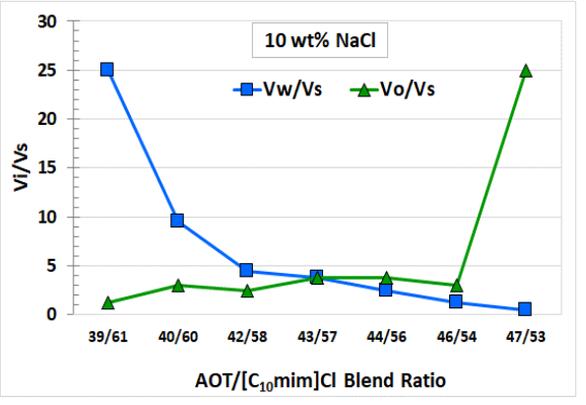
Figure S6. Blend scans for AOT/[C_{10}mim]Cl at 50°C and at salinity concentration of (a) 15 wt%, (b) 10 wt%, (c) 5 wt% and (d) 1 wt% NaCl.

USC UNIVERSIDADE DE SANTIAGO DE COMPOSTELA

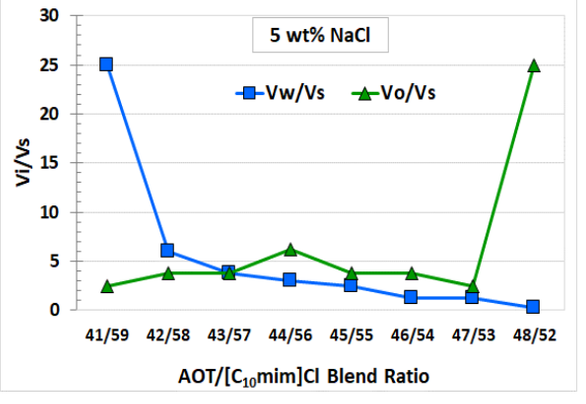
(a)



(b)



(c)



(d)

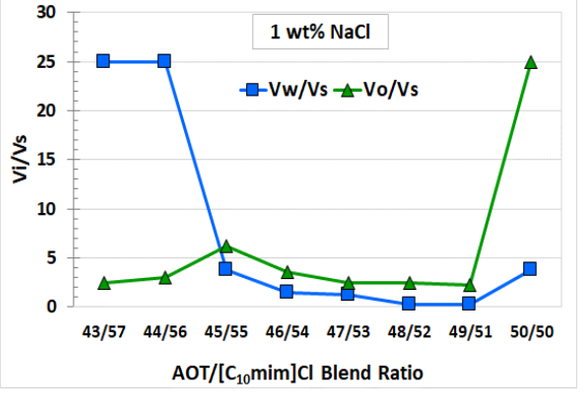


Figure S7. Solubilization parameters (V_i/V_s) for AOT/[C_{10}mim]Cl at 50°C and at salinity concentration of (a) 15 wt%, (b) 10 wt%, (c) 5 wt% and (d) 1 wt% NaCl.

USC UNIVERSIDADE DE SANTIAGO DE COMPOSTELA

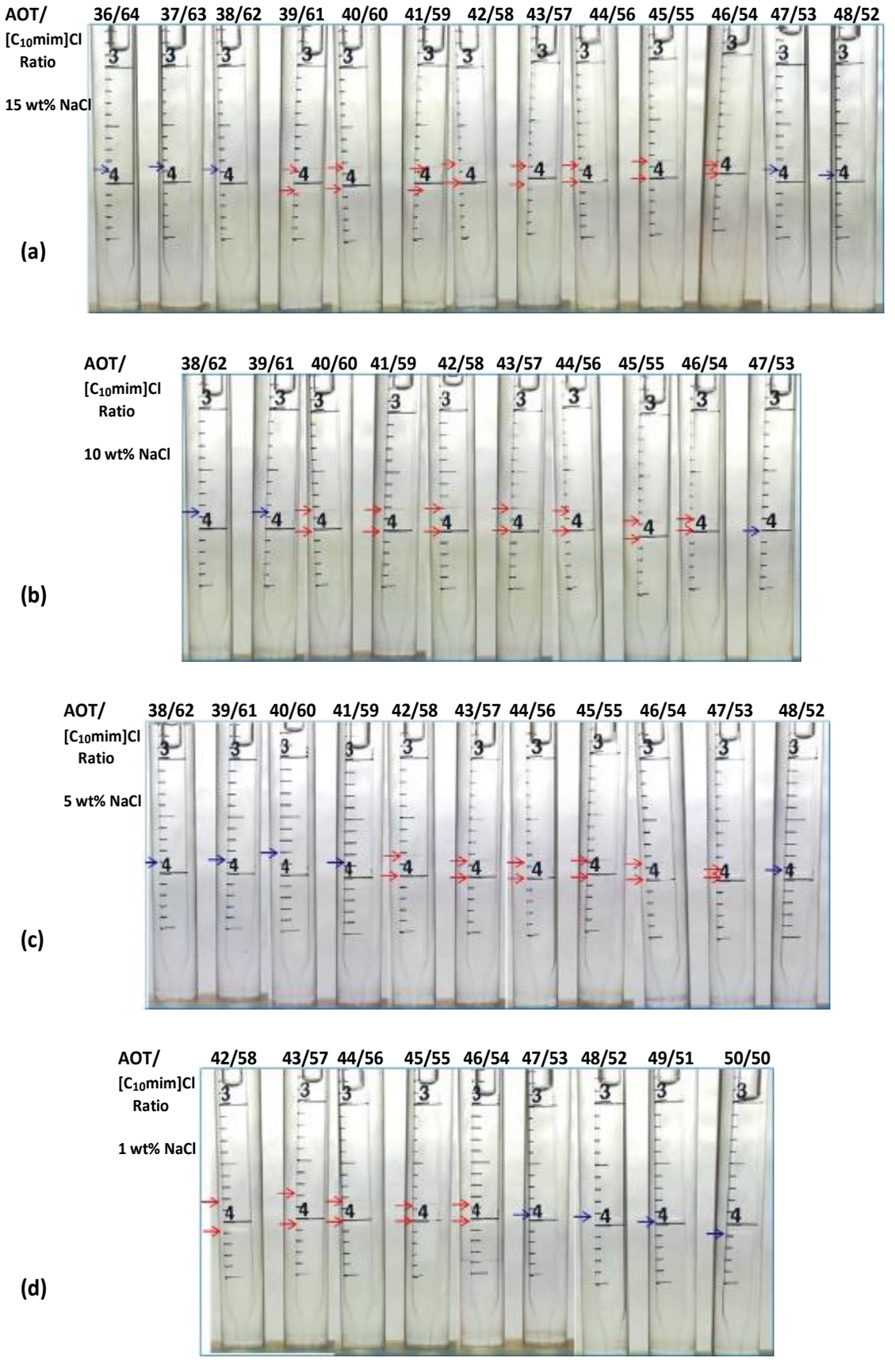
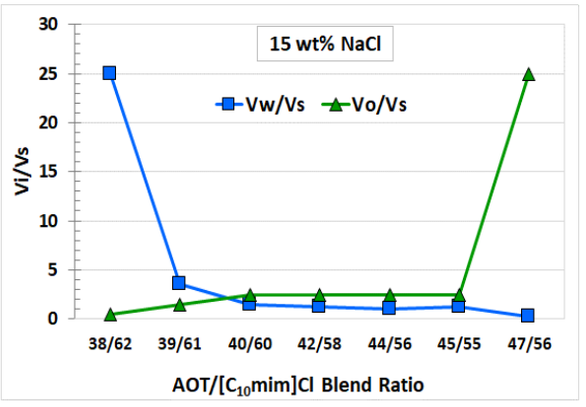


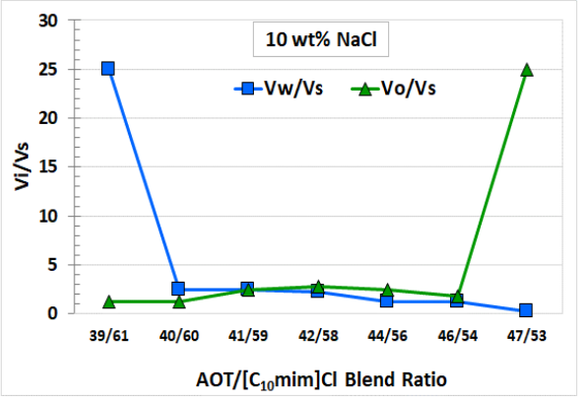
Figure S8. Blend scans for AOT/[C_{10}mim]Cl at 75°C and at salinity concentration of (a) 15 wt%, (b) 10 wt%, (c) 5 wt% and (d) 1 wt% NaCl.

USC UNIVERSIDADE DE SANTIAGO DE COMPOSTELA

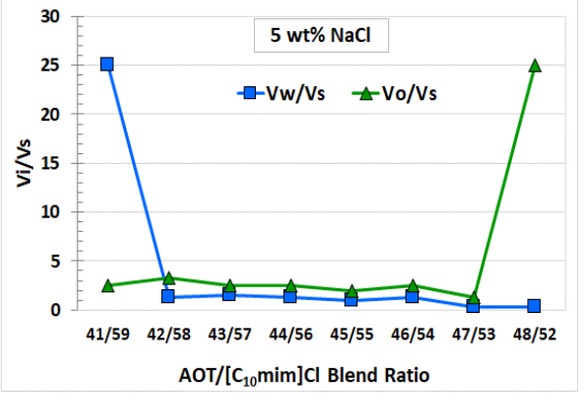
(a)



(b)



(c)



(d)

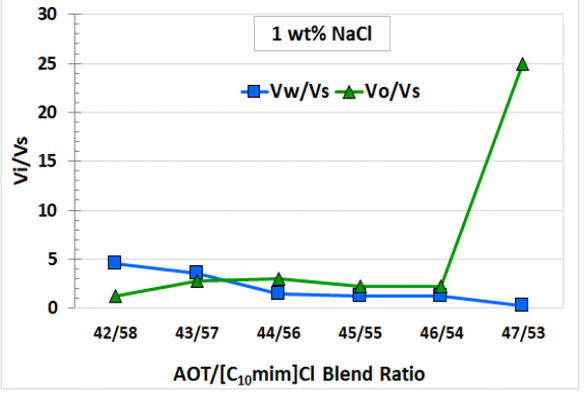


Figure S9. Solubilization parameters (V_i/V_s) for AOT/[C_{10}mim]Cl at 75°C and at salinity concentration of (a) 15 wt%, (b) 10 wt%, (c) 5 wt% and (d) 1 wt% NaCl.

USC UNIVERSIDADE DE SANTIAGO DE COMPOSTELA

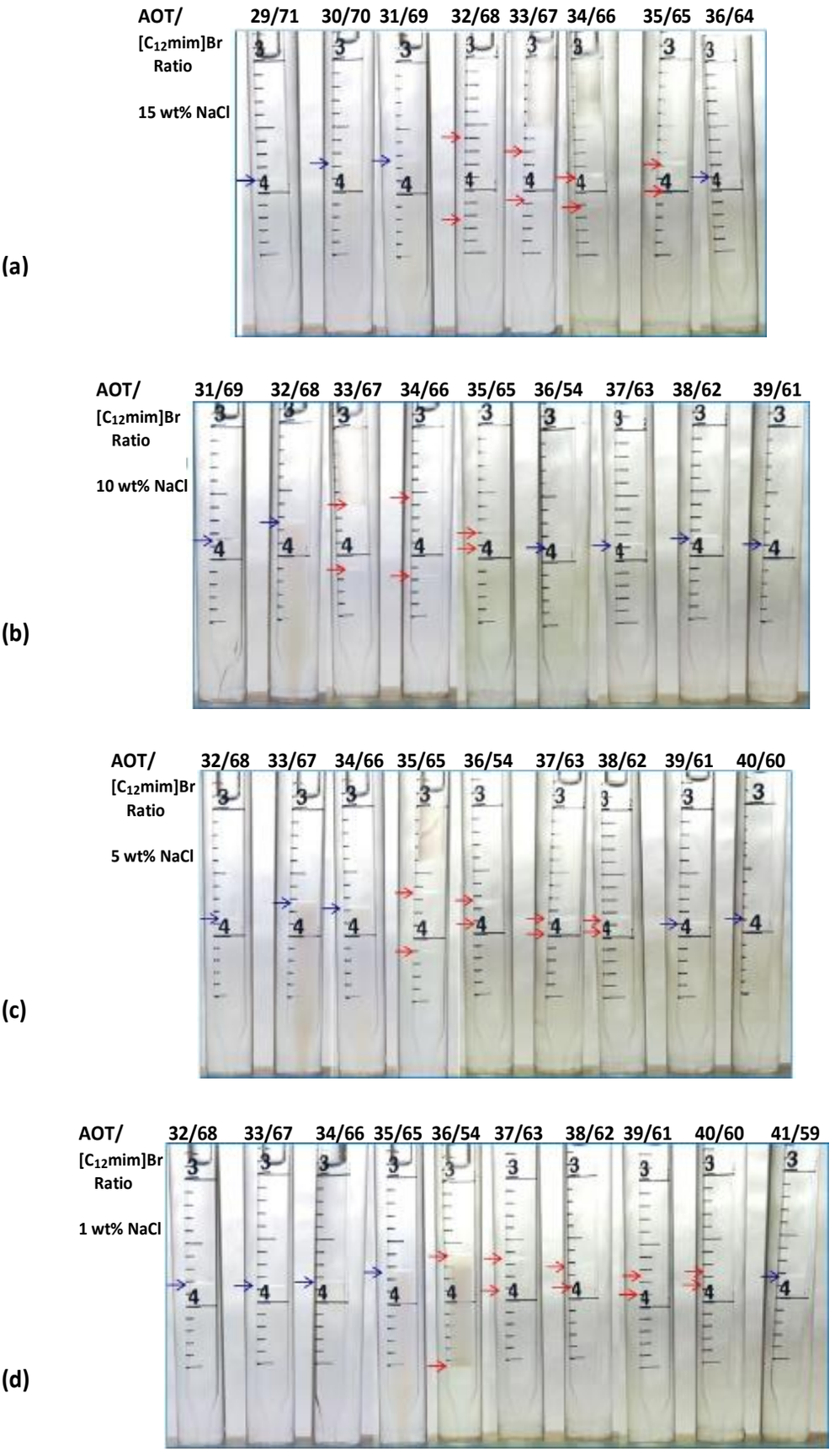
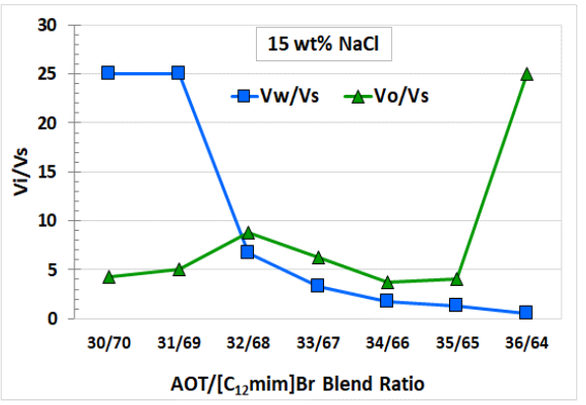


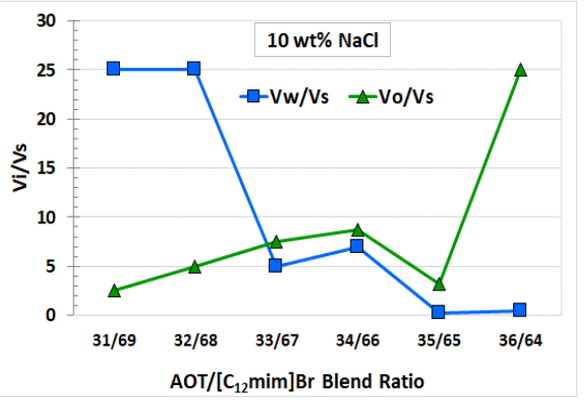
Figure S10. Blend scans for AOT/[C_{12}mim]Br at 50°C and at salinity concentration of (a) 15 wt%, (b) 10 wt%, (c) 5 wt% and (d) 1 wt% NaCl.

USC UNIVERSIDADE DE SANTIAGO DE COMPOSTELA

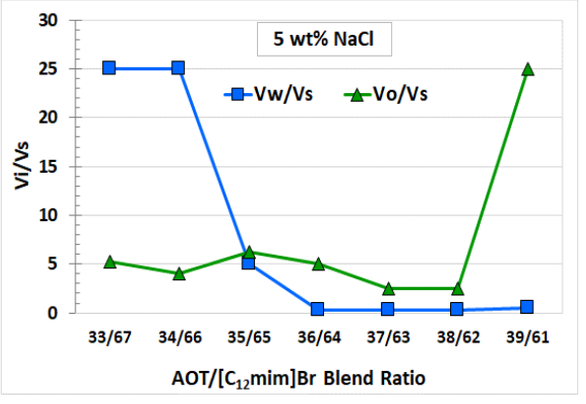
(a)



(b)



(c)



(d)

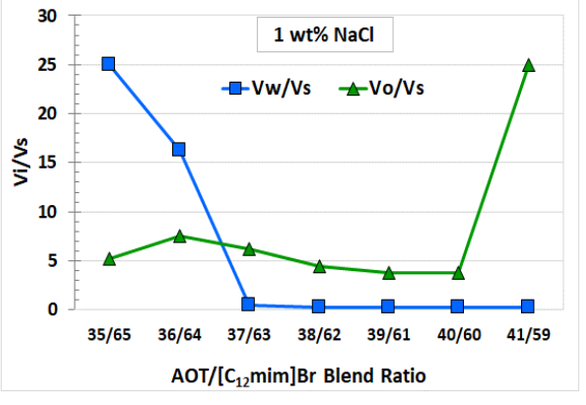


Figure S11. Solubilization parameters (V_i/V_s) for AOT/[C_{12}mim]Br at 50°C and at salinity concentration of (a) 15 wt%, (b) 10 wt%, (c) 5 wt% and (d) 1 wt% NaCl.

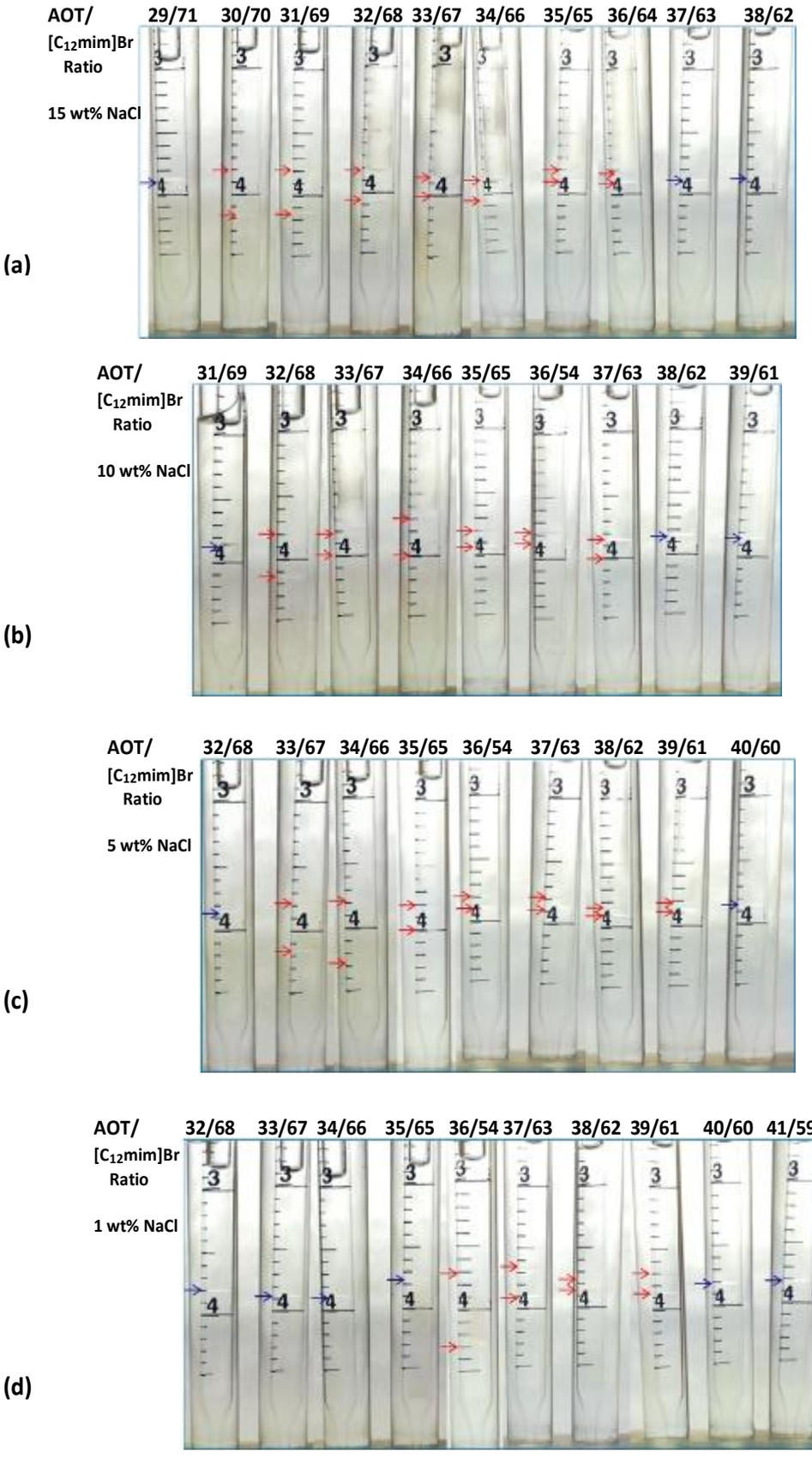
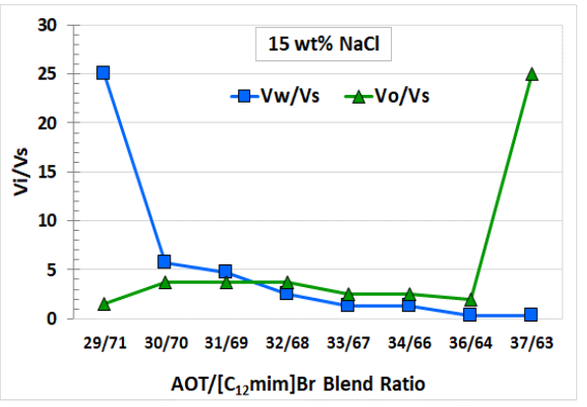


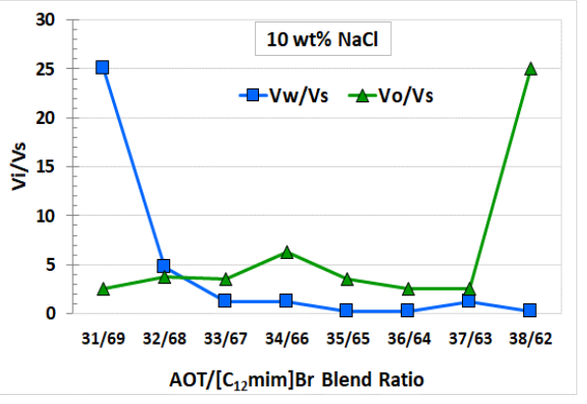
Figure S12. Blend scan for AOT/[C_{12}mim]Br at 75°C and at salinity concentration of (a) 15 wt%, (b) 10 wt%, (c) 5 wt% and (d) 1 wt% NaCl.

USC UNIVERSIDADE DE SANTIAGO DE COMPOSTELA

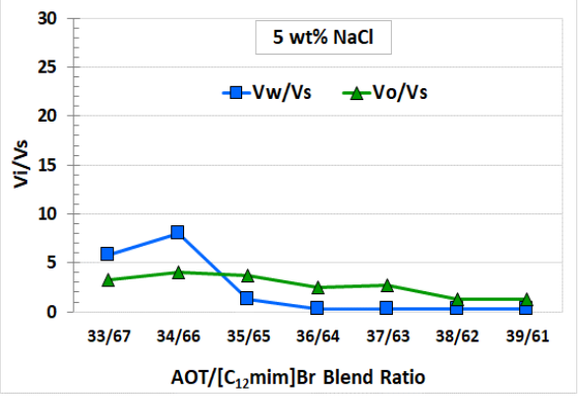
(a)



(b)



(c)



(d)

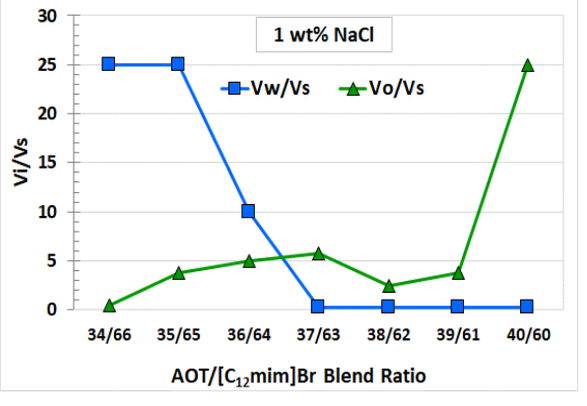


Figure S13. Solubilization parameters (V_i/V_s) for AOT/[C_{12}mim]Br at 75°C and at salinity concentration of (a) 15 wt%, (b) 10 wt%, (c) 5 wt% and (d) 1 wt% NaCl.

USC UNIVERSIDADE DE SANTIAGO DE COMPOSTELA

International Journal of
Molecular Sciences

MDPI

Article

Improvement of a Surfactant Blend for Enhanced Oil Recovery in Carbonate Reservoirs by Means of an Ionic Liquid

Nestor Tafur [1], Alberto P. Muñuzuri [2] and Ana Soto [1,*]

[1] CRETUS, Department of Chemical Engineering, Universidade de Santiago de Compostela, 15782 Santiago de Compostela, Spain
[2] Group of Nonlinear Physics, Galician Center for Mathematical Research and Technology (CITMAga), 15782 Santiago de Compostela, Spain
* Correspondence: ana.soto@usc.es

Abstract: The promising experimental performance of surfactant blends encourages their use in recovering the large quantity of crude oil still remaining in carbonate reservoirs. Phase behavior studies were carried out in this work to propose a blend for practical application. To that aim, the surfactants dioctyl sulfosuccinate sodium (AOT) and polyoxyethylene(8) octyl ether carboxylic acid (Akypo LF2) were mixed. A formulation consisting of 1 wt% of $AOT_{50wt\%}/LF2_{50wt\%}$ blend in synthetic sea water (SSW) led to a low value of interfacial tension with crude oil of $1.50 \cdot 10^{-2}$ mN/m, and 0.42 mg/g_{rock} of dynamic adsorption. A moderate additional oil recovery (7.3% of the original oil in place) was achieved in a core flooding test. To improve this performance, the surface-active ionic liquid 1-dodecyl-3-methylimidazolium bromide ($[C_{12}mim]Br$) was added to the system. The electrostatic interactions between the oppositely charged surfactants (AOT and $[C_{12}mim]Br$) led to a higher surface activity. Thus, a formulation consisting of 0.8 wt% of $AOT_{20.7wt\%}/[C_{12}mim]Br_{25.3wt\%}/LF2_{54wt\%}$ in SSW reduced the interfacial tension and surfactant adsorption achieved with the binary blend to 1.14×10^{-2} mN/m and 0.21 mg/g_{rock}, respectively. The additional oil recovery achieved with the blend containing the ionic liquid was 11.5% of the original oil in place, significantly improving the efficiency of the binary blend.

Keywords: blend; microemulsion; Winsor III; ionic liquid; surfactant flooding

check for updates

Citation: Tafur, N.; Muñuzuri, A.P.; Soto, A. Improvement of a Surfactant Blend for Enhanced Oil Recovery in Carbonate Reservoirs by Means of an Ionic Liquid. *Int. J. Mol. Sci.* **2023**, *24*, 726. https://doi.org/10.3390/ijms24010726

Academic Editors: Senentxu Lanceros-Mendez, Carlos Miguel Costa and Daniela M. Correia

Received: 30 November 2022
Revised: 23 December 2022
Accepted: 27 December 2022
Published: 31 December 2022

Copyright: © 2022 by the authors. Licensee MDPI, Basel, Switzerland. This article is an open access article distributed under the terms and conditions of the Creative Commons Attribution (CC BY) license (https://creativecommons.org/licenses/by/4.0/).

1. Introduction

Although surfactant flooding has been studied and used as an effective enhanced oil recovery (EOR) method for sandstone rock reservoirs [1], the use of surfactants in carbonate rocks has been limited because of their high adsorption on the rock surface (anionic surfactants) and their inability to reduce the interfacial tension (IFT) to ultralow values (cationic and nonionic surfactants) [2–6]. Since carbonate rock reservoirs represent around 50–60% of the total oil around the world [7,8], several methods such as the use of low salinity water and nanoparticles are being tested for their exploitation [9]. However, the successful application in this kind of reservoir of the traditionally most efficient surfactants for EOR would be of high interest, which is why this has been the target of many studies. Among the tested possibilities, several works have taken advantage of the better performance of surfactant blends in comparison with their pure components used individually. These mixtures commonly show a synergistic effect on the reduction of interfacial tension between water and oil, and in some cases, surfactant adsorption on the rock surface is also reduced [10–14].

In our previous work [15], the phase behavior of three binary blends was studied at different salinity and temperature conditions. An anionic/nonionic blend was formulated with dioctyl sulfosuccinate sodium salt (AOT) and polyoxyethylene(8) octyl ether carboxylic acid (Akypo LF2). AOT is an anionic surfactant with a high lipophilic character [16–18]. Akypo LF2 is a triblock alkyl ethoxy carboxylate surfactant, tolerant to high

salinity and long-term stable at high temperature, with a hydrophilic character [19–21]. Thus, a hydrophilic-lipophilic balance associated with a Winsor III behavior [22] was achieved blending both chemicals. In the same work [15], two anionic/cationic blends were formulated with AOT and surface-active ionic liquids (SAILs). These salts have been found promising for EOR applications [23–27]. However, they are usually not able to achieve ultra-low IFT by themselves. As far as we know, only one work can be found in the literature [28] where a Winsor type III system was achieved with a single SAIL: (S)-2-prolinolium dodecylbenzene sulfonate. Therefore, their blending with other surfactants is a technique that is gaining attention for EOR purposes [26,29,30]. Blends of AOT and 1-decyl-3-methylimidazolium chloride ([C_{10}mim]Cl) or 1-dodecyl-3-methylimidazolium bromide ([C_{12}mim]Br) led to Winsor III systems [15]. The AOT/SAIL blends showed high optimal solubilization parameters (good capacity to solubilize oil and water at the same proportion) but were unstable in the absence of oil, so they only could be injected in the reservoir as microemulsions. In contrast, the AOT/LF2 blend showed good stability in brine and lower sensitivity to blend ratio changes, but lower optimal solubilization parameters than the AOT/SAIL blends.

The purpose of the present work is to evaluate the AOT/LF2 blend for EOR by means of core flooding tests, and also to test the possibility of improving the blend's efficiency by adding SAIL [C_{12}mim]Br. On one hand, this ternary mixture would take advantage of the strong electrostatic interactions between oppositely charged surfactant head groups of AOT and [C_{12}mim]Br, leading to catanionic micelle formation with higher surface activity and greater capacity of solubilization than the individual surfactants [15,26,27,30–33]. On the other hand, the incorporation of LF2 would provide stability under harsh salinity and temperature conditions [19–21].

2. Results and Discussion

2.1. Experimental Section

2.1.1. Blend Scans

The surfactant LF2 and the ionic liquid [C_{12}mim]Br are highly hydrophilic, showing microemulsion Winsor type I (according to Winsor's classification) from 1 to 15 wt% NaCl and from 25 to 75 °C [15]. The surfactant AOT is highly lipophilic, being Winsor type II from 0.21 wt% NaCl [15,26]. The pseudo-component A-C (45 wt% AOT, 55 wt% [C_{12}mim]Br) was found to be lipophilic, with a Winsor type II behavior in SSW at 25 °C (See Supporting Information, SI). Figure 1 shows the AOT/LF2 and A-C/LF2 blend scans at 25°C. Winsor type I microemulsions were obtained from 0 to 40 wt% AOT in the AOT/LF2 blend (Figure 1a). Winsor type III was observed at 50 wt% AOT, and the microemulsion shifted to Winsor type II at 60 wt% and higher AOT concentrations. Precipitation and high viscosity emulsions were observed for blends with high AOT proportions. A similar phase behavior was observed for the A-C/LF2 blend (Figure 1b), the difference being that the volume of the middle phase (shown in the figure between red arrows) was higher for this ternary blend. The behavior of the AOT/LF2 slightly differs from our previous study [15] where *n*-octane was used as the oil phase, and brine solution (5 wt% NaCl without divalent ions) as the aqueous phase. The Winsor III region found in tests with crude oil was slightly smaller. As expected, the capacity of solubilization of the blend is affected by the different compounds of the crude [12,17,32,34–37].

The blends were also evaluated at 50 °C and 75 °C. The results are shown in Figures 2 and 3 for AOT/LF2 and A-C/LF2, respectively. In the case of the AOT/LF2 blend, the range of ratios where Winsor III systems were found increased with temperature. At 50 °C, triphasic systems were found from 50 to 60 wt% AOT, and at 75 °C, from 10 to 70 wt% AOT (Figure 2). However, the volume of the middle phase slightly reduced with temperature. Similar behavior was found for the A-C/LF2 blend: in a range between 10 and 40 wt% A-C, small Winsor type III systems were found (Figure 3). No further studies were carried out at 75 °C since both blends showed loss of efficiency to solubilize water and oil phases.

USC UNIVERSIDADE DE SANTIAGO DE COMPOSTELA

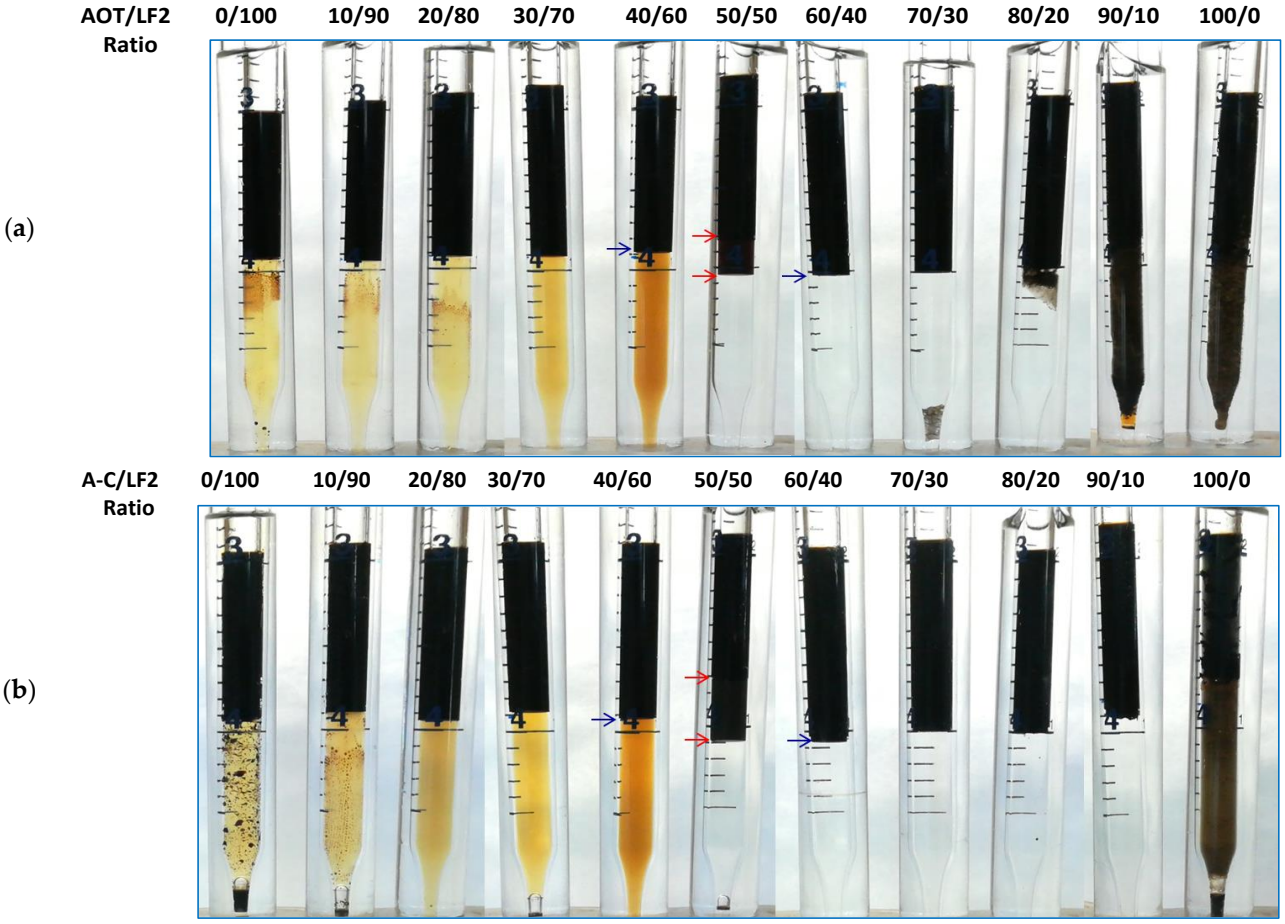


Figure 1. Blend scans at 25 °C: (**a**) AOT/LF2 and (**b**) A-C/LF2.

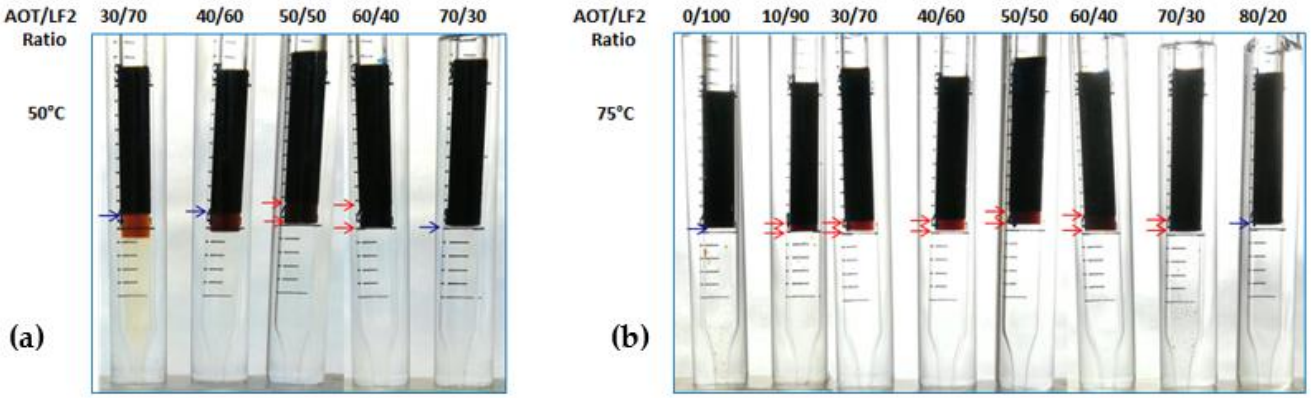


Figure 2. AOT/LF2 blend scans at (**a**) 50 °C and (**b**) 75 °C.

USC UNIVERSIDADE DE SANTIAGO DE COMPOSTELA

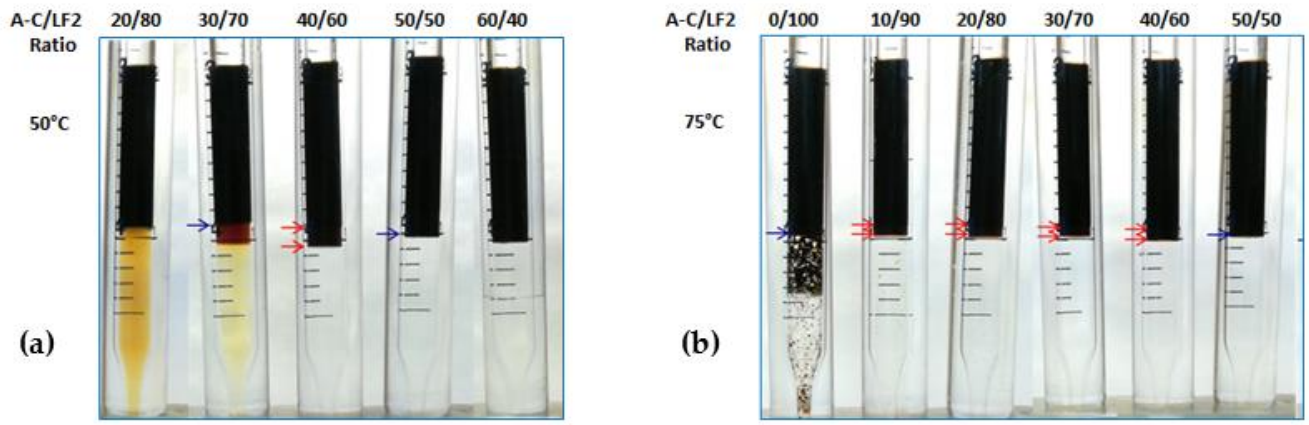


Figure 3. A-C/LF2 blend scans at (**a**) 50 °C and (**b**) 75 °C.

Oil (V_o/V_s) and water (V_w/V_s) solubilization parameters, as a function of the blend ratio, were calculated for both blends at 25 °C and 50 °C. A decrease in the optimal solubilization parameters (V_i/V_s*, $V_o/V_s = V_w/V_s$) with temperature was observed. The optimal solubilization parameters for the blend AOT/LF2 were 3 and 2.1 at 25 °C and 50 °C, respectively (Figure 4). In the case of the A-C/LF2 blend, V_i/V_s* decreased from 4.7 to 2.5 at the same evaluated temperatures (Figure 5). Table 1 shows the values of the optimal blend ratios, corresponding solubilization parameters, and estimated IFT by Huh's equation, for both blends.

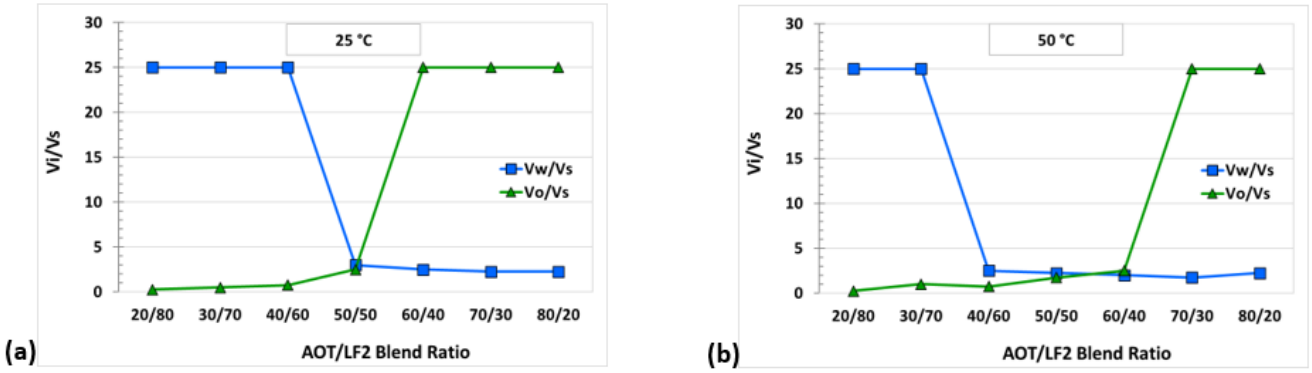


Figure 4. Solubilization parameters (V_i/V_s) for AOT/LF2 blend at (**a**) 25 °C and (**b**) 50 °C.

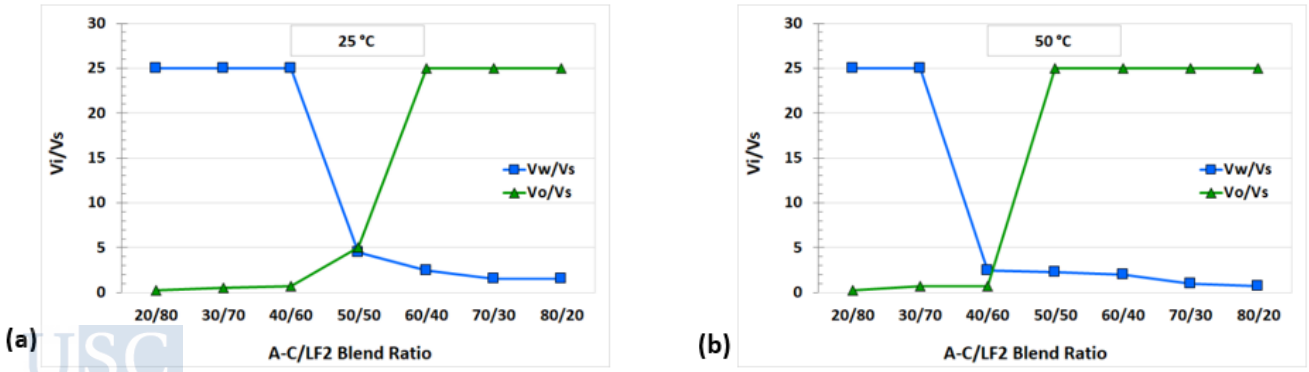


Figure 5. Solubilization parameters (V_i/V_s) for A-C/LF2 blend at (**a**) 25 °C and (**b**) 50 °C.

Table 1. Optimal blend ratios, solubilization parameters and IFT_{Huh} at 25 °C and 50 °C, for AOT/LF2 and A-C/LF2 blends.

	AOT/LF2		A-C/LF2	
Temperature	25 °C	50 °C	25 °C	50 °C
Optimal blend ratio	50.2/49.8	55/45	49.9/50.1	40.7/59.3
V_i/V_s*	3.0	2.1	4.7	2.5
IFT_{Huh} (mN/m)	3.36×10^{-2}	6.64×10^{-2}	1.32×10^{-2}	4.87×10^{-2}

Table 1 shows a clearly different behavior of the blends studied regarding the influence of temperature on the optimal blend ratio. In the case of AOT/LF2, the estimated optimal blend ratio shifted from 50.2 to 55 wt% AOT when the temperature increased from 25 °C to 50 °C. The range of ratios where the blend behaves as hydrophilic increased with temperature due to a stronger interaction of the ionic head groups of the surfactants with the water molecules, as in the case of anionic surfactants. On the other hand, for the same temperature increase, the estimated optimal blend ratio for A-C/LF2 moved from 49.9 to 40.7 wt% A-C. Lipophilicity increased with temperature, as in the case of traditional nonionic surfactants. This last behavior was also observed for the blends AOT/[C_{12}mim]Br and AOT/[C_{10}mim]Cl in our previous study [15], and it may be explained by the reduction or cancellation of free electrostatic charges due to the high synergy between the oppositely charged head groups of the anionic surfactant and the cationic SAIL [31,32]. The surfactant LF2 is a weak carboxylic acid which behaves as a nonionic surfactant in neutral to acid solution [19].

2.1.2. Stability Tests

The stability of the aqueous formulations was initially evaluated at 1 wt% blend (AOT/LF2 and A-C/LF2) concentration at room temperature. During the evaluation, the A-C/LF2 concentration was reduced from 1 to 0.9 wt% to improve the stability of the blend. Figure 6 shows the results of this test with different AOT/LF2 ratios, from 10 wt% to 90 wt% AOT. Around the 50/50 blend ratio, the formulations remained translucent during the 4 weeks of the test.

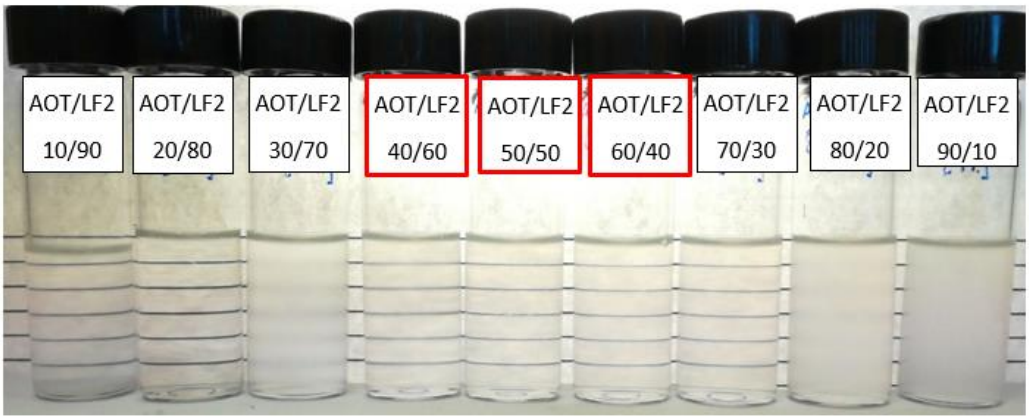


Figure 6. Stability test of aqueous formulations with 1 wt% AOT/LF2 blend (different ratios) at room conditions. The range of interest for further dynamic IFT evaluation is shown with red squares.

In the case of A-C/LF2, the stability evaluation was performed from 10 wt% to 90 wt% A-C. The blend remained translucent during 4 weeks in the range of interest from the 40/60 to 50/50 A-C/LF2 ratio (Figure 7).

USC UNIVERSIDADE DE SANTIAGO DE COMPOSTELA

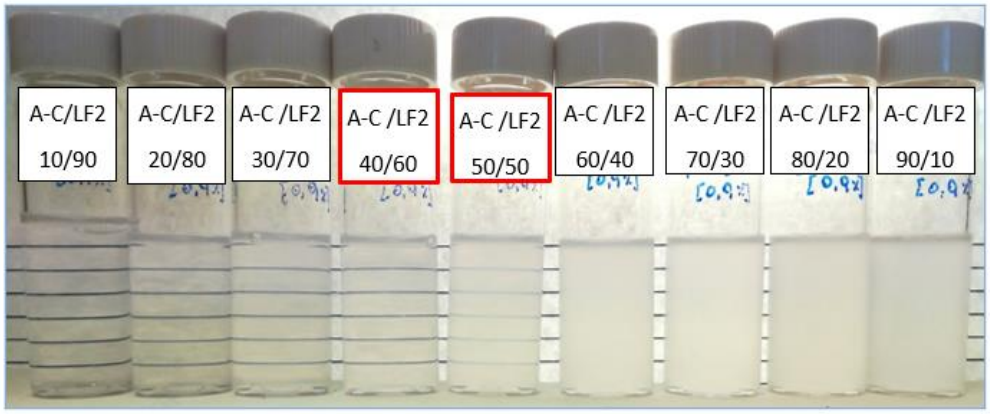


Figure 7. Stability test of aqueous formulations with 0.9 wt% A-C/LF2 blend (different ratios) at room conditions. The range of interest for further dynamic IFT evaluation is shown with red squares.

2.1.3. Dynamic Interfacial Tension (IFT)

As part of the optimal blend ratio definition, several ratios considered of interest according to the phase behavior evaluation (Section 2.1.1) and the stability tests (Section 2.1.2) were selected to measure dynamic IFT. Other close concentrations were also considered. Figure 8 shows the equilibrated interfacial tensions measured at 25 °C, as a function of blend ratio and concentration, for the AOT/LF2 (Figure 8a) and A-C/LF2 blends (Figure 8b).

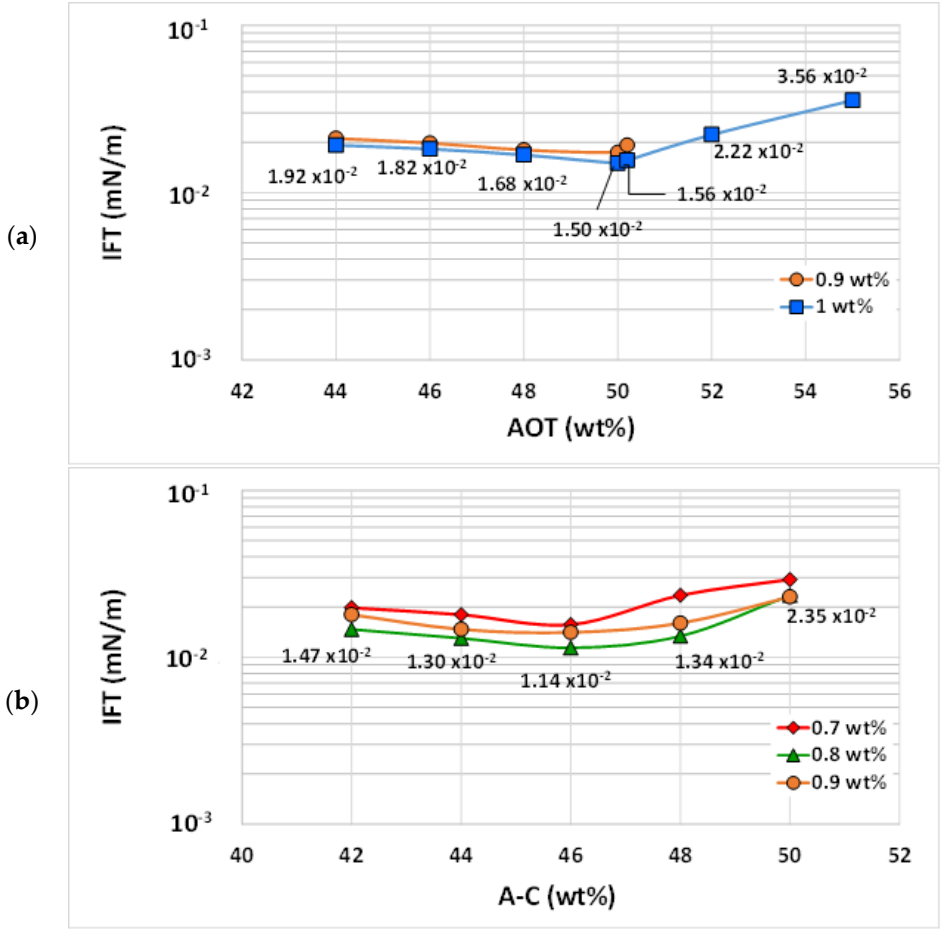


Figure 8. Interfacial tension measurements as a function of blend ratio and concentration at 25 °C for (**a**) AOT/LF2 and (**b**) A-C/LF2 blends.

The lowest IFT value achieved with the AOT/LF2 blend was 1.50×10^{-2} mN/m at the 50/50 blend ratio and at 1 wt% concentration in SSW. A slight increase in the IFT values was observed when the blend concentration was reduced to 0.9 wt%. In the case of the A-C/LF2 blend, the lowest IFT value was 1.14×10^{-2} mN/m, observed at a 46/54 ratio (the composition in the ternary blend was $AOT_{20.7wt\%}/[C_{12}mim]Br_{25.3wt\%}/LF2_{54wt\%}$) and at 0.8 wt% concentration in SSW. A higher concentration (0.9 wt%) and a lower one (0.7 wt%) were also evaluated, resulting in slightly higher IFT values.

2.1.4. Dynamic Adsorption

The results of the dynamic adsorption tests carried out in carbonate rocks are shown in Figure 9. This figure shows the relative concentrations (C/C_0) of the tracer and the optimal blends in the effluent as a function of the injected pore volume (*PV*) at room conditions. The tracer front achieved 50% of the initial concentration ($C/C_0 = 0.5$) at 1.09 *PV* injected, while for the optimal blends AOT/LF2 and A-C/LF2 this concentration ratio was achieved at 1.75 and 1.43 *PV*, respectively. Using Eq. 2, the dynamic adsorptions were estimated as 0.42 mg/g of rock for AOT/LF2 and 0.21 mg/g of rock for the A-C/LF2 blend.

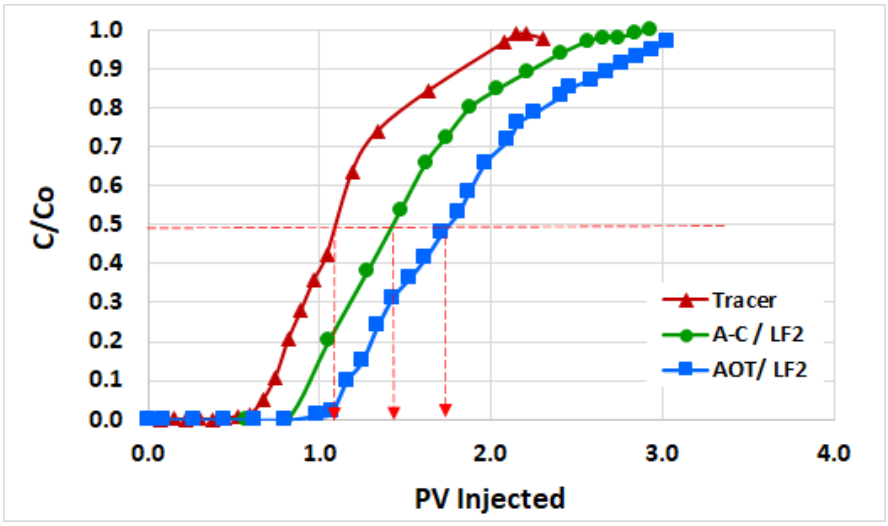


Figure 9. Estimation of dynamic adsorptions for optimal blends AOT/LF2 and A-C/LF2 in carbonate core at room conditions.

The lower adsorption of the A-C/LF2 blend compared with AOT/LF2 could be due to the high electrostatic interaction between the oppositely charged head groups of AOT and $[C_{12}mim]Br$, increasing the synergy between them and tending to form ion pairs [32,33] which reduce the free negative charges of AOT. The AOT/LF2 blend is less synergistic than A-C/LF2. An analysis of the AOT/LF2 and AOT/$[C_{12}mim]Br$ electrostatic interactions is discussed in our previous study [15].

2.1.5. Core Flooding Tests

In the AOT/LF2 core flooding test, during the water flooding stage, 1.97 *PV* of SSW was injected (until water production reached around 99% of the total production) through the carbonate core at 0.05 mL/min. The oil recovery was 47.7% of OOIP. For the chemical flooding, a slug of around 0.5 *PV* of the optimal formulation (1 wt% of 50/50 AOT/LF2 prepared in SSW) was injected followed by 1.26 *PV* of polymer flooding, both at 0.05 mL/min. The achieved AOR was 7.3% OOIP.

In the case of the A-C/LF2 core flooding test, the core was water flooded at 0.05 mL/min with 1.96 *PV* of SSW (no oil production was observed at that point), and an oil recovery of 40.8% of OOIP was obtained. Then, the core was flooded with 0.51 *PV* of the optimized blend (0.8 wt% of 46/54 A-C/LF2 prepared in SSW) at 0.05 mL/min, followed by 1.38 *PV* of polymer flooding

USC UNIVERSIDADE DE SANTIAGO DE COMPOSTELA

at the same injection rate. The AOR in this case was 11.5% OOIP. The apparent viscosity of the FloPAM 920 SH polymer solution for both core flooding tests at 2000 ppm of concentration and at 25°C was 5.7 mPa S, measured at a shear rate of 10 s^{-1}.

Table 2 presents a summary of the two core flooding tests, and Figure 10 shows the evolution of the oil recovery during water, surfactant, and polymer flooding. It can be seen that in the case of the AOT/LF2, oil production started after the injection of 0.85 *PV* of chemicals, whereas only 0.65 *PV* was required with A-C/LF2. This might be due to the higher adsorption found with the AOT/LF2 blend (Section 2.1.4).

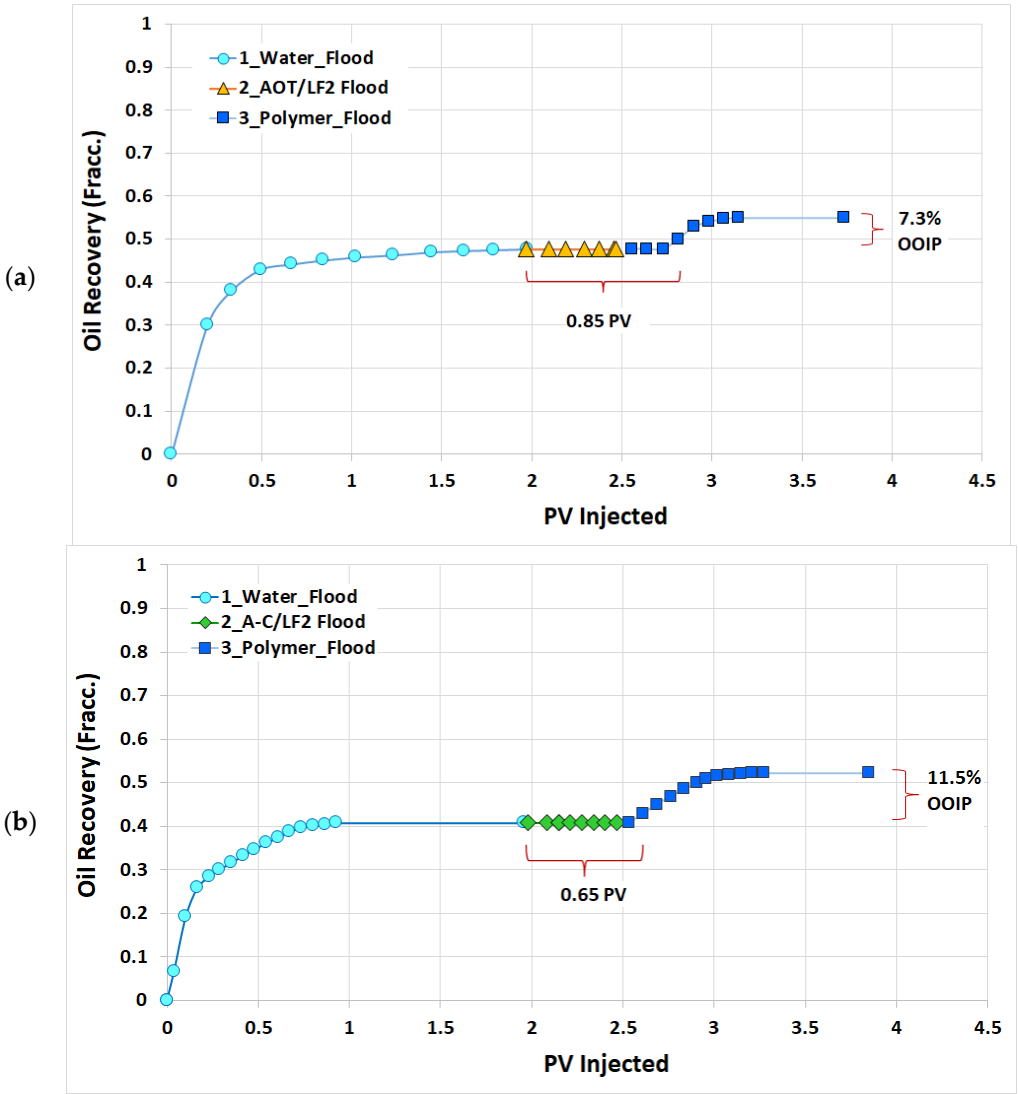


Figure 10. Oil recovery during water, blend and polymer injections in core flooding tests at room temperature: (**a**) AOT/LF2 and (**b**) A-C/LF2.

USC UNIVERSIDADE DE SANTIAGO DE COMPOSTELA

Table 2. Results of the core flooding experiments.

	Formulation	
Blend Composition	**AOT (50 wt%) LF2 (50 wt%)**	**AOT (20.7 wt%) [C_{12}mim]Br (25.3 wt%) LF2 (50 wt%)**
Concentration in SSW (wt%)	1	0.8
Initial conditions		
Porosity, $ø$	0.136	0.18
Permeability, K_a (mD)	16.81	19.16
Pore volume, PV (mL)	12.03	15.6
Oil visc. (mPa S) at 25 °C	12	12
OOIP (mL)	6.80	8.20
Initial water saturation, S_{wi}	0.43	0.47
Water Flooding		
Injection rate, Q_i (mL/min)	0.05	0.05
Injected SSW Volume (PV)	1.97	1.96
Oil recovery (%OOIP)	47.7	40.8
Residual oil saturation, S_{orw}	0.36	0.37
Chemical Flooding		
Injection rate (Q_i, mL/min)	0.05	0.05
Injected blend volume (PV)	0.495	0.511
Injected polymer volume (PV)	1.26	1.38
AOR (%OOIP)	7.3	11.5
Residual oil saturation, Sor_2	0.33	0.32

3. Materials and Methods

3.1. Experimental

3.1.1. Materials

The AOT surfactant, dioctyl sulfosuccinate sodium salt, and potassium iodide (KI) were purchased from Sigma-Aldrich with purities of $\geq$ 97 wt% and > 99 wt%, respectively. The surfactant polyoxyethylene(8) octyl ether carboxylic acid ($C_8EO_8OCH_2COOH$), commercially named Akypo LF2, was kindly provided by KAO Chemicals with a purity $\geq$ 98 wt%. The SAIL 1-dodecyl-3-methylimidazolium bromide ([C_{12}mim]Br) was purchased with a purity > 98 wt% from Iolitec. Figure 11 presents the chemical structures of the surfactants and the SAIL.

Polyacrylamide FloPAM FA 920 SH polymer (6.5–8.5 $\times$ 10^6 Da) was kindly provided by SNF Floerger. Synthetic sea water (SSW) was prepared with salts. Its composition is detailed in Table 3.

Dead crude oil was kindly supplied by CEPSA. Table 4 shows its main characteristics. Outcrop carbonate rock cores (Indiana Limestone), supplied by Kocurek Industries, were used for the dynamic adsorption and core flooding experiments. The mineral details can be found in a previous work [27].

USC UNIVERSIDADE DE SANTIAGO DE COMPOSTELA

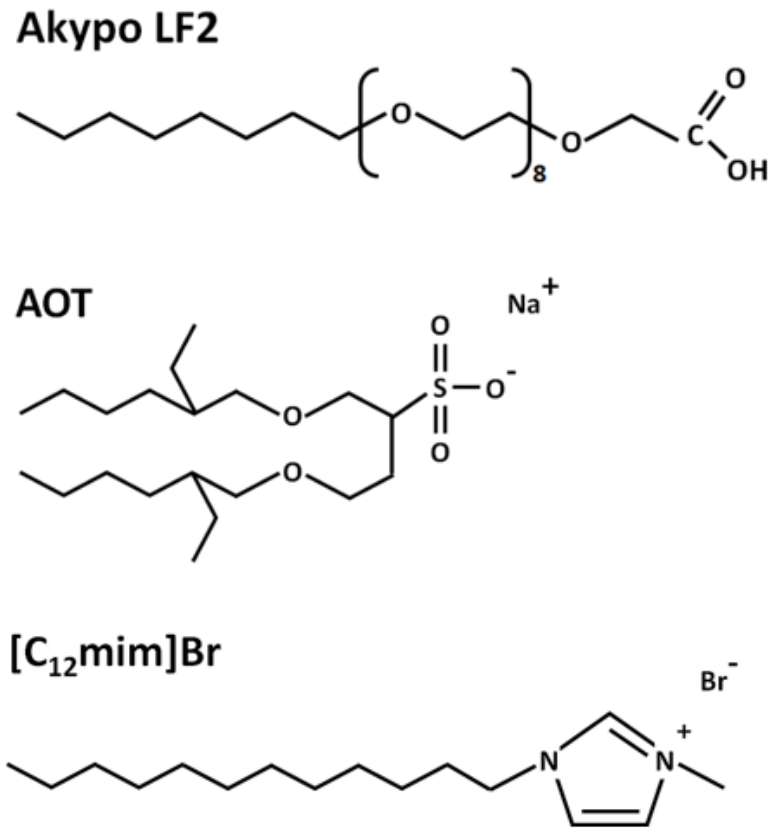


Figure 11. Chemical structure of surfactants and SAIL.

Table 3. Synthetic sea water (SSW) composition.

Salt	Purity (wt%)/ Commercial	SSW (g/L)
Na_2SO_4	>99%/Sigma-Aldrich	4.84
$CaCl_2{\cdot}2H_2O$	>99%/Sigma-Aldrich	1.89
$MgCl_2{\cdot}6H_2O$	>99%/Sigma-Aldrich	15.06
NaCl	>99%/Panreac	27.94
TDS (g/L)		49.73
Density at 25 °C (g/mL)		1.028

Table 4. Main properties of crude oil.

Property	Crude Oil A
Density at 25 °C (g/mL)	0.853
°API	34.1
Viscosity at 25 °C (mPa·s)	15.3
Saturates (wt%)	61
Aromatics (wt%)	33
Resins (wt%)	4.6
Asphaltenes (wt%)	1.4

USC UNIVERSIDADE DE SANTIAGO DE COMPOSTELA

3.1.2. Methods

Stock solutions of the surfactants AOT, LF2 and the ionic liquid ([C_{12}mim]Br were prepared individually in distilled water at 8 wt% concentration, to prevent possible in-

teractions of each component with divalent salts prior to blending them. The required amounts of surfactant solutions were mixed to obtain aqueous formulations with a blend concentration of 4 wt%. Aiming to carry out phase behavior studies, a brine solution twice the concentration shown in Table 3 was added to obtain an aqueous solution of 4 wt% surfactant blend in SSW. Lower blend concentrations for the adsorption and core flooding tests were prepared in a similar way. A Mettler Toledo XPE205 analytical balance was used for the preparation of the solutions by weight.

Blend Scans

To evaluate the phase behavior of the microemulsions and identify the blend ratio corresponding to the optimal formulations (lowest interfacial tension), blend scans were carried out using the encased-glass-pipette methodology [33,34]. The binary and ternary blends were prepared at 4 wt% concentration in SSW (a concentration higher than usual in practice but one that allowed the easy visualization of the phases). The water-oil ratio in the pipettes was about 1:1, with ~1 mL of aqueous blend solution and ~1 mL of crude oil as the oil phase. For AOT/LF2, the blend scan was performed varying the ratio from 0/100 to 100/0 wt%. In the case of the AOT/[C_{12}mim]Br/LF2 blend, the AOT/[C_{12}mim]Br was considered as a pseudo component (hereinafter termed A-C), so the ratios were changed from 0/100 A-C/LF2 to 100/0 A-C/LF2. Preliminary studies were carried out to fix the composition of A-C to 45 wt% AOT (55 wt% [C_{12}mim]Br). This initial work can be found in Figure S1 in Supporting Information. Phase behavior was evaluated at 25 °C, 50 °C and 75 °C using an OVAN dry-block heater (model BD200-RE).

The oil and aqueous phase volumes were measured in the pipettes to calculate the solubilization parameters for water (V_w/V_s) and oil (V_o/V_s), defined as the volume of water (V_w) and the volume of oil (V_o) solubilized in the microemulsion phase per volume of surfactant (V_s), assuming that all the surfactant is present in the microemulsion phase [20,33]. An optimal formulation is obtained when the system shows a middle microemulsion in equilibrium with excess oil (upper) and excess water (lower) phases and the solubilization parameters are equal and large. Interfacial tensions between the aqueous and oleic phases at optimal solubilization parameters (V_i/V_s*, when $V_o/V_s = V_w/V_s$) were estimated using the Huh's correlation [38]:

$$IFT_{Huh} = \frac{C}{\left(\frac{V_i}{V_S}^*\right)^2} \quad (1)$$

where C = 0.3 mN/m.

Stability Tests

To determine the possible precipitation or separation of the blend's components, the stability of the blends in the absence of oil was evaluated by preparing 1 wt% blend (a concentration commonly used in the application), with different ratios, in SSW at room temperature. The evaluation was carried out considering the translucence of the solutions [11,27,30].

Dynamic Interfacial Tension

This evaluation was performed, taking into account the range of interest found in the pipette tests, to precisely determine the optimal blend ratio for both blends. Measurements of the interfacial tension between the aqueous phase and the crude oil were carried out using a Krüss spinning drop tensiometer (model SITE100) at 25 °C, as in our previous reports [27,30]. A drop of 4 µL of the crude oil was left in the middle of the capillary tube filled with the aqueous formulations, and the rotation velocity was set to obtain an oil drop length at least four times larger than its diameter [39,40]. Densities of the aqueous blends were measured with the help of an Anton Paar density meter (model DMA 5000 M).

USC UNIVERSIDADE DE SANTIAGO DE COMPOSTELA

Dynamic Adsorption

Determination of the adsorption of the blends on carbonate rocks was conducted in a Hassler core holder equipment (model H00-021-0) for each optimal blend through single-phase dynamic adsorption tests at room temperature. The cores were vacuumed for 24 h and then saturated with SSW for 24 h at 0.05 mL/min. Absolute permeabilities (*Ka*) were estimated by Darcy's law at different injection rates, while pore volumes (*PV*) and porosities (*Ø*) were calculated using wet and dry core weights, their bulk volume, and the SSW density. Potassium iodide (KI) was injected at 0.1 mL/min as the tracer. The effluent was sampled until it achieved the initial KI concentration. The cores were cleaned by injecting SSW until no KI was produced. Then, the optimized blend was injected at 0.1 mL/min. Samples of effluent were taken until they achieved a blend concentration equal to the initial value. The difference between the tracer and the blend fronts (defined as the 50% of their initial concentration in effluents) was used to determine the blend adsorption [20,27,41]:

$$\tau = \frac{(PV_{blend,50\%} - PV_{tracer,50\%}) \times PV \times [C_0]_{blend}}{mass_{rock}} \quad (2)$$

where τ is the blend adsorption in mg/g, $PV_{blend,50\%}$ and $PV_{tracer,50\%}$ are the pore volumes in which effluent has reached 50% of initial concentration of blend and tracer, respectively, $mass_{rock}$ is the dry core weight in grams, PV is the pore volume in mL and $[C_0]_{blend}$ is the initial blend concentration in mg/mL. To estimate the concentrations of KI and the blend in effluents, an HP UV/Vis-spectrophotometer (model Presario SR1000) was used.

Core Flooding Tests

Two core flooding experiments using fresh carbonate cores were performed at room temperature following a similar protocol to that described above for the adsorption test. The cores were initially vacuumed and saturated with SSW at 0.05 mL/min (~1 ft/d) for 24 h. After the estimation of the absolute permeability, pore volume, and porosity, dead crude oil was injected at 0.05 mL/min for 24 h, and the expelled water was used to calculate the original oil in place (OOIP) and the initial water saturation (S_{wi}). The cores were left to equilibrate for 8 days and then water flooded with SSW at 0.05 mL/min. Volumes of injected water, produced water and produced oil were recorded. Oil recovery was measured during the tests, and the residual oil saturation for water flooding (S_{orw}) was estimated by material balance. Surfactant flooding was performed by injecting optimized blend formulations at 0.05 mL/min, and finally, polymer flooding was carried out by injecting the polymer PAM 920 SH (2000 ppm) at 0.05 mL/min until no oil was detected in the effluents. Residual oil saturation after chemical flooding (S_{or2}) and additional oil recovery (AOR) were estimated. The apparent viscosities of the polymer at 25°C as a function of shear rates were measured using an Anton Paar rheometer (model MCR 102).

4. Conclusions

In this work, the evaluation of the blend AOT/LF2 for enhanced oil recovery in carbonate reservoirs was carried out, and the improvement of its efficiency by adding the SAIL [C_{12}mim]Br to the formulation was also assessed. From this study, some conclusions may be established.

The phase behavior of AOT/LF2 and A-C/LF2 (A-C being a mixture containing 45 wt% AOT and 55 wt% [C_{12}mim]Br) in SSW is very similar, leading in both cases to Winsor type III systems of interest for EOR applications.

A decrease in solubilization parameters with temperature suggests, in both cases, the application of the formulations in reservoirs without excessively high temperatures.

According to phase behavior and IFT studies, the best formulation with the binary blend consists of 1 wt% of $AOT_{50wt\%}/LF2_{50wt\%}$ blend in SSW. In the case of the ternary blend, the optimal formulation contains 0.8 wt% of $AOT_{20.7wt\%}/[C_{12}mim]Br_{25.3wt\%}/\ LF2_{54wt\%}$.

USC UNIVERSIDADE DE SANTIAGO DE COMPOSTELA

Both blends are stable without oil and in the presence of divalent ions, thus ensuring their injectability in surfactant flooding.

When the SAIL is added to the formulation, the electrostatic interactions between the oppositely charged surfactants (AOT and [C_{12}mim]Br) led to a greater reduction in the water–oil IFT and lower adsorption of the blend on carbonate rocks.

Tertiary oil recovery with the ternary blend increases the AOR achieved with the binary blend by 57.5% (in both cases surfactant being followed by polymer flooding), pointing to the former as most promising for the application.

Supplementary Materials: The following supporting information can be downloaded at: https://www.mdpi.com/article/10.3390/ijms24010726/s1.

Author Contributions: Formal analysis, N.T.; Investigation, N.T.; Writing—original draft, N.T.; Writing—review & editing, A.P.M. and A.S.; Supervision, A.S.; Funding acquisition, A.S. All authors have read and agreed to the published version of the manuscript.

Funding: The authors acknowledge the Ministry of Science and Innovation and State Research Agency (AEI, 10.13039/501100011033) for financial support throughout project PGC2018-097342-B-I00, including European Regional Development Fund.

Institutional Review Board Statement: Not applicable.

Informed Consent Statement: Not applicable.

Data Availability Statement: Not applicable.

Acknowledgments: The authors thank Kao Corporation S.A. and SNF Floerger for supplying the Akypo LF2 surfactant and FloPAM FA 920 SH polymer, respectively.

Conflicts of Interest: The authors declare no conflict of interest.

References

1. Sheng, J. *Enhanced Oil Recovery Field Case Studies*, 2nd ed.; Elsevier Inc.: Amsterdam, The Netherlands, 2013.
2. Barati-Harooni, A.; Najafi-Marghmaleki, A.; Tatar, A.; Mohammadi, A.H. Experimental and modeling studies on adsorption of a nonionic surfactant on sandstone minerals in enhanced oil recovery process with surfactant flooding. *J. Mol. Liq.* **2016**, *220*, 1022–1032. [CrossRef]
3. Ma, K.; Cui, L.; Dong, Y.; Wang, T.; Da, C.; Hirasaki, G.J.; Biswal, S.L. Adsorption of cationic and anionic surfactants on natural and synthetic carbonate materials. *J. Colloid Interf. Sci.* **2013**, *408*, 164–172. [CrossRef] [PubMed]
4. Scamehorn, J.F.; Schechter, R.S.; Wade, W.H. Adsorption of surfactants on mineral oxide surfaces from aqueous solutions. I: Isomerically pure anionic surfactants. *J. Colloid Interf. Sci.* **1982**, *85*, 463–478. [CrossRef]
5. Sheng, J. *Modern Chemical Enhanced Oil Recovery: Theory and Practice*, 2nd ed.; Elsevier Inc.: Amsterdam, The Netherlands, 2011.
6. Wang, J.; Han, M.; Fuseni, A.B.; Cao, D. Surfactant adsorption in Surfactant-Polymer flooding for carbonate reservoirs. In Proceedings of the SPE Middle East Oil & Gas Show and Conference, Manama, Bahrain, 8–11 March 2015; pp. 1736–1746. [CrossRef]
7. Akbar, M.; Alghamdi, A.H.; Herron, M.; Allen, D.; Carnegie, A.; Dutta, D.; Olesen, J.-R.; Chourasiya, R.D.; Logan, D.; Stief, D.; et al. A Snapshot of Carbonate Reservoir Evaluation. *Oilf. Rev.* **1995**, *1*, 38–57.
8. Burchette, T.P. Carbonate rocks and petroleum reservoirs: A geological perspective from the industry. *Geol. Soc. Spec. Publ.* **2012**, *370*, 17–37. [CrossRef]
9. Khormali, A.; Rezaei-Koochi, M.; Varfolomeev, M.A.; Ahmadi, S. Experimental study of the low salinity water injection process in the presence of scale inhibitor and various nanoparticles. *J. Petrol. Expl. Prod. Technol.* **2022**. [CrossRef]
10. Feng, H.; Hou, J.; Ma, T.; Meng, Z.; Wu, H.; Yang, H.; Kang, W. The ultra-low interfacial tension behavior of the combined cationic/anionic-nonionic gemini surfactants system for chemical flooding. *Colloid Surf. A* **2018**, *554*, 74–80. [CrossRef]
11. Kurnia, I.; Zhang, G.; Han, X.; Yu, J. Zwitterionic-anionic surfactant mixture for chemical enhanced oil recovery without alkali. *Fuel* **2020**, *259*, 116236. [CrossRef]
12. Li, Y.; Zhang, W.; Bailing, K.; Puerto, M.; Bao, X.; Ou, S.; Zhiqin, S.; Yiqing, Y.; Yanhua, L.; Songyuan, G.; et al. Mixtures of anionic/cationic surfactants: A new approach for enhanced oil recovery in low-salinity, high-temperature sandstone reservoir. *SPE J.* **2016**, *21*, 1164–1177. [CrossRef]
13. Li, Z.; Wu, H.; Hu, Y.; Chen, X.; Yuan, Y.; Luo, Y.; Hou, J.; Bai, B.; Kang, W. Ultra-low interfacial tension biobased and catanionic surfactants for low permeability reservoirs. *J. Mol. Liq.* **2020**, *309*, 113099. [CrossRef]

14. Pal, N.; Vajpayee, M.; Mandal, A. Cationic/nonionic mixed surfactants as enhanced oil recovery fluids: Influence of mixed micellization and polymer association on interfacial, rheological, and rock-wetting characteristics. *Energ. Fuel* **2019**, *33*, 6048–6059. [CrossRef]
15. Tafur, N.; Somoza, A.; Soto, A. Evaluation of surfactant blends for enhanced oil recovery through activity maps. *J. Mol. Liq.* **2022**, *364*, 119984. [CrossRef]
16. Sheu, E.Y.; Chen, S.H.; Huang, J.S. Structure and growth of Bis(2-ethylhexyl) Sulfosuccinate Micelles in Aqueous Solutions. *J. Phys. Chem.* **1987**, *91*, 3306–3310. [CrossRef]
17. Wan, W.; Zhao, J.; Harwell, J.H.; Shiau, B.J. Characterization of crude oil equivalent alkane carbon number (EACN) for surfactant flooding design. *J. Dispers. Sci. Technol.* **2016**, *37*, 280–287. [CrossRef]
18. Wu, B.; Shiau, B.J.; Sabatini, D.A.; Harwell, J.H.; Vu, D.Q. Formulating microemulsion systems for a weathered jet fuel waste using surfactant/cosurfactant mixtures. *Sep. Sci. Technol.* **2000**, *35*, 1917–1937. [CrossRef]
19. Denk, P.; El Maangar, A.; Lal, J.; Kleber, D.; Zemb, T.; Kunz, W. Phase diagrams and microstructures of aqueous short alkyl chain polyethylene glycol ether carboxylate and carboxylic acid triblock surfactant solutions. *J. Colloid Interf. Sci.* **2021**, *590*, 375–386. [CrossRef]
20. Montes, J.; Blin, N.; Alvarez, A.E.; Barrio, I.; Panadero, A.; Rodriguez, R.; Coca, M.; Trujillo, F. Novel anionic surfactant formulation for high temperature carbonate reservoirs. In Proceedings of the SPE EOR Conference at Oil and Gas West Asia, Muscat, Oman, 26–28 March 2018. [CrossRef]
21. Negin, C.; Ali, S.; Xie, Q. Most common surfactants employed in chemical enhanced oil recovery. *Petroleum* **2017**, *3*, 197–211. [CrossRef]
22. Winsor, P.A. Hydrotropy, solubilisation and related emulsification processes. Part I. *Trans. Farad. Soc.* **1948**, *44*, 376–398. [CrossRef]
23. Hezave, A.Z.; Dorostkar, S.; Ayatollahi, S.; Nabipour, M.; Hemmateenejad, B. Effect of different families (imidazolium and pyridinium) of ionic liquids-based surfactants on interfacial tension of water/crude oil system. *Fluid Phase Equilibr.* **2013**, *360*, 139–145. [CrossRef]
24. Hezave, A.Z.; Dorostkar, S.; Ayatollahi, S.; Nabipour, M.; Hemmateenejad, B. Investigating the effect of ionic liquid (1-dodecyl-3-methylimidazolium chloride ([C_{12}mim]Cl) on the water/oil interfacial tension as a novel surfactant. *Colloid Surf. A* **2013**, *421*, 63–71. [CrossRef]
25. Pillai, P.; Kumar, A.; Mandal, A. Mechanistic studies of enhanced oil recovery by imidazolium-based ionic liquids as novel surfactants. *J. Ind. Eng. Chem.* **2018**, *63*, 262–274. [CrossRef]
26. Rodriguez-Escontrela, I.; Puerto, M.C.; Miller, C.A.; Soto, A. Ionic liquids for low-tension oil recovery processes: Phase behavior tests. *J. Colloid Interf. Sci.* **2017**, *504*, 404–416. [CrossRef] [PubMed]
27. Somoza, A.; Arce, A.; Soto, A. Oil recovery tests with ionic liquids: A review and evaluation of 1-decyl-3-methylimidazolium triflate. *Pet. Sci.* **2022**, *19*, 1877–1887. [CrossRef]
28. Fernández-Stefanuto, V.; Corchero, R.; Rodríguez-Escontrela, I.; Soto, A.; Tojo, E. Ionic Liquids Derived from Proline: Application as Surfactants. *ChemPhysChem* **2018**, *19*, 2885–2893. [CrossRef] [PubMed]
29. Nandwani, S.K.; Chakraborty, M.; Bart, H.J.; Gupta, S. Synergism, phase behaviour and characterization of ionic liquid-nonionic surfactant mixture in high salinity environment of oil reservoirs. *Fuel* **2018**, *229*, 167–179. [CrossRef]
30. Somoza, A.; Tafur, N.; Arce, A.; Soto, A. Design and performance analysis of a formulation based on SDBS and ionic liquid for EOR in carbonate reservoirs. *J. Pet. Sci. Eng.* **2022**, *209*, 109856. [CrossRef]
31. Kume, G.; Gallotti, M.; Nunes, G. Review on anionic/cationic surfactant mixtures. *J. Surfactants Deterg.* **2008**, *11*, 1–11. [CrossRef]
32. Li, Y.; Puerto, M.; Bao, X.; Zhang, W.; Jin, J.; Su, Z.; Shen, S.; Hirasaki, G.; Miller, C. Synergism and performance for systems containing binary mixtures of anionic/cationic surfactants for enhanced oil recovery. *J. Surfactants Deterg.* **2017**, *20*, 21–34. [CrossRef]
33. Puerto, M.; Hirasaki, G.J.; Miller, C.A.; Barnes, J.R. Surfactant systems for EOR in high-temperature, high-salinity environments. *SPE J.* **2012**, *17*, 11–19. [CrossRef]
34. Barnes, J.R.; Smit, J.P.; Smit, J.R.; Shpakoff, P.G.; Raney, K.H.; Puerto, M.C. Development of surfactants for chemical flooding at difficult reservoir conditions. *SPE Symp. Improv. Oil Recover.* **2008**, *1*, 435–452. [CrossRef]
35. Antón, R.E.; Andérez, J.M.; Bracho, C.; Vejar, F.; Salager, J.L. Practical surfactant mixing rules based on the attainment of microemulsion-oil-water three-phase behavior systems. *Adv. Polym. Sci.* **2008**, *218*, 83–113. [CrossRef]
36. Salager, J.L.; Forgiarini, A.M.; Bullón, J. How to attain ultralow interfacial tension and three-phase behavior with surfactant formulation for enhanced oil recovery: A review. Part 1. Optimum formulation for simple surfactant-oil-water ternary systems. *J. Surfactants Deterg.* **2013**, *16*, 449–472. [CrossRef]
37. Salager, J.L.; Morgan, J.C.; Schechter, R.S.; Wade, W.H.; Vasquez, E. Optimum formulation of surfactant-water-oil systems for minimum interfacial tension or phase behaviour. *Soc. Pet. Eng. J.* **1979**, *19*, 107–115. [CrossRef]
38. Huh, C. Interfacial tensions and solubilizing ability of a microemulsion phase that coexists with oil and brine. *J. Colloid Interf. Sci.* **1979**, *71*, 408–426. [CrossRef]
39. Hu, H.; Joseph, D. Evolution of a liquid drop in a spinning drop tensiometer. *J. Colloid Interf.* **1994**, *162*, 331–339. [CrossRef]

USC DE SANTIAGO DE COMPOSTELA

40. Vonnegut, B. Rotating bubble method for the determination of surface and interfacial tensions. *Rev. Sci. Instrum.* **1942**, *13*, 6–9. [CrossRef]
41. Sharma, H.; Lu, J.; Weerasooriya, U.P.; Pope, G.A.; Mohanty, K.K. Adsorption in chemical floods with ammonia as the alkali. In Proceedings of the SPE Improved Oil Recovery Conference, Tulsa, OK, USA, 11–13 April 2016. [CrossRef]

Disclaimer/Publisher's Note: The statements, opinions and data contained in all publications are solely those of the individual author(s) and contributor(s) and not of MDPI and/or the editor(s). MDPI and/or the editor(s) disclaim responsibility for any injury to people or property resulting from any ideas, methods, instructions or products referred to in the content.

USC UNIVERSIDADE DE SANTIAGO DE COMPOSTELA

Supporting Information

Improvement of a Surfactant Blend for Enhanced Oil Recovery in Carbonate Reservoirs by Means of an Ionic Liquid

Nestor Tafur [1], Alberto P. Muñuzuri [2] and Ana Soto [1,*]

[1] CRETUS, Department of Chemical Engineering, Universidade de Santiago de Compostela, 15782 Santiago de Compostela, Spain
[2] Group of Nonlinear Physics, Galician Center for Mathematical Research and Technology (CITMAga), 15782 Santiago de Compostela, Spain
* Correspondence: ana.soto@usc.es

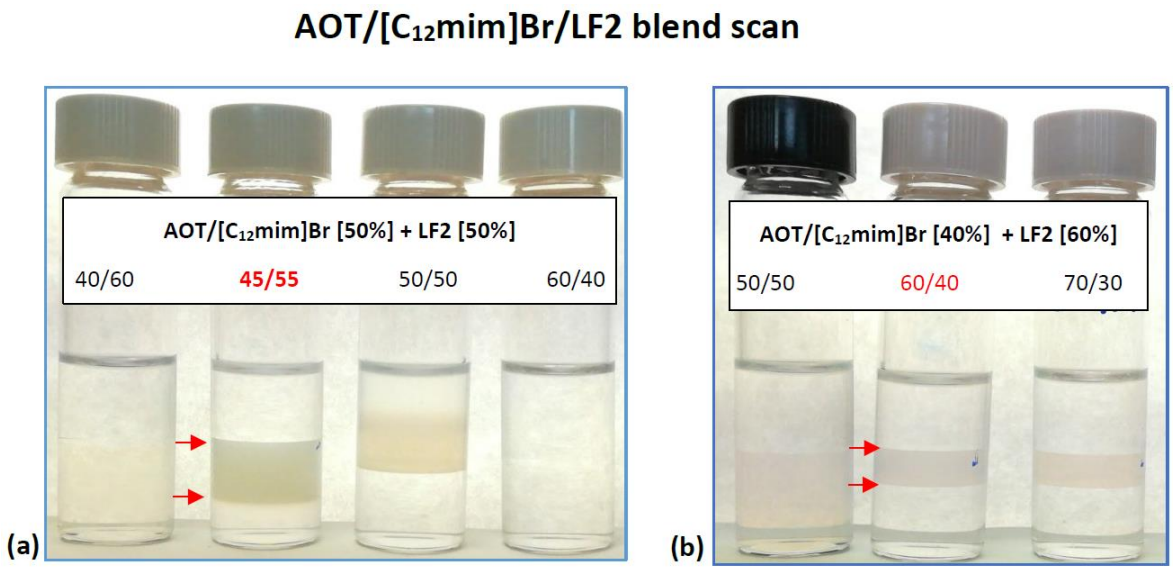


Figure S1. AOT/[C12mim]Br + LF2 blend scan as a function of AOT/[C12mim]Br ratio. (a) AOT/[C12mim]Br [50%] + LF2 [50%]. (b) AOT/[C12mim]Br [40%] + LF2 [60%]. Test temperature 25°C. N-octane as oil phase.

USC UNIVERSIDADE DE SANTIAGO DE COMPOSTELA

224 (2023) 211619

Contents lists available at ScienceDirect

Geoenergy Science and Engineering

journal homepage: www.sciencedirect.com/journal/geoenergy-science-and-engineering

Assessment of a surface-active ionic liquid formulation for EOR applications: Experimental and simulation studies

Nestor Tafur [a,**], Alba Somoza [a], Alberto P. Muñuzuri [b], Borja Rodríguez-Cabo [c], Izaskun Barrio [c], Asier Panadero [d], M. Flor García-Mayoral [d], Ana Soto [a,*]

[a] CRETUS, Department of Chemical Engineering, Universidade de Santiago de Compostela, E-15782, Santiago de Compostela, Spain
[b] Group of Nonlinear Physics, Dept. of Physics, Universidade de Santiago de Compostela, E-15782, Santiago de Compostela, Spain
[c] CEPSA-Química, Research Center, E-28805, Madrid, Spain
[d] CEPSA, Research Center, E-28805, Madrid, Spain

ARTICLE INFO

Keywords:
Blend
Microemulsion
Flooding
History match

ABSTRACT

This study aims to assess a surfactant blend for enhanced oil recovery from carbonate rocks. Due to the abundance of these reservoirs, their profitable exploitation would ensure our petrochemical needs are met, and maintain current quality of life. The objective of this work is to increase the technology readiness level of our previous proposal based on the use of a blend of pure sodium dodecylbenzene sulfonate and the surface-active ionic liquid cocosalkylpentaethoximethyl ammonium methylsulfate. To that aim, the method was adapted for its application with a commercially available petrochemical surfactant (RECOLAS103, a mixture of lineal alkyl benzene sulfonates), and reservoir simulations were carried out to evaluate its effectiveness. Phase behavior, stability, dynamic interfacial tension, adsorption and core flooding were the experimental tests carried out. An optimized formulation consisting of 1 wt% of blend (40 wt% RECOLAS103) in synthetic sea water was found stable and able to reduce water-oil interfacial tension down to 0.02 mN/m. The dynamic blend adsorption in carbonate rocks was found to be 0.60 mg/grock, a promising value for the application. Core flooding tests were conducted at 25 and 120 °C and additional oil recoveries achieved ranged from 10.2 to 12.7% of the original oil in place, the lowest production obtained at the highest temperature. This work offers an advance in the application of surfactants for EOR in carbonate reservoirs, since it improves previous proposals that show stability or high adsorption problems. Moreover, a chemical injection optimization was also carried out by simulation with the CMG-STARS software. Results point to the possibility of reaching higher oil recoveries than those obtained experimentally if the extraction method is optimized.

1. Introduction

In the current world energy scenario, it is expected that oil fields at developing and mature stages optimize their production. During the transition to the use of renewable energies, a more efficient extraction of the recoverable oil reserves must be achieved with the implementation of Enhanced Oil Recovery (EOR) techniques. These methods are mainly focused on the reduction of the residual oil saturation after water flooding by increasing the capillary number (N_C), which represents the ratio of viscous to capillary forces. This dimensionless number ranges normally from the order of 10^{-7} to 10^{-6} for water flooding. To reduce the water flooding residual oil saturation, N_C needs to be increased higher than the critical capillary number (normally around 10^{-5} to 10^{-4}) to mobilize the residual oil (Ghadami et al., 2015; Green and Willhite, 2018; Hakiki et al., 2015; Sheng, 2013, 2011). To achieve such a high N_C, low or ultralow values (around 10^{-3} to 10^{-2} mN/m) of water-oil interfacial tension (IFT) are required. These values can be obtained by injecting certain surfactants at specific conditions (Abbaszadeh and Ren, 2013; Kamal et al., 2017; Spildo et al., 2012), promoting the formation of optimal microemulsions within the reservoir. Surfactant injection reduces capillary pressure within the porous medium and alters the original relative permeability curves, reducing the residual oil saturation.

It is currently known that anionic surfactants show much greater

* Corresponding author.
** Corresponding author.
E-mail addresses: nestor.tafur@usc.es (N. Tafur), ana.soto@usc.es (A. Soto).

https://doi.org/10.1016/j.geoen.2023.211619
Received 16 September 2022; Received in revised form 6 February 2023; Accepted 24 February 2023
Available online 5 March 2023
2949-8910/© 2023 The Authors. Published by Elsevier B.V. This is an open access article under the CC BY-NC-ND license (http://creativecommons.org/licenses/by-nc-nd/4.0/).

efficiency in reducing IFT compared to cationic and non-ionic surfactants. However, they work better in sandstone reservoirs, whose surface rock has a negative electrical charge, than in carbonate reservoirs that are positively charged. In the latter case, a greater electrostatic adsorption of the anionic surfactant during injection drastically reduces the efficiency of the EOR project (Barati-Harooni et al., 2016; Ma et al., 2013; Scamehorn et al., 1982; Sheng, 2011; Wang et al., 2015). Several recent works propose the use of binary mixtures of anionic, cationic and nonionic surfactants for EOR applications, aiming to improve certain properties (i.e., IFT or surfactant adsorption) in comparison to the use of the single surfactants (Feng et al., 2018; Kurnia et al., 2020; Li et al., 2017, 2020; Pal et al., 2019).

Recently, the use of certain ionic liquids (salts with melting or glass transition temperatures below 100 °C) with surface-active properties has also been investigated. These salts, at very low concentrations in water formulations act as surfactants (Cooper et al., 2004; Hanke and Lynden-Bell, 2003) and are being studied to improve current EOR methods. A summary of these works was presented by Somoza et al. (2022a). Although those surface-active ionic liquids (SAILs) are capable of lowering IFT, they are rarely able to achieve ultra-low values by themselves (Fernández-Stefanuto et al., 2018). However, mixtures of SAILs and traditional surfactants have been shown able to achieve low IFT values ($<10^{-1}$ mN/m). Core flooding tests, in sandstone rocks or sand packs, have been used to validate the interest of these blends for EOR in these kinds of rocks (Jia et al., 2017; Nandwani et al., 2018).

The percentage of the world's oil found in carbonate reservoirs is commonly estimated at around 50–60% (Akbar et al., 1995; Burchette, 2012), so one of the priorities of the oil industry is to maximize the oil recovery from these rocks. The challenging conditions of carbonate reservoirs have led to a limited number of studies with surfactants in this kind of rocks. The SAIL [C_{18}mim]Cl was tested by Manshad et al. (2017) and Zabihi et al., (2019) leading to an additional oil recovery (AOR) of 13 and 16.5% OOIP, respectively. However, a high adsorption took place (according to the presented Freundlich isotherm) in the first study, and no information about this parameter was given in the second case. Nandwani et al. (2019b) proposed the use of a blend constituted by Tergitol 15-S-9 and the SAIL [P_{44416}]Br, achieving an AOR of 16.7% OOIP. The same authors exchanged the phosphonium SAIL for [C_{16}mim]Br to work at high salt concentration (31 wt%) and achieved an AOR of 20.9 %OOIP (Nandwani et al., 2019). However, those studies did not consider the presence of divalent ions, and were performed with an unconsolidated calcite powder packed bed. Montes et al. (2018) achieved an AOR of 32 %OOIP with a blend of alkyl benzene sulfonate + alkyl ethoxy carboxylate (40/60). However, the high adsorption of the blend (3.51 mg/g rock) would likely limit its application. Thus, the design of a formulation based on surfactants, or SAILs, able to satisfactorily extract oil from carbonate reservoirs is still a research goal.

In our previous report (Somoza et al., 2022b), a blend constituted of the anionic surfactant sodium dodecyl benzene sulfonate (SDBS) and the SAIL cocosalkylpentaethoximethyl ammonium methylsulfate was shown promising for EOR in carbonate reservoirs. As a continuation of that previous work, in this study the pure commercial SDBS was exchanged for a lineal alkyl benzene sulfonate surfactant (RECOLAS103) developed by CEPSA. The novelty and main contribution of this paper is, therefore, an approach to the real application of the proposed blend in EOR projects. To that aim, new laboratory tests were carried out to optimize the formulation with this petrochemical surfactant according to IFT and adsorption parameters. Further, numerical simulation studies were carried out to evaluate key chemical displacement parameters and to optimize the field chemical injection protocol, using the commercial reservoir simulator CMG-STARS (CMG, 2016).

USC UNIVERSIDADE DE SANTIAGO DE COMPOSTELA

2. Materials and methods

2.1. Experimental

2.1.1. Materials

The cationic SAIL cocosalkylpentaethoximethyl ammonium methylsulfate, commercially named IoLiLyte C1EG (hereinafter called "C1EG"), was purchased with purity ≥95 wt% from Iolitec. The surfactant RECOLAS103 is a sodium alkyl benzene sulfonate provided by CEPSA with a concentration of 20 wt%, with alkyl chain lengths C_{10}–C_{13}. The nonionic polymers polyacrylamide FloPAM FA 920 SH (6.5–8.5 × 10^6 Da) and FloPAM FA 920 VHM (≥8.5 × 10^6 Da) were kindly provided by SNF Floerger.

Two brines, synthetic formation water (SFW) and synthetic sea water (SSW), were used for initial water saturation and water flooding processes. The composition and densities of the SFW and the SSW are shown in Table 1.

Potassium iodide (KI), used as tracer for dynamic adsorption tests, was purchased from Sigma-Aldrich with purity >99 wt%. No further purification was done for the received chemical reagents. Distilled water was used to prepare C1EG and RECOLAS103 stock solutions, as well as the SFW and SSW.

N-octane was purchased from Sigma-Aldrich with a purity >99 wt%. Two dead crude oils were used in this work, both provided by CEPSA. Their main characteristics are presented in Table 2.

Indiana Limestone carbonate rocks were used for dynamic adsorption and core flooding experiments at room conditions (plug of 8–20 mD permeability and dimensions of 75.3 mm length and 38.2 mm diameter) and 120 °C (plug of 2–5 mD permeability and dimensions of 111.1 mm length and 37.7 mm diameter).

2.1.2. Methods

To avoid individual interactions of C1EG and RECOLAS103 with divalent salts before mixing, stock solutions were prepared for each component in distilled water at 8 wt% concentration of active matter. All of the solutions were prepared by weight using a Mettler Toledo XPE205 analytical balance. Weighing uncertainty was 0.0001 g.

2.1.2.1. Blend scans. Phase behavior of the surfactant blend was evaluated through mixing ratio scan tests using the encased-glass-pipette methodology (Barnes et al., 2008; Puerto et al., 2012). The aqueous and oily phases were introduced into tip sealed borosilicate glass pipettes, then heat-sealed at the top, and mixed slowly for 24 h at ambient temperature with the use of a rotary mixer. Finally, pipettes were placed in 10 mL test tubes containing silicon oil, and set to equilibrate in an OVAN bath dry block (model BD200-RE) at the required temperature until no change in interfacial position was observed.

The water-oil ratio in the pipettes was around 1:1, with ~1 mL of *n*-octane as the oil phase and ~1 mL of aqueous phase with 4 wt% surfactant concentration. The blend scan was performed at different RECOLAS103/C1EG mass ratios, from 100/0 to 0/100 (weight). The salinity of the aqueous phase was 4.97 wt% TDS (SSW). Phase behavior was evaluated at 25 °C, 50 °C and 75 °C. Phase volumes were measured to calculate solubilization parameters defined as either volume of oil (V_o)

Table 1
Compositions, salt purities and densities for synthetic formation water (SFW) and synthetic sea water (SSW).

Salt	Purity (wt%)/Commercial	SFW (g/L)	SSW (g/L)
Na_2SO_4	>99%/Sigma-Aldrich	0.4	4.84
$CaCl_2{\cdot}2H_2O$	>99%/Sigma-Aldrich	61.1	1.89
$MgCl_2{\cdot}6H_2O$	>99%/Sigma-Aldrich	13.1	15.06
NaCl	>99%/Panreac	153.5	27.94
$NaHCO_3$	>99%/Scharlau	0.5	0
TDS (g/L)		228.6	49.73
Density at 25 °C (g/mL)		1.100	1.028

Table 2
Main properties of used crude oils.

Property	Crude oil A	Crude oil B
Density at 25°C (g/mL)	0.853	0.836
°API	34.1	37.3
Viscosity at 25°C (mPa·s)	15.3	5.38
Saturates (wt%)	61	71
Aromatics (wt%)	33	28
Resins (wt%)	4.6	1
Asphaltenes (wt%)	1.4	<1

or water (V_w) solubilized per volume of surfactant (V_s) in the micro-emulsion phase (Montes et al., 2018; Puerto et al., 2012; Rodriguez-Escontrela et al., 2017; Somoza et al., 2022b). The optimal solubilization parameters (V_i/V_s*, when $V_o/V_s = V_w/V_s$) were used to estimate the IFT between the aqueous and oleic phases by using the Huh's correlation (Huh, 1979):

$$IFT_{Huh} = \frac{C}{\left(V_i/V_S^*\right)^2} \quad \text{(Eq. 1)}$$

where C is an empirical constant ranging between 0.1 and 0.35 mN/m. It was fixed at 0.3 in the present work.

The presence of liquid crystals in the systems was evaluated through the search of birefringence under polarized light.

2.1.2.2. Compatibility tests. The stability of the blend in the absence of oil was evaluated at different mixing ratios to determine the possible separation of the components, leading to their non-uniform distribution in the reservoir during injection, as well as the appearance of precipitates. The evaluation was carried out visually based on the translucence of the solution. To this end, formulations at several blend ratios were prepared (1 wt% blend concentration) in SSW (4.97 wt% TDS) at room temperature (Kurnia et al., 2020; Somoza et al., 2022a,b).

2.1.2.3. Dynamic interfacial tension. IFT measurements between crude oil A and the aqueous formulations (1 wt% blend concentration) were performed at 25 °C with the use of a Krüss spinning drop tensiometer (model SITE100) as in our previous reports (Somoza et al., 2022a,b). The main purpose of this study was the selection, among the promising blends found with the phase behavior studies, of the mixture leading to the lowest IFT. During the measurements, an oil drop of 4 μL was injected into the capillary tube of the equipment previously filled with the aqueous formulation. The rotation speed was set in order to obtain a drop length at least four times larger than its diameter. An Anton Paar density meter (model DMA 5000 M) was used to measure the densities of the phases. The relative standard uncertainty of equilibrium IFT was estimated to be 10%.

2.1.2.4. Dynamic adsorption. Single-phase dynamic adsorption tests were carried out in a Hassler core holder equipment (model H00-021-0) at room temperature. A carbonate rock core was used for these tests with a confining pressure set to 700 psi. After vacuuming the core for 24 h, it was saturated with SSW at an injection rate of 0.05 mL/min, also for 24 h. The absolute permeability (K_a) was estimated by Darcy's Law at different injection rates with their stabilized differential pressures. After the estimation of pore volume and porosity, potassium iodide (KI) was injected as the tracer at 0.1 mL/min, and effluent samples were taken roughly every 1 mL until reaching the initial KI concentration (C_0). Next, the core was cleaned by injecting SSW until no traces of KI were detected. The optimized RECOLAS103/C1EG formulation was then injected with the same protocol and conditions. An HP UV/Vis-spectrophotometer (model Presario SR1000) was used to estimate the concentrations of tracer and blend in effluents during the test. The blend adsorption was estimated based on the delay in the surfactant front in comparison with the tracer front by using the following equation (Montes et al., 2018; Sharma et al., 2016; Somoza et al., 2022b):

$$\tau = \frac{\left(PV_{blend,50\%} - PV_{tracer,50\%}\right) \times PV \times [C_0]_{blend}}{mass_{rock}} \quad \text{(Eq. 2)}$$

where τ is the blend adsorption in mg/g, $PV_{blend,50\%}$ and $PV_{tracer,50\%}$ are the pore volume in which blend or tracer concentration reached 50% of initial concentration, PV is the pore volume in mL, $[C_0]_{blend}$ is initial blend concentration in mg/mL, and $mass_{rock}$ is the dry core weight in grams. Adsorption uncertainty was estimated to be 0.02 mg/g rock.

2.1.2.5. Polymer solution evaluation. Although the optimum selection of a polymer to efficiently sweep a 15.3 mPa s crude oil through low permeability carbonate cores (25 mD or less) is outside the scope of this study, a preliminary evaluation of two polymers was performed to define the type and the polymer concentration to use in this work. Two nonionic polymers (FloPAM FA 920 SH and FloPAM FA 920 VHM) were analyzed. Polymer solutions were prepared by weight adding polymer powder to SSW. 5000 ppm stock solution was prepared by stirring the solution at 80 rpm with a magnetic stirrer for 3 h, ensuring the absence of large slugs or "fish-eyes", then allowing the solution to settle overnight. More diluted polymer solutions were prepared by mixing the stock solutions with SSW gently stirring overnight (14 h). The whole process was carried out at room temperature and following the recommended practices for evaluation of polymers used in enhanced oil recovery operations (American Petroleum Institute- Production Department, 1990).

Apparent viscosities (η) for both polymer solutions were determined as a function of polymer concentration and shear rate at 25 °C, using an Anton Paar rheometer (model MCR 102), to choose the suitable polymer and concentration. The relative standard uncertainty of viscosity was 3%. Injectivity tests of the polymer solutions were carried out in fresh carbonate cores saturated with SSW at room conditions to define the polymer formulation to be used in flooding tests.

2.1.2.6. Core flooding tests. In general, for each displacement test, the cores were initially vacuumed and then saturated with brine using the core holder equipment. Absolute permeabilities (K_a) were estimated using Darcy's law, while pore volumes (PV) and porosities ($Ø$) were calculated using wet and dry core weights and the water density. Water was drained by injecting dead crude oil to reach the initial water saturation (S_{wi}) and the cores were left to equilibrate or for ageing. The total expelled water was used to calculate the original oil in place (OOIP). Fresh oil was injected, and maximum oil relative permeability (K_{romax}) was estimated. Then, the cores were water flooded with SSW and volumes of produced oil, produced water, injected water and differential pressures were recorded. The residual oil saturation for water flooding (S_{orw}) and the oil recovery were estimated from material balance. The end-point water relative permeability (K_{rwmax}) was estimated at the end of the water flooding process. Surfactant flooding was conducted by injecting optimized blend formulation (1 wt% concentration), and residual oil saturation after chemical flooding (S_{or2}) and oil recovery were calculated.

Three core flooding experiments were carried out to determine the efficiency of the blend under different conditions. The CF-1 test was an initial study carried out at room temperature with the sole purpose of evaluating the EOR capacity of the proposed blend, and the comparison of the results with previous studies (Somoza et al. 2022b). This test was not considered in posterior simulation studies. CF-2 was conducted at 120 °C to evaluate the effect of the temperature on the oil recovery. The third test (CF-3) was carried out using a more realistic protocol of injection, flooding a slug of the blend followed by a polymer flood at injection rate around 1 ft/D. In this test, effluent samples were collected for salinity analysis with a Crison conductivity meter (model Basic 30). Finally, chase water was injected to estimate the residual resistance

factor (RRF) of the polymer using the following equation:

$$RRF = \frac{\Delta P_{Chase\ water\ flood}}{\Delta P_{Water\ flood}} \quad \text{(Eq. 3)}$$

where ΔP_{Water_flood} and $\Delta P_{Chase_Water_flood}$ are the stabilized differential pressures at the end of the water and the chase water flooding, respectively. A summary of the protocols for CF-1, CF-2 and CF-3 is presented in Table 3.

2.2. Simulation

Dynamic numerical simulations were performed using the compositional reservoir simulator CMG-STARS (CMG, 2016) with the main objective of confirming the surfactant blend parameters (IFT and adsorption measurements) during flooding, and also determining unknown parameters involved in the process.

2.2.1. Model system

The fluids flow along the core mainly in one direction during core flooding, with the radial flow being negligible (Kornilov et al., 2020; Kumar and Mandal, 2020). Thus, for the simulation of CF-2 and CF-3 tests, the cores were represented using 3D grids in Cartesian coordinates (X, Y, Z), with 11 grid blocks in the flow direction X (11 × 1 × 1). Fig. S1 and S.2 in the Supplementary Information (SI) show the grid sensitivity study carried out to determine the independence of the results from the grid resolution. Inlet and outlet flow points were set at each end of the grid. The grids were built to represent the core dimensions (length and cross-sectional area) and introduce rock characteristics (porosity and absolute permeability) and fluid properties at the corresponding test temperature (density and viscosity of water and oil phases). The flow of the fluids through the porous medium was modeled by the incorporation of relative permeability curves, which were built using Corey's correlations, and the end-points from the core flooding tests (S_{wi}, S_{orw}, K_{romax}, *and* K_{rwmax}). Data were initially introduced into the models with no changes and without considering any error range in their measurements. This original set of relative permeability curves (Set 1) was generated for each experiment (CF-2 and CF-3) to simulate the water flooding process.

Regarding surfactant flooding, experimental IFT measurements and adsorption were also set in the models. CMG-STARS models the surfactant effects by using sets of relative permeabilities curves, which are a function of the capillary number *Nc* (Abbaszadeh and Ren, 2013; CMG, 2016; Van Quy and Labrid, 1983). Since the incorporation of surfactant decreases the IFT to ultra-low values it can theoretically straighten the relative permeability curves (Bardon and Longeron, 1980; Harbert, 1983; Ronde, 1992), CMG-STARS was used to generate this second set of curves (Set 2). In the simulation, both sets were used for surfactant flooding: Set 1 obtained through water flooding conditions (at normal interfacial tension) and Set 2 for completely miscible flooding (ideal straight lines for ultra-low interfacial tension). The interpolation between these two sets allowed the generation of multiple intermediate relative permeability curves for semi-miscible flooding by simulation, and also the reproduction of the experimental data.

To represent polymer flooding, the experimental data of the viscosity of SSW polymer formulations, as a function of polymer concentration and shear rates, were introduced into the model. Since polymer adsorption was not measured, an approximate value was used as a starting point, and it was considered one of the history matching parameters. Accessible Pore Volume (*APV*) was also initially estimated.

Table 3
Summary of core flooding protocols.

	CF-1	CF-2	CF-3
Test Temperature (°C)	25	120	25
Carbonate core aging	No	Yes	No
Initial saturation fluid	SSW	SFW	SFW
Crude oil	A	B	A
Water Flooding			
Injection rate (mL/min)	2.00	0.066 (~1 ft/D)	0.050 (~1 ft/D)
Injected fluid	SSW	SSW	SSW
Chemical Flooding			
Injection rate (mL/min)	2.00	0.066 (~1 ft/D)	0.050 (~1 ft/D)
Injected fluid	Blend	Blend	Blend slug + Polymer
Chase water Flooding			
Injection rate (mL/min)	–	–	0.050 (~1 ft/D)
Injected fluid	–	–	SSW

2.2.2. Model validation (history match)

Some parameters entered in the numerical models were not measured experimentally and were assumed as starting points for initial simulations, and others were estimated experimentally but not directly measured during the displacement tests. Therefore, those properties had to be validated and re-evaluated through model calibration (history matching study). After building the initial models for CF-2 and CF-3 flooding tests, history matching was carried out in two stages, the first one was done for the water flooding and the second one for the chemical flooding periods.

For the water flooding history matching, the parameters to validate were the endpoints related to the relative permeability curves, mainly K_{romax} and K_{rwmax}, since S_{wi} and S_{or} were experimentally determined. The absolute permeability as well as the Corey's exponents for water (N_w) and oil phases (N_o) were also considered. In the case of the surfactant injection, the re-evaluation parameters were the blend adsorption and the IFT, this latter through the intermediate sets of relative permeability curves for semi-miscible conditions. CMG-STARS uses the wetting phase and the non-wetting phase interpolation factors, DTRAPW and DTRAPN respectively, to modify the interpolated relative permeability curves. Both are functions of the capillary number (CMG, 2016; Hakiki et al., 2015; Kumar and Mandal, 2020). For polymer injection, the main tuning parameters considered were the adsorption and the accessible pore volume (APV). The residual resistance factor (RRF) was also considered in the study with a lower range of variations since it was approximated during the experimental test.

The objective variables (outcome to match) were the produced fluids (oil and water), the injection scheme, and the differential pressures. For the assisted history match processing, the CMG-CMOST-AI tool, which combines experimental design and artificial intelligence, was used. For the matching of each model (CF-2 and CF-3), the range of evaluation for the parameters was based on the uncertainty of their determination. The process finished once the global error between experimental and simulated results of the objective variables achieved a value lower than 10%. This study was performed through the CMG Bayesian engine.

2.2.3. Chemical slug optimization

The model with the lower deviation, obtained during the history matching process, was used as base case for the chemical injection. The effects of the formulation, slug size and injection rate, as well as the polymer viscosity when applicable, were used to determine the optimized injection protocol.

3. Results and discussion

3.1. Experimental section

3.1.1. Blend scans

The results of the blend scan at 25 °C can be seen in Fig. 1. Pure surfactants RECOLAS103 and C1EG presented Winsor I behavior at 25 °C and 5 wt% TDS of salinity. As in the case of the blend SDBS/C1EG (Somoza et al., 2022b), increasing the proportion of the sulfonate surfactant from 0 wt% to 50 wt%, the blend became more lipophilic and a

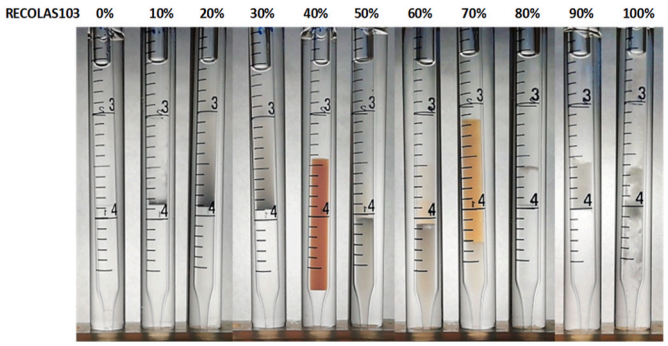


Fig. 1. Phase behavior evaluation for RECOLAS103/C1EG blend at 25 °C. Aqueous phase: 4 wt% blend in SSW; Oily phase: *n*-octane.

transition from Winsor I to Winsor III (at ~40 wt% RECOLAS103) and then to Winsor II (at equilibrated proportion of the components) was observed. The cationic C1EG and the anionic RECOLAS103, when blended, generated an optimal blend in Winsor III region (associated to ultra-low IFT and high oil recovery) caused by the electrostatic attraction between the oppositely charged surfactant head groups. The electrostatically neutral complex formed (a catanionic surfactant) exhibits many unique properties, due to the effective reduction of the area of surfactant head groups, and is less hydrophilic than the individual surfactants (Li et al., 2017; Puerto et al., 2012; Rodriguez-Escontrela et al., 2017; Somoza et al., 2022b). Increasing the proportion of RECOLAS103 from 50 to 100 wt% provoked the change of the microemulsion behavior from Winsor II to Winsor I, with a second Winsor III microemulsion at ~70 wt% RECOLAS103. This second blend leading to a Winsor III microemulsion was also found with SDBS (Somoza et al., 2022b) and was concluded to be less promising (higher adsorption, higher IFT and lower recovered oil) than the first one. For that reason, this work was focused on the applicability of the first blend for EOR applications.

As the behavior of the blend RECOLAS103/C1EG was very similar to SDBS/C1EG at 25 °C (Somoza et al., 2022b), similar behavior was also expected at higher temperatures. To confirm the hypothesis, blend scans were carried out at 50 °C and 75 °C (Fig. S3 and S4 in SI). A slightly different behavior was found at 50 °C, the blend presenting a three-phase region between 40 and 70 wt% RECOLAS103, with a significant reduction of the volume of water and oil solubilized. At 75 °C, as in the case of the SDBS/RECOLAS103 blend, a Winsor I-III-II-III-I transition was again found, with a Winsor III region corresponding to compositions ranging from 40 to 50 wt% RECOLAS103 and another Winsor III region at 70–80 wt% RECOLAS103. Fig. S5 (SI) shows the absence of liquid crystals for Winsor III microemulsions at 25 °C and 75 °C, although some liquid crystals were noticed at 50 °C between 40 and 60 wt% RECOLAS103.

In order to obtain the optimal solubilization parameters (V_i/V_s*), the solubilization parameters for oil (V_o/V_s) and water (V_w/V_s) were calculated for the optimal blend of interest (first one) at the three evaluated temperatures. Results are shown in Fig. 2. Increasing temperature from 25 °C to 75 °C reduced the V_i/V_s* value, which translates into reduced solubilization capacity of the formula. Table 4 shows the numerical values of the optimal solubilization parameters and optimal blend ratios, as well as the IFT estimated by Eq. (1). Slightly lower concentrations of sulfonate surfactant at the optimal blend ratio were found in this work

Table 4
Optimal blend ratios and solubilization parameters, and IFT_{Huh}, for the RECOLAS103/C1EG blend at 25 °C, 50 °C, and 75 °C.

	25 °C	50 °C	75 °C
Optimal blend ratio RECOLAS103/C1EG	42.3/57.7	39.1/60.9	38.7/61.3
V_i/V_s[a]	14.37	6.83	5.46
IFT_{Huh} (mN/m)	1.45×10^{-3}	6.43×10^{-3}	1.01×10^{-2}

[a] First optimum (see the text).

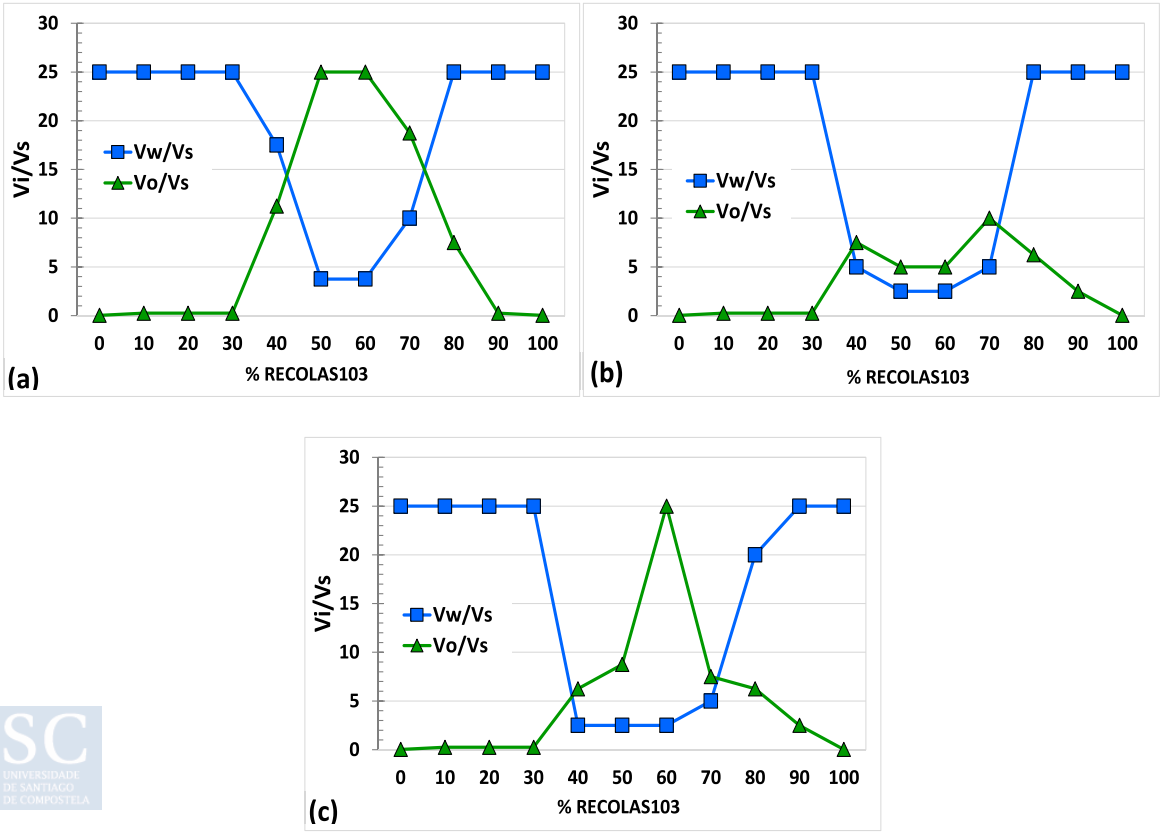


Fig. 2. Solubilization parameters (V_i/V_s) for RECOLAS103/C1EG blend at (a) 25 °C, (b) 50 °C, and (c) 75 °C. Aqueous phase: 4 wt% blend in SSW; Oily phase: *n*-octane.

with a petrochemical surfactant (used in practical applications) compared to our previous study with a pure commercial product (Somoza et al., 2022b). In addition, optimal solubilization parameters slightly decreased at 25 °C (14.4 with RECOLAS103 and 15.5 with SDBS) and increased at 50 and 75 °C (6.8 and 5.5 with RECOLAS103 and 3.7 and 3.3 with SDBS, at 50 and 75 °C, respectively). The differences being justified due to the mixture of chain lengths of the petrochemical surfactant.

3.1.2. Compatibility test

To ensure their compatibility, the stability of some formulations close to the optimal blend ratio was tested in SSW at 1 wt% blend concentration and room temperature. Mixtures with compositions in the blend ranging from 34 wt% to 44 wt% RECOLAS103 (step 2 wt%) were tested. As shown in Fig. 3, the blend presented stability in the evaluated ratios, keeping clear until the end of the test, after 4 weeks.

3.1.3. Dynamic interfacial tension (IFT)

The final selection of the best RECOLAS103/C1EG blend ratio was made based on IFT measurements. According to blend scan tests, Winsor III behavior (minimum IFT) was achieved at 38.7 wt% RECOLAS103 at 75 °C, and 42.3 wt% RECOLAS103 at 25 °C (see Table 4), so blend proportions ranging from 38 wt% to 45 wt% RECOLAS103 were selected. Fig. 4 shows the equilibrated IFT data at 25 °C as a function of blend ratios (for comparative purposes pure C1EG was also included, but RECOLAS103 precipitates in SSW). As shown, the RECOLAS103/C1EG blend reached the lowest IFT (2.1×10^{-2} mN/m) at a 40/60 ratio. In our previous work (Somoza et al., 2022b), the same optimal blend ratio was decided through IFT measurements, however, the IFT achieved was clearly lower (2.2×10^{-3} mN/m) than in the present case. As the surfactants behaved very similarly in previous tests, the reason is likely to be the type of crude. Crude oil components, especially resins and asphaltenes have significant influence on the IFT (Zhu and Lei, 2015). In the case of the work with SDBS (Somoza et al., 2022b), crude oil had a resin content of 11.6 wt%, 41.7 wt% of aromatics and 43.5 wt% of saturates. The crude oil used for IFT measurements in this work only has a 4.6 wt% resin content, and the content of aromatics is also lower (33 wt%), the saturate content clearly being higher (61 wt%). According to Zhu and Lei (2015), crude oil group components with the greatest effect on ITF reduction capacity are resins, followed by aromatic and finally saturates and wax content. So, the different composition of crude oils justifies the differences found in IFT measurements.

3.1.4. Adsorption

The adsorption obtained in our previous work for the blend SDBS/C1EG (Somoza et al., 2022b) was much lower in carbonate than in sandstone rocks, therefore the adsorption evaluation for the optimal blend RECOLAS103/C1EG was performed in a carbonate core at room temperature. Fig. 5 shows the relative concentration of the sampled effluents for the tracer (blue curve) and for the blend (green curve) as a function of the injected pore volume (PV) at room conditions. 50% of the initial tracer concentration (when $C/C_0 = 0.5$) was detected at 1.23 injected PV, while for the blend 2.13 PV was required. Using Eq. (2), the dynamic adsorption was estimated around 0.60 mg/g of rock. The electrostatic attraction between the surfactant head group and the rock surface is the most important mechanism of adsorption. The catanionic surfactant formed with the blend is an electrostatically neutral complex, which explains why the adsorption in carbonate material is low.

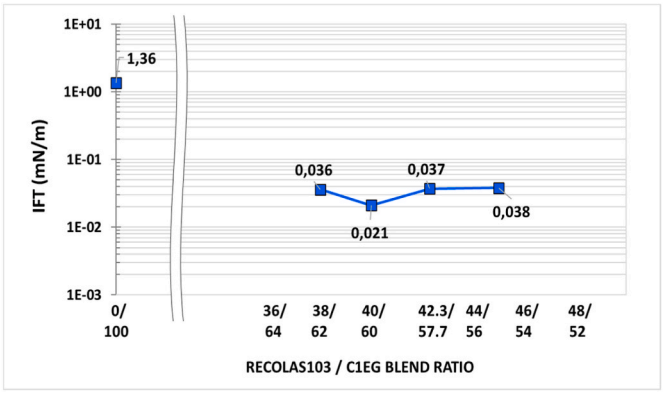


Fig. 4. Interfacial tension measurements at 25 °C and atmospheric pressure for RECOLAS103/C1EG formulations as a function of blend ratio. Aqueous phase: 1 wt% blend in SSW; Oily phase: crude oil.

3.1.5. Polymer solution evaluation

The apparent viscosity of different solutions, prepared in SSW, of two nonionic polymers (FloPAM FA 920 SH and FloPAM FA 920 VHM) was determined at 25 °C as a function of polymer concentration and shear rate (from 1 to 100 s^{-1}). Data are shown in SI (Fig. S6). Fig. 6 shows apparent viscosities at a shear rate of 10 s^{-1}. Due to the difficulty of getting an efficient displacement control with any of the polymers, injectivity tests for different polymer solutions were conducted in fresh carbonate cores. The results of those tests are presented in Fig. S7 and show the difficulty of matching polymer formulation and oil viscosities without plugging the core face due to the low permeability (17.7 mD) of the core. So, a compromise was struck: approaching the oil viscosity whilst also limiting polymer concentration to avoid plugging. The PAM 920 VHM polymer was selected to achieve an apparent viscosity $\eta = 6.3$ mPa s (at 10 s^{-1}) at a lower concentration (1500 ppm) than that required by the polymer PAM 920 SH (see Fig. 6).

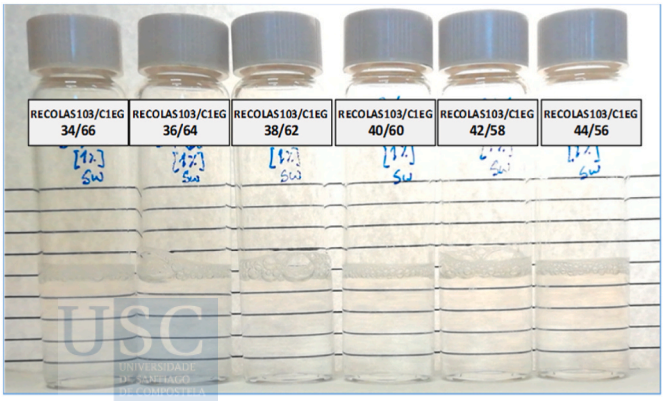


Fig. 3. Compatibility tests at room conditions for RECOLAS103/C1EG blends, at 1 wt% blend concentration and different surfactant ratios, in SSW and absence of oil phase.

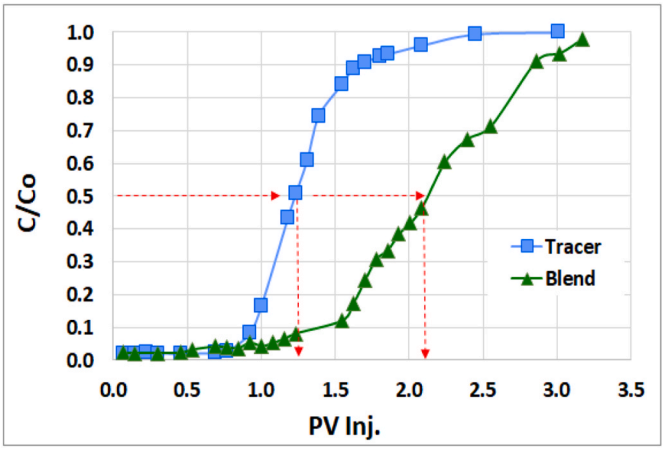


Fig. 5. Estimation of dynamic adsorption at room conditions for the optimal formulation (1 wt% blend - 40/60 RECOLAS103/C1EG-in SSW) in a carbonate core.

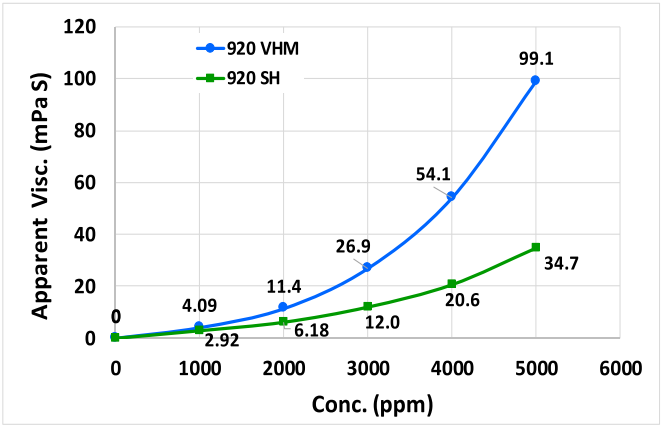


Fig. 6. Apparent viscosity, at 25 °C, atmospheric pressure and 10 s^{-1}shear rate, of FloPAM FA 920 VHM (blue) and FloPAM FA 920 SH (green) solutions prepared in SSW.

3.1.6. *Core flooding tests*

In the CF-1 test, the carbonate core (water-wet) was flooded with 4.2 PV of SSW at 2 mL/min (no oil production was observed by the end of the flood). Then, 4.34 PV of the optimized blend (1 wt% - 40 wt% RECOLAS103 - in SSW) were injected at 2 mL/min obtaining an AOR of 12.7% OOIP for this chemical flooding.

CF-2 was conducted at 120 °C and pore pressure of 91.4 psi with an intermediate-wet rock. The oil displacement was done by injecting SSW at 0.066 mL/min (~1 ft/D) until about 99% watercut and stable differential pressure across the core were observed, followed by 10.25 PV of the blend formulation at the same rate. The AOR was in this case 10.2% OOIP. Due to the very low permeability of the core (3.35 mD), no polymer was injected to avoid face plugging. The results of this test can be observed in Fig. 7.

For the CF-3 test, a water-wet carbonate rock was water flooded at 0.05 mL/min (~1 ft/D) until about 99% watercut and stable differential pressure across the core was observed. A blend slug of 0.56 PV was injected followed by 1.6 PV of polymer flooding, both at 0.05 mL/min. The AOR with this method was 11.7% OOIP. The chase water flooding was carried out to estimate the residual resistance factor (RRF) of the polymer, which was 1.4. Fig. 8 presents the oil recovery, differential pressures, residual oil saturation and salinity of the effluents for this core flooding test during the water (WF), blend (SF), and polymer (PF) floods. As shown, at 1.9 PV injected, the salinity of the effluent had already reached the SSW salinity used during the water flooding. Despite the polymer evaluation and the precautions taken, the rise of the injection pressure during polymer flooding shows slight but continuous face plugging. However, that did not influence the final efficiency of the blend greatly. The optimization of the polymer slug is outside the scope of this work.

Table 5 presents a summary of the three core flooding tests. The main mechanism associated to the improvement of oil recovery is IFT reduction. The blend of the cationic and anionic surfactants led to a catanionic species. Its aqueous formulation in contact with oil forms a Winsor III system associated with a very low IFT. This reduction is related to an increase in the capillary number, explaining the mobilization of trapped oil and the reduction of the residual oil saturation. The differences in the performance of the chemical flooding among the CF-2 with respect to the other two tests should be noted: the surfactant formulation lost efficiency at 120 °C when compared to CF-1 and CF-3 tests. Experimental conditions are different (core in CF-2 was aged), but the outcome is partially explained from results obtained in section 3.1.1, where a clearly low solubility of oil and water was achieved at the higher temperature. In the CF-2 test, the injection of more than 10 PV of blend was required to obtain an AOR of about 10% OOIP. Fig. 7 shows that 3 PV of blend formulation were required to start the oil displacement during surfactant flooding. When production ceased, a further 3.26 PV of blend formulation was injected to restart it.

3.2. *Simulation*

3.2.1. *Model validation (history match)*

In general, the numerical models of CF-2 and CF-3 tests were initialized for a first verification of the pore volume and OOIP. Afterwards, the models were run for the water flooding stage using initial values of the tuning parameters described in section 2.2.2. As indicated, the four end-points were obtained during the core flooding experiments. S_{wi} and S_{orw} (shown in Table 5), were directly taken from experimental data, while K_{romax} and K_{rwmax} were estimated by Darcy's law. A value of 2 was initially assigned to Corey's exponents, N_w and N_o, as a starting point for the iteration process. The simulated oil production, water production and differential pressures were compared with laboratory data from the CF-2 and CF-3 tests (Figs. 7 and 8). Results were not satisfactory, so to improve the match among them, parameters were tuned by a history matching process, to define the relative permeability curves that govern the water flooding (Set 1).

- ***CF-2 test***

For the CF-2 test, the simulation was done for better understanding and validate the mechanisms involved in the loss of productivity of blend flooding and in the differential pressure behavior. Table 6 shows the tuning parameters involved in this evaluation for water flooding, with the initial values for each parameter before history matching, their range of evaluation, as well as the defined values after the history matching.

Next, the simulation of blend injection was run with IFT and surfactant adsorption data obtained experimentally. Since the simulated

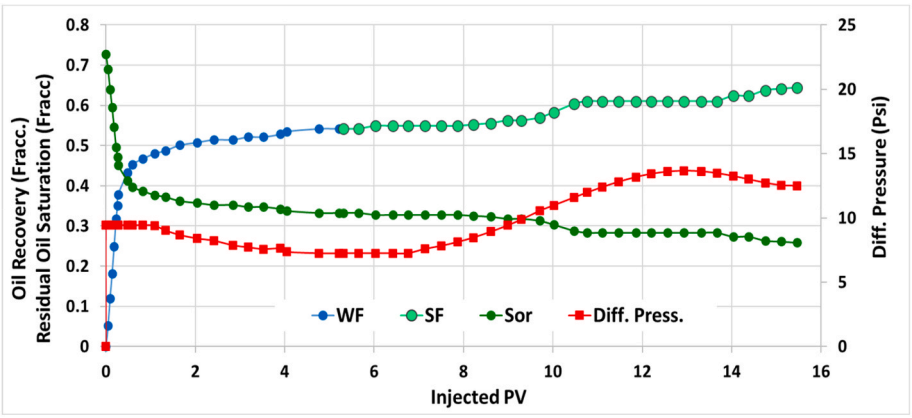


Fig. 7. Results of the displacement test CF-2 during the water (WF) and optimal blend (SF) floods at injection rate of 0.066 mL/min (~1 ft/D) and at 120 °C.

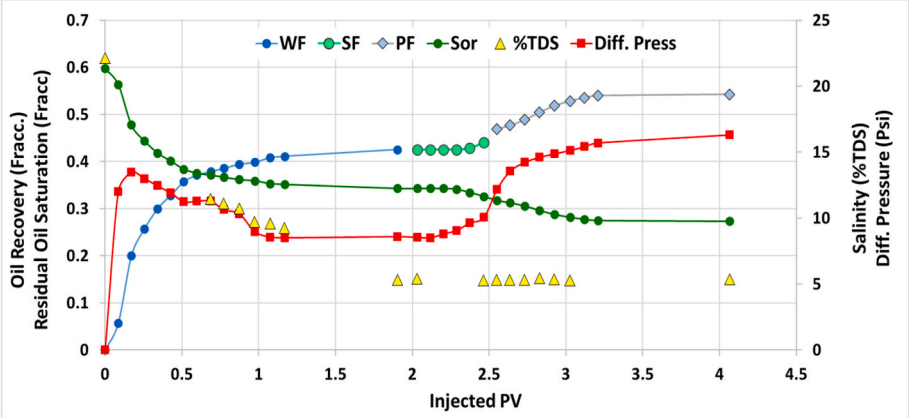


Fig. 8. Results of the displacement test CF-3 during the water (WF), optimal blend (SF), and polymer (PF) floods at injection rate of 0.05 mL/min (~1 ft/D) and at room conditions.

Table 5
Results of the core flooding experiments.

	CF-1	CF-2	CF-3
Porosity, ϕ (frac.)	0.147	0.177	0.134
Permeability, K_a (mD)	7.99	3.35	17.69
Pore Volume, PV (mL)	12.7	22.05	11.71
Oil Visc (mPa S) at test temp.	12	0.82	12
OOIP (mL)	8.4	16.03	7.0
Initial water saturation, S_{wi} (frac.)	0.338	0.273	0.402
Initial oil saturation, S_{oi} (frac.)	0.661	0.726	0.597
Water Flooding			
Injection rate, Qi (mL/min)	2.00	0.066	0.050
Injected SSW Volume (PV)	4.21	5.21	1.9
Oil Recovery (%OOIP)	59.5	54.2	42.5
Residual oil saturation, S_{orw} (frac.)	0.267	0.333	0.343
Chemical Flooding			
Injection rate (Q_i, mL/min)	2.00	0.066	0.050
Injected blend volume (PV)	4.34	10.25	0.56
Injected polymer volume (PV)	–	–	1.6
AOR (%OOIP)	12.7	10.2	11.7
Residual oil saturation, S_{or2} (frac.)	0.183	0.258	0.273

Table 6
Set of parameters for history matching of water flooding, test CF-2.

Parameter	Initial Value	Range Evaluated	History matched
K_a (mD)	3.35	2.51/4.18	3.7
S_{wi} (%)	0.273	0.270/0.275	0.273
S_{orw} (%)	0.333	0.32/0.34	0.34
K_{romax}	0.425	0.32/0.53	0.460
K_{rwmax}	0.334	0.25/0.42	0.465
N_w	2	1.5/2.5	1.8
N_o	2	1.5/2.5	1.6

results were not able to represent experimental results found in the core flooding CF-2, especially the delay in oil production, history matching was performed using the tuning parameters described in section 2.2.2 (blend adsorption and IFT). Preliminary attempts were made to adjust the oil production profile by increasing the IFT value and the surfactant adsorption. Rising the IFT value above 0.1 mN/m did not properly reproduce the delay in oil production (neither the slope of the production profile nor the total recovered oil). However, it was noticed that an increase in surfactant adsorption to very high levels (30 mg/g) better matched the simulated results with the experimental ones. At that point, it was obvious that surfactant adsorption would have a greater influence on the performance of chemical flooding than other parameters. Thus, a history matching study was carried out using the tuning parameters described previously for chemical flooding, but with special attention on the surfactant adsorption, expanding its evaluation range. The relative permeability curves for water flooding (Set 1) and completely miscible flooding (Set 2) used for curve interpolation during history matching are shown in Fig. 9.

Table 7 presents the initial values and range of evaluation used in the simulation. A total of 800 models were generated with different values and combinations of these parameters, using the established range of variations. Fig. S8 and S9 (in SI) show outcomes of the 800 models. The defined values after the history matching are also shown in Table 7. With these parameters, the model's global error was 8.21%.

Since the blend adsorption was already evaluated experimentally at 25 °C, the most likely explanation for this performance is to assume that this adsorption is actually the total retention of the surfactant in the porous medium, which involves the adsorption on the rock and also retention in the immovable oily phase contained in the pores of the rocks. The partitioning of the surfactant towards the oil phase (phase trapping) would justify the excess retention levels (Glover et al., 1979; Jang et al., 2016; Novosad, 1982). That would mean the microemulsion has shifted from Winsor type III to Winsor type II (water in oil microemulsion). Once the surfactant concentration in the oil phase is equilibrated, the oil begins to be movable. Moreover, the incorporation of water into the oil phase induces an increase in the emulsion viscosity, which would justify increases of the differential pressure along the surfactant injection (Izadi et al., 2014). The pressure behavior was therefore modeled by increasing the emulsion viscosity along the injection (Al-Murayri et al., 2019; CMG, 2016; Goudarzi et al., 2013).

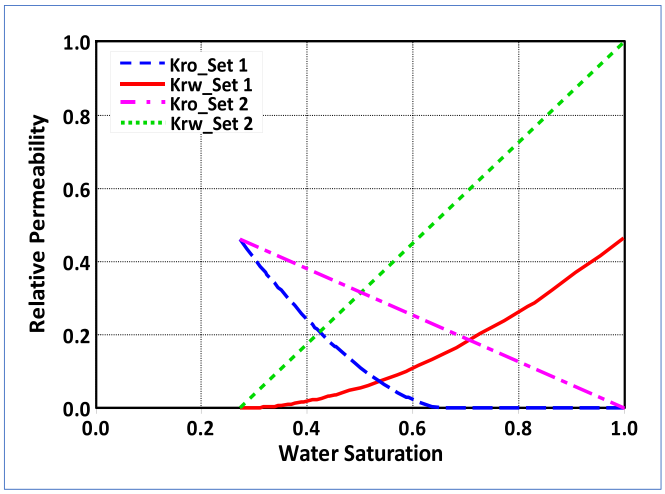


Fig. 9. Relative permeability curves for high IFT (Set 1) and ultralow IFT (Set 2), CF-2 model.

Table 7
Set of parameters for history matching of surfactant flooding, test CF-2.

Parameter	Initial value	Range evaluated	History matched
Dtrapw_Set 1	−5	−6.25/−3.75	−4.01
Dtrapn_Set 1	−5	−6.25/−3.75	−5.13
Dtrapw_Set interm	−3.5	−4.37/−2.62	−2.84
Dtrapn_Set interm	−3.5	−4.37/−2.62	−3.38
Dtrapw_Set 2	−2	−2.5/−1.5	−2.15
Dtrapn_Set 2	−2	−2.5/−1.5	−2.12
Surfactant Adsorp (mg/g)	0.60	0.60/50	36.4

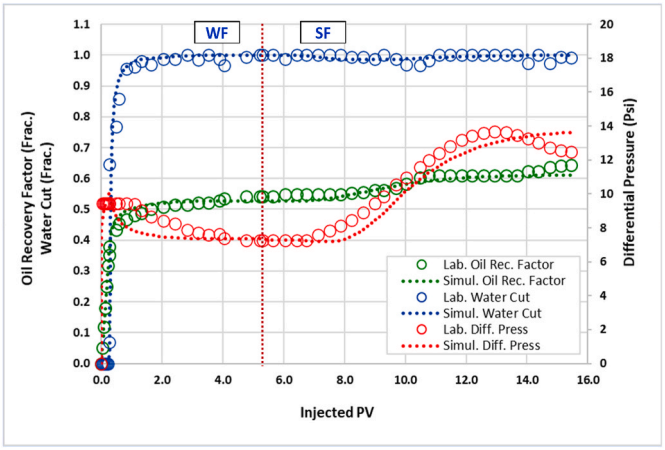


Fig. 10. Results of history matching process for core flooding test CF-2. Injection rate of 0.066 mL/min (~1 ft/D) at 120 °C.

Fig. 10 shows the results of the history matching evaluation, with experimental and best matched profiles for the objective variables.

The shift of the microemulsion behavior from Winsor type III to type II found by simulation could be due to an increase in water phase salinity or temperature. The phase behavior of the blend SDBS/C1EG was evaluated for salinity increase until 10% TDS and no shift was observed (Somoza et al., 2022b). In this work, microemulsion behavior was analyzed up to a temperature of 75 °C (see section 3.1.1), and despite showing a reduction of solubilization parameters with increasing temperature, the microemulsion always remained Winsor type III. Higher temperatures could not be tested due to working at atmospheric pressure and the corresponding boiling temperatures of the fluids. Taking into account the change of salinity from SFW to SSW inside the core during the SSW flooding, the amount of PV of SSW injected in CF-2 test, and the low effect of the salinity increase on the very similar blend SDBS/C1EG, the possible change of microemulsion type during the flooding could be very likely due to the increase of the test temperature.

- ***CF-3 test***

With regard to the CF-3 test, a simulation was done to validate the IFT and adsorption values obtained experimentally in sections 3.1.3 and 3.1.4 respectively, and later to optimize the process. The steps followed to simulate and to history match the water flooding were analogous to those described above for the CF-2 model. Initial and final values for the fitting parameters are shown in Table 8.

Table 8
Set of parameters for history matching of water flooding, test CF-3.

Parameter	Initial value	Range evaluated	History matched
K_a (mD)	17.69	16/20	17.7
S_{wi} (frac.)	0.402	0.39/0.405	0.402
S_{orw} (frac.)	0.343	0.33/0.35	0.345
K_{romax}	0.801	0.3/0.9	0.776
K_{rwmax}	0.353	0.3/0.9	0.383
N_w	2	1.5/3	1.8
N_o	2	1.5/3	1.9

Once the relative permeability curve Set 1 for the CF-3 water flooding was defined (see Fig. 9), a simulation was run for the blend and polymer injections, using experimental surfactant IFT and adsorption, and polymer RRF. Since a first suitable match was not obtained among the simulated and experimental objective variables at this stage, history matching was performed. Fig. 11 presents the relative permeability curves for water flooding (Set 1) and the ideal miscible flooding (Set 2), used for interpolation during history matching.

Table 9 shows initial and adjusted values of the tuning parameters, before and after history matching. The global error was found to be 7.91%. Fig. S10 to S.12 show several outcomes of the 800 generated models.

Fig. 12 shows a comparison between laboratory and simulated (with parameters shown in Table 9) data for produced oil, differential pressure and water cut profiles for core flooding test CF-3. It can be seen that in the case of the pressure profile for polymer injection, the simulation shows a certain deviation from experimental data, this is likely due to the plugging face not being appropriately modeled. However, regarding the surfactant parameters, a perfect match was found. So, the IFT and surfactant adsorption values were validated, and the model can be considered suitable to represent the oil displacement process.

3.2.2. Chemical injection optimization

Once the best matched simulation for the CF-3 test was obtained (base case), several schemes of chemical injection were designed (see Table 10) to determine the effects of the size of the slug and the injection rate over the final oil recovery, working at 25 °C. The ranges of variation were kept within realistic operational conditions.

The optimization focused on the blend injection. Polymer injection conditions of the base case were not modified for the first 4 cases, to avoid those improvements in the displacement control influencing the final oil recovery. Only the last case (Case 5) was simulated with a low residual resistance factor (RRF = 1.0) and a high viscosity (20 mPa S) for the polymer slug. Table 10 presents the EOR achieved in simulations of the different cases.

As expected, decreasing the mobility of the displacing fluid by injection of a more viscous polymer improves the volumetric sweep efficiency, reaching the highest values of recovered oil for the EOR process. For the other cases, although differences among them can be noted, a huge increase of the oil recovery with respect to the base case was not observed. Fig. 13 shows the oil recovery profiles for all the cases studied.

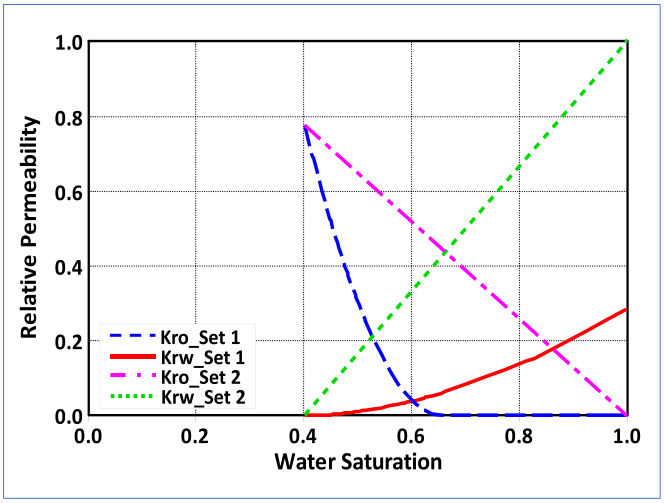


Fig. 11. Relative permeability curves for high IFT (Set 1) and ultralow IFT (Set 2), CF-3 model.

Table 9
Set of parameters for history matching of surfactant flooding, test CF-3.

Parameter	Initial value	Range evaluated	History matched
Dtrapw_Set 1	−5	−6.25/−3.75	−3.82
Dtrapn_Set 1	−5	−6.25/−3.75	−4.52
Dtrapw_Set interm	−3.5	−4.37/−2.62	−3.16
Dtrapn_Set interm	−3.5	−4.37/−2.62	−2.63
Dtrapw_Set 2	−2	−2.5/−1.5	−1.76
Dtrapn_Set 2	−2	−2.5/−1.5	−1.95
Surfactant Adsorp (mg/g)	0.60	0.45/0.75	0.63
Polymer RRF	1.4	1.05/1.75	1.69
Polymer Adsorp (mg/g)	0.50	0.37/0.62	0.38
Polymer APV	0.9	0.4/1.0	0.88

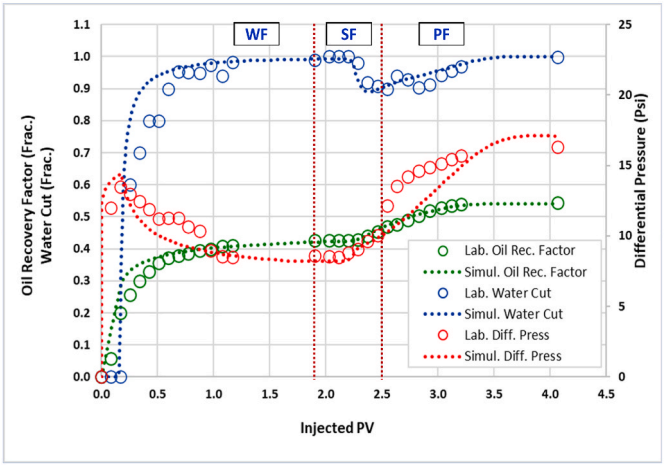


Fig. 12. Results of history matching process for core flooding test CF-3. Injection rate of 0.05 mL/min (~1 ft/D) at 25 °C.

Table 10
Case studies for the blend flooding and simulated EOR results, CF-3 test.

Case	Slug volume (PV)	Injection Rate (mL/min)	Polymer Visc. (mPa S)	AOR (% OOIP)
Base	0.56	0.05	6.3	11.5
Case 1	0.4	0.05	6.3	11.1
Case 2	1.0	0.05	6.3	12.1
Case 3	0.56	0.025	6.3	10.5
Case 4	0.56	0.075	6.3	11.7
Case 5	0.56	0.05	20	15.4

4. Conclusions

In a previous work, we proposed the use of a formulation based on the surfactant SDBS and the SAIL C1EG for EOR. The novelty of this new work lies in the approach to the industrial application of the method. To that aim, the ABS petroleum surfactant RECOLAS103 (developed by Cepsa) was blended with the SAIL, and the formulation was evaluated for EOR, both experimentally and through simulation. From the work carried out, some conclusions can be established.

The substitution of the pure commercial surfactant SDBS for the RECOLAS103 (a mixture of lineal alkyl benzene sulfonates with an average length of 11.6 carbons) did not affect any significant change regarding phase behavior, IFT and adsorption of the formulation. Blend scans showed two Winsor type III microemulsions at 25 °C, the first one around 40 wt% RECOLAS103 and the second one around 70 wt% RECOLAS103. Based on our previous study, further evaluation was focused on the first system. The Winsor type III behavior found at 40 wt % RECOLAS103 also continued at 50 and 75 °C although the optimal solubilization parameter decreased significantly. The oil-water IFT is more affected by the type of crude oil than by the small variations in the alkyl chain length of the sulfonate surfactant.

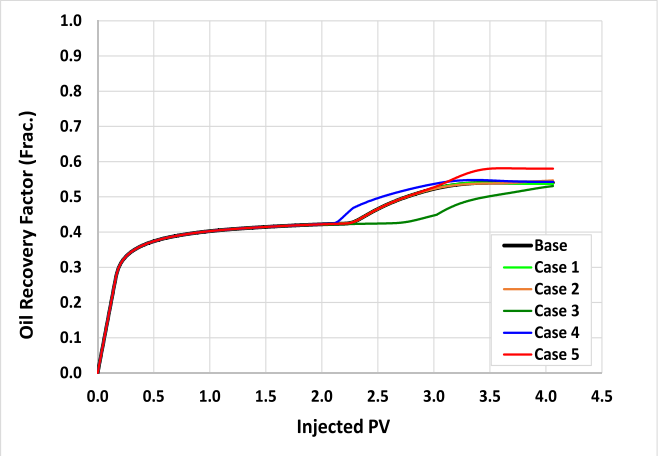


Fig. 13. Results of the optimization process for the blend injection. Injection rate of 0.05 mL/min (~1 ft/D) at 25 °C.

Oil recoveries achieved at 25 and 120 °C, using different injection conditions, were higher than 10 %OOIP. High productivity was achieved at 25 °C. The combination with a polymer formulation maintains the level of recovery and can decrease the cost of the surfactant.

The numerical simulations suggest that the main cause of blend efficiency loss at reservoir conditions (120 °C) was oil trapping due to a shift of the microemulsion type from Winsor Type III to Type II, likely due to the influence of temperature. Higher oil recoveries than those obtained experimentally could be achieved if the surfactant ratio at 120 °C, to avoid the shift to a Winsor II system, and type and concentration of polymer were optimized.

Funding

Ministry of Science and Innovation and State Research Agency (AEI, 10.13039/501100011033) throughout project PGC2018-097342-B-I00, including European Regional Development Fund.

Author contributions

N. Tafur: Experimental, Simulation, Formal analysis, Writing. A. Somoza: Experimental, Review & Editing. A. Panadero: Experimental, Review & Editing. B. Rodríguez-Cabo, I. Barrio: Resources, Review & Editing. M.F. García-Mayoral: Experimental, Resources, Review & Editing. A.P. Muñuzuri: Review & Editing. A Soto: Conceptualization, Supervision, Review & Editing, Funding acquisition.

Declaration of competing interest

The authors declare that they have no known competing financial interests or personal relationships that could have appeared to influence the work reported in this paper.

Data availability

No data was used for the research described in the article.

Acknowledgements

The authors would like to thank SNF Floerger for supplying polymer

samples.

Appendix A. Supplementary data

Supplementary data to this article can be found online at https://doi.org/10.1016/j.geoen.2023.211619.

References

Abbaszadeh, M., Ren, G., 2013. Simulation techniques for surfactant phase behavior and foam flow modeling in fractured reservoirs. In: Soc. Pet. Eng. - SPE Reserv. Characterisation Simul. Conf. Exhib. RCSC 2013 New Approaches Characterisation and Modelling Complex Reserv, vol. 2, pp. 927–942. https://doi.org/10.2118/166032-ms.

Akbar, M., Alghamdi, A.H., Herron, M., Allen, D., Carnegie, A., Dutta, D., Olesen, J.-R., Chourasiya, R.D., Logan, D., Stief, D., Netherwood, R., Russell, S.D., Saxena, K., 1995. A snapshot of carbonate reservoir evaluation carbonate. Oilfield Rev. 1, 38–57.

Al-Muraryi, M.T., Ghedan, S.G., Skoreyko, F., Hassan, A.A., Lara, R., Qubian, A., 2019. Compositional modeling and calibration of ASP carbonate corefloods. In: SPE Middle East Oil Gas Show Conf. MEOS, Proc.. https://doi.org/10.2118/195039-ms, 2019-March.

American Petroleum Institute- Production Department, 1990. Recommended Practices for Evaluation of Polymers Used in Enhanced Oil Recovery Operations, First. ed. American Petroleum Institute - Official Publication, Washington, DC.

Barati-Harooni, A., Najafi-Marghmaleki, A., Tatar, A., Mohammadi, A.H., 2016. Experimental and modeling studies on adsorption of a nonionic surfactant on sandstone minerals in enhanced oil recovery process with surfactant flooding. J. Mol. Liq. 220, 1022–1032. https://doi.org/10.1016/j.molliq.2016.04.090.

Bardon, C., Longeron, D.G., 1980. Influence of very low interfacial tensions on relative permeability. Soc. Petrol. Eng. J. 391–401. https://doi.org/10.2118/7609-pa.

Barnes, J.R., Smit, J.P., Smit, J.R., Shpakoff, P.G., Raney, K.H., Puerto, M.C., 2008. Development of surfactants for chemical flooding at difficult reservoir conditions. SPE Symp. Improv. Oil Recover. 1, 435–452. https://doi.org/10.2118/113313-ms.

Burchette, T.P., 2012. Carbonate rocks and petroleum reservoirs: a geological perspective from the industry. Geol. Soc. Spec. Publ. 370, 17–37. https://doi.org/10.1144/SP370.14.

CMG, 2016. In: STARS User Guide-Advanced Processes & Thermal Reservoir Simulator, Version 20. Computer Modelling Group Ltd., Calgary, Canada.

Cooper, E.R., Andrews, C.D., Wheatley, P.S., Webb, P.B., Wormald, P., Morris, R.E., 2004. Ionic liquids and eutectic mixtures as solvent and template in synthesis of zeolite analogues. Nature 430, 1012–1016. https://doi.org/10.1038/nature02860.

Feng, H., Hou, J., Ma, T., Meng, Z., Wu, H., Yang, H., Kang, W., 2018. The ultra-low interfacial tension behavior of the combined cationic/anionic-nonionic gemini surfactants system for chemical flooding. Colloids Surfaces A Physicochem. Eng. Asp. 554, 74–80. https://doi.org/10.1016/j.colsurfa.2018.06.028.

Fernández-Stefanuto, V., Corchero, R., Rodríguez-Escontrela, I., Soto, A., Tojo, E., 2018. Ionic liquids derived from proline: application as surfactants. ChemPhysChem 19, 2885–2893. https://doi.org/10.1002/cphc.201800735.

Ghadami, N., Arsanti, D., Faizal Sedaralit, M., 2015. Uncertainty assessment of chemical EOR in one of the offshore fields in Malaysia. Soc. Pet. Eng. - SPE Asia Pacific Enhanc. In: Oil Recover. Conf. EORC 2015, pp. 522–536. https://doi.org/10.2118/174614-ms.

Glover, C.J., Puerto, M.C., Maerker, J.M., Sandvik, E.L., 1979. Surfactant phase behavior and retention in porous media. Soc Pet Eng AIME J 19, 183–193. https://doi.org/10.2118/7053-pa.

Goudarzi, A., Delshad, M., Sepehrnoori, K., 2013. A critical assessment of several reservoir simulators for modeling chemical enhanced oil recovery processes. Soc. Pet. Eng. - SPE Reserv. Simul. Symp. 1, 33–48. https://doi.org/10.2118/163578-ms, 2013.

Green, D., Willhite, G.P., 2018. Enhanced Oil Recovery, second ed. Society of Petroleum Engineers, Inc, Richardson, Texas.

Hakiki, F., Maharsi, D.A., Marhaendrajana, T., 2015. Surfactant-polymer coreflood simulation and uncertainty analysis derived from laboratory study. J. Eng. Technol. Sci. 47, 706–725. https://doi.org/10.5614/j.eng.technol.sci.2015.47.6.9.

Hanke, C.G., Lynden-Bell, R.M., 2003. A simulation study of water-dialkylimidazolium ionic liquid mixtures. J. Phys. Chem. B 107, 10873–10878. https://doi.org/10.1021/jp034221d.

Harbert, L.W., 1983. Low interfacial tension relative permeability. In: Proc. - SPE Annu. Tech. Conf. Exhib, pp. 2–9. https://doi.org/10.2523/12171-ms, 1983-Octob.

Huh, C., 1979. Interfacial tensions and solubilizing ability of a microemulsion phase that coexists with oil and brine. J. Colloid Interface Sci. 71, 408–426. https://doi.org/10.1016/0021-9797(79)90249-2.

Izadi, M., Kazemi, H., Manrique, E.J., Kazempour, M., Rohilla, N., 2014. Microemulsion flow in porous media : potential impact on productivity loss. In: Soc. Pet. Eng. - SPE EOR Conf. Oil Gas West Asia, Muscat, Oman. https://doi.org/10.2118/169726-MS.

Jang, S.H., Liyanage, P.J., Tagavifar, M., Chang, L., Upamali, K.A.N., Lansakara-P, D., Weerasooriya, U., Pope, G.A., 2016. A systematic method for reducing surfactant retention to extremely low levels. SPE - DOE Improv. Oil Recover. Symp. Proc. 2016-Janua. https://doi.org/10.2118/179685-ms.

Jia, H., Leng, X., Hu, M., Song, Y., Wu, H., Lian, P., Liang, Y., Zhu, Y., Liu, J., Zhou, H., 2017. Systematic investigation of the effects of mixed cationic/anionic surfactants on the interfacial tension of a water/model oil system and their application to enhance crude oil recovery. Colloids Surfaces A Physicochem. Eng. Asp. 529, 621–627. https://doi.org/10.1016/j.colsurfa.2017.06.055.

Kamal, M.S., Hussein, I.A., Sultan, A.S., 2017. Review on surfactant flooding: phase behavior, retention, IFT, and field applications. Energy Fuel. 31, 7701–7720. https://doi.org/10.1021/acs.energyfuels.7b00353.

Kornilov, A., Zhirov, A., Petrakov, A., Rogova, T., Kurelenkova, Y., Afanasiev, I., Sansiev, G., Fedorchenko, G., Fursov, G., Kubrak, M., Altmann, T., Lichterfeld-Weber, N., Bittner, C., Oetter, G., Helwig, E., 2020. Selection of effective surfactant composition to improve oil displacement efficiency in carbonate reservoirs with high salinity formation water. In: Soc. Pet. Eng. - SPE Russ. Pet. Technol. Conf. RPTC 2019. https://doi.org/10.2118/196772-ms, 2019.

Kumar, A., Mandal, A., 2020. Core-scale modelling and numerical simulation of zwitterionic surfactant flooding: designing of chemical slug for enhanced oil recovery. J. Pet. Sci. Eng. 192 https://doi.org/10.1016/j.petrol.2020.107333.

Kurnia, I., Zhang, G., Han, X., Yu, J., 2020. Zwitterionic-anionic surfactant mixture for chemical enhanced oil recovery without alkali. Fuel 259, 116236. https://doi.org/10.1016/j.fuel.2019.116236.

Li, Y., Puerto, M., Bao, X., Zhang, W., Jin, J., Su, Z., Shen, S., Hirasaki, G., Miller, C., 2017. Synergism and performance for systems containing binary mixtures of anionic/cationic surfactants for enhanced oil recovery. J. Surfactants Deterg. 20, 21–34. https://doi.org/10.1007/s11743-016-1892-x.

Li, Z., Wu, H., Hu, Y., Chen, X., Yuan, Y., Luo, Y., Hou, J., Bai, B., Kang, W., 2020. Ultra-low interfacial tension biobased and catanionic surfactants for low permeability reservoirs. J. Mol. Liq. 309 https://doi.org/10.1016/j.molliq.2020.113099.

Ma, K., Cui, L., Dong, Y., Wang, T., Da, C., Hirasaki, G.J., Biswal, S.L., 2013. Adsorption of cationic and anionic surfactants on natural and synthetic carbonate materials. J. Colloid Interface Sci. 408, 164–172. https://doi.org/10.1016/j.jcis.2013.07.006.

Manshad, A.K., Rezaei, M., Moradi, S., Nowrouzi, I., Mohammadi, A.H., 2017. Wettability alteration and interfacial tension (IFT) reduction in enhanced oil recovery (EOR) process by ionic liquid flooding. J. Mol. Liq. 248, 153–162. https://doi.org/10.1016/j.molliq.2017.10.009.

Montes, J., Blin, N., Alvarez, A.E., Barrio, I., Panadero, A., Rodriguez, R., Coca, M., Trujillo, F., 2018. Novel anionic surfactant formulation for high temperature carbonate reservoirs. In: Soc. Pet. Eng. - SPE EOR Conf. Oil Gas West Asia. https://doi.org/10.2118/190353-ms, 2018 2018-March.

Nandwani, S.K., Chakraborty, M., Bart, H.J., Gupta, S., 2018. Synergism, phase behaviour and characterization of ionic liquid-nonionic surfactant mixture in high salinity environment of oil reservoirs. Fuel 229, 167–179. https://doi.org/10.1016/j.fuel.2018.05.021.

Nandwani, S.K., Chakraborty, M., Gupta, S., 2019. Chemical flooding with ionic liquid and nonionic surfactant mixture in artificially prepared carbonate cores: a diffusion controlled CFD simulation. J. Petrol. Sci. Eng. 173, 835–843. https://doi.org/10.1016/j.petrol.2018.10.083.

Nandwani, S.K., Malek, N.I., Chakraborty, M., Gupta, S., 2019b. Potential of a novel surfactant slug in recovering additional oil from highly saline calcite cores during the EOR process: synergistic blend of surface active ionic liquid and nonionic surfactant. Energy Fuel. 33, 541–550. https://doi.org/10.1021/acs.energyfuels.8b03419.

Novosad, J., 1982. Surfactant retention in berea sandstone-effects of phase behavior and temperature. Soc. Petrol. Eng. J. 22, 962–970. https://doi.org/10.2118/10064-PA.

Pal, N., Vajpayee, M., Mandal, A., 2019. Cationic/nonionic mixed surfactants as enhanced oil recovery fluids: influence of mixed micellization and polymer association on interfacial, rheological, and rock-wetting characteristics. Energy Fuel. 33, 6048–6059. https://doi.org/10.1021/acs.energyfuels.9b00671.

Puerto, M., Hirasaki, G.J., Miller, C.A., Barnes, J.R., 2012. Surfactant systems for EOR in high-temperature, high-salinity environments. SPE J. 17, 11–19. https://doi.org/10.2118/129675-PA.

Rodriguez-Escontrela, I., Puerto, M.C., Miller, C.A., Soto, A., 2017. Ionic liquids for low-tension oil recovery processes: phase behavior tests. J. Colloid Interface Sci. 504, 404–416. https://doi.org/10.1016/j.jcis.2017.05.102.

Ronde, H., 1992. Relative permeability at low interfacial tensions. In: Proc. - SPE Annu. Tech. Conf. Exhib. Sigma, pp. 123–134. https://doi.org/10.2523/24877-ms.

Scamehorn, J.F., Schechter, R.S., Wade, W.H., 1982. Adsorption of surfactants on mineral oxide surfaces from aqueous solutions. I: isomerically pure anionic surfactants. J. Colloid Interface Sci. 85, 463–478. https://doi.org/10.1016/0021-9797(82)90013-3.

Sharma, H., Lu, J., Weerasooriya, U.P., Pope, G.A., Mohanty, K.K., 2016. Adsorption in chemical floods with ammonia as the alkali. SPE - DOE Improv. In: Oil Recover. Symp. Proc. https://doi.org/10.2118/179682-MS, 2016-Janua.

Sheng, J., 2013. Enhanced Oil Recovery Field Case Studies, second ed. Elsevier Inc., Amsterdam.

Sheng, J., 2011. Modern Chemical Enhanced Oil Recovery: Theory and Practice, second ed. Elsevier Inc., Amsterdam.

Somoza, A., Arce, A., Soto, A., 2022a. Oil recovery tests with ionic liquids: a review and evaluation of 1-decyl-3-methylimidazolium triflate. Petrol. Sci. 19, 1877–1887. https://doi.org/10.1016/j.petsci.2021.10.025.

Somoza, A., Tafur, N., Arce, A., Soto, A., 2022b. Design and performance analysis of a formulation based on SDBS and ionic liquid for EOR in carbonate reservoirs. J. Pet. Sci. Eng. 209, 109856 https://doi.org/10.1016/j.petrol.2021.109856.

Spildo, K., Johannessen, A., Skauge, A., 2012. Low salinity waterflood at reduced capillarity. SPE - DOE Improv. Oil Recover. Symp. Proc. 2, 1264–1276. https://doi.org/10.2118/154236-ms.

Van Quy, N., Labrid, J., 1983. Numerical study of chemical flooding - comparison with experiments. Soc. Petrol. Eng. J. 23, 461–474. https://doi.org/10.2118/10202-pa.

Wang, J., Han, M., Fuseni, A.B., Cao, D., 2015. Surfactant adsorption in Surfactant-Polymer flooding for carbonate reservoirs. In: SPE Middle East Oil Gas Show Conf. MEOS, Proc, pp. 1736–1746. https://doi.org/10.2118/172700-ms, 2015-Janua.
Zabihi, S., Faraji, D., Rahnama, Y., Zeinolabedini Hezave, A., Ayatollahi, S., 2019. Relative permeability measurement in carbonate rocks, the effects of conventional surfactants vs. Ionic liquid-based surfactants. J. Dispersion Sci. Technol. 41, 1797–1811. https://doi.org/10.1080/01932691.2019.1637262.
Zhu, Y., Lei, M., 2015. Effects of crude oil components on the interfacial tension between oil and surfactant solutions. In: Soc. Pet. Eng. - SPE Asia Pacific Enhanc. Oil Recover. Conf. EORC, pp. 341–349. https://doi.org/10.2118/174593-ms, 2015.

USC UNIVERSIDADE DE SANTIAGO DE COMPOSTELA

ASSESMENT OF A SURFACE-ACTIVE IONIC LIQUID FORMULATION FOR EOR APPLICATIONS: EXPERIMENTAL AND SIMULATION STUDIES

Nestor Tafur[1*], Alba Somoza[1], Alberto P. Muñuzuri[2], Borja Rodríguez-Cabo[3], Izaskun Barrio[3], Asier Panadero[4], M. Flor García-Mayoral[4], and Ana Soto[1*]

[1] CRETUS. Department of Chemical Engineering, Universidade de Santiago de Compostela, E-15782, Santiago de Compostela, Spain.
[2] Group of Nonlinear Physics. Dept. of Physics. Universidade de Santiago de Compostela, E-15782, Santiago de Compostela, Spain.
[3] CEPSA-Química. Research Center, E-28805, Madrid, Spain
[4] CEPSA. Research Center, E-28805, Madrid, Spain

SUPPLEMENTARY INFORMATION

[*] Corresponding authors. E-mails: ana.soto@usc.es / nestor.tafur@usc.es

USC UNIVERSIDADE DE SANTIAGO DE COMPOSTELA

1. Grid Sensitivity Study

This study was carried out to identify the optimal grid resolution for simulations. To that aim, the selected control property was the final oil recovery.

As the radial flow was considered negligible, grid resolution in Y and Z directions were fixed to 1 (nY=nZ=1) and the grid sensitivity evaluation was performed increasing the grid block number in the direction X (nX), maintaining the original dimensions of the core (length and cross-sectional area). In all cases, independently of the grid resolution, the outlet and inlet points of the models were set close to the ends of the core model. The objective was the representation of real operational conditions and the achievement of the convergence of the results with the lowest number of cells. Figure S.1 shows examples of the core models with different resolutions (nX).

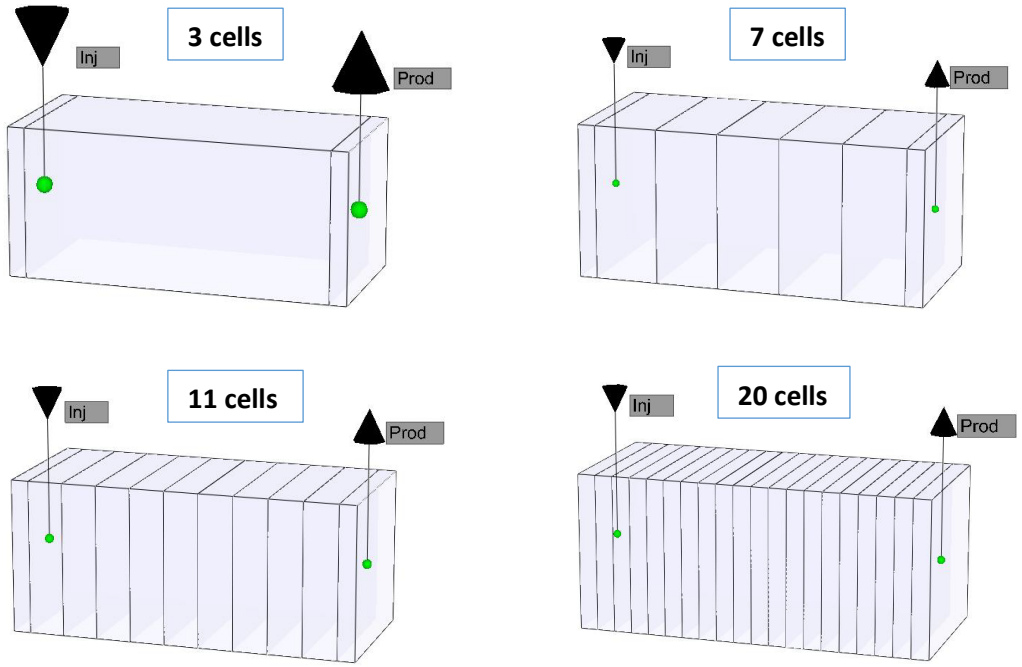


Figure S.1. Examples for the one direction Cartesian grid models with different resolutions (nX=3, 7, 11 and 20 cells).

Figure S.2 shows the results of the final oil recovery as a function of grid resolution. As the number of grid blocks in X direction increases, the results start to converge to a single solution. According to these results, the grid resolution with 11 cells in the X direction was selected for simulations.

USC UNIVERSIDADE DE SANTIAGO DE COMPOSTELA

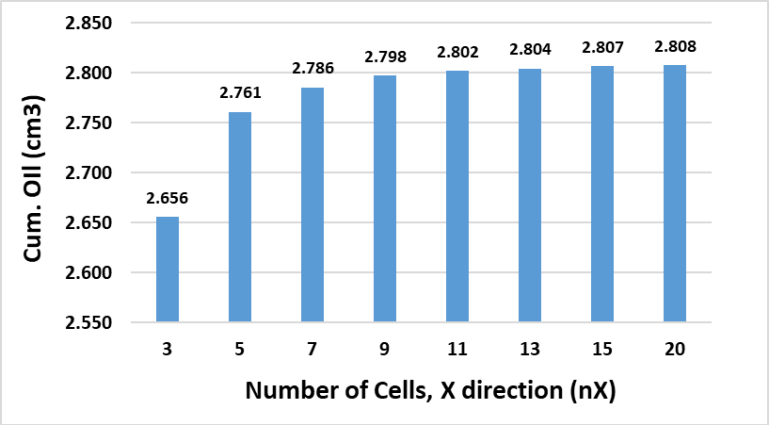


Figure S.2. Final oil recovery response as a function of grid resolution.

2. Blend scan for RECOLAS103/C1EG at 50°C and 75°C.

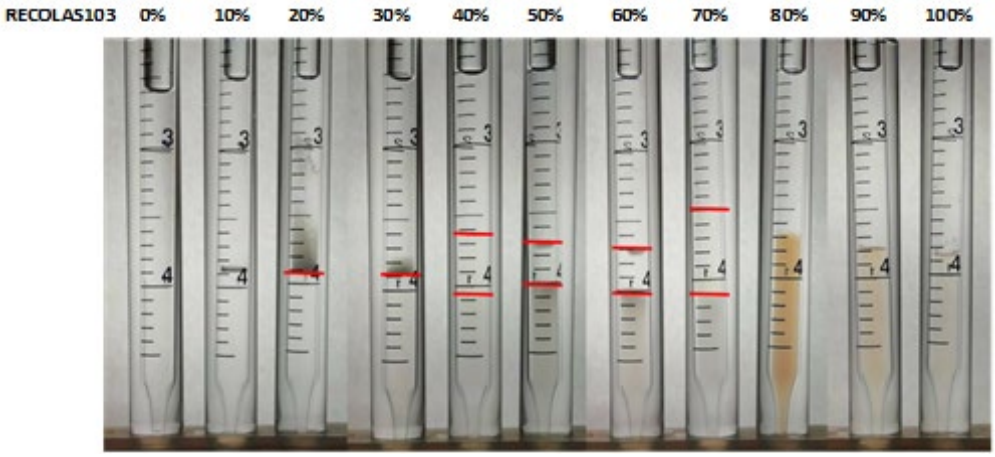


Figure S.3. Blend scan for RECOLAS103 / C1EG at 50°C.

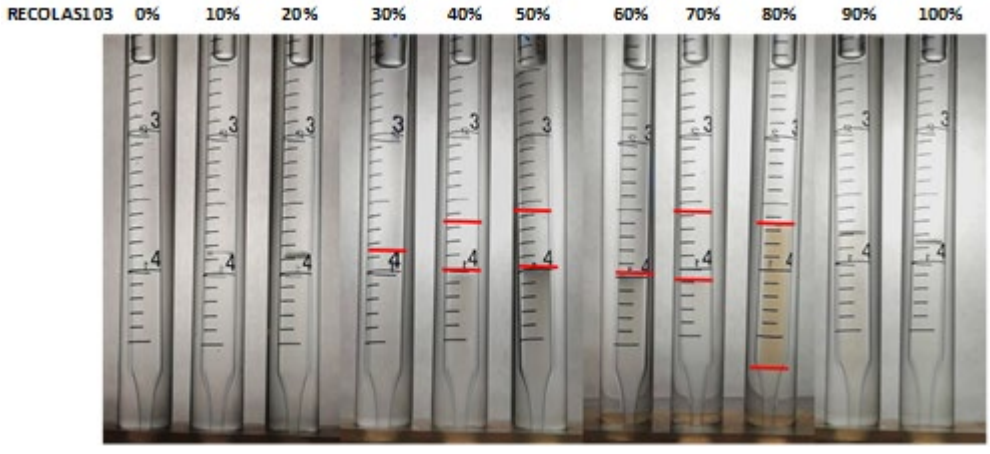


Figure S.4. Blend scan for RECOLAS103 / C1EG at 75°C.

3. Blend scans for RECOLAS103/C1EG under polarized light at 25°C, 50°C and 75°C.

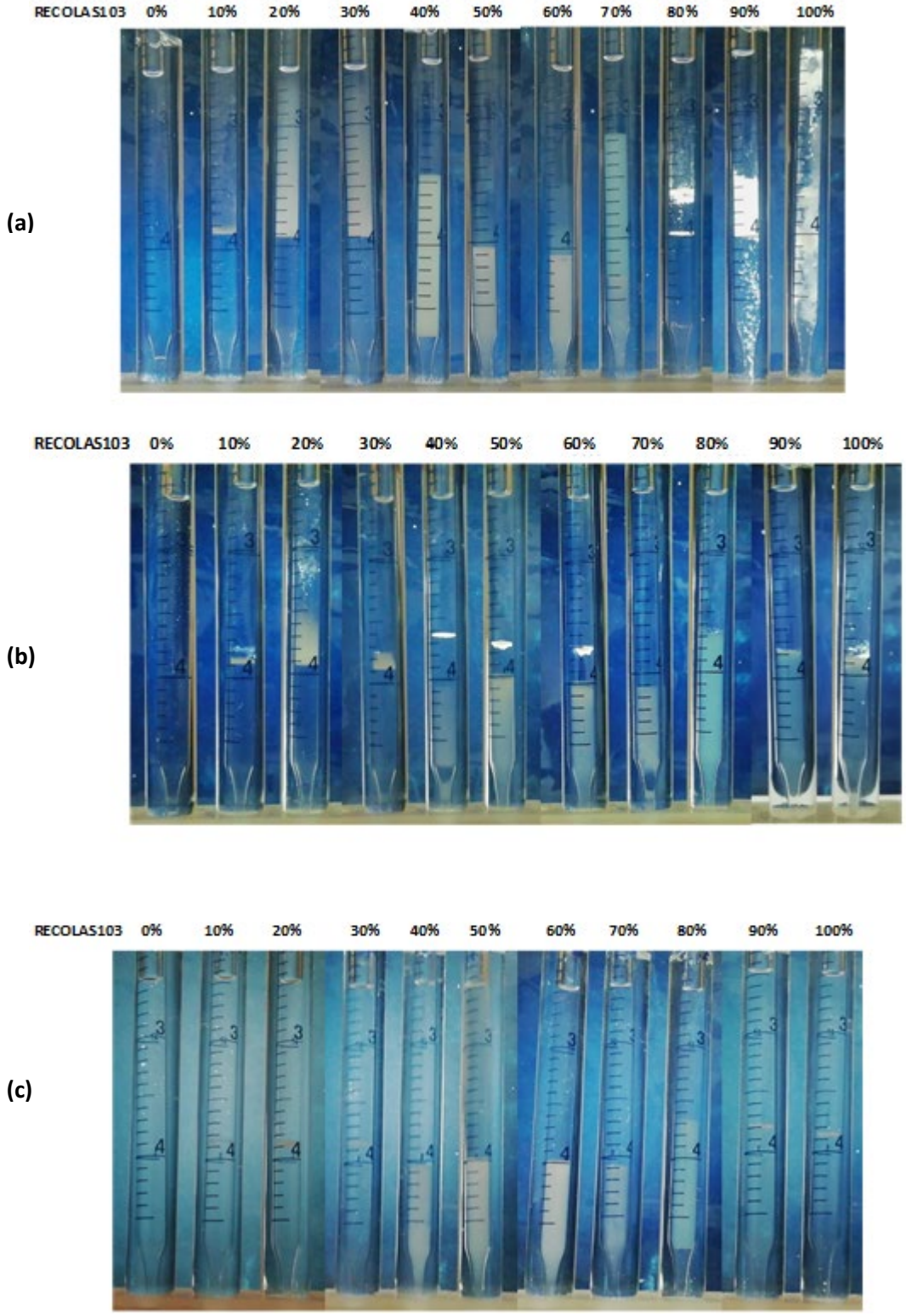
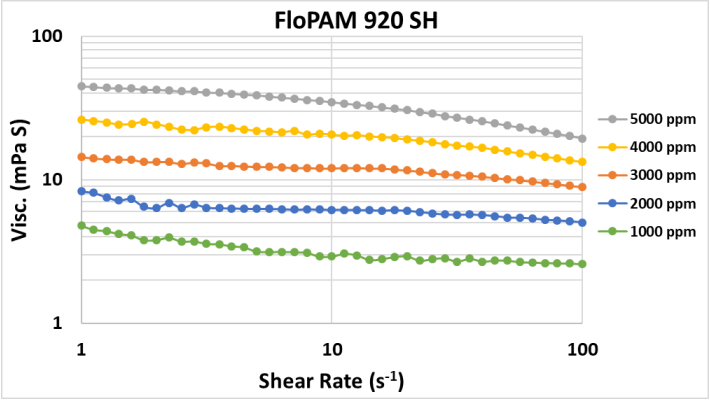


Figure S.5. Blend scan for RECOLAS103/C1EG under polarized light at (a) 25°C, (b) 50°C and (c) 75°C.

USC UNIVERSIDADE DE SANTIAGO DE COMPOSTELA

4. Polymer solution evaluation.

(a)



(b)

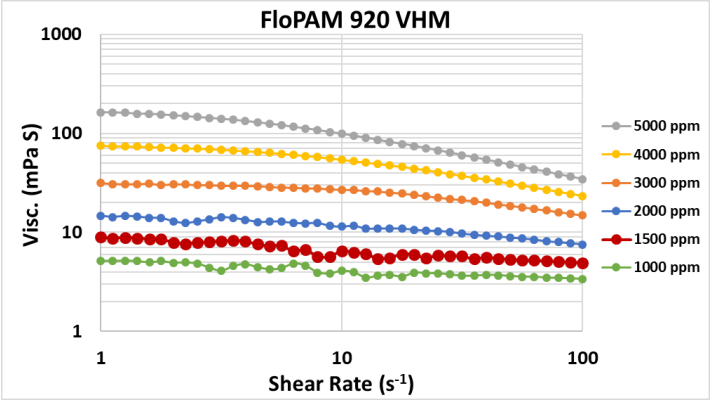


Figure S.6. Polymer apparent viscosity behavior as a function of shear rates for (a) FloPAM 920 SH and (b) FloPAM 920 VHN at 25°C.

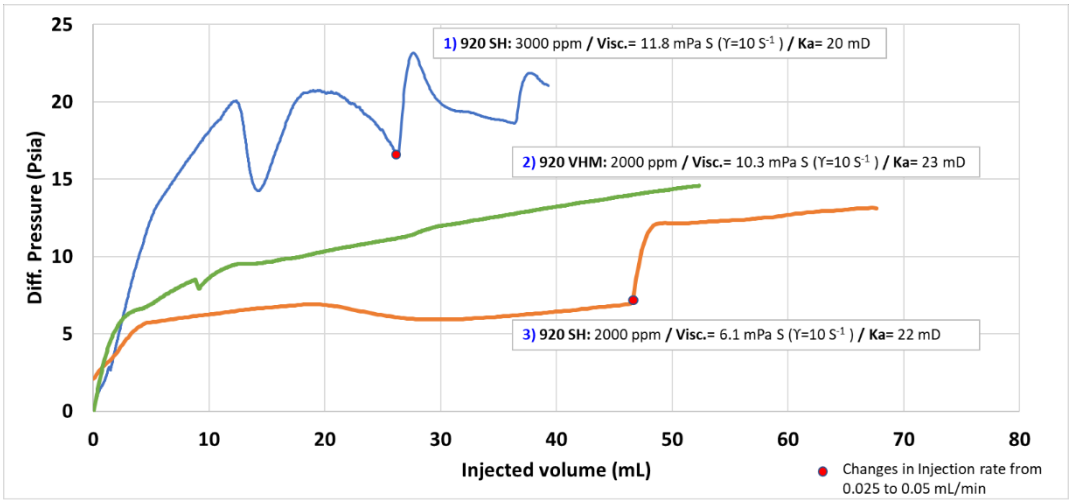


Figure S.7. Injectivity tests three polymer solutions at room conditions.

USC UNIVERSIDADE DE SANTIAGO DE COMPOSTELA

5. Results of the history matching for surfactant flooding, test CF-2.

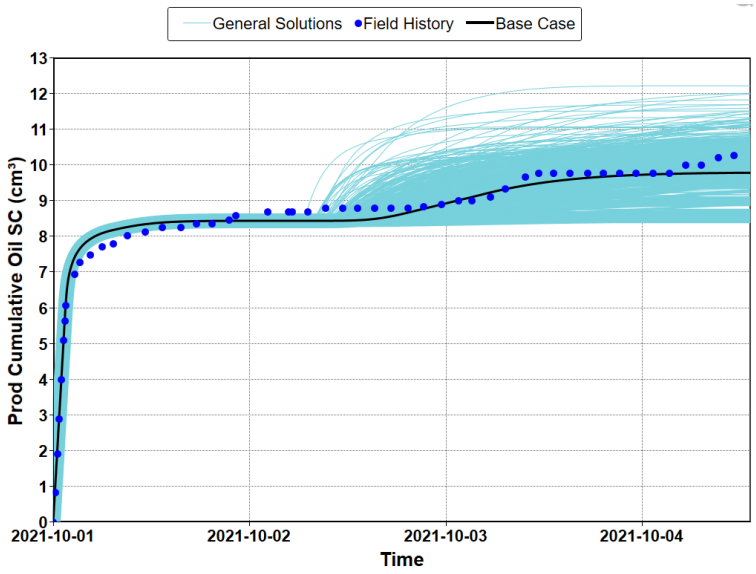


Figure S.8. History matching for produced oil during surfactant flooding, test CF-2.

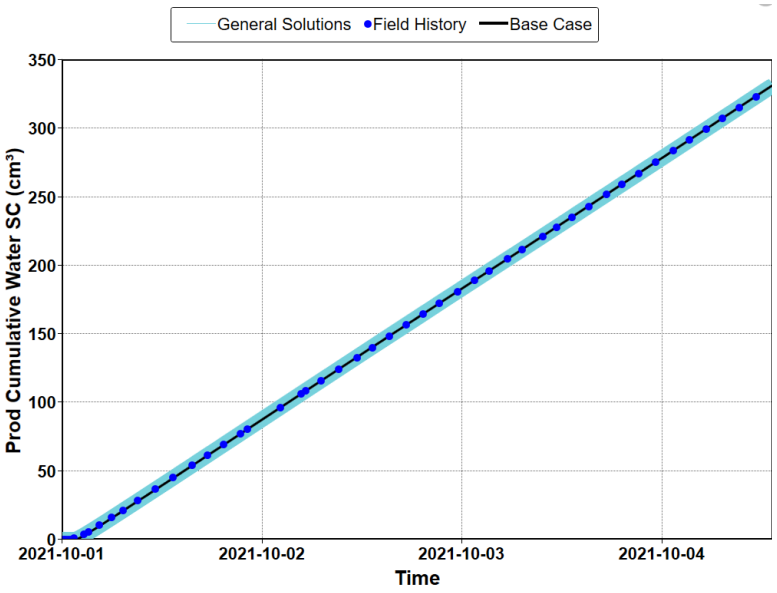


Figure S.9. History matching for produced water during surfactant flooding, test CF-2.

6. Results of the history matching for chemical flooding, test CF-3.

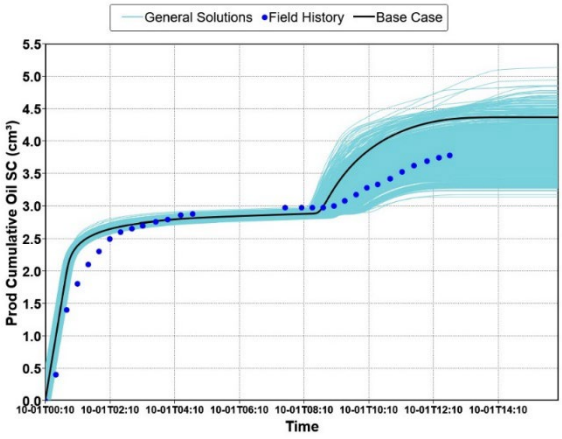


Figure S.10. History matching for produced oil during surfactant and polymer flooding, test CF-3.

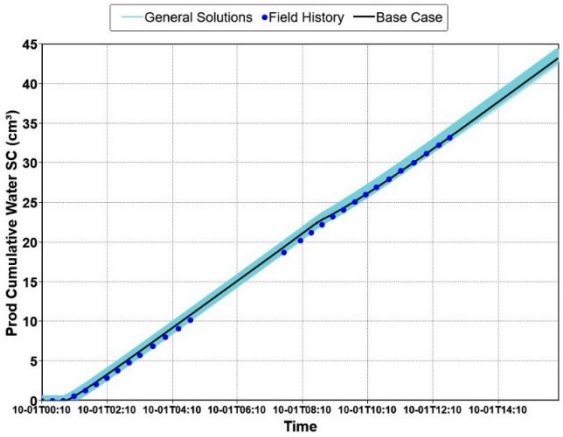


Figure S.11. History matching for produced water during surfactant and polymer flooding, test CF-3.

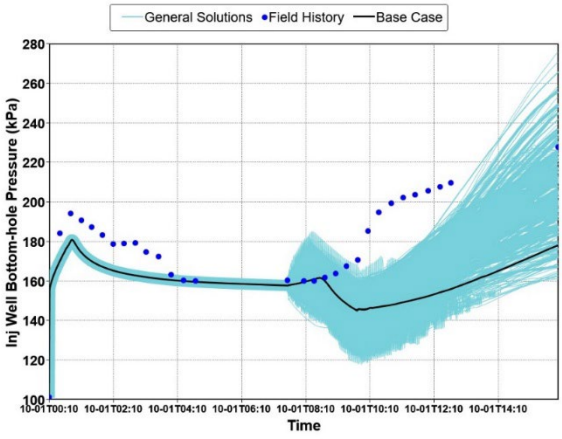


Figure S.12. History matching for injection pressure during surfactant and polymer flooding, test CF-3.

USC
UNIVERSIDADE DE SANTIAGO DE COMPOSTELA

USC
UNIVERSIDADE
DE SANTIAGO
DE COMPOSTELA

energy&fuels

pubs.acs.org/EF

Article

Evaluation of Surface-Active Ionic Liquids in Smart Water for Enhanced Oil Recovery in Carbonate Rocks

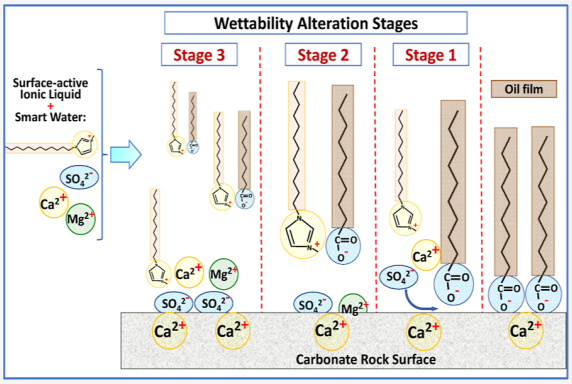
Nestor Tafur, Aleksandr Mamonov, Md Ashraful Islam Khan, Ana Soto, Tina Puntervold,* and Skule Strand

Cite This: *Energy Fuels* 2023, 37, 11730–11742

Read Online

ACCESS | Metrics & More | Article Recommendations

ABSTRACT: Ionic modification of injected brines (Smart Water EOR) has previously demonstrated great potential for wettability alteration in carbonates from initially mixed-wet toward more water-wet conditions. However, the efficiency of Smart Water application is temperature-dependent, which reduces its ability as a rock wettability modifier at low temperatures (below 100 °C). Moreover, at low temperature conditions, the acid number of crude oils tends to increase in the reservoir, causing a stronger oil wetting character and less water-wet initial conditions. This paper evaluates the wettability alteration potential of surface-active ionic liquids added to Smart Water to obtain a synergistic enhanced oil recovery effect in low-temperature carbonate reservoirs. [C_{12}mim]Br, [C_{12}Py]Cl, and [C_{16}Py]Cl were formulated in Smart Water (SW0Na) and tested as wettability modifiers in mixed-wet carbonate chalk cores. Spontaneous imbibition oil recovery tests showed that the addition of [C_{12}mim]Br and [C_{12}Py]Cl can cause wettability changes, resulting in increased oil recovery compared to pure SW0Na brine at 90 °C. The highest incremental oil recovery in tertiary mode of 24.6 % OOIP was obtained using [C_{12}mim]Br in SW0Na, followed by [C_{12}Py]Cl in SW0Na with 22.4 % OOIP, and only 11.5 % OOIP was recovered by pure SW0Na brine. The potential for wettability alteration for carbonate rocks was further evaluated in viscous flooding tests using the best formulation from the results obtained in the spontaneous imbibition experiments ([C_{12}mim]Br in SW0Na). The core flooding results showed an ultimate recovery of 79.3 % OOIP achieved in secondary mode injection. Despite the difference in the head groups of the cationic [C_{12}mim]Br and [C_{12}Py]Cl ionic liquids, both formulations showed abilities to desorb polar organic components of crude oil from the chalk mineral surfaces, thus improving the performance of Smart Water EOR at 90 °C.



Downloaded via 139.47.57.33 on August 17, 2023 at 12:25:48 (UTC).
See https://pubs.acs.org/sharingguidelines for options on how to legitimately share published articles.

1. INTRODUCTION

Around 60% of the discovered oil reserves worldwide are located in carbonate formations, and most of them are mixed to oil-wet, naturally fractured, and low permeability reservoirs.[1−3] The injection of water as a secondary recovery method in those reservoirs (fractured mixed-wet or oil-wet) shows low recovery efficiency due to the high capillary pressure differences between fractures and matrix pores, making the penetration of water into the matrix difficult. In water-wet reservoirs, injected water can penetrate from fractures to matrix blocks through the spontaneous imbibition process, thus expelling the crude oil and increasing the recovery.[4−6] However, conventional water injection is normally carried out using the produced water from the reservoir, which is similar in composition to the initial formation water. As a result, the chemical equilibrium between crude oil, brine, and rock (COBR) systems cannot be altered, and wettability modification toward a more water-wet state is hard to achieve.[7]

Carbonate rock surfaces are positively charged below their isoelectric point of pH ~9.5[8] and, hence, are sensitive to negatively charged components at reservoir conditions. Accordingly, anionic polar compounds present in crude oil (mainly carboxylates, R-COO$^-$, which are dissociated carboxylic acids) can adsorb onto the carbonate surface, modifying the original water-wet state toward less water-wet conditions.[9−11] The alteration of rock wettability toward a more water-wet state using surfactants has previously been investigated.[12,13] Surfactants are amphiphilic molecules, possessing both a hydrophilic polar moiety and a hydrophobic non-polar moiety (generally a hydrocarbon chain), with

Received: April 28, 2023
Revised: July 5, 2023
Published: August 8, 2023



© 2023 The Authors. Published by American Chemical Society

significant surface activity. Conventional surfactants can be classified on the basis of their hydrophilic groups as anionic, cationic, zwitterionic, or non-ionic.[13,14] Currently, bio-based surfactants (from natural sources) are gaining interest due to their environmental benefits.[15,16] The potential of different types of surfactants to alter the wettability in oil-wet carbonate rocks has been evaluated through imbibition tests.[17−19] Spontaneous imbibition with cationic surfactants (primarily from the quaternary ammonium and phosphonium families) showed a clearly higher potential to expel oil compared to anionic surfactants (mainly from the ethoxylated sulfonate and sulfate families). The proposed imbibition mechanism for cationic surfactants suggests that the positive head groups electrostatically interact with the adsorbed negative compounds of the crude oil on the rock surface, forming ion pairs. These ion pairs are stabilized by hydrophobic interactions between their alkyl chains, and the material is desorbed from the carbonate surface.[17,19] The spontaneous imbibition is driven by capillary forces, turning oil-wet cores more water-wet. As a result, the capillary force increases and overcomes the low capillary force due to the surfactant.[17,20] The ability of anionic surfactants to displace oil was generally low. Among them, ethoxylated sulfonates showed relatively higher efficiency. For anionic surfactants, the formation of a surfactant layer was suggested, in which the hydrophobic chains were oriented toward the hydrophobic carbonate surface, exposing the hydrophilic part, thereby making the surface double-layer water-wet.[17,20,21] Moreover, assessments of non-ionic surfactants (specifically ethoxylated alcohol types) showed that they were much less effective than the tested cationic surfactants.[18,22] Similar to anionic surfactants, the wettability alteration mechanism for non-ionic surfactants was suggested to involve the formation of a bilayer structure.[22]

Furthermore, several studies revealed that alteration of carbonate wetting toward water-wet conditions can be achieved by injecting water with a different composition than that originally found in reservoirs (i.e., seawater, SW), thus improving oil recovery.[5,23,24] The injection of SW, or smart water (SmW), is categorized as an enhanced oil recovery (EOR) method since it can alter the chemical equilibrium of the COBR system, change the wettability state toward more water-wet, and improve the oil recovery. SmW is designed by adjusting the composition of ions present in the injection water to a specific COBR system.

Focusing on chalk rocks, potential determining ions (PDI) Ca^{2+}, Mg^{2+}, and SO_4^{2-} present in SW and SmW can modify the charges on the surface rock and trigger favorable wettability conditions. The suggested mechanism[24,25] for that process indicates that when SW or SmW is injected in chalk rocks, SO_4^{2-} ions are adsorbed on the positively charged surface due to their high affinity to Ca^{2+}. The positive charge on the surface is reduced, and the electrostatic interaction of surface Ca^{2+} with the carboxylate groups of the crude oil diminishes, and in addition, the repulsion between surface Ca^{2+} and water Ca^{2+} is reduced. Then, the water Ca^{2+} concentration near the surface increases, and Ca^{2+} ions interact electrostatically with carboxylate groups, inducing their desorption from the chalk surface.[24,25] The Mg^{2+} ion has the ability to replace Ca^{2+} from the carbonate surface; hence, it can also help to remove the carboxylic group--Ca^{2+} complex from the rock surface.[26] However, the interaction between PDIs and the carbonate surface is dependent on temperature: the higher the temperature, the higher SO_4^{2-} adsorption on the carbonate surface. This means a higher affinity for water Ca^{2+} on the surface and higher oil recovery by wettability modification.[25,27] Mg^{2+} is also more reactive at high temperatures due to dehydration, that is, the breaking of the hydrogen bonds between the water molecules, solvating the Mg^{2+} ions and reducing their reactivity.[26,28] Hence, SW and SmW have reduced efficiency as wettability modifiers at low temperatures below 100 °C.

It has also been shown that at lower temperatures, the acid number (AN) of crude oils tends to increase because carboxylic acids suffer from decarboxylation at high temperatures.[29] Knowing that crude oils with high AN induce higher oil wetting, carbonate reservoirs will be likely more oil-wet at lower temperatures than at higher temperatures.[30]

This work aims to assess a new method, based on ionic liquids, to improve the performance of SmW for EOR in carbonate reservoirs at low temperatures. Taking into account that cationic have shown effectiveness over anionic and nonionic surfactants for wettability alteration processes,[17,31] some cationic ionic liquids were selected as possible alternatives to the widely proposed cationic surfactant C_{12}TAB. Ionic liquids are salts with melting or glass transition temperatures below 100 °C. They are characterized by high thermal stability, a high capacity of solvation, and the possibility of being functionalized. They can be designed to be stable in harsh environmental conditions.[32,33] Due to their negligible vapor pressure, these salts avoid atmospheric contamination and are cataloged as environmentally friendly.[34] Ionic liquids with long alkyl chains (more than six carbon atoms) are surface-active agents (SAILs), self-aggregating in micelles when dissolved in water and being able to decrease the interfacial tension (IFT).[35−38] In recent years, the potential of SAILs to be used in EOR applications as a surfactant agent has been studied. Analyzing the first publications on this topic, Bera and Belhaj[33] highlighted the SAILs' ability to reduce water-oil IFT and their tolerance at harsh conditions (salinity and temperature). Somoza et al.[39] reviewed core-flooding tests conducted with these salts and found that the majority of the studies were carried out in sandstone rocks, despite the expected high adsorption of cationic surfactants in this kind of rock. Additional oil recoveries (AOR) of about 5−12% original oil in place (% OOIP)[32,40,41] were found. Evaluations of SAILs in carbonate cores achieved AOR values in the range of 8−20 % OOIP.[39,42−44] Despite these positive results, ultra-low IFT with pure SAILs is not easy to achieve. For this reason, cationic SAILs have also been blended with traditional anionic surfactants to promote the formation of mixed micelles (also named catanionic micelles), thus increasing the surface activity with the oil phase. Core flooding tests injecting these kinds of blends suggested an improvement in performance when the blends were compared to the pure surfactants.[45,46] According to contact-angle measurements, some SAILs were also able to change wettability toward a more water-wet state.[42,47,48] However, a few studies[49,50] conducted imbibition tests with SAILs to evaluate the capability for wettability alteration of these salts. Sakthivel and Elsayed[49] and Manshad et al.[50] carried out spontaneous imbibition tests in carbonate cores at 80−100 °C (secondary mode), with SAIL formulations prepared in formation brine or seawater. Spontaneous imbibition values up to 34% AOR were found.

In this study, SAILs are combined with Smart Water for the first time, investigating potential synergistic effects in the wettability alteration process. Three imidazolium and pyridinium SAILs with different alkyl chain lengths

https://doi.org/10.1021/acs.energyfuels.3c01488
Energy Fuels 2023, 37, 11730−11742

([C_{12}mim]Br, [C_{12}Py]Cl, and [C_{16}Py]Cl) were considered to improve the performance of SmW for EOR in carbonate rocks. SAIL formulations were prepared in SmW, and their wetting alteration capacity was tested on mixed-wet chalk cores by spontaneous imbibition tests at 90 °C in tertiary mode. The efficiency of the best performing formulation was additionally evaluated by means of viscous flooding tests in secondary and tertiary modes.

2. EXPERIMENTAL WORK

2.1. Material. *2.1.1. Ionic Liquids.* Three cationic SAILs were evaluated in this study. 1-dodecyl-3-methylimidazolium bromide ([C_{12}mim]Br) with a purity >98 wt % was purchased from Iolitec. 1-dodecylpyridinium chloride ([C_{12}Py]Cl) and 1-hexadecylpyridinium chloride ([C_{16}Py]Cl) with purity grades of 98 wt % and 99 wt %, respectively, were supplied by Sigma-Aldrich. Figure 1 shows the chemical structures of the evaluated SAILs.

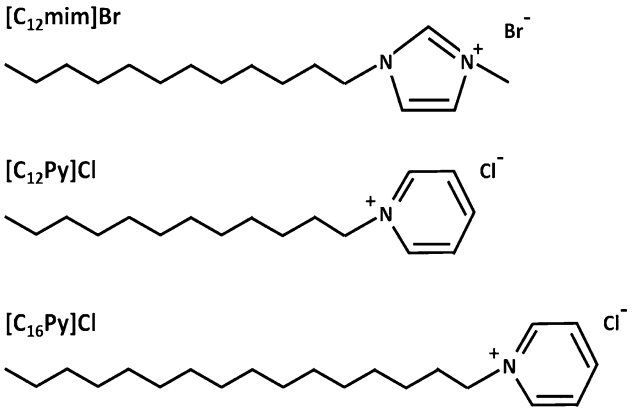


Figure 1. Chemical structures of the used SAILs.

2.1.2. Brines. Synthetic brines were used in the experimental work. The Valhall formation brine (VB0S) was employed to initially saturate the cores and as the first spontaneous imbibition fluid, in secondary mode. The composition of the VB0S brine is similar to that of the reservoir formation water of the Valhall chalk field in the North Sea, but it is depleted in sulfate ions (SO_4^{2-}) to not induce initial wettability alteration. Synthetic North Sea SW was only used as make-up water in initial evaluations of the phase behavior and thermal stability of the SAIL formulations. The Smart Water SW0Na was used in secondary and tertiary modes in spontaneous imbibition and viscous core flooding tests, as well as make-up water for SAIL formulations. The SW0Na composition is similar to that of SW but depleted in NaCl salt. For sulfate influence evaluations, SW0S brine (SW0Na without sulfate ions) was also prepared. The brines SW1/2T and SW0T (with and without tracer ions, SCN^-), previously tested in chromatographic wettability tests for chalk,[25] were used in the adsorption test. All brines were prepared by dissolving reagent-grade salts in deionized water, stirring overnight, and then filtering through a 0.22 μm filter. The brine compositions are listed in Table 1.

2.1.3. Oil. A model crude oil, termed Res40-m, was used for the core preparation process and oil recovery tests. This model oil was obtained by mixing the crude oils Res40 and Res40-0, with ANs of 1.8 and 0.0 mg KOH/g, respectively, in a ratio of 1:2 Res40/Res40-0.[25,51] The crude oil Res40 was prepared by diluting Heidrun crude oil and *n*-heptane at a 3:2 Heidrun/heptane blend ratio, and no precipitation of asphaltenes was observed. Res40-0 oil was obtained by treating Res40 oil with 10 wt % of silica gel under stirring at room temperature for 3 days to remove the acidic material present in the crude oil.[30] After preparation, the oils were centrifuged and filtered through a 5 μm filter. The resulting AN and base number (BN) of Res40-m oil were 0.6 and 0.3 mgKOH/g, respectively, measured with a Mettler Toledo T50 auto-titrator using methods developed by Fan and Buckley,[52] which are modified versions of ASTM D2896 and D664 for BN and AN titration, respectively. Res40-m oil density was 0.803 g/cm^3, measured using an Anton Paar density meter (model DMA 4500).

2.1.4. Core Samples. Ten outcrop chalk cores from the Stevns Klint (SK) quarry in Denmark were used as carbonate rock models in the experimental work. SK cores have often been used to represent North Sea chalk reservoirs.[53] This material generally contains around 98% $CaCO_3$[54] with most of the pore sizes ranging from 0.1−0.5 μm,[55] has high porosity (40−50%) and low permeability (1−3 mD), and has shown reproducible results in wettability and recovery tests in previous studies.[53,55,56]

2.2. Methodology - SAILs Evaluation. To prevent possible interactions between SAILs and divalent salts contained in the SW0Na brine, before blending them, stock solutions of the SAILs [C_{12}mim]Br, [C_{12}Py]Cl, and [C_{16}Py]Cl were first prepared individually in deionized water at 8 wt % SAIL concentration. To avoid dilution of the make-up brines, these were prepared at a higher concentration than the original (1.2 times the original concentration of each brine) so that, when they were mixed with the SAIL stock solutions, the formulations reached both the original brine concentration and the desired SAIL concentration. To compare the obtained results with previously performed work with cationic surfactants at 1 wt % concentration,[17] 1 wt % was also selected as the SAIL concentration.

2.2.1. Phase Behavior Evaluation. The phase behavior of crude oil and SAILs prepared in VB0S, SW, and SW0Na brines was visually evaluated following the so-called encased-glass-pipette method.[57,58] Borosilicate glass pipettes were heat-sealed at the tip, and SAIL formulations, prepared in the different brines, were placed into the pipettes at a 1:1 aqueous phase/oil phase ratio. Initial interfaces were recorded to easily identify the type of microemulsion. Thereafter, each pipette was heat-sealed at the top and gently mixed for 24 h in a rotary mixer at room temperature. They were enclosed in a 10 cm^3

Table 1. Brine Properties and Compositions

ions	VB0S (mM)	SW (mM)	SW0Na (mM)	SW0S (mM)	SW0T (mM)	SW1/2T (mM)
Na^+	996.6	450.1	50.0	60.0	460.0	427.0
K^+	5.3	10.1	10.1	10.1	10.0	22.0
Li^+	0.0	0.0	0.0	0.0	0.0	12.0
Ca^{2+}	28.9	13.0	13.0	13.0	13.0	13.0
Mg^{2+}	7.8	44.5	44.5	44.5	44.5	44.5
Cl^-	1066.0	525.1	125.1	126.0	583.0	538.0
HCO_3^-	9.3	2.0	2.0	2.0	2.0	2.0
SO_4^{2-}	0.0	24.0	24.0	0.0	0.0	12.0
SCN^-	0.0	0.0	0.0	0.0	0.0	12.0
TDS (g/L)	62.83	33.39	10.01	10.01	33.39	33.39
density (g/cm^3)	1.039	1.023	1.01	1.01	1.022	1.022
ionic strength	1.112	0.657	0.257	0.657	0.643	0.644

USC UNIVERSIDADE DE SANTIAGO DE COMPOSTELA

https://doi.org/10.1021/acs.energyfuels.3c01488
Energy Fuels 2023, 37, 11730−11742

Pyrex test tube filled with silicone oil to ensure temperature control and then introduced into an OVAN dry-block heater (model BD200-RE). Phase behavior was monitored at different temperatures, from 50 °C to 130 °C, increasing temperature by 20 °C every 72 h. In this kind of study, the SAIL concentration in the aqueous phase is normally high (4 wt % SAIL) just to easily visualize oil in the aqueous phase[58,59] and determine the type of microemulsion, Winsor type I, II, or III, according to the Winsor classification.[60]

2.2.2. Thermal Stability Test. The possible precipitation of components in SAIL formulations was visually evaluated by preparing 1 wt % SAIL concentration in different brines (VB0S, SW, and SW0Na), aiming to use those formulations in spontaneous imbibition and viscous flooding tests. As in the phase behavior evaluation, the formulations were placed into sealed pipettes in the absence of crude oil and monitored when increasing the temperature from 50 to 130 °C using the OVAN dry-block heater. The evaluation was done based on the translucence of the solutions.[45,61]

2.2.3. Dynamic Interfacial Tension. The interfacial tension (IFT) between the SAIL formulations (at 1 wt % SAIL concentration) and crude oil was measured using a Krüss spinning drop tensiometer (model SITE100) at 50 °C. For each formulation, a 4 μL crude oil sample was injected into the capillary tube, which was filled with the SAIL formulation. The rotation speed was set at 5000 rpm to guarantee an oil droplet length at least four times larger than its diameter, according to Vonnegut's theory.[62,63] SAIL formulation densities were obtained using an Anton Paar density meter (model DMA 5000 M).

2.3. Methodology—Core Preparation. *2.3.1. Core Cleaning.* The cores were drilled in the same direction from the same outcrop chalk block. The core cleaning procedure followed the methodology suggested by Puntervold et al.[56] By using Hassler core holder equipment and a compressed nitrogen piston cell to support a confining pressure of 10 bar, each core was flooded with 5 pore volumes (PV) of deionized water at 0.1 cm^3/min at room temperature. The objective was to remove any easily dissolvable salts, especially those containing SO_4^{2-} ions, which might influence the initial wettability behavior of the cores.[56] The absence of sulfates in the effluent was checked by the addition of Ba^{2+} ions, which will react with available sulfate ions to form $BaSO_4$ (s), according to the following reaction equation

$$Ba^{2+}(aq) + SO_4^{2-}(aq) \rightarrow BaSO_4(s)$$

When no more precipitation of $BaSO_4$ was observed, each core was dried in an oven at 90 °C until a constant weight was reached (after about 3 days) and thereafter kept in a sealed container.

2.3.2. Initial Water Saturation (S_{wi}). The initial water saturation of the cores was established at around 10% by using the desiccator method.[64] This method is fast compared to desaturation by, e.g., porous plates, and it results in evenly distributed and reproducible S_{wi}. The dried cores were first evacuated to be 100% vacuum-saturated with ten times diluted VB0S brine at room temperature. Thereafter, the saturated cores were placed in a desiccator with silica gel until reaching the desired S_{wi} of ∼10%, obtained by water evaporation from the cores, controlled by weight. Each core was stored in a sealed container and left to equilibrate for 3 days.

2.3.3. Initial Core Wettability. After equilibrating the S_{wi} established by the desiccator, reproducible initial oil saturation and initial core wettability were established by introducing a controlled, equal amount of crude oil into each core.[65] Using a Hassler core holder in horizontal position at a confining pressure of 20 bar, each core was first vacuum-saturated with 1 PV of Res40-m oil and then flooded with 4 PV Res40-m oil at 0.2 cm^3/min (injecting 2 PV in each direction). The whole process was performed at 50 °C. Then, the cores were wrapped in Teflon tape to avoid unrepresentative adsorption of active polar organic components on the outer core surface during the aging stage. Each core was placed on marble balls in sealed stainless-steel aging cells surrounded by the effluent Res40-m oil and aged in an oven at 90 °C for 2 weeks.

2.4. Methodology—Oil Recovery Tests. *2.4.1. Spontaneous Imbibition (SI) Tests.* Seven spontaneous imbibition (SI) tests were conducted. Each aged core was unwrapped and placed vertically on marble balls submerged in VB0S imbibition brine into steel HPHT (high pressure−high temperature) SI cells. The SI cells were connected to compressed nitrogen piston cells, supplying the VB0S brine and keeping the system pressurized at 10 bar. The SI test temperature was kept at 90 °C. VB0S was used as the first imbibition fluid in secondary mode to avoid changes in wettability at this stage and be able to infer the initial wetting state of the chalk cores more accurately. The cumulative oil produced was measured in a graded glass burette and reported as the percentage of OOIP versus time. Once oil recovery reached the plateau, the VB0S imbibition brine was replaced by another imbibition fluid to perform tertiary-mode spontaneous imbibition. This last imbibition brine varied depending on the SI test performed (SW0Na or SAIL-SW0Na formulation at 1 wt % SAIL).

2.4.2. Viscous Flooding Tests. To validate the efficiency of the best-performing SAIL-SW0Na formulation (1 wt % SAIL), two viscous flooding (VF) experiments were conducted at 90 °C. The aged core was placed in the Hassler core holder, positioned horizontally, with confining and back pressure established at 20 and 10 bar, respectively. Each core was flooded at an injection rate of ∼1 PV/D with the desired brine or formulation. Volumes of produced oil as a percentage of OOIP were measured, and differential pressures were recorded during the tests until the oil production plateau was reached.

2.4.3. Dynamic Adsorption Test. SAIL adsorption on chalk rock was estimated using the best-performing formulation in a single-phase dynamic adsorption test based on the breakthrough difference between the SAIL and tracer fronts. Similar to the chromatographic wettability method used for chalk,[25] the first part of the test allowed the determination of the flow behavior of the non-adsorbing tracer thiocyanate (SCN^-). Also, the SO_4^{2-} profile from the same effluent samples was tracked for comparative purposes. A cleaned, not exposed to oil, chalk core was 100% vacuum-saturated with SW0T brine (without SCN^-) and placed horizontally in the Hassler core holder. Once the confining and back pressure were established at 20 and 10 bar, respectively, and the temperature reached 90 °C, the core was first flooded at ∼1 PV/D by the same brine, SW0T, until the differential pressure stabilized, after which it was flooded by the SW1/2T brine. The effluent was sampled with an autosampler and analyzed using an ion chromatographer for tracer concentration estimation. Thereafter, the core was cleaned by injecting SW0Na for 24 h at the same injection rate to finally be flooded by the best-performing SAIL-SW0Na formulation (1 wt % SAIL). Effluent samples were collected until the SAIL concentration achieved the value of the injected formulation. The SAIL concentration in the samples was determined by using an HP UV/vis-spectrophotometer (model Presario SR1000). Normalized concentrations (C/C_0) of SAIL and tracer profiles were obtained. Then, SAIL adsorption was estimated using the theory of diffuse percolation, that means, the difference in pore volumes corresponding to 0.5 normalized concentration between SCN^- and SAIL profiles (eq 1).[45,59,66] The theory of diffuse percolation suggests that when a solution is flooding a water-saturated core at an injection velocity of V, the front at $C/C_0 = 0.5$ also moves at that velocity, indicating breakthrough of the fronts when the effluents reach that normalized concentration.[67]

$$\tau = \frac{(PV_{SAIL,50\%} - PV_{tracer,50\%}) \times PV \times [C_0]_{SAIL}}{Mass_{rock}} \quad (1)$$

where τ is the SAIL adsorption on the chalk rock surface in mg/g, $[C_0]_{SAIL}$ is the initial SAIL concentration in mg/cm^3, PV is the core pore volume in cm^3, $PV_{SAIL,50\%}$ and $PV_{tracer,50\%}$ are the pore volumes at 50% injection concentration of SAIL and tracer, respectively, in the effluent, and $Mass_{rock}$ is the dry core weight in grams. As an alternative, the adsorption was also estimated using the area between the SCN^- and $[C_{12}mim]Br$ curves.

https://doi.org/10.1021/acs.energyfuels.3c01488
Energy Fuels 2023, 37, 11730−11742

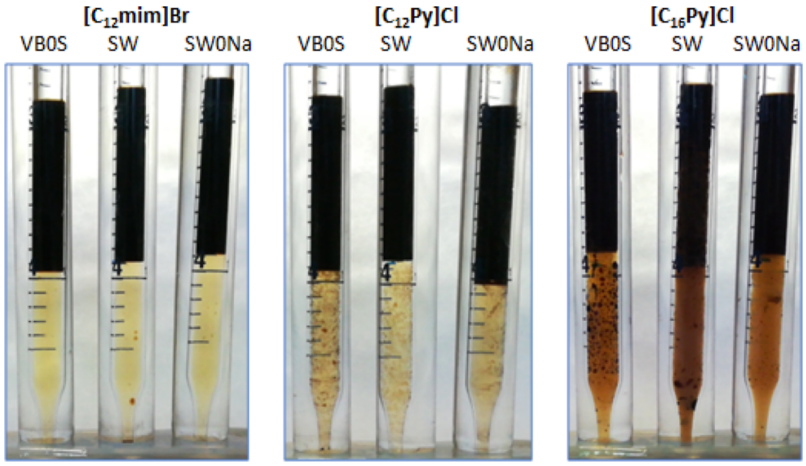


Figure 2. Phase behavior evaluation at 130 °C of the [C_{12}mim]Br, [C_{12}Py]Cl, and [C_{16}Py]Cl SAIL formulations prepared at 4 wt % SAIL concentration in VB0S, SW, and SW0Na brines in contact with crude oil.

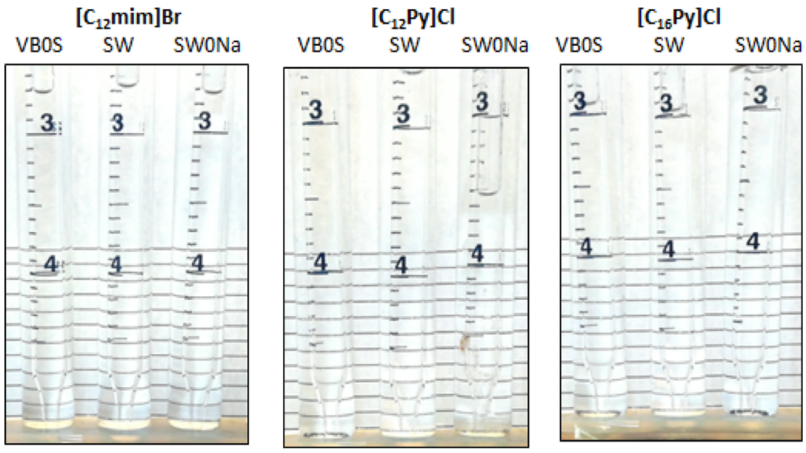


Figure 3. Thermal stability test at 130 °C for the [C_{12}mim]Br, [C_{12}Py]Cl, and [C_{16}Py]Cl SAIL formulations prepared in VB0S, SW, and SW0Na brines at 1 wt % SAIL concentration in the absence of an oil phase.

Table 2. Properties of Outcrop Chalk Cores

property/core ID	C#1	C#2	C#3	C#4	C#5	C#6	C#7	C#8	C#9	C#10
length, cm	7.2	7.3	6.6	6.4	7.0	6.7	6.9	7.3	7.5	6.9
diameter, cm	3.8	3.8	3.8	3.8	3.8	3.8	3.8	3.8	3.8	3.8
bulk volume, cm^3	81.7	82.7	74.3	72.5	79.2	75.5	77.7	83.7	86.0	78.8
dry weight, g	109.6	111.4	101.6	101.6	106.8	100.7	106.7	114.7	116.9	107.6
pore volume, cm^3	40.3	41.3	36.1	34.6	39.2	38.1	38.1	40.9	42.4	39.2
porosity, %	49.3	49.9	48.6	47.7	49.5	50.4	49.1	48.8	49.3	49.8
K_{abs}, mD	3.7	3.1	4.2	3.8	3.4	4.2	3.9	3.2	3.9	3.0
S_{wi}, %	10.1	10.0	11.3	10.0	10.1	9.9	10.0	10.0	10.2	100.0
OOIP, cm^3	37.4	35.7	30.6	32.1	33.5	34.2	36.6	36.6	38.5	0.0

3. RESULTS AND DISCUSSION

3.1. SAILs Evaluation. *3.1.1. Phase Behavior Evaluation.* The hydrophilicity of the [C_{12}mim]Br, [C_{12}Py]Cl, and [C_{16}Py]Cl SAILs, each one prepared in three brines (VB0S, SW, and SW0Na), was evaluated through phase behavior studies with crude oil. The purpose was to ensure that microemulsion Winsor type I (oil in water) was kept when the temperature increased from 50 to 130 °C. Since polar interactions between water molecules and ionic surfactant head groups can be reduced by the aqueous phase salinity, the partition of surfactant to the oil phase can be induced, and a shift of microemulsion from Winsor I to Winsor II could take place.[14,68−71] Winsor II, water in oil emulsion, means loss of formulation efficiency due to the increase of both SAIL retention and oil viscosity.[72−74] On the other hand, rising temperatures provoke stronger interactions between ionic surfactant head groups and water molecules, making them more hydrophilic as the temperature increases.[70,75−77] Figure 2 presents the results of the phase behavior study of the SAIL formulations at 130 °C. The evaluated SAILs behaved highly hydrophilic during the test, showing microemulsion Winsor type I in the tested temperature interval and at the highest evaluated salinity (VB0S).

3.1.2. Thermal Stability Test. The thermal stability of the SAIL formulations presented in the previous section was evaluated from 50 to 130 °C. The SAIL formulations were prepared at a 1 wt % SAIL concentration using brines VB0S,

https://doi.org/10.1021/acs.energyfuels.3c01488
Energy Fuels 2023, 37, 11730−11742

Table 3. Summary of Spontaneous Imbibition Tests Performed at 90 °C

test ID	SI-1	SI-2	SI-3	SI-4	SI-5	SI-6	SI-7
core ID	C#1	C#2	C#3	C#4	C#5	C#6	C#7
OOIP, cm^3	37.4	35.7	30.6	32.1	33.5	34.2	36.6
secondary mode fluid	VB0S	VB0S	VB0S	VB0S	VB0S	VB0S	VB0S
oil recovery, (% OOIP)	27.0	23.0	19.0	38.7	35.8	28.1	26.2
tertiary mode fluid	SW0Na	$[C_{12}Py]Cl$ SW0Na	$[C_{16}Py]Cl$ SW0Na	$[C_{12}mim]Br$ SW0Na	$[C_{12}Py]Cl$ SW0Na	SW0S	$[C_{12}mim]Br$ SW0S
AOR, (% OOIP)	11.5	22.7	4.9	24.6	22.4	1.2	5.2

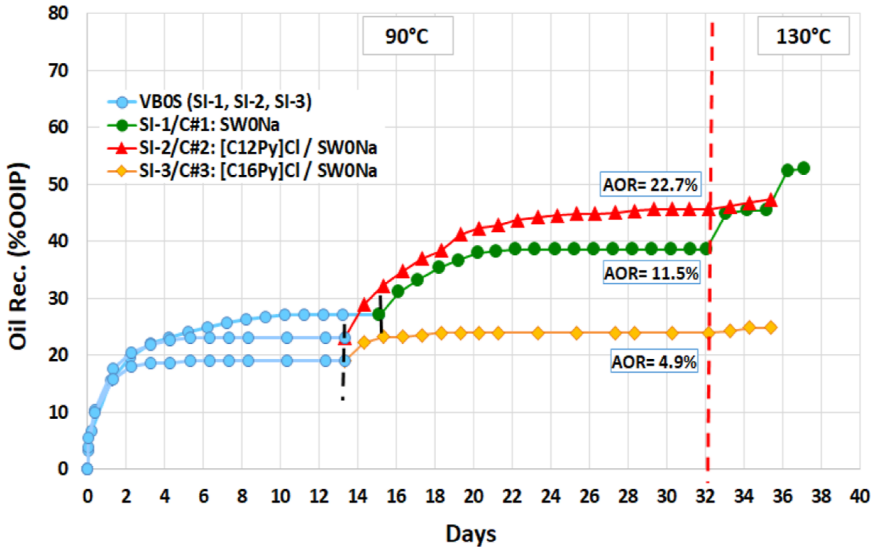


Figure 4. Effect of the SAIL alkyl chain length on spontaneous imbibition at 90 °C, SI-1 (SW0Na), SI-2 ($[C_{12}Py]Cl$-SW0Na), and SI-3 ($[C_{16}Py]Cl$-SW0Na). VB0S was used as the first imbibition brine in all three tests.

SW, and SW0Na as make-up water. During the evaluation, no precipitation was observed in the pipettes, and the formulations remained translucent until the end of the test, after 2 weeks. Figure 3 shows the results of this evaluation at 130 °C.

3.1.3. Dynamic Interfacial Tension. As seen in Figure 2, a dark aqueous phase was noticed for all $[C_{16}Py]Cl$ formulations, meaning a higher capacity to solubilize the oil phase inside the aqueous phase and therefore lower expected IFT with crude oil than that corresponding to the other SAIL formulations. That expectation was confirmed through the dynamic IFT measurements performed at 50 °C with the SAIL formulations prepared at a 1 wt % SAIL concentration in SW0Na. The IFT between crude oil and $[C_{12}mim]Br$ was 1.2 mN/m; for $[C_{12}Py]Cl$, it resulted in 1.7 mN/m, while for the $[C_{16}Py]Cl$ formulation, it was 0.4 mN/m.

3.2. Core Characterization. The characterization of the cores was performed during the core preparation stage. Dimensions, porosity, absolute permeability (K_{abs}), pore volume, initial water saturation (S_{wi}), and OOIP are shown in Table 2 for the 10 used outcrop SK chalk cores.

The physical properties of the outcrop chalk cores were similar to those in previously published research.[78,79]

3.3. Oil Recovery Tests. Several oil recovery tests were performed to evaluate the ability of the three cationic SAILs to increase oil recovery from outcrop chalk cores when they are formulated in SW0Na brine as make-up water. The evaluation involved seven spontaneous imbibition tests and two additional viscous flooding tests with the best-performing formulation.

3.3.1. Spontaneous Imbibition Tests. The purpose of the SI tests was to determine the efficiency of the SAILs, formulated in smart water (SW0Na), to induce wettability alteration of chalk cores from mixed-wet to more water-wet at 90 °C. For efficient oil displacement by SI of water in mixed-wet to more oil-wet cores, the capillary forces acting against water intrusion into oil-wet pores must be overcome. As suggested in previous studies,[17,20,80] SI driven by capillary forces can occur in oil-wet rocks with cationic surfactant formulations, despite their low capillary pressure (low IFT). Cationic elements present in surfactant solutions have the ability to desorb anionic polar compounds of the crude oil from the rock surface and modify the wetting state toward a more water-wet state. However, it has been shown[17,20] that in addition to the capacity to desorb polar compounds from the rock surface, the cationic surface-active formulations must have a moderate IFT with the oil to promote the penetration of the aqueous phase into the core by capillary forces during the wettability alteration process. On the other hand, anionic surfactants were not able to desorb polar organic compounds from the chalk surface, but could, due to a low to ultra-low IFT, imbibe water and produce oil because of weak capillary forces and sufficient gravity forces.[17,81] Seven SI tests (SI-1 to SI-7) were carried out at 90 °C using cores C#1 to C#7 (core properties in Table 2). All SI tests were performed with VB0S as the first imbibition fluid (in secondary mode) until the oil recovery plateau was reached. Oil recovery is reported in % OOIP. The moderate oil recoveries obtained after this first imbibition stage showed that the cores were mixed-wet at initial conditions[12] (Table 3). Previously, it has been shown that a very water-wet SK chalk core spontaneously imbibed VB0S, producing 75 % OOIP of the *n*-heptane saturated core in the presence of S_{wi} = 10% VB0S.[82] After treating the same core material with 15 PV crude oil, the core spontaneously imbibed a limited volume of

https://doi.org/10.1021/acs.energyfuels.3c01488
Energy Fuels 2023, 37, 11730−11742

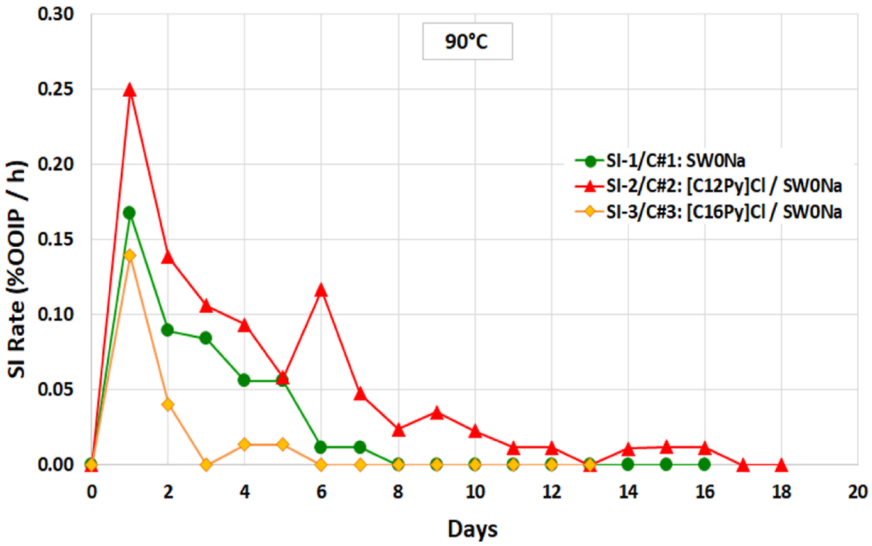


Figure 5. Effect of the SAIL alkyl chain length on spontaneous imbibition rates at 90 °C during tertiary imbibition of SI-1 (SW0Na), SI-2 ([C_{12}Py]Cl-SW0Na), and SI-3 ([C_{16}Py]Cl-SW0Na) tests.

VB0S, producing only 6 % OOIP crude oil at 50 °C, confirming mixed-wet conditions after crude oil exposure. In the SI-1 test (core C#1), the tertiary mode imbibition was carried out with SW0Na as the base case. In the SI-2 to SI-7 tests, VB0S brine was replaced by a SAIL formulation (1 wt % SAIL) in the tertiary mode, according to the designed assessment plan with three objectives: (1) evaluation of the effect of two different alkyl chain length SAILs with the same head group (pyridinium ring), (2) evaluation of the effect of different head groups (pyridinium and imidazolium rings) having the same hydrophobic tail length, and (3) evaluation of the effect of sulfate ions on the wettability alteration behavior of the best-performing SAIL formulation.

3.3.2. Effect of the SAIL Alkyl Chain Length. The influence of the alkyl chain length of SAILs on the wettability alteration process was evaluated using the pyridinium SAILs [C_{12}Py]Cl and [C_{16}Py]Cl. In the experiment SI-2 and SI-3, [C_{12}Py]Cl and [C_{16}Py]Cl formulations were used as tertiary mode imbibition fluids using the cores C#2 and C#3. The potential of the formulations was inferred by the recovered oil during the tertiary mode (named additional oil recovery, AOR) and by the imbibition rates. The produced aqueous phase from the SI-2 and SI-3 tests contained a fraction of oil in the form of an emulsion, but this was not taken into account for the AOR results. The results of these tests are shown in Figure 4, which also includes the base case (SI-1 test). As it can be seen, the [C_{12}Py]Cl formulation reached a final AOR almost twice that obtained with SW0Na, 22.7 % OOIP and 11.5 % OOIP at 90 °C, respectively. In the case of the [C_{16}Py]Cl formulation, AOR was only 4.9 % OOIP, resulting in poorer imbibition performance than the other tests. Imbibition rates corresponding to these tests are shown in Figure 5. The figure shows that the rate of oil expulsion with the [C_{12}Py]Cl formulation was clearly higher than that corresponding to SW0Na during the whole imbibition process. The oil production with the [C_{12}Py]Cl formulation stopped after 17 days, whereas the oil production with SW0Na was only maintained for 8 days. The [C_{16}Py]Cl formulation presented the lowest imbibition rates, with oil production ceasing after 6 days.

The imbibition mechanism for the [C_{12}Py]Cl formulation may be analogous to that suggested for the C_{12}TAB surfactant.[17−19] At first imbibition flood with VB0S in mixed-wet cores, when no change of wettability state has taken place, the capillary forces are unfavorable for the water to imbibe into the cores and expel the oil. Once VB0S brine has been switched to the [C_{12}Py]Cl formulation, which has even lower IFT (lower capillary pressure) than the VB0S brine, cationic monomers interact with the adsorbed anionic polar components of the oil, desorbing them from the rock surface. The aqueous phase continues to imbibe into the core and expel oil, making the chalk rock more and more water-wet as the process continues. At this point, the capillary pressure between the aqueous and oil phases is now high enough (because water has now become the wetting phase), and the imbibition is driven by capillary forces. Desorbed anionic polar components are solubilized into the oil phase but are also produced through micelles in the aqueous phase.

Regarding the clearly different performance between [C_{12}Py]Cl and [C_{16}Py]Cl, similar behavior between the cationic surfactants C_{12}TAB and C_{16}TAB was observed in previous work, where C_{12}TAB obtained a higher imbibition rate and oil recovery than C_{16}TAB.[17] In that study, the authors suggested that in the wettability alteration process, only cationic monomers of the surfactants have an active role in the polar component desorption. As explained above, it was also shown that a moderate IFT between the aqueous and oil phases was required to facilitate the imbibition process in which cationic surfactants desorb carboxylates from the chalk surface, improving spontaneous imbibition of water because of sufficient capillary forces present at a moderate IFT.[80] The capability of the [C_{16}Py]Cl for wettability alteration should be similar to SW0Na and [C_{12}Py]Cl since all the formulations have the same Ca^{2+} concentration. However, the water-oil IFT generated by the [C_{16}Py]Cl SAIL could be too low to overcome the capillary forces of the core to invade it and trigger the wettability alteration. To evaluate the influence of high temperatures on the formulation's performance, the temperature was increased to 130 °C. It is known that the efficiency of SmW increases with temperature.[25−27,83] As expected, the raised temperature from 90 °C to 130 °C reactivated the oil production for the SI-1 test with SW0Na brine (Figure 4). Surprisingly, this behavior was not repeated in the SI-2 and SI-3 tests performed with the SAIL formulations. After 5 days, it was clear that SW0Na greatly

https://doi.org/10.1021/acs.energyfuels.3c01488
Energy Fuels 2023, 37, 11730−11742

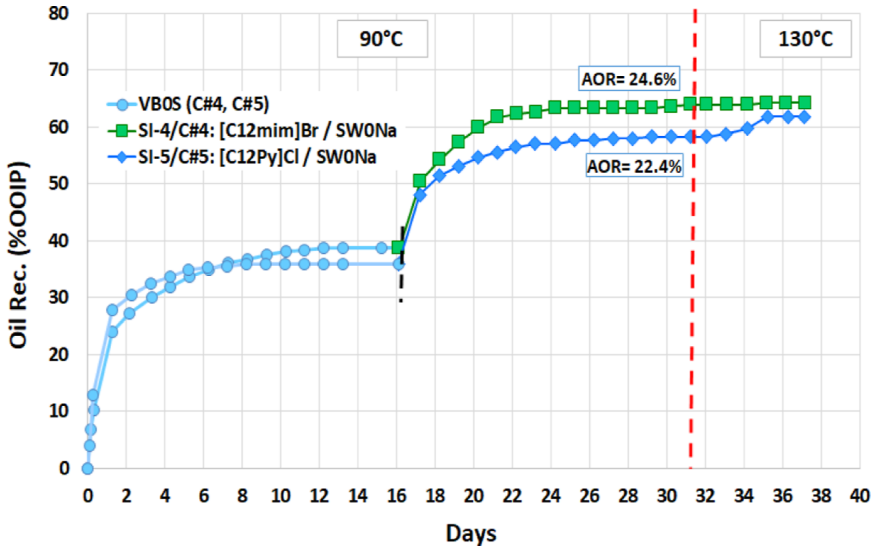


Figure 6. Effect of the SAIL head group on spontaneous imbibition at 90 °C, SI-4 ([C_{12}Py]Cl-SW0Na) and SI-5 ([C_{12}mim]Br-SW0Na). VB0S was used as the first imbibition brine in both tests.

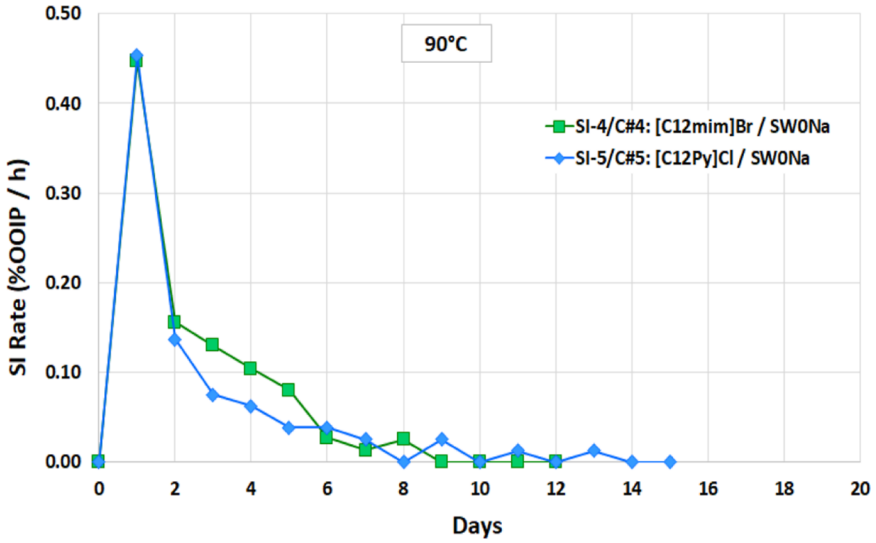
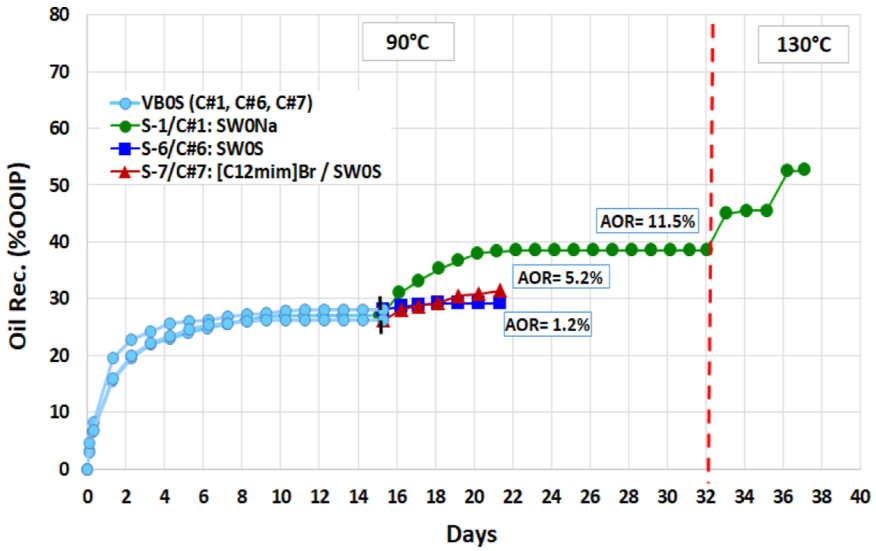


Figure 7. Effect of the SAIL head group on spontaneous imbibition rates at 90 °C during tertiary imbibition of SI-4 ([C_{12}Py]Cl-SW0Na) and SI-5 ([C_{12}mim]Br-SW0Na).



USC UNIVERSIDADE DE SANTIAGO DE COMPOSTELA

Figure 8. Influence of sulfate on the efficiency of the [C_{12}mim]Br formulation in chalk wettability alteration at 90 °C through spontaneous imbibition tests.

https://doi.org/10.1021/acs.energyfuels.3c01488
Energy Fuels 2023, 37, 11730−11742

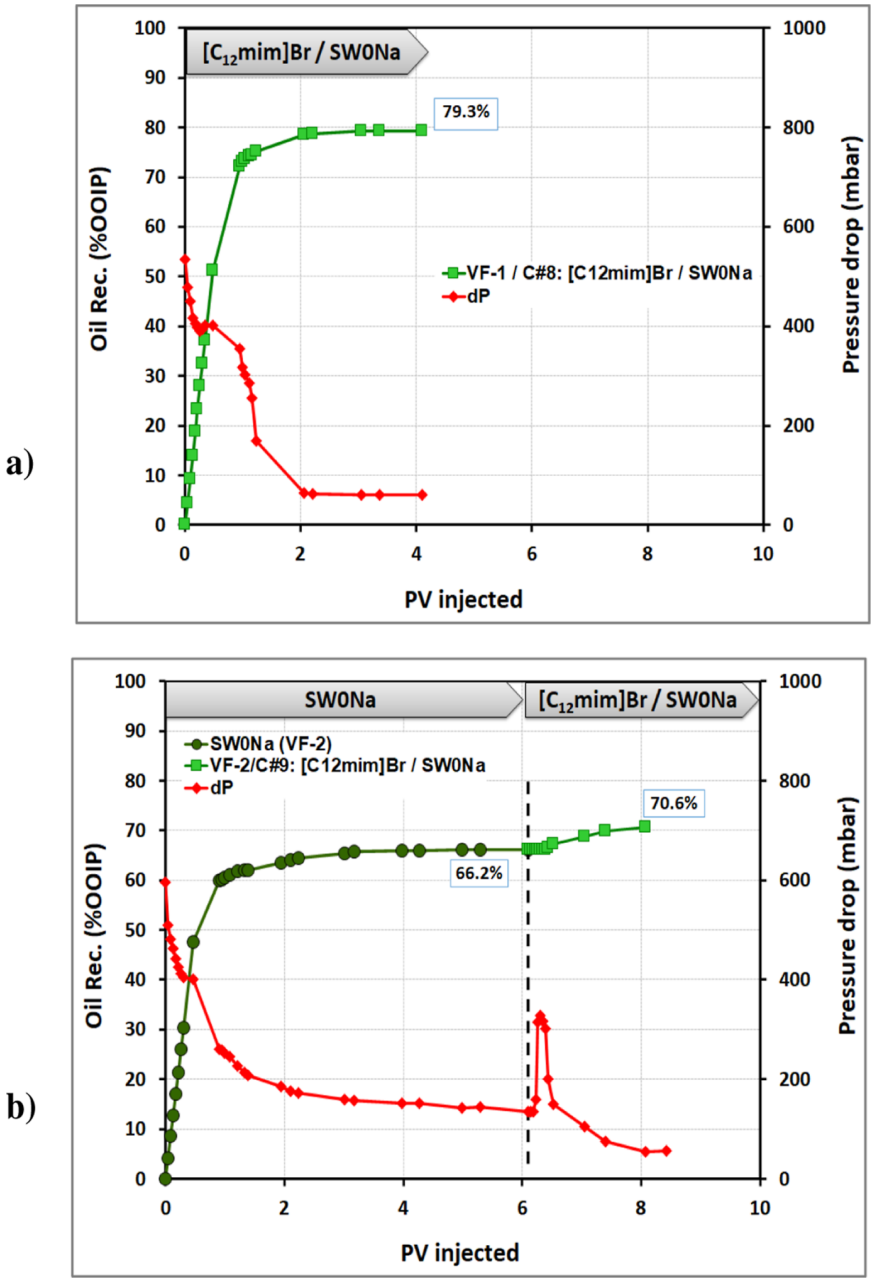


Figure 9. Oil recovery by viscous flooding tests (a) VF-1 using [C_{12}mim]Br formulation in secondary mode; and (b) VF-2 using SW0Na brine in the secondary mode and [C_{12}mim]Br formulation in the tertiary mode. Injection rate: 0.03 cm^3/min, test temperature: 90 °C.

improved its efficiency, reaching an AOR of 25.7 % OOIP with the temperature increase. This might be due to the cationic head group of the ionic liquids deactivating the interactions of the temperature-sensitive PDIs with the rock surface during the imbibition process.

3.3.3. Effect of the SAIL Head Group. In order to determine the influence of SAIL head groups on wettability changes, the SI tests SI-4 (using C#4) and SI-5 (using C#5) were carried out with [C_{12}mim]Br and [C_{12}Py]Cl. These SAILs have the same hydrophobic chain length but different rings (imidazolium and pyridinium). The result of this evaluation is shown in Figure 6. As seen, the AOR for the [C_{12}mim]Br formulation was around 24.6 % OOIP, while the [C_{12}Py]Cl formulation achieved an AOR of 22.4 % OOIP. Figure 7 shows that [C_{12}mim]Br kept a slightly higher imbibition rate than [C_{12}Py]Cl for a few days, which resulted in a somewhat higher oil recovery obtained with [C_{12}mim]Br. This outcome could indicate that neither the ring type nor the contra-ion had great influence on the final AOR (Figure 6) or imbibition rates (Figure 7). The aqueous phase produced in the SI-4 and SI-5 tests had oil in the form of an oil-in-water emulsion, but it was not considered for final oil recoveries. The test temperature was raised from 90 to 130 °C, and in this case, a slight increase in AOR was noticed only with [C_{12}Py]Cl (Figure 6). The [C_{12}mim]Br formulation was selected for further assessments at 90 °C.

3.3.4. Effect of Sulfate. The sulfate ion is one of the three PDIs involved in the wettability alteration of chalk rocks. As discussed above, when SW or SmW are injected, SO_4^{2-} is adsorbed onto the chalk surface, and divalent Ca^{2+} and Mg^{2+} favor the desorption process of the carboxylate from the rock.[84−86] Removal of SO_4^{2-} from the imbibition fluids has a negative impact on oil recovery.[5,26,87,88] To evaluate if the sulfate ion has a significant influence on the wettability alteration capacity of the best-performing SAIL formulation, SO_4^{2-} was removed from the SW0Na brine. The new brine

https://doi.org/10.1021/acs.energyfuels.3c01488
Energy Fuels 2023, 37, 11730−11742

SW0S (SW0Na without SO_4^{2-}) was then used as make-up brine for a new [C_{12}mim]Br formulation (termed [C_{12}mim]Br-SW0S). Both imbibition fluids, SW0S and [C_{12}mim]Br-SW0S, were evaluated at 90 °C in the tertiary imbibition mode in the SI-6 and SI-7 tests using cores C#6 and C#7. Figure 8 presents the results of this evaluation together with the base-case SI-1 test. According to these results, the presence of sulfate in the [C_{12}mim]Br formulation was crucial to maintaining the efficiency of the formulation for oil recovery, with a similar role as that observed in SW0Na imbibition tests.

Table 3 shows a summary of the main outcomes obtained for the seven spontaneous imbibition tests.

3.3.5. Viscous Flooding Tests. The best performing SAIL formulation (1 wt % [C_{12}mim]Br in SW0Na) was additionally evaluated at 90 °C through two viscous flooding tests, VF-1 and VF-2, in the secondary mode and tertiary mode after SW0Na flooding, respectively. In the VF-1 test, 4.11 PV of the [C_{12}mim]Br formulation was injected through the chalk core C#8 at an injection rate of 0.03 cm^3/min (~1 PV/D) until the oil production ceased. The oil recovery was 79.3 % OOIP (Figure 9a). In the VF-2 test, core C#9 was first flooded by 6.1 PV of SW0Na brine at 0.03 cm^3/min until no more oil production was observed, reaching an oil recovery of 66.2 % OOIP. Then, the core was flooded by 1.97 PV of the [C_{12}mim]Br formulation at the same injection rate, obtaining a final oil recovery of 70.6 % OOIP (AOR in the tertiary mode was 4.4 % OOIP) (Figure 9b).

The viscous flooding tests show a beneficial effect of flooding the SAIL formulation (1 wt % [C_{12}mim]Br in SW0Na) compared to flooding pure SW0Na, both in secondary and tertiary injection modes. This is believed to be because of the improved wettability alteration taking place with [C_{12}mim]Br present in SW0Na, as observed in Figures 4 and 6, with values summarized in Table 3.

Moreover, the differential pressure behavior between VF-1 and VF-2 tests after ~0.48 PV was injected was not similar. As observed for VF-1 (Figure 9a), at 0.48 PV, the pressure started to decline slower than for VF-2 (Figure 9b). Then, the pressure in VF-1 dropped sharply to 65 mbar after 2 PV injection. In comparison, the pressure in VF-2 declined smoothly from 0.48 PV to 6.1 PV, ending at 135 mbar. That dissimilar performance may indicate the creation of an oil bank in VF-1, resulting from both the wettability alteration process and the promotion of Winsor type I emulsion (oil in water) due to the IFT between the SAIL formulation and the oil phase. In VF-2, the increase in pressure during the SAIL formulation injection (from 6.1 PV injection) can also be attributed to the formation of a smaller oil bank. After its production, the pressure declined abruptly to 56 mbar. A small fraction of oil was observed in the aqueous phase collected in the burettes during the SAIL formulation core floods; however, it was not considered in the total recovered oil.

The lower tertiary recovery efficiency of the SAIL formulation seen in VF-2 compared to that obtained in VF-1 might be due to the reduced potential of wettability alteration and emulsion formation after the SW0Na flooding in core C#9 due to its already low residual oil saturation (S_{or}).

3.3.6. Dynamic Adsorption. The adsorption of SAIL [C_{12}mim]Br on chalk core at 90 °C was estimated using the core C#10 and the best-performing formulation (1 wt % [C_{12}mim]Br in SW0Na) in the dynamic adsorption single-phase test. Figure 10 presents the results of this evaluation, showing normalized concentration (C/C_0) profiles of tracer and SAIL formulations as a function of injected PV. According to diffuse percolation methodology, the fronts (C/C_0 = 0.5) for the tracer SCN^- and [C_{12}mim]Br injection were detected at 0.96 and 1.48 PV injected, respectively (Figure 10). The SO_4^{2-} profile was also included in the figure for comparative purposes.

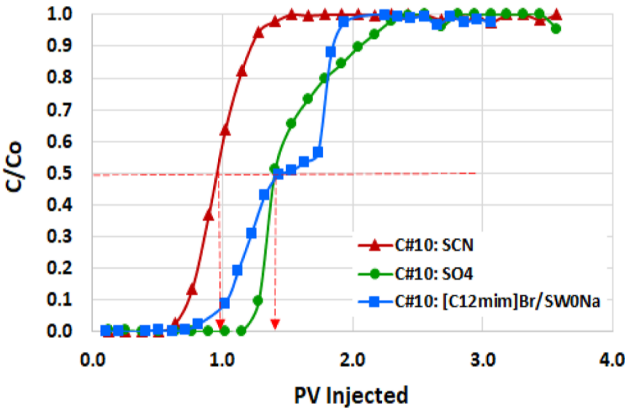


Figure 10. Dynamic adsorption of [C_{12}mim]Br prepared in SW0Na brine on chalk. Single-phase condition. Water-wet chalk core C#10. Injection rate of 0.1 cm^3/min, test temperature of 90 °C.

With the use of eq 1, [C_{12}mim]Br adsorption was estimated to be 1.91 mg/g of rock. Using the area between curves SCN^- and [C_{12}mim]Br (around 0.51), a similar value was achieved (1.85 mg/g). This output seems quite high since recent work[44] with this SAIL prepared in a synthetic SW showed very low dynamic adsorption on Indiana limestone cores of around 0.08 mg/g (at 100 °C and an injection rate of 0.5 cm^3/min). It was found that increasing the SAIL concentration slightly increased the adsorption until the CMC (250 ppm), where the adsorption increments were not significant.

However, the SK chalk, a biogenic $CaCO_3$ material, has a much larger surface area than the Indiana limestone. Khan et al.[78] measured a SK BET surface area of 2.0 m^2/g, which is 3–4 times higher than the BET values in the range of 0.49 to 0.71 m^2/g reported for Indiana limestone by Churcher et al.[89] Thus, in SK chalk, there is a much larger surface area available for the adsorption of SAIL; therefore, more adsorption should be expected. In addition, the biogenic chalk surface has previously been found to be more reactive than the recrystallized outcrop limestone surface. The surface reactivity of two outcrop limestones toward the PDIs, Ca^{2+}, Mg^{2+}, and SO_4^{2-}, was tested by Ravari et al.[90] and was found to be much lower than that observed for SK chalk or reservoir limestone.[91]

Nonetheless, a suggested explanation for this high adsorption of cationic ions onto the positively charged chalk surface is a possible binding between surface Ca^{2+}, SO_4^{2-}, and [C_{12}mim]$^+$ ions, which should become more prominent in the absence of NaCl salts. It is known that SO_4^{2-} adsorbs onto the chalk surface, which then can aid additional adsorption of [C_{12}mim]$^+$ ions.

4. CONCLUSIONS

The potential of three cationic SAILs, [C_{12}mim]Br, [C_{12}Py]Cl, and [C_{16}Py]Cl, prepared in Smart Water (SW0Na), to trigger wettability alteration of chalk cores from mixed-wet toward more water-wet conditions, was evaluated by means of spontaneous imbibition and viscous flooding tests. Some conclusions can be drawn:

https://doi.org/10.1021/acs.energyfuels.3c01488
Energy Fuels 2023, 37, 11730–11742

- The [C_{12}mim]Br and [C_{12}Py]Cl formulations showed higher potential to alter wetting state of the mixed-wet chalk cores toward more water-wet at 90 °C compared to pure SW0Na brine, as confirmed by a more efficient spontaneous imbibition process using SAIL formulations.
- Although it was observed that the efficiency of the [C_{12}mim]Br formulation was slightly higher than that of the [C_{12}Py]Cl formulation in spontaneous imbibition evaluations, the rings of [C_{12}mim]Br and [C_{12}Py]Cl SAIL did not show a significant effect on additional oil recovered or imbibition rates at 90 °C.
- Solutions formulated with [C_{12}Py]Cl and [C_{16}Py]Cl in SW0Na had a very different performance in imbibition tests. The potential of the [C_{16}Py]Cl formulation to induce changes in rock wetting state was quite low in comparison to [C_{12}Py]Cl and SW0Na due to differences in formulation-oil IFT.
- Contrary to SmW SW0Na brine, an increase of temperature from 90 to 130 °C did not improve the efficacy of the SAIL formulations.
- The evaluation of the effect of sulfate demonstrated that this ion remains key for the chalk wettability alteration by [C_{12}mim]Br formulation, a behavior previously observed with Smart Water, also using the cationic surfactant C_{12}TAB.
- The evaluation of the [C_{12}mim]Br formulation with two viscous core floodings showed that the formulation was more efficient than pure Smart Water, injected both in the secondary and tertiary modes.

This work is a preliminary study about the influence of cationic SAIL parameters, such as type of ring and alkyl chain length, on the performance of SmW as an EOR method. Significant further assessments need to be done to have a full understanding of the SAIL behavior in the wettability alteration processes.

AUTHOR INFORMATION

Corresponding Author

Tina Puntervold − *University of Stavanger, Stavanger 4036, Norway;* orcid.org/0000-0002-5944-7275; Email: tina.puntervold@uis.no

Authors

Nestor Tafur − *CRETUS. Department of Chemical Engineering, Universidade de Santiago de Compostela, Santiago de Compostela E-15782, Spain*

Aleksandr Mamonov − *University of Stavanger, Stavanger 4036, Norway;* orcid.org/0000-0002-3800-9364

Md Ashraful Islam Khan − *University of Stavanger, Stavanger 4036, Norway;* orcid.org/0000-0001-9946-3360

Ana Soto − *CRETUS. Department of Chemical Engineering, Universidade de Santiago de Compostela, Santiago de Compostela E-15782, Spain*

Skule Strand − *University of Stavanger, Stavanger 4036, Norway*

Complete contact information is available at: https://pubs.acs.org/10.1021/acs.energyfuels.3c01488

Notes

The authors declare no competing financial interest.

ACKNOWLEDGMENTS

The author acknowledges CRETUS, the Centre for Cross-disciplinary Research in Environmental Technologies, for financial support (mobility grant for research stays, 2022). We also gratefully acknowledge the University of Stavanger for providing material, equipment, and laboratory facilities.

REFERENCES

(1) Roehl, P. O.; Choquette, P. W. *Carbonate Petroleum Reservoirs*; Springer Science & Business Media: New York, USA, 1985.

(2) Akbar, M.; Alghamdi, A. H.; Herron, M.; Allen, D.; Carnegie, A.; Dutta, D.; Olesen, J.-R.; Chourasiya, R. D.; Logan, D.; Stief, D.; Netherwood, R.; Russell, S. D.; Saxena, K. A Snapshot of Carbonate Reservoir Evaluation Carbonate. *Oilf. Rev.* **1995**, *1*, 38−57.

(3) Burchette, T. P. Carbonate Rocks and Petroleum Reservoirs: A Geological Perspective from the Industry. *Geol. Soc. Spec. Publ.* **2012**, *370*, 17−37.

(4) Chen, H. L.; Lucas, L. R.; Nogaret, L. A. D.; Yang, H. D.; Kenyon, D. E. Laboratory Monitoring of Surfactant Imbibition Using Computerized Tomography. *SPE Reservoir Evaluation \& Engineering*, 2000, No. February.

(5) Strand, S.; Standnes, D. C.; Austad, T. Spontaneous Imbibition of Aqueous Surfactant Solutions into Neutral to Oil-Wet Carbonate Cores: Effects of Brine Salinity and Composition. *Energy and Fuels* **2003**, *17*, 1133−1144.

(6) Austad, T.; Matre, B.; Milter, J.; Sævareid, A.; Øyno, L. Chemical Flooding of Oil Reservoirs 8. Spontaneous Oil Expulsion from Oil- and Water-Wet Low Permeable Chalk Material by Imbibition of Aqueous Surfactant Solutions. *Colloids Surfaces A Physicochem. Eng. Asp.* **1998**, *137*, 117−129.

(7) Puntervold, T.; Austad, T. Injection of Seawater and Mixtures with Produced Water into North Sea Chalk Formation: Impact on Wettability, Scale Formation, and Rock Mechanics Caused by Fluid-Rock Interaction. *Soc. Pet. Eng. - SPE/EAGE Reserv. Charact. Simul. Conf.* **2007**, *2007*, 102−113.

(8) Jaafar, M. Z.; Nasir, A. M.; Hamid, M. F. Measurement of Isoelectric Point of Sandstone and Carbonate Rock for Monitoring Water Encroachment. *Journal of Applied Sciences* **2014**, *14*, 3349−3353.

(9) Dubey, S. T.; Waxman, M. H. Asphaltene Adsorption and Desorption from Mineral Surfaces. *SPE Reserv. Eng.* **1991**, *6*, 389−395.

(10) Buckley, J. S.; Liu, Y.; Monsterleet, S. Mechanisms of Wetting Alteration by Crude Oils. *SPE J* **1998**, *3*, 54−61.

(11) Standnes, D. C.; Austad, T. Wettability Alteration in Chalk 1. Preparation of Core Material and Oil Properties. *J. Pet. Sci. Eng.* **2000**, *28*, 111−121.

(12) Austad, T.; Milter, J.; Rogaland, R. F. Spontaneous Imbibition of Water Into Low Permeable Chalk at Different Wettabilities Using Surfactants. *SPE International Conference on Oilfield Chemistry* Soc. Pet. Eng. J., 1997; SPE 37236, 257−266.

(13) Spinler, E. .; Baldwin, B. Surfactant Induced Wettability Alteration in Porous Media. In *Surfactant Fundamental and Application in the Petroleum Industry*; Schramm, L. L., Ed.; Cambridge University Press: Cambridge, 2000, pp 159−202.

(14) Green, D.; Willhite, G. P. *Enhanced Oil Recovery*, 2nd Ed.; Society of Petroleum Engineers, Inc: Richardson, Texas, 2018.

(15) Singh, A.; Chaturvedi, K. R.; Sharma, T. Natural Surfactant for Sustainable Carbon Utilization in Cleaner Production of Fossil Fuels: Extraction, Characterization and Application Studies. *J. Environ. Chem. Eng.* **2021**, *9*, 106231.

(16) Singh, A.; Sharma, T.; Kumar, R. S.; Arif, M. Biosurfactant Derived from Fenugreek Seeds and Its Impact on Wettability Alteration, Oil Recovery, and Effluent Treatment of a Rock System of Mixed Composition. *Energy and Fuels* **2023**, *37*, 6683−6696.

(17) Standnes, D. C.; Austad, T. Wettability Alteration in Chalk 2. Mechanism for Wettability Alteration from Oil-Wet to Water-Wet Using Surfactants. *J. Pet. Sci. Eng.* **2000**, *28*, 123−143.

(18) Wu, Y.; Shuler, P. J.; Blanco, M.; Tang, Y.; Goddard, W. A. An Experimental Study of Wetting Behavior and Surfactant EOR in Carbonates with Model Compounds. *SPE J.* **2008**, *13*, 26−34.
(19) Chen, P.; Mohanty, K. K. Surfactant-Enhanced Oil Recovery from Fractured Oil-Wet Carbonates: Effects of Low IFT and Wettability Alteration. *Proc. - SPE Int. Symp. Oilf. Chem.* **2015**, *2*, 1225−1248.
(20) Austad, T.; Standnes, D. C. Spontaneous Imbibition of Water into Oil-Wet Carbonates. *J. Pet. Sci. Eng.* **2003**, *39*, 363−376.
(21) Jarrahian, K.; Seiedi, O.; Sheykhan, M.; Sefti, M. V.; Ayatollahi, S. Wettability Alteration of Carbonate Rocks by Surfactants: A Mechanistic Study. *Colloids Surfaces A Physicochem. Eng. Asp.* **2012**, *410*, 1−10.
(22) Standnes, D. C.; Nogaret, L. A. D.; Chen, H. L.; Austad, T. An Evaluation of Spontaneous Imbibition of Water into Oil-Wet Carbonate Reservoir Cores Using a Nonionic and a Cationic Surfactant. *Energy and Fuels* **2002**, *16*, 1557−1564.
(23) Pierre, A.; Lamarche, J. M.; Mercier, R.; Foissy, A.; Persello, J. Calcium as Potential Determining Ion in Aqueous Calcite Suspensions. *J. Dispers. Sci. Technol.* **1990**, *11*, 611−635.
(24) Zhang, P.; Tweheyo, M. T.; Austad, T. Wettability Alteration and Improved Oil Recovery in Chalk: The Effect of Calcium in the Presence of Sulfate. *Energy and Fuels* **2006**, *20*, 2056−2062.
(25) Strand, S.; Høgnesen, E. J.; Austad, T. Wettability Alteration of Carbonates - Effects of Potential Determining Ions (Ca2+ and SO42-) and Temperature. *Colloids Surfaces A Physicochem. Eng. Asp.* **2006**, *275*, 1−10.
(26) Zhang, P.; Tweheyo, M. T.; Austad, T. Wettability Alteration and Improved Oil Recovery by Spontaneous Imbibition of Seawater into Chalk: Impact of the Potential Determining Ions Ca2+, Mg2+, and SO42-. *Colloids Surfaces A Physicochem. Eng. Asp.* **2007**, *301*, 199−208.
(27) Zhang, P.; Austad, T. Wettability and Oil Recovery from Carbonates: Effects of Temperature and Potential Determining Ions. *Colloids Surfaces A Physicochem. Eng. Asp.* **2006**, *279*, 179−187.
(28) Burgess, J. *Metal Ions in Solution*; Ellis Horwood Limited: Chichester, Sussex, UK, 1978.
(29) Rao, D. N. Wettability Effects in Thermal Recovery Operations. *Proc. - SPE Symp. Improv. Oil Recover.* **1999**, *2*, 420−430.
(30) Zhang, P.; Austad, T. The Relative Effects of Acid Number and Temperature on Chalk Wettability. *SPE International Conference on Oilfield Chemistry*; SPE, 2005; pp 185−191.
(31) Qi, Z.; Han, M.; Chen, S.; Wang, J. Surfactant Enhanced Imbibition in Carbonate Reservoirs: Effect of IFT Reduction and Surfactant Partitioning. *JCIS Open* **2022**, *5*, 100045.
(32) Bin Dahbag, M.; AlQuraishi, A.; Benzagouta, M. Efficiency of Ionic Liquids for Chemical Enhanced Oil Recovery. *J. Pet. Explor. Prod. Technol.* **2015**, *5*, 353−361.
(33) Bera, A.; Belhaj, H. Ionic Liquids as Alternatives of Surfactants in Enhanced Oil Recovery—A State-of-the-Art Review. *J. Mol. Liq.* **2016**, *224*, 177−188.
(34) Nandwani, S. K.; Chakraborty, M.; Bart, H. J.; Gupta, S. S. Synergism, phase behaviour and characterization of ionic liquid-nonionic surfactant mixture in high salinity environment of oil reservoirs. *Fuel* **2018**, *229*, 167−179.
(35) Cooper, E. R.; Andrews, C. D.; Wheatley, P. S.; Webb, P. B.; Wormald, P.; Morris, R. E. Ionic Liquids and Eutectic Mixtures as Solvent and Template in Synthesis of Zeolite Analogues. *Nature* **2004**, *430*, 1012−1016.
(36) Hanke, C. G.; Lynden-Bell, R. M. A Simulation Study of Water-Dialkylimidazolium Ionic Liquid Mixtures. *J. Phys. Chem. B* **2003**, *107*, 10873−10878.
(37) Vaghela, N. M.; Sastry, N. V.; Aswal, V. K. Surface Active and Aggregation Behavior of Methylimidazolium-Based Ionic Liquids of Type [C n Mim] [X], N∈=∈4, 6, 8 and [X]∈=∈Cl-Br-and I- in Water. *Colloid Polym. Sci.* **2011**, *289*, 309−322.
(38) Hezave, A. Z.; Dorostkar, S.; Ayatollahi, S.; Nabipour, M.; Hemmateenejad, B. Investigating the Effect of Ionic Liquid (1-Dodecyl-3-Methylimidazolium Chloride ([C12mim] [Cl])) on the Water/Oil Interfacial Tension as a Novel Surfactant. *Colloids Surfaces A Physicochem. Eng. Asp.* **2013**, *421*, 63−71.
(39) Somoza, A.; Arce, A.; Soto, A. Oil Recovery Tests with Ionic Liquids: A Review and Evaluation of 1-Decyl-3-Methylimidazolium Triflate. *Pet. Sci.* **2022**, *19*, 1877−1887.
(40) Rodríguez-Palmeiro, I.; Rodríguez-Escontrela, I.; Rodríguez, O.; Soto, A.; Reichmann, S.; Amro, M. M. Tributyl(Tetradecyl)-Phosphonium Chloride Ionic Liquid for Surfactant-Enhanced Oil Recovery. *Energy and Fuels* **2017**, *31*, 6758−6765.
(41) Liu, J.; Huang, P.; Feng, Q.; Lian, P.; Liang, Y.; Huang, W.; Yan, H.; Jia, H. Systematic Investigation of the Effects of an Anionic Surface Active Ionic Liquid on the Interfacial Tension of a Water/Crude Oil System and Its Application to Enhance Crude Oil Recovery. *J. Dispers. Sci. Technol.* **2019**, *40*, 1657−1663.
(42) Nabipour, M.; Ayatollahi, S.; Keshavarz, P. Application of Different Novel and Newly Designed Commercial Ionic Liquids and Surfactants for More Oil Recovery from an Iranian Oil Field. *J. Mol. Liq.* **2017**, *230*, 579−588.
(43) Zabihi, S.; Faraji, D.; Rahnama, Y.; Zeinolabedini Hezave, A.; Ayatollahi, S. Relative Permeability Measurement in Carbonate Rocks, the Effects of Conventional Surfactants vs. Ionic Liquid-Based Surfactants. *J. Dispers. Sci. Technol.* **2020**, *41*, 1797−1811.
(44) Sakthivel, S. Imidazolium Based Ionic Liquids for Enhanced Oil Recovery on the Carbonate Reservoir. *J. Mol. Liq.* **2022**, *366*, 120284.
(45) Somoza, A.; Tafur, N.; Arce, A.; Soto, A. Design and Performance Analysis of a Formulation Based on SDBS and Ionic Liquid for EOR in Carbonate Reservoirs. *J. Pet. Sci. Eng.* **2022**, *209*, 109856.
(46) Jia, H.; Leng, X.; Hu, M.; Song, Y.; Wu, H.; Lian, P.; Liang, Y.; Zhu, Y.; Liu, J.; Zhou, H. Systematic Investigation of the Effects of Mixed Cationic/Anionic Surfactants on the Interfacial Tension of a Water/Model Oil System and Their Application to Enhance Crude Oil Recovery. *Colloids Surfaces A Physicochem. Eng. Asp.* **2017**, *529*, 621−627.
(47) Sakthivel, S. Wettability Alteration of Carbonate Reservoirs Using Imidazolium-Based Ionic Liquids. *ACS Omega* **2021**, *6*, 30315−30326.
(48) Cao, N.; Almojtaba Mohammed, M.; Babadagli, T. Wettability Alteration of Heavy-Oil-Bitumen-Containing Carbonates by Use of Solvents, High-PH Solutions, and Nano/Ionic Liquids. *SPE Reserv. Eval. Eng.* **2017**, *20*, 363−371.
(49) Sakthivel, S.; Elsayed, M. Enhanced Oil Recovery by Spontaneous Imbibition of Imidazolium Based Ionic Liquids on the Carbonate Reservoir. *J. Mol. Liq.* **2021**, *340*, 117301.
(50) Manshad, A. K.; Rezaei, M.; Moradi, S.; Nowrouzi, I.; Mohammadi, A. H. Wettability Alteration and Interfacial Tension (IFT) Reduction in Enhanced Oil Recovery (EOR) Process by Ionic Liquid Flooding. *J. Mol. Liq.* **2017**, *248*, 153−162.
(51) Klewiah, I.; Piñerez Torrijos, I. D.; Strand, S.; Puntervold, T.; Konstantinopoulos, M. Adsorption of Crude Oil Polar Components onto Silica-Rich Chalk and Its Impact on Wetting. *SPE Norway Subsurface Conference*; SPE, 2019.
(52) Fan, T.; Buckley, J. S. Acid Number Measurements Revisited. *SPE J.* **2007**, *12*, 496−500.
(53) Frykman, P. Spatial Variability in Petrophysical Properties in Upper Maastrichtian Chalk Outcrops at Stevns Klint, Denmark. *Mar. Pet. Geol.* **2001**, *18*, 1041−1062.
(54) Pinerez Torrijos, I. D.; Strand, S.; Puntervold, T.; Kahlbom Wathne, A.; Harestad, A.; Radenkovic, K.; Andersen, P. Ø. The Effect of Core Wettability on Oil Mobilization, Capillary Forces and Relative Permeability in Chalk. *SPE EuropEC-Europe Energy Conference featured at the 83rd EAGE Annual Conference Exhibition*; OnePetro, 2022.
(55) Piñerez, I.; Puntervold, T.; Strand, S.; Hopkins, P.; Aslanidis, P.; Yang, H. S.; Kinn, M. S. Core Wettability Reproduction: A New Solvent Cleaning and Core Restoration Strategy for Chalk Cores. *J. Pet. Sci. Eng.* **2020**, *195*, 107654.

(56) Puntervold, T.; Strand, S.; Austad, T. New Method to Prepare Outcrop Chalk Cores for Wettability and Oil Recovery Studies at Low Initial Water Saturation. *Energy and Fuels* **2007**, *21*, 3425−3430.
(57) Barnes, J. R.; Smit, J. P.; Smit, J. R.; Shpakoff, P. G.; Raney, K. H.; Puerto, M. C. Development of Surfactants for Chemical Flooding at Difficult Reservoir Conditions. *SPE Symp. Improv. Oil Recover.* **2008**, *1*, 435−452.
(58) Puerto, M.; Hirasaki, G. J.; Miller, C. A.; Barnes, J. R. Surfactant Systems for EOR in High-Temperature, High-Salinity Environments. *SPE J* **2012**, *17*, 11−19.
(59) Montes, J.; Blin, N.; Alvarez, A. E.; Barrio, I.; Panadero, A.; Rodriguez, R.; Coca, M.; Trujillo, F. Novel Anionic Surfactant Formulation for High Temperature Carbonate Reservoirs. *SPE EOR Conference at Oil and Gas West Asia*; OnePetro, 2018, 2018.
(60) Winsor, P. A. Hydrotropy, solubilisation and related emulsification processes. *Trans. Faraday Soc.* **1948**, *44*, 376−398.
(61) Kurnia, I.; Zhang, G.; Han, X.; Yu, J. Zwitterionic-Anionic Surfactant Mixture for Chemical Enhanced Oil Recovery without Alkali. *Fuel* **2020**, *259*, 116236.
(62) Hu, H.; Joseph, D. Evolution of a Liquid Drop in a Spinning Drop Tensiometer. *J. Colloid Interface Sci.* **1994**, *162*, 331−339.
(63) Vonnegut, B. Rotating Bubble Method for the Determination of Surface and Interfacial Tensions. *Rev. Sci. Instrum.* **1942**, *13*, 6−9.
(64) Springer, N.; Survey, G. Resistivity Index Measurement without the Porous Plate: A Desaturation Technique Based on Evaporation Produces Uniform Water Saturation Profiles and More Reliable Results for Tight North Sea Chalk. *International Symposium of the Society of Core Analysts Pau, France*, 2003.
(65) Piñerez Torrijos, I. D.; Puntervold, T.; Strand, S.; Aslanidis, P.; Fjelde, I.; Mamonov, A. *Core Restoration. A Guide for Improved Wettability Assessments*; UiS Scholarly Publishing Services, 2022.
(66) Sharma, H.; Lu, J.; Weerasooriya, U. P.; Pope, G. A.; Mohanty, K. K. Adsorption in Chemical Floods with Ammonia as the Alkali. *SPE Improved Oil Recovery Conference*; OnePetro, 2016, 2016-Janua.
(67) Li, K.; Jing, X.; He, S.; Wei, B. Static Adsorption and Retention of Viscoelastic Surfactant in Porous Media: EOR Implication. *Energy and Fuels* **2016**, *30*, 9089−9096.
(68) Salager, J. L.; Forgiarini, A. M.; Bullón, J. How to Attain Ultralow Interfacial Tension and Three-Phase Behavior with Surfactant Formulation for Enhanced Oil Recovery: A Review. Part 1. Optimum Formulation for Simple Surfactant-Oil-Water Ternary Systems. *J. Surfactants Deterg.* **2013**, *16*, 449−472.
(69) Salager, J. L.; Morgan, J. C.; Schechter, R. S.; Wade, W. H.; Vasquez, E. Optimum Formulation of Surfactant/Water/Oil Systems for Minimum Interfacial Tension or Phase Behavior. *Soc. Pet. Eng. J.* **1979**, *19*, 107−115.
(70) Oh, K. H.; Baran, J. R.; Wade, W. H.; Weerasooriya, V. Temperature Insensitive Microemulsion Phase Behavior with Non-Ionic Surfactants. *J. Dispers. Sci. Technol.* **1995**, *16*, 165−188.
(71) Nan, Y. Q.; Hao, L. S. Salt-Induced Phase Inversion in Aqueous Cationic/Anionic Surfactant Two-Phase Systems. *J. Phys. Chem. B* **2008**, *112*, 12326−12337.
(72) Glover, C. J.; Puerto, M. C.; Maerker, J. M.; Sandvik, E. L. Surfactant Phase Behavior and Retention in Porous Media. *Soc. Pet. Eng. AIME J.* **1979**, *19*, 183−193.
(73) Jang, S. H.; Liyanage, P. J.; Tagavifar, M.; Chang, L.; Upamali, K. A. N.; Lansakara-P, D.; Weerasooriya, U.; Pope, G. A. A Systematic Method for Reducing Surfactant Retention to Extremely Low Levels. *SPE improved oil recovery conference*, 2016-Janua, 2016.
(74) Novosad, J. Surfactant Retention in Berea Sandstone-Effects of Phase Behavior and Temperature. *Soc. Pet. Eng. J.* **1982**, *22*, 962−970.
(75) Aarra, M. G.; Høiland, H.; Skauge, A. Phase Behavior and Salt Partitioning in Two- and Three-Phase Anionic Surfactant Micro-emulsion Systems: Part II, Partitioning of Salt. *J. Colloid Interface Sci.* **1999**, *215*, 216−225.
(76) Antón, R. E.; Gómez, D.; Graciaa, A.; Lachaise, J.; Salager, J. L. Surfactant-Oil-Water Systems Near the Affinity Inversion Part IX: Optimum Formulation and Phase Behavior of Mixed Anionic-Cationic Systems. *J. Dispers. Sci. Technol.* **1993**, *14*, 401−416.
(77) Skauge, A.; Fotland, P. Effect of Pressure and Temperature on the Phase Behavior of Microemulsions. *SPE Reserv. Eng.* **1990**, *5*, 601−608.
(78) Khan, M. A. I.; Piñerez Torrijos, I. D.; Aldeen Algazban, S. H.; Strand, S.; Puntervold, T. Polysulphate: A New Eor Additive to Maximize the Oil Recovery from Carbonate Reservoirs at High Temperature. *ADIPEC*; OnePetro, 2022, No. August, 1−15.
(79) Khan, M. A. I.; Kleiberg, S. H.; Pinerez Torrijos, I. D.; Puntervold, T.; Strand, S. Carbonated Smart Water Injection for Optimized Oil Recovery in Chalk at High Temperature. *E3S Web of Conferences*; EDP Sciences, 2023; Vol. *367*.
(80) Standnes, D. C.; Austad, T. Wettability Alteration in Carbonates: Interaction between Cationic Surfactant and Carboxylates as a Key Factor in Wettability Alteration from Oil-Wet to Water-Wet Conditions. *Colloids Surfaces A Physicochem. Eng. Asp.* **2003**, *216*, 243−259.
(81) Li, Y.; Pope, G. A.; Lu, J.; Churchwell, L.; Tagavifar, M.; Weerasooriya, U. Scaling of Low-Interfacial-Tension Imbibition in Oil-Wet Carbonates. *SPE Symp. Improv. Oil Recover.* **2017**, *22*, 1349−1361.
(82) Puntervold, T.; Mamonov, A.; Piñerez Torrijos, I. D.; Strand, S. Adsorption of Crude Oil Components onto Carbonate and Sandstone Outcrop Rocks and Its Effect on Wettability. *Energy and Fuels* **2021**, *35*, 5738−5747.
(83) Strand, S.; Puntervold, T.; Austad, T. Effect of Temperature on Enhanced Oil Recovery from Mixed-Wet Chalk Cores by Spontaneous Imbibition and Forced Displacement Using Seawater. *Energy and Fuels* **2008**, *22*, 3222−3225.
(84) Karimi, M.; Al-Maamari, R. S.; Ayatollahi, S.; Mehranbod, N. Mechanistic Study of Wettability Alteration of Oil-Wet Calcite: The Effect of Magnesium Ions in the Presence and Absence of Cationic Surfactant. *Colloids Surfaces A Physicochem. Eng. Asp.* **2015**, *482*, 403−415.
(85) Liu, J.; Wani, O. B.; Alhassan, S. M.; Pantelides, S. T. Wettability Alteration and Enhanced Oil Recovery Induced by Proximal Adsorption of Na+, Cl-Ca2+, Mg2+, and SO42- Ions on Calcite. *Phys. Rev. Appl.* **2018**, *10*, 034064.
(86) Alotaibi, M. B.; Yousef, A. A. The Role of Individual and Combined Ions in Waterflooding Carbonate Reservoirs: Electrokinetic Study. *SPE Reserv. Eval. Eng.* **2017**, *20*, 077−086.
(87) Montazeri, M.; Fazelabdolabadi, B.; Shahrabadi, A.; Nouralishahi, A.; HallajiSani, A.; Moosavian, S. M. A. An Experimental Investigation of Smart-Water Wettability Alteration in Carbonate Rocks−Oil Recovery and Temperature Effects. *Energy Sources, Part A Recover. Util. Environ. Eff.* **2020**, 1−13.
(88) Safavi, M. S.; Masihi, M.; Safekordi, A. A.; Ayatollahi, S.; Sadeghnejad, S. Effect of SO4−2 Ion Exchanges and Initial Water Saturation on Low Salinity Water Flooding (LSWF) in the Dolomite Reservoir Rocks. *J. Dispers. Sci. Technol.* **2020**, *41*, 841−855.
(89) Churcher, P. L.; French, P. B.; Shaw, J. C.; Schramm, L. L. Rock Properties of Berea Sandstone, Baker Dolomite, and Indiana Limestone. *SPE International Conference on Oilfield Chemistry*, 1991; pp 431−446.
(90) Ravari, R. R.; Strand, S.; Austad, T. Care Must Be Taken to Use Outcrop Limestone Cores to Mimic Reservoir Core Material in SCAL Linked to Wettability Alteration. In *11th International Symposium on Reservoir Wettability: Calgary, Canada*, 2010.
(91) Strand, S.; Austad, T.; Puntervold, T.; Høgnesen, E. J.; Olsen, M.; Barstad, S. M. F. Smart Water for Oil Recovery from Fractured Limestone: A Preliminary Study. *Energy and Fuels* **2008**, *22*, 3126−3133.

https://doi.org/10.1021/acs.energyfuels.3c01488
Energy Fuels 2023, 37, 11730−11742

USC
UNIVERSIDADE
DE SANTIAGO
DE COMPOSTELA

4. GENERAL DISCUSSION



USC
UNIVERSIDADE
DE SANTIAGO
DE COMPOSTELA

USC
UNIVERSIDADE
DE SANTIAGO
DE COMPOSTELA

As the world transitions towards cleaner energy, EOR methods can help to extend the productive life of oil reservoirs, providing a bridge between traditional energy sources and more sustainable ones. The ability to increase the recovery factor of reservoirs, while remaining environmentally friendly and cost-effective, makes certain EOR methods crucial tools in the oil and gas industry's efforts to meet the growing demand for energy while reducing its environmental impact.

This thesis focused on studying novel techniques and chemical agents to improve existing chemical EOR methods. Several proposals to enhance both volumetric sweep and displacement efficiencies were evaluated.

In the oil industry, volumetric sweep efficiency is commonly improved through the injection of a polymer solution after a water injection process. The polymer solution must have higher viscosity than the injected water and, if operational conditions allow, should also have equal or higher viscosity than the crude oil in the reservoir. Polymers are macromolecules whose average size in solution must be adjusted to the porous throat size of the reservoir rock to prevent face plugging [57] (blockages or restrictions of pores at the face rock in the well-reservoir interface caused by high polymer size or concentration). When the crude oil at reservoir conditions has a much higher viscosity than the injected water, it becomes necessary to increase the viscosity of the polymer solution to achieve more favourable mobility ratios. Therefore, the polymer solution requires either an increase in polymer concentration or the use of higher molecular weight polymers, which have larger molecular sizes but can reach the desired viscosity at lower concentrations. For low permeability reservoirs and high oil viscosity, the manoeuvrable window is narrow because face plugging can occur due to polymer sizes or high concentrations of smaller polymers. A possible solution to this limitation of traditional polymers in EOR processes is proposed in the first part of this thesis.

An initial evaluation, conducted in **Paper 1** of this compendium of articles, was related to the areal sweep efficiency (macroscopic efficiency). To that end, numerical simulations were conducted, modelling displacement processes in a Helle Shaw cell (without a porous medium), using a commercial simulator (Ansys Fluent 20.1). Viscous fingering is caused by the displacement of a higher viscosity fluid by a lower viscosity one. A previous experimental work [58], it was shown that this instability is also present in reactive displacement systems, where a lower viscosity displacing fluid reacts with the higher viscosity displaced fluid throughout the process. The reaction gives rise to the formation of a product at the interface with higher viscosity than the displacing and displaced fluids. When the fingering pattern reaches a certain distance from the injection point, the injection of the displacing fluid can be closed to allow the fluids to react

USC UNIVERSIDADE DE SANTIAGO DE COMPOSTELA

without convective mass transfer. The fingering pattern attenuates or disappears because of the reaction at this stage. Since the flow is radial, this product may form a ring at the interface between the displaced and displacing fluids, around the inlet point, at a certain distance from it (radius of the ring). Looking for the application of this phenomenon to EOR, the first paper of this thesis involved a systematic evaluation of the main parameters influencing the reactive displacement process, including injection rates, ring radius, and the closing time required to improve ring formation. Moreover, the volume of the displaced fluid was estimated once restored the injection and the boundaries of the system were reached. Higher values of displaced fluid recovery were mainly found by adjusting the radius of the ring and the closing time. The study showed that it might be possible to displace a higher viscosity fluid (e.g., crude oil) with high efficiency (around 90% recovery) using a lower viscosity fluid (e.g., aqueous phase). This is due to the improvement of the areal sweep by means of the chemical reaction. However, the success of this proposal depends on several key parameters such as the chemical reaction rate, displacing and displaced viscosity ratio, and diffusion coefficients of the fluids.

This technique was considered for use during or after water flooding recovery. Chemical agents could be added to the injection water to react either with crude oil in the reservoir or other previously injected fluids. As bottleneck of the method, finding such reactions (taking into account, for instance, some specific functional groups of crude oils) is not an easy task. The main idea is to design specific chemical interfacial reactions that allow a personalized oil recovery. Although from a fundamental point of view, this technique works, it still requires more research in order to become useful.

The second part of the thesis evaluates displacement efficiency (microscopic efficiency) when reducing interfacial tension (IFT) values between oil and aqueous phases present in reservoirs. As mentioned in section 2.1.3, the most effective approach to significantly increasing displacement efficiency consists of reducing the IFT to very low levels using surface-active agents. Surfactant flooding is a well-known chemical EOR method, primarily due to fundamental studies, extensive laboratory evaluations and several pilot tests. However, the number of surfactant flooding projects conducted in oil reservoirs has remained relatively low [13,35]. This could be attributed to the profitability of the projects, as the cost of many surfactants is tightly linked to the oil price [21], and to the delicate balance of surfactant formulations, which can be disrupted during their passage through reservoirs due to changes in parameters such as salinity, rock mineralogy, and rock heterogeneity. This second part of this thesis involves three papers which testing blends of surfactants and SAILs to design formulations capable of reducing IFT to very low values.

USC UNIVERSIDADE DE SANTIAGO DE COMPOSTELA

Typical ionic surfactants are known to exhibit good aqueous phase solubility at low salinity, with some oil solubilised in the aqueous phase in micelles and an excess oil phase essentially free of surfactant (Winsor type I microemulsion). At high salinity, surfactant shifts to the oil phase, and the system separates into an excess water phase free of surfactant and an oil phase with water solubilised by means of inverse micelles (Winsor type II microemulsion). Normally, this transition between microemulsion types passes through an intermediate microemulsion (Winsor type III), which has water and oil solubilised in bicontinuous micelles (a combination of direct and inverse micelles) with excess water and oil phases [25]. In contrast, nonionic surfactants can exhibit less sensitivity to electrolyte changes and maintain a Winsor type I microemulsion at higher salinity concentration than ionic surfactants [10,59].

Significant changes in reservoir salinity can occur after water flooding, where gradients between the formation water (original brine present) and injected water salinities may form. When using formation brine as the injected water this gradient is not produced. In reservoirs that have been flooded SW, a salinity gradient should be present. However, in some cases, after years of water flooding and several injected PV, some reservoirs have reached brine salinities similar to injected brines [35].

The evaluation of surfactant blends, taking into account salinity gradients, was initiated in **Paper 2**. Several blend systems were studied simultaneously varying salinity and blend ratio. The aim was to build activity maps to represent the behaviour of the middle-phase in Winsor type III microemulsions graphically, as a function of salinity concentration and blend ratio at a fixed temperature. By interpolating the data of the third-phase regions in the activity maps, it was possible to define their boundaries and identify blend ratios less sensitive to salinity. Thus, adjusting the injection water salinity could be a way to maintain the stability of the microemulsion inside the reservoir. Moreover, during the injection of a formulation with a surfactant blend, the adsorption of one of the surfactants may occur. If the adsorption of that surfactant is too high, it triggers changes in the microemulsion type. In that case, knowing the proportion of the surfactant adsorbed, the activity maps might provide useful insight into the phase behaviour changes in the reservoir by altering the blend ratio.

In Paper 2, several surfactant/SAIL blends were formulated in vials at room temperature to achieve a 4 wt% surfactant concentration in 5 wt% NaCl brine. *N*-octane was used as a model oil phase, for simplicity and to enable easy identification of the interfaces between microemulsions and excess phases, particularly the two interfaces found in Winsor III microemulsions. The use of SAILs was proposed to expand the options of cationic surface-active agents, since a wide variety

USC UNIVERSIDADE DE SANTIAGO DE COMPOSTELA

(with different alkyl chain lengths and polar head groups) are available. The formulation work focused on obtaining binary blends capable of both reaching Winsor type III microemulsions and maintaining them for as long as possible during salinity increases. The surfactant blend technique has been shown effective in improving the performance of pure surfactant formulations when they fail to achieve the desired IFT or adsorption levels under required conditions [60,61]. It is known that the combination of different surfactants, especially those with different head group charges, promotes the formation of mixed micelles that enhance surface activity between the oil and aqueous phases. Therefore, binary blends were formulated using traditional surfactants and SAILs. The surfactant dioctyl sulfosuccinate sodium salt (Aerosol® OT, AOT) was used as a tuning agent due to its anionic and large hydrophobic character. This surfactant was blended with nonionic and cationic surfactants, as well as cationic SAILs, all of which being highly hydrophilic. Figure 4.1 presents the formulations that were able to achieve Winsor type III microemulsions or at least a transition from Winsor type I to type II in this preliminary evaluation. Three promising blends were selected:

- AOT and the surfactant polyoxyethylene(8) octyl ether carboxylic acid ($C_8EO_8OCH_2COOH$) (Akypo LF2®, LF2)
- AOT and the SAIL 1-decyl-3-methylimidazolium chloride ([C_{10}mim]Cl)
- AOT and the SAIL 1-dodecyl-3-methylimidazolium bromide ([C_{12}mim]Br)

Those blends are shown in the first row of Figure 4.1. In the second row, the binary formulations of AOT with the traditional cationic surfactant dodecyl trimethyl ammonium bromide (C12TAB) and with the SAIL 1-dodecyl-3-methylimidazolium Acetate ([C_{12}mim][OAc]) are also shown. These blends also led to Winsor type III microemulsions. However, with respect to their potential application for EOR methods, these formulations were excluded from further evaluation due to the formation of precipitates at high or low AOT concentrations.

To delineate the experimental work for building the activity maps, a simple experimental design based on the Doehlert model [62,63] with two variables was conducted in vials at room temperature. Variables were salinity concentration (wt% NaCl) and the blend ratio between surfactants. Although an experimental design is not necessary for building activity maps, it was a helpful tool in saving time and resources, allowing efforts to be focused on the regions of interest.

USC UNIVERSIDADE DE SANTIAGO DE COMPOSTELA

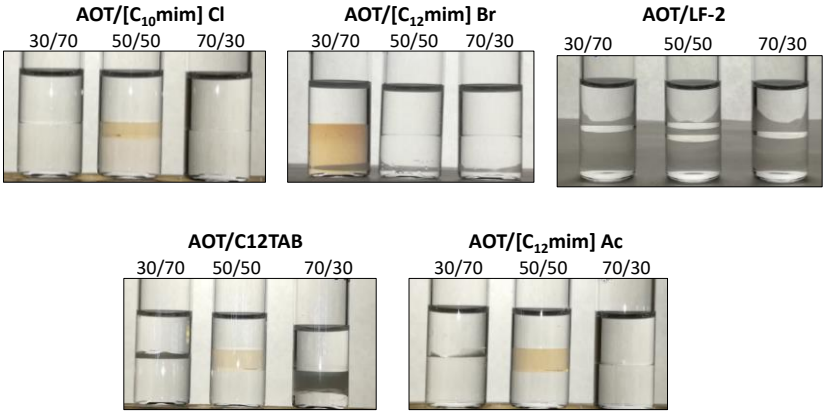


Figure 4.1. Promising blend formulations (Winsor type III microemulsions) at different blend ratios (30/70, 50/50 and 70/30) in 5 wt% NaCl aqueous solution at room temperature. Overall surfactant concentration of 4 wt%. *N*-octane was used as oil phase.

For more accurate evaluations, further studies of the blends were performed using visual tests with pipettes. These evaluations began by examining the phase behaviour of the blends (4 wt%) at different ratios prepared in brine with a fixed salinity concentration of 5 wt% NaCl, and at a controlled temperature of 25 °C. This salinity concentration was selected as starting point since it is close to the total dissolved solids in SW. The changes in the type of microemulsion were obtained by first formulating the blends at low AOT concentration and then increasing it in steps of 5% in blend ratios (e.g., 30/70, 35/65, etc). This method increased the hydrophobic character of the blends, which are highly hydrophilic at low AOT concentrations. The transition from Winsor type I to type II microemulsion for the AOT/LF2 formulation was smooth, as a Winsor type III region was observed in several pipettes with blend ratios ranging from 50/50 to 60/40. For the AOT/[C_{10}mim]Cl blend, a Winsor III microemulsion was only observed at 45/55 blend ratio. However, for the AOT/[C_{12}mim]Br blend, there was a sharp shift from Winsor I to Winsor II microemulsions, and no three-phase region was seen in the pipettes. Thus, the test was repeated by reducing the blend ratio step size. The same detailed study was applied to the AOT/[C_{10}mim]Cl blend for comparative purposes. A Winsor III microemulsion was observed at a 35/65 blend ratio in the AOT/[C_{12}mim]Br system. For the AOT/[C_{10}mim]Cl blend, the three-phase region was observed from 43/57 to 45/55 ratios.

The surface activity of the blends was reflected in the capacity of the Winsor III microemulsions to solubilise aqueous and oil phases. The solubilisation of the phases was measured by the volume of the Winsor III microemulsion in the pipettes. The highest solubilisation capacity is directly related to the optimal solubilisation parameter and the lowest IFT according to Huh's equation

USC UNIVERSIDADE DE SANTIAGO DE COMPOSTELA

[64]. The AOT/LF2, AOT/[C_{10}mim]Cl, and AOT/[C_{12}mim]Br blends achieved optimal solubilisation parameters of 2.5, 6.6 and 14.5, respectively.

The most important characteristic observed at this point was the existence of a relationship between the abruptness with which the microemulsion shifts from Winsor I to II and the magnitude of the optimal solubilisation parameter. In other words, the greater this value the more abrupt the transition of the microemulsion. The amplitude of the third-phase region for AOT/LF2 was the widest, ranging from 50/50 to 60/40 blend ratios. However, the solubilisation capacity of this blend was the lowest, and each pipette showed a thinner third-phase (smaller volume of Winsor III microemulsion) compared to the other blends. In contrast, with the AOT/[C_{12}mim]Br blend, Winsor III behaviour was only observed in one pipette (at 35/65 blend ratio), resulting in the narrowest Winsor III region among the three blends studied, but its optimal solubilisation parameter was the highest. AOT/[C_{10}mim]Cl presented an intermediate amplitude of Winsor III region as well as solubilisation capacity, with values between the other two blends. It should be noted that larger electrostatic interactions between the opposite charges of the surfactant head groups result in higher surface activity in mixed micelles [65,66].

As mentioned above, one of the most important concerns in surfactant flooding is the formulation's behaviour when it faces salinity variations in the reservoir. To evaluate this situation, the three blends (with different blend ratios) were prepared at different salt concentrations ranging from 1 to 15 wt% NaCl. As the salinity decreased, the AOT/LF2 blend became more hydrophilic. Thus, the AOT fractions were adjusted to promote the Winsor I-III-II transition depending on salinity. It is worth mentioning the reduction in the amplitude of the Winsor III region at low salinity. At 1 wt% NaCl, this microemulsion type was only obtained in one pipette (85/15 AOT/LF2 ratio). However, at 13 wt% NaCl, Winsor III systems were found from 25/75 to 45/55 blend ratios. Furthermore, the optimal solubilisation parameter increased as salinity decreased, being 5.7 at 1 wt% NaCl and 1.9 at 13 wt% NaCl. Formulations with salinity above 13 wt% NaCl showed very low values of the parameter. Regarding the evolution of the AOT/SAIL blends with salinity, they were found to be less sensitive to this variable, with the size of the narrow Winsor III region being hardly affected. It was also found that the larger the optimal solubilisation parameter, the more abrupt the transition of the microemulsion behaviour (the narrower Winsor III region).

Concerning temperature changes, these only occur when the surfactant formulation enters the reservoir and goes from ambient to the reservoir temperature. As this remains constant, it serves as the working temperature for surfactant flooding studies. The average reservoir temperature

USC UNIVERSIDADE DE SANTIAGO DE COMPOSTELA

for alkaline-surfactant projects undertaken is around 27 °C, while for polymer projects, it is about 49 °C [2]. However, most global oil fields have temperatures of about 80 °C. Figure 4.2 shows a distribution of reservoir temperatures worldwide [67].

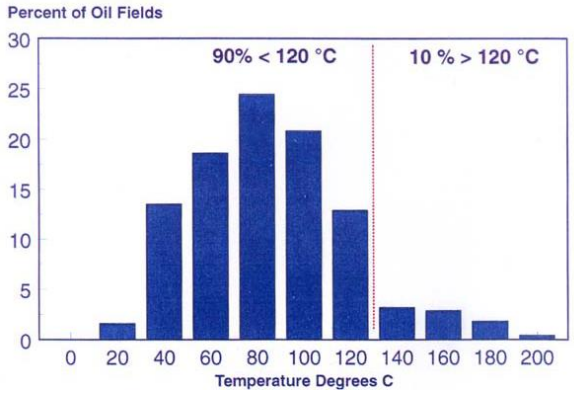


Figure 4.2. Reservoir temperature distributions of oil resources from a worldwide sampling of oil fields IFT (Figure reproduced from [67]. Permission to publish by CSIRO Publishing).

To determine the influence of temperature on the behaviour of the blends, new studies were carried out at 50 °C and 75 °C. The general behaviour was the expansion of the initial three-phase region amplitude (at 25 °C) with increased temperature. This expansion occurred on both sides of the initial Winsor III regions. So, Winsor I microemulsions (low AOT blend proportion) and Winsor II (high AOT proportion) shifted to Winsor III with increasing temperature. This behaviour, previously reported by others [68,69], makes defining trends for the blends under temperature changes challenging. To identify general performance, the evaluation focused on the shift of the optimal blend ratio.

In the case of AOT/LF2, the formulation became more hydrophilic, and thus required higher AOT proportion to maintain optimal Winsor III conditions, with increased temperature. This behaviour is similar to that found in ionic surfactant solutions. In contrast, for both AOT/SAIL blends the behaviour was the opposite. Optimal blend ratios shifted to lower AOT proportions with increasing temperature. The blends became more lipophilic, behaving as nonionic surfactants [70]. The expansion of the three-phase region with increased temperature was accompanied by a reduction of the optimal solubilisation parameters. The highest reduction being observed for the AOT/[C_{12}mim]Br blend. About 50% reduction was found when the temperature changed from 25°C to 50 °C. Despite this reduction, this blend exhibited the best solubilisation capacity.

The results presented in Paper 2 allow the design of a suitable formulation addressing the conditions of a given reservoir: salinity and hardness of brines and reservoir temperature.

USC UNIVERSIDADE DE SANTIAGO DE COMPOSTELA

The outcomes of this study were used to design a new surfactant formulation for EOR in **Paper 3** of the thesis. The first step was to identify the limitations of the studied blends, such as maximum operational temperature, tolerance to brine hardness, and useful blend ratios for specific operational conditions. For core flooding tests, a lengthy water flooding process with SW before the blend injection was assumed, so that no salinity gradient was considered along the cores. This approach allowed the evaluation to be focused on the efficiency, at SW salinity, of the blends to improve oil recovery by reduction of the IFT.

A preliminary evaluation of hardness tolerance was conducted for AOT/LF2, AOT/[C_{10}mim]Cl and AOT/[C_{12}mim]Br blends at 1 wt% surfactant concentration in synthetic SW at room temperature. The presence of divalent ions in the brine (Ca^{2+} and Mg^{2+}) affected the stability of the AOT/SAIL blends, causing cloudiness and consequently a problem for practical applications. AOT/LF2 blends displayed a larger tolerance to hardness, particularly at low AOT concentrations. Paper 2 showed that AOT/[C_{12}mim]Br blend presented the highest surface activity, as reflected in the highest optimal solubilisation parameters at the studied temperatures, among the three blends considered. This is due to the formation of ion pairs, making these blends behave as nonionic surfactants [70]. The design of a formulation using these components is consequently considered of high interest. However, the instability problems would have to be solved.

Several attempts were made to achieve a ternary blend with AOT, [C_{12}mim]Br and LF2, with the highest possible proportion of AOT/[C_{12}mim]Br to obtain better surface activity performance while maintaining stability against hardness. According to phase behaviour studies, AOT/[C_{12}mim]Br with 45/55 blend ratio (from now on A-C) was considered the most adequate to be blended with LF2. Thus, a ternary formulation was defined by means of a A-C/LF2 blend scan, stability, and IFT tests.

Comparing the optimal formulations of both AOT/LF2 and A-C/LF2 blends, A-C/LF2 showed slightly better surface activity with crude oil, reaching an optimal solubilisation parameter of 4.7 at 25 °C. This value was greater than 3, the value achieved with the binary blend AOT/LF2 at the same temperature. As expected, the IFT measurements also demonstrated improvements for A-C/LF2 (1.14×10^{-2} mN/m) compared to AOT/LF2 (1.50×10^{-2} mN/m). The blends exhibited the opposite behaviour with temperature increases. At 50 °C, the optimal Winsor III microemulsion for the AOT/LF2 blend was obtained with a higher AOT proportion (behaving like an ionic surfactant formulation). In contrast, at the same temperature, the A-C/LF2 blend reached the optimal microemulsion at a lower A-C proportion (behaving like a nonionic surfactant). The

USC UNIVERSIDADE DE SANTIAGO DE COMPOSTELA

solubilisation capacity of both blends significantly decreased at higher temperatures, so the application was focused on an operational temperature of 25 °C.

It is known that high surfactant adsorption is a significant drawback in EOR projects, since it reduces the concentration of surfactants available for IFT reduction and oil mobilisation. Therefore, minimising adsorption is vital to ensure the effectiveness of a surfactant flooding process. Surfactants are typically expensive chemicals, so their adsorption leads to significant economic losses. When surfactants adsorb onto the reservoir rock, injecting larger quantities of surfactants becomes necessary to ensure an effective concentration in the reservoir. This can significantly increase the operational cost of the EOR project. In this regard, single-phase dynamic adsorption tests were conducted at room temperature using both blends. First the tests were performed using carbonate (limestone) cores and then sandstone was used. The evaluation for both blends showed relatively low surfactant adsorption on carbonate rocks. AOT/LF2 adsorption (0.42 mg/g rock) was cut in half using the A-C/LF2 blend. The reduction in the adsorption for the A-C/LF2 blend is attributed to the formation of ion pairs between AOT and [C_{12}mim]Br head groups, leading to the reduction of mainly free negative charges. Strong attraction between the head groups also contributed to the improved surface activity with the oil phase, as observed in the solubility and IFT evaluations. The tests in sandstone cores were conducted under the same flow and temperature conditions as those in carbonate cores. However, in this case, a very high adsorption was found. For both blends, after injecting 3.5 PV of the surfactant solution, the blend concentration in the effluent was approximately 50% of the injected concentration. As a result, further tests with sandstone rocks were discounted.

Core flooding tests were performed using the blends (1 wt% of 50/50 AOT/LF2 and 0.8 wt% of 46/54 A-C/LF2, both prepared in synthetic SW) to estimate their efficiencies in AOR. To optimise the required surfactant, a polymer slug was injected after surfactant flooding. The results of this evaluation showed higher AOR for the A-C/LF2 blend after water flooding, recovering 11.5% of OOIP, while for AOT/LF2, the AOR was 7.3% OOIP. One notable observation during the secondary recovery stage was the smaller volume of chemicals (blend and polymer solutions) needed to mobilise the trapped oil for the A-C/LF2 flood (0.65 PV) compared to the AOT/LF2 flood (0.85 PV). This difference in performance might be attributed to the difference in surfactant adsorption of the blends. In practice, after economic evaluations and estimations of ultimate oil recovery, EOR projects with shorter oil recovery times are desired as they lead to earlier returns of investment.

USC UNIVERSIDADE DE SANTIAGO DE COMPOSTELA

Paper 4 also aimed to design a blend formulation to improve oil recovery after water flooding via IFT reduction. The new blend was studied to determine its real potential for industrial applications in carbonate rocks, as an initial investigation prior to its consideration by the oil industry. After experimental tests, numerical simulations were used to further investigate the blend performance, identify potential causes of efficiency loss during the core flooding, and optimise the EOR process. The blend was formulated using the cationic SAIL cocosalkylpentaethoximethyl ammonium methylsulfate (C1EG) and a petrochemical sodium lineal alkyl (C_{10}-C_{13}) benzene sulfonate named RECOLAS103®, kindly provided by the Spanish oil company CEPSA. This study was built upon an evaluation of C1EG blended with the commercial surfactant sodium dodecylbenzene sulfonate (SDBS) conducted in our research group [71]. Due to the favourable outcomes of that previous work, this research aimed to test the efficacy of the proposal with a petrochemical surfactant in an approximation to a real application.

The RECOLAS103/C1EG blend was prepared in synthetic SW at 1 wt% concentration. It underwent the same sequence of tests described above to determine its phase behaviour, optimal blend ratio, performance at several temperatures, solubilisation capacity, surfactant adsorption, and oil recovery efficiency. Additionally, evaluations of two polymers were carried out to choose the one most suitable for the flow conditions.

In phase behaviour studies, RECOLAS103/C1EG exhibited a peculiar behaviour, showing two Winsor III microemulsions when varying the blend ratio. This phenomenon, also observed with the SDBS/C1EG blend, is characteristic of the ion pairs formed between the opposite head groups of the surfactants. In this case, both the cationic SAIL C1EG and the anionic surfactant RECOLAS103 are hydrophilic. As the proportion of one of the surfactants increases, the formation of paired micelles is promoted. These micelles present lesser or even near neutral charge. This leads the blend to become globally less charged, and thus less hydrophilic. Further decreases in hydrophilicity yield the formation of Winsor III and subsequently Winsor II microemulsions, at the evaluated salinity and temperature. Mixed micelles can interact with either the excess cationic or anionic surfactant [65,72]. At 25 °C, the two Winsor III microemulsions were obtained at approximately 40% and 70% RECOLAS103. The Winsor III system with 40% RECOLAS103 is richer in cationic surfactant. Even though the surface charge of the mixed micelles has been neutralised by the opposite charges, the overall charge of the microemulsion is still positive [65]. This is more favourable for positively charged rocks such as carbonates [72]. Therefore, the study was further focused on this blend ratio.

USC
UNIVERSIDADE DE SANTIAGO DE COMPOSTELA

One important feature of the blend was its ability to maintain an acceptable magnitude of the optimal solubilisation parameter when the temperature increased. Although it dropped from 14.37 at 25 °C to 5.46 at 75 °C, the latter value is still higher than those obtained with the A-C/LF2 blend at 25 °C (which was 4.7) and more than double the value at 50 °C (which was 2.5). The estimated IFT by Huh's equation at 75 °C was 1.01 $\times 10^{-2}$ mN/m. Dynamic IFT measurements at 25 °C with the crude oil confirmed the optimal blend ratio, being IFT 2.1 $\times 10^{-2}$ mN/m.

Concerning surfactant adsorption, it was estimated to be about 0.6 mg/g of rock. Although higher than those obtained with the AOT/LF2 and A-C/LF2 blends, the adsorption is relatively low and acceptable for this type of project, especially for carbonate rocks, considering the limitations of cationic and nonionic surfactants to reach low IFTs at similar conditions. Values accepted for surfactant adsorption in EOR processes range from near zero to 2.5 mg/g [21].

The potential of the RECOLAS103/C1EG blend to be used in EOR was inferred from the AOR obtained through three core flooding tests (CF-1, CF-2 and CF-3), conducted at 25 °C (CF-1 and CF-3) and 120 °C (CF-2). The injected formulation was 1 wt% of the blend (40 wt% RECOLAS103) in synthetic SW. In the case of CF-3, to approximate real applications, a polymer flooding step was carried out with PAM 920 VHM polymer solution with an apparent viscosity optimised to 6.3 mPa·s (at 10 s^{-1}), after surfactant flooding. AOR values ranging from 10.2% to 12.7% OOIP were achieved. The lowest AOR value was observed in test CF-2 at 120 °C, which could be attributed to a decrease in blend efficiency at higher temperatures. Utilising numerical simulation, the causes of the efficiency loss in reservoir were identified. After conducting several history matching simulations to adjust the numerical model to the laboratory tests, it was found that a surfactant retention of approximately 36 mg/g of rock delayed oil production in this test at high temperature. As simulations also confirmed the low adsorption found experimentally, additional surfactant retention might be caused by oil phase trapping, indicating the partitioning of surfactant towards the oil phase (Winsor type III shifted to Winsor type II microemulsion). Simulations with those conditions better matched the laboratory outcomes. Further simulations were carried out to estimate the blend's maximum AOR achievable by varying several parameters: the volume of the injected blend, injection rate, and the polymer solution's apparent viscosity (at 10 s^{-1} shear rate). The results showed that the maximum AOR for the blend flooding would be approximately 15% OOIP, which could be achieved by maintaining the same injection parameter magnitudes as in the CF-3 test while increasing the apparent viscosity of the polymer solution to 20 mPa·s. As mentioned in the first part of the general discussion, the magnitude of polymer solution viscosity can be adjusted by increasing the polymer concentration or using polymers with higher molecular weights. However, both options may lead to face plugging in low permeability reservoirs.

Chemical flooding in low permeability reservoirs can be more challenging when they contain fractures. The situation becomes even more unfavourable when these reservoirs are oil-wet, mixed-wet or intermediate-wet. Surfactant and injected water will tend to flow through fractures preventing flooding the reservoir matrix. Some cationic surfactants, SW and modified SW (known as Smart Water, SmW) have been studied to overcome this situation by promoting changes in the rock wettability towards a more water-wet condition. The cationic divalent ions present in SW and SmW, as well as the cationic head groups of specific surfactants, induce the desorption of negatively charged carboxylic acid oil groups, which were adhered to the rock surface in oil-wet rocks. This process spontaneously induces the imbibition of the aqueous phase into the now more water-wet reservoir matrix, expelling the trapped oil towards production wells.

In this context, the last part of the thesis, developed in **Paper 5**, evaluates the efficacy of three cationic SAIL formulations in improving the wettability alteration properties of a SmW in mixed-wet low permeability carbonate (Chalk) cores at 90 °C. This temperature was selected since SW and SmW are efficient enough in changing wetting states of rocks at high temperatures (120-130 °C), while the efficiency decreases when temperature decreases.

To select the SAILs, solutions of eleven hydrophilic SAILs (see table 4.1) were prepared at 1 wt% SAIL in formation brine VB0S, SW and SmW (SW0Na brine). The thermal stability of these formulations was evaluated at high temperature (up to 130 °C) in sealed pipettes to ensure that no precipitation appeared. The phase behaviour of the same formulations with crude oil was also studied. The purpose of this evaluation was to guarantee that the SAIL formulations would remain Winsor type I microemulsions as the temperature increased, preventing the shift to Winsor II and the potential oil-phase trapping. Additionally, the test was used to visually identify formulations with high surface activity and consequently high oil solubilisation in the aqueous phase (evidenced by the darkness of this phase). This was a quick method to select SAIL formulations leading to low IFT. Therefore, formulations with darkest aqueous phases were chosen for IFT measurements with crude oil.

The SAILs were also selected to facilitate analysis of the influence of the head groups and alkyl chain lengths on oil recovery with SmW. Thus, 1 wt% of $[C_{16}Py]Cl$, $[C_{12}Py]Cl$ and $[C_{12}mim]Br$ in SW0Na were selected as formulations for further studies. This allowed the evaluation of imidazolium versus pyridinium ring, and hexadecyl (C_{16}) versus dodecyl (C_{12}) alkyl chain.

Spontaneous imbibition tests were conducted mainly at 90 °C to assess the capacity of the SAIL formulations in modifying chalk rock wettability. Additionally, core flooding tests were performed to validate the results and study the differential pressure profile during the flooding process. In

USC DE SANTIAGO DE COMPOSTELA

general, the [C_{12}Py]Cl and [C_{12}mim]Br formulations were demonstrated to be the most effective options for changing the wetting state from intermediate to a more water-wet condition at 90 °C. Longer alkyl chain lengths led to worse results. Both formulations enhanced the performance of SW0Na brine as a wettability modifier at the evaluated temperature. However, the [C_{12}mim]Br formulation exhibited a slightly better performance in terms of imbibition rate and recovery. Thus, two core flooding tests were conducted at 90 °C using the [C_{12}mim]Br formulation in secondary and tertiary modes. In the first case, a total oil recovery of 79.3% of OOIP was achieved, and in the second case the AOR was 4.4% after SW0Na flooding (66.2% OOIP), for a total oil recovery of 70.6% OOIP. Moreover, the differential pressure profiles in both core flooding tests revealed that the low IFT led to the formation of oil banks ahead of the surfactant formulation.

Table 4.1. SAILs evaluated in thermal stability and phase behaviour tests.

SAIL Name	Abbreviation
1-dodecyl-3-methylimidazolium bromide	[C_{12}mim]Br
1-decyl-3-methylimidazolium chloride	[C_{10}mim]Cl
1-octyl-3-methylimidazolium chloride	[C_8mim]Cl
1-hexyl-3-methylimidazolium chloride	[C_6mim]Cl
1-hexadecylpyridinium chloride	[C_{16}Py]Cl
1-dodecylpyridinium chloride	[C_{12}Py]Cl
1-octylpyridinium chloride	[C_8Py]Cl
Tributyl tetradecyl phosphonium chloride	[$P_{444\ 14}$]Cl
221PG	Iolilyte 221PG
Cocosalkylpentaethoximethyl ammonium methylsulfate	Iolilyte C1EG
Tallow polyoxyethylene ethyl ammonium ethosulfate	Iolilyte T2EG

USC UNIVERSIDADE DE SANTIAGO DE COMPOSTELA

USC
UNIVERSIDADE
DE SANTIAGO
DE COMPOSTELA

5. CONCLUSIONS

USC
UNIVERSIDADE
DE SANTIAGO
DE COMPOSTELA

USC
UNIVERSIDADE
DE SANTIAGO
DE COMPOSTELA

The potential of novel techniques and formulations to improve the performance of certain chemical EOR methods was evaluated. Promising results were obtained through the proposed technologies by means of laboratory and simulation tests, demonstrating advancements in both volumetric sweep (macroscopic) and displacement (microscopic) efficiencies. The following summarises the general conclusions that can be derived from all the work carried out and presented in the manuscripts comprising this thesis.

Numerical simulations have shown the possibility of controlling viscous fingering instability during a hydrodynamically unfavourable displacement process, by means of chemical reactions and modifying injection protocols. However, achieving successful displacement requires controlling several parameters such as: the ratio between the reaction and convective mass transport rates, the ratio of convection and diffusion rates, the maximum viscosity of the product at the interface, and the viscosity gradient between the product and displacing fluid. It can be concluded that finding such a reaction, and adjusting the required variables, is a difficult task that greatly limits the method's possibilities.

Focusing on surfactant EOR, blends are usually required to meet all the requirements of a specific reservoir. Activity maps for surfactant blends are very useful tools for understanding their phase behaviour. Given the more complex nature of blends, these maps help illustrate the microemulsion types under varying conditions of salinity, temperature, and blend ratio. This is crucial for short water flooding processes or highly heterogeneous reservoirs, where the injected water may not fully replace the formation brine, leading to salinity gradients. Additionally, activity maps take on greater importance for blends where one component is more prone to being adsorbed onto the rock surface, altering the effective blend ratio.

The literature presents SAILs as promising chemicals for EOR. The evaluated cationic SAILs [C_{10}mim]Cl and [C_{12}mim]Br, by themselves, do not possess the capacity to reduce the interfacial tension between the aqueous and oil phase to ultra-low values. However, SAILs can form mixed micelles in blends with anionic surfactants, thus increasing the formulation surface activity and the oil recovery achieved with single surfactants. The vast range of options for synthesising SAILs opens the possibility of creating successful blends with oppositely charged surfactants. That makes those kinds of blends more promising than traditional cationic and non-ionic surfactants for use in reservoirs with positively charged surface rocks.

Experimental and simulation work carried out with the RECOLAS103/C1EG blend showed its potential for use in surfactant flooding at high temperatures. The hydrophilicity of the blend needs

USC UNIVERSIDADE DE SANTIAGO DE COMPOSTELA

to be adjusted, by varying the blend ratio, to achieve the optimal surfactant for specific reservoir temperatures.

Adding specific SAILs to smart water improved its ability to change wettability in intermediate wet carbonate cores at low temperatures, making cores more water-wet. The higher imbibition rate and final recovery suggest improved oil desorption from the rock surface. However, further evaluation is necessary to assess the selected cationic SAIL adsorption on the cationic rock surface. This is crucial due to the higher cost of SAILs compared to the salts presented in smart water, thus economic evaluations are needed to confirm the project's profitability. The combination of SAILs and smart water seems to be promising for EOR. Future works should be focused on the influence of SAIL head groups and alkyl chains on oil recovery, considering the type of smart water and rock, and salinity and temperature conditions of the reservoir.

As a global conclusion, it can be said that there is still room for the improvement of EOR methods. The combination of SAILs with traditional surfactants or smart water are the most promising techniques. The economy of the process would be the key factor for the application and must be the goal of future studies.

USC
UNIVERSIDADE DE SANTIAGO DE COMPOSTELA

LIST OF SYMBOLS

USC
UNIVERSIDADE
DE SANTIAGO
DE COMPOSTELA

USC
UNIVERSIDADE
DE SANTIAGO
DE COMPOSTELA

Symbols

A_c	Cross-sectional area of the rock across flow direction
AOR	Additional Oil Recovery
A_{swept}	Swept horizontal area
A_{Total}	Total horizontal area
CDC	Capillary Desaturation Curve
CMC	Critical Micelle Concentration
COBR	Crude oil-brine-rock system
dP/dL	Pressure drop in the flow direction
E	Total efficiency
E_A	Areal sweep efficiency
E_D	Displacement efficiency (microscopic efficiency)
EOR	Enhanced Oil Recovery
E_V	Vertical sweep efficiency
E_{Vol}	Volumetric sweep efficiency (macroscopic efficiency)
HLB	Hydrophilic-Lipophilic Balance
HPAM	Partially hydrolysed polyacrylamide
IFT	Interfacial tension
IL	Ionic Liquid
K	Permeability of the porous rock,
k_a	Absolute permeability
k_i	Effective permeability of fluid i
k_{ri}	Relative permeability of fluid i
L	Length of approximated cylindrical shape of oil spinning drop
M	Mobility Ratio
M_w	Molecular weight
M_{wD}	Molecular weight distribution
N_C	Capillary number
Nc_c	Critical capillary number
Nc_{max}	Maximum capillary number
O	Oil
O/W	oil-in-water
OOIP	Original Oil In Place
PAM	Polyacrylamide
P_c	Capillary pressure

USC UNIVERSIDADE DE SANTIAGO DE COMPOSTELA

P_{nw}	Pressure of the non-wetting fluid
PV	Pore volume
P_w	Pressure of the wetting fluid
q	Flow rate
R	Radical substituent or alkyl associated group
R	Radius of approximated cylindrical shape of oil spinning drop
r_c	Pore or capillary radius
S	surfactant
SAIL	Surface-Active Ionic Liquids
S_i	Saturation of fluid i
S_{ii}	Initial saturation of fluid i
S_{ir}	Residual saturation of fluid i
SmW	Smart Water
SW	Seawater
VA_{swept}	Swept vertical area
VA_{total}	Total vertical area
V_b	Bulk volume
V_f	Volume of fluid
V_{grain}	Grain volume
V_i	Volume of fluid i
V_p	Pore volume
W	Water
W/O	water-in-oil
WI	Winsor type I microemulsion
WII	Winsor type II microemulsion
WIII	Winsor type III microemulsion

Greek letters

Δ	Property variation
θ	Contact angle
λ_i	Mobility of fluid i
ρ	Density
σ	Interfacial tension
ϕ	Porosity
μ	Viscosity of the flowing fluid

USC UNIVERSIDADE DE SANTIAGO DE COMPOSTELA

v	Apparent fluid flowing velocity
ω	Angular velocity

Subscript

i	Fluids oil (o), water (w) or gas (g)
X, Y	Polymerisation degree of monomer

USC
UNIVERSIDADE DE SANTIAGO DE COMPOSTELA

USC
UNIVERSIDADE
DE SANTIAGO
DE COMPOSTELA

REFERENCES

USC
UNIVERSIDADE
DE SANTIAGO
DE COMPOSTELA

USC
UNIVERSIDADE
DE SANTIAGO
DE COMPOSTELA

[1] International Energy Agency (IEA) (2022). World Energy Outlook 2022. Available from: Https://Iea.Blob.Core.Windows.Net/Assets/830fe099-5530-48f2-A7c1-11f35d510983/WorldEnergyOutlook2022.Pdf. (Last accessed: July-2023).

[2] Sheng, J. (2011). Modern chemical enhanced oil recovery: Theory and practice. 2nd Ed., Elsevier Inc., Amsterdam.

[3] Muggeridge, A., Cockin, A., Webb, K., Frampton, H., Collins, I., Moulds, T., and Salino, P. (2014). Recovery rates, enhanced oil recovery and technological limits. *Philos. T. R. Soc. A*. 372, 1–25.

[4] Craft, B.C. and Hawkins, M.F. (1991). Applied Petroleum Reservoir Engineering. 2nd Ed., Prentice Hall Inc., New Jersey.

[5] Chilingar, G.V., Buryakovsky, L.A., Eremenko, N.A., and Gorfunkel, M.V. (2005). Geology and Geochemistry of Oil and Gas. Elsevier B.V, Amsterdam.

[6] Roehl, P.O. and Choquette, P.W. (1985). Carbonate Petroleum Reservoirs. Springer Science & Business Media, New York.

[7] Tiab, D. and Donaldson, E. (2004). Petrophysics: theory and practice of measuring reservoir rock and fluid transport properties. 2nd Ed., Gulf Professional Publishing, Burlington, Massachusetts.

[8] Ertekin, T., Abou-Kassem, J.H., and King, G.R. (2001). Basic Applied Reservoir Simulation. Society of Petroleum Engineers Inc., Richardson, Texas.

[9] Ahmed, T. (2019). Reservoir Engineering Handbook. 5th Ed., Gulf Professional Publishing, Cambridge, Massachusetts.

[10] Green, D. and Willhite, G.P. (2018). Enhanced oil recovery. 2nd Ed., Society of Petroleum Engineers Inc., Richardson, Texas.

[11] Vishnyakov, V., Suleimanov, B., Salmanov, A., and Zeynalov, E. (2020). Primer on Enhanced Oil Recovery. Gulf Professional Publishing, Cambridge, Massachusetts.

[12] Puntervold, T. and Austad, T. (2007). Injection of seawater and mixtures with produced water into North Sea chalk formation: Impact on wettability, scale formation, and rock mechanics caused by fluid-rock interaction. *Soc. Petrol. Eng. J.* SPE 111237 ,1-12.

[13] Massarweh, O. and Abushaikha, A.S. (2020). The use of surfactants in enhanced oil recovery: A review of recent advances. *Energy Reports*. 6, 3150–3178.

[14] Thomas, A., Gaillard, N., and Favero, C. (2012). Some key features to consider when studying acrylamide-based polymers for chemical enhanced oil recovery. *Oil Gas Sci. Technol.* 67 (6), 887–902.

[15] Craig, F.F. (1975). The Reservoir Engineering Aspects of Waterflooding. Society of Petroleum Engineers Inc., Dallas.

USC UNIVERSIDADE DE SANTIAGO DE COMPOSTELA

[16] Saffman, P.G. and Taylor, G.I. (1958). The penetration of a fluid into a porous medium or Hele-Shaw cell containing a more viscous liquid. *Proc. R. Soc. London A*. 245, 312–329.

[17] Moore, T.F. and Slobod, R.L. (1955). Displacement of oil by water-effect of wettability, rate, and viscosity on recovery. *Soc. Petrol. Eng. J.* 502-G, 1–16.

[18] Ghadami, N., Arsanti, D., and Faizal Sedaralit, M. (2015). Uncertainty assessment of chemical EOR in one of the offshore fields in Malaysia. *Soc. Petrol. Eng. J.* SPE-174614 ,1-15.

[19] Spildo, K., Johannessen, A., and Skauge, A. (2012). Low salinity waterflood at reduced capillarity. *Soc. Petrol. Eng. J.* SPE-154236 ,1-13.

[20] Kamal, M.S., Hussein, I.A., and Sultan, A.S. (2017). Review on surfactant flooding: phase behavior, retention, IFT, and field applications. *Energ Fuel*. 31 (8), 7701–7720.

[21] Schramm, L.L. (2000). Surfactants: Fundamentals and Applications in the Petroleum Industry. Cambridge University Press, Cambridge.

[22] Strand, S., Standnes, D.C., and Austad, T. (2003). Spontaneous imbibition of aqueous surfactant solutions into neutral to oil-wet carbonate cores: Effects of brine salinity and composition. *Energ Fuel*. 17 (5), 1133–1144.

[23] Austad, T., Milter, J., and Rogaland, R.F. (1997). Spontaneous Imbibition of Water Into Low Permeable Chalk at Different Wettabilities Using Surfactants. *Soc. Petrol. Eng. J.* SPE-37236, 257–266.

[24] Standnes, D.C. and Austad, T. (2000). Wettability alteration in chalk 2. Mechanism for wettability alteration from oil-wet to water-wet using surfactants. *J. Petrol. Sci. Eng.* 28, 123–143.

[25] Sheng, J. (2013). Enhanced oil recovery field case studies. 2nd Ed., Elsevier Inc., Amsterdam.

[26] Holmberg, K., Jönsson, B., Kronberg, B., and Lindman, B. (2002). Surfactants and polymers in aqueous solution. 2nd Ed., John Wiley & Sons Ltd., Chichester.

[27] Teraoka, I. (2002). Polymer Solutions: An Introduction to Physical Properties. John Wiley & Sons Ltd., New York.

[28] Gbadamosi, A.O., Junin, R., Manan, M.A., Agi, A., and Yusuff, A.S. (2019). An overview of chemical enhanced oil recovery: recent advances and prospects. *Int. Nano Letters*. 9, 171–202.

[29] Negin, C., Ali, S., and Xie, Q. (2017). Most common surfactants employed in chemical enhanced oil recovery. *Petroleum*. 3 (2), 197–211.

[30] Brennecke, J.F. and Maginn, E.J. (2001). Ionic liquids: Innovative fluids for chemical processing. *AICHE J*. 47 (11), 2384–2389.

[31] Eftekhari, A. (2018). Polymerized Ionic Liquids. The Royal Society of Chemistry,

Cambridge.

[32] Cao, H., Hu, Y., Xu, W., Wang, Y., and Guo, X. (2020). Recent progress in the assembly behavior of imidazolium-based ionic liquid surfactants. *J. Mol. Liq.* 319, 114354.

[33] Seddon, K.R., Stark, A., and Torres, M.J. (2000). Influence of chloride, water, and organic solvents on the physical properties of ionic liquids. *Pure Appl. Chem.* 72 (12), 2275–2287.

[34] Han, X., Lu, M., Fan, Y., Li, Y., and Holmberg, K. (2021). Recent Developments on Surfactants for Enhanced Oil Recovery. *Tenside Surfact. Det.* 58 (3), 164–176.

[35] Sheng, J.J. (2015). Status of surfactant EOR technology. *Petroleum*. 1 (2), 97–105.

[36] Church, J., Willner, M.R., Renfro, B.R., Chen, Y., Diaz, D., Lee, W.H., Dutcher, C.S., Lundin, J.G., and Paynter, D.M. (2021). Impact of Interfacial Tension and Critical Micelle Concentration on Bilgewater Oil Separation. *J. Water Proc. Eng.* 39, 101684.

[37] Salager, J.L., Forgiarini, A.M., Márquez, L., Manchego, L., and Bullón, J. (2013). How to attain an ultralow interfacial tension and a three-phase behavior with a surfactant formulation for enhanced oil recovery: A Review. Part 2. performance improvement trends from Winsor's premise to currently proposed inter- and intra-molecular mixtu. *J. Surfactants Deterg.* 16 (5), 631–663.

[38] Winsor, P.A. (1948). Hydrotropy, solubilisation and related emulsification processes. Part I. *T. Faraday Soc.* 44, 376–398.

[39] Healy, R.N. and Reed, R.L.. (1976). Multiphase Microemulsion Systems. *Soc. Petrol. Eng. J.* SPE-5565, 147–160.

[40] Benzagouta, M.S., AlNashef, I.M., Karnanda, W., and Al-Khidir, K. (2013). Ionic liquids as novel surfactants for potential use in enhanced oil recovery. *Korean J. Chem. Eng.* 30 (11), 2108–2117.

[41] Spildo, K., Sun, L., Djurhuus, K., and Skauge, A. (2014). A strategy for low cost, effective surfactant injection. *J. Petrol. Sci. Eng.* 117, 8–14.

[42] Vonnegut, B. (1942). Rotating bubble method for the determination of surface and interfacial tensions. *Rev. Sci. Instrum.* 13 (6), 6–9.

[43] Rapp, B. (2016). Microfluidics: Modeling, Mechanics and Mathematics. Elsevier, Amsterdam.

[44] Viades-Trejo, J. and Gracia-Fadrique, J. (2007). Spinning drop method. From Young-Laplace to Vonnegut. *Colloid Surfaces A*. 302 (1–3), 549–552.

[45] Schlumberger (2003). Energy Glossary. Coreflooding. Https://Glossary.Slb.Com/En/Terms/c/Coreflooding. (Last accessed: March-2023).

[46] National Geosequestration Laboratory (2023). Core-flooding and imaging. Http://Ngl.Org.Au/Facility/Core-Flooding/. (Last accessed: May-2023).

USC UNIVERSIDADE DE SANTIAGO DE COMPOSTELA

[47] Morrow, N.R. and Mason, G. (2001). Recovery of oil by spontaneous imbibition. *Curr. Opin. Colloid In.* 6 (4), 321–337.

[48] Aziz, K. and Settari, A. (1979). Petroleum Reservoir Simulation. Applied Science Publishers Ltd., London.

[49] Abou-Kassem, J.H., Farouq Ali, S.M., and Rafiq Islam, M. (2006). Petroleum Reservoir Simulation: A Basic Approach. Gulf Publishing Company, Houston, Texas.

[50] Kumar, A. and Mandal, A. (2020). Core-scale modelling and numerical simulation of zwitterionic surfactant flooding: Designing of chemical slug for enhanced oil recovery. *J. Petrol. Sci. Eng.* 192, 107333.

[51] Rai, S.K., Bera, A., and Mandal, A. (2015). Modeling of surfactant and surfactant–polymer flooding for enhanced oil recovery using STARS (CMG) software. *J. Petrol. Explor. Prod. Technol.* 5 (1), 1–11.

[52] Goudarzi, A., Delshad, M., and Sepehrnoori, K. (2013). A critical assessment of several reservoir simulators for modeling chemical enhanced oil recovery processes. *Soc. Petrol. Eng. J.* SPE-163578 ,1-16.

[53] CMG (2016). STARS user guide-Advanced Processes & Thermal Reservoir Simulator. Version 20 Computer Modelling Group Ltd., Calgary, Canada.

[54] Al-Muraryi, M.T., Ghedan, S.G., Skoreyko, F., Hassan, A.A., Lara, R., and Qubian, A. (2019). Compositional modeling and calibration of ASP carbonate corefloods. *Soc. Petrol. Eng. J.* SPE-195039 ,1-19.

[55] Hakiki, F., Maharsi, D.A., and Marhaendrajana, T. (2015). Surfactant-polymer coreflood simulation and uncertainty analysis derived from laboratory study. *J. Eng. Technol. Sci.* 47 (6), 706–725.

[56] Tang, Y., Su, Z., He, J., and Yang, F. (2016). Numerical Simulation and Optimization of Enhanced Oil Recovery by the In Situ Generated CO2 Huff-n-Puff Process with Compound Surfactant. *J. Chem.-NY*. 6731848, 1–13.

[57] Ghosh, P., Sharma, H., and Mohanty, K.K. (2017). Chemical flooding in low permeability carbonate rocks. *Soc. Petrol. Eng. J.* SPE-187274 ,1-22.

[58] Escala, D.M. and Muñuzuri, A.P. (2021). A bottom-up approach to construct or deconstruct a fluid instability. *Sci. Rep.-UK*. 11 (24368), 1–16.

[59] Salager, J.L., Forgiarini, A.M., and Bullón, J. (2013). How to attain ultralow interfacial tension and three-phase behavior with surfactant formulation for enhanced oil recovery: A review. Part 1. Optimum formulation for simple surfactant-oil-water ternary systems. *J. Surfactants Deterg.* 16 (4), 449–472.

[60] Bharadwaj, S. and Ahluwalia, J.C. (1996). Mixed-surfactant system of dodecylbenzene

USC UNIVERSIDADE DE SANTIAGO DE

sulfonate and alpha-olefin sulfonate: Micellar and volumetric studies. *J. Am. Oil Chem. Soc.* 73 (1), 39–45.

[61] Park, I.J. and Lee, B.H. (2012). Mixed micellization of sodium dodecylbenzene sulfonate with polyoxyethylene lauryl ether surfactants (POLE4 and POLE23) in n-butanol aqueous solution. *J. Surfactants Deterg.* 15 (1), 41–46.

[62] Ferreira, S.L.C., Dos Santos, W.N.L., Quintella, C.M., Neto, B.B., and Bosque-Sendra, J.M. (2004). Doehlert matrix: A chemometric tool for analytical chemistry - Review. *Talanta*. 63 (4), 1061–1067.

[63] Borges, F.J., Roux-de Balmann, H., and Guardani, R. (2008). Investigation of the mass transfer processes during the desalination of water containing phenol and sodium chloride by electrodialysis. *J. Membrane Sci.* 325 (1), 130–138.

[64] Huh, C. (1979). Interfacial tensions and solubilizing ability of a microemulsion phase that coexists with oil and brine. *J. Colloid Interf. Sci.* 71 (2), 408–426.

[65] Antón, R.E., Gómez, D., Graciaa, A., Lachaise, J., and Salager, J.L. (1993). Surfactant-Oil-Water Systems Near the Affinity Inversion Part IX: Optimum Formulation and Phase Behavior of Mixed Anionic-Cationic Systems. *J. Disper. Sci. Technol.* 14 (4), 401–416.

[66] Li, Y., Zhang, W., Bailing, K., Puerto, M., Bao, X., Ou, S., Zhiqin, S., Yiqing, Y., Yanhua, L., Songyuan, G., Miller, C., and Hirasaki, G.J. (2016). Mixtures of anionic/cationic surfactants: A new approach for enhanced oil recovery in low-salinity, high-temperature sandstone reservoir. *Soc. Petrol. Eng. J.* SPE-169051 ,1-14.

[67] Bjorkum, P.A. and Nadeau, P.H. (1998). Temperature Controlled Porosity/Permeability Reduction, Fluid Migration, and Petroleum Exploration in Sedimentary Basins. *APPEA J.* 38 (1), 453.

[68] Antón, R.E., Graciaa, A., Lachaise, J., and Salager, J.L. (1992). Surfactant-Oil-Water Systems Near the Affinity Inversion, Part VIII : Optimum Formulation and Phase Behavior of Mixed Anionic-Nonionic Systems Versus Temperature. *J. Disper. Sci. Technol.* 13 (5), 565–579.

[69] Sassen, C.L., Gonzalez Casielles, A., de Loos, T.W., and de Swaan Arons, J. (1992). The influence of pressure and temperature on the phase behaviour of the system H2O+C12+C7E5 and relevant binary subsystems. *Fluid Phase Equilibr.* 72, 173–187.

[70] Graciaa, A., Ben Ghoulam, M., Marion, G., and Lachaise, J. (1989). Critical concentrations and compositions of mixed micelles of sodium dodecylbenzenesulfonate, tetradecyltrimethylammonium bromide, and polyoxyethylene octylphenols. *J. Phys. Chem.-US*. 93 (10), 4167–4173.

[71] Somoza, A., Tafur, N., Arce, A., and Soto, A. (2022). Design and performance analysis of a formulation based on SDBS and ionic liquid for EOR in carbonate reservoirs. *J. Petrol. Sci.*

USC UNIVERSIDADE DE SANTIAGO DE COMPOSTELA

Eng. 209, 109856.

[72] Li, Y., Puerto, M., Bao, X., Zhang, W., Jin, J., Su, Z., Shen, S., Hirasaki, G., and Miller, C. (2017). Synergism and performance for systems containing binary mixtures of anionic/cationic surfactants for enhanced oil recovery. *J. Surfactants Deterg.* 20 (1), 21–34.

USC
UNIVERSIDADE DE SANTIAGO DE COMPOSTELA

Appendix A:

Journal articles in which this thesis is based

USC
UNIVERSIDADE
DE SANTIAGO
DE COMPOSTELA

USC
UNIVERSIDADE
DE SANTIAGO
DE COMPOSTELA

[1] Highly viscous fluid displaced by a chemically controlled reactive interface

Néstor Tafur[1], Darío M. Escala[1], Ana Soto[2], and Alberto P. Muñuzuri[1]

[1]Institute CRETUS, Group of Nonlinear Physics, Department of Physics, Universidade de Santiago de Compostela, 15782 Santiago de Compostela, Spain

[2]Institute CRETUS, Group EQUIFASE, Department of Chemical Engineering, Universidade de Santiago de Compostela, 15782 Santiago de Compostela, Spain

Journal: Chaos (2021), AIP Publishing (ISSN: 1054-1500),31, 023135.

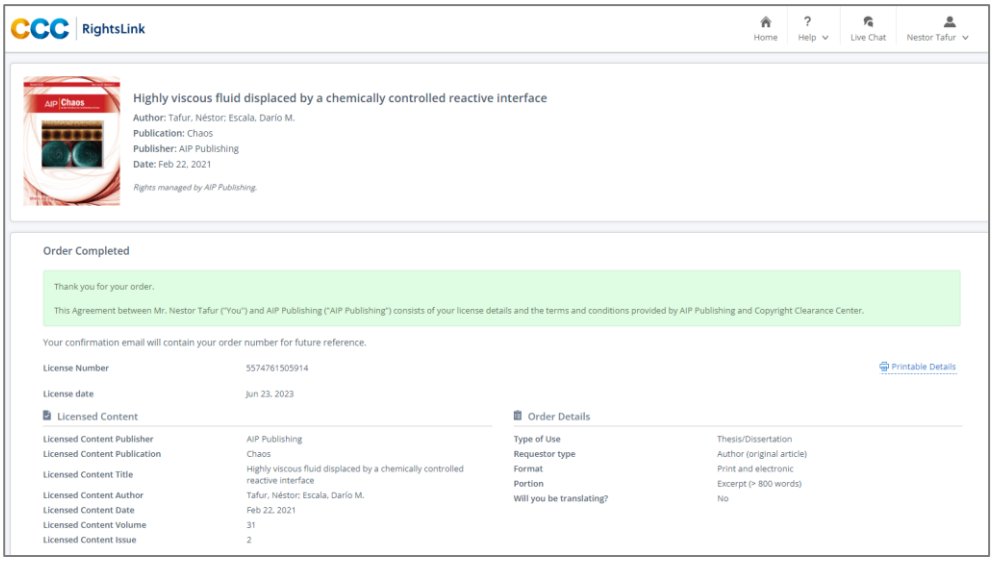
DOI: https://doi.org/10.1063/5.0031058.

Impact factor = 3.741 (2021), ranking it 7/56 in Physics, Mathematical (Q1).

Author contribution (CRediT taxonomy): simulation, formal analysis, writing.

Chapters reproducing the article content: Chapter 3.

This journal has provided permissions for the use of this full article on the present thesis, both in print an electronic format.



[2] Evaluation of surfactant blends for enhanced oil recovery through activity maps

Nestor Tafur, Alba Somoza, Ana Soto

CRETUS. Department of Chemical Engineering, Universidade de Santiago de Compostela, E-15782, Santiago de Compostela, Spain.

Journal: Journal of Molecular Liquids (2022), ed. Elsevier (ISSN: 0167-7322), 364, 119984

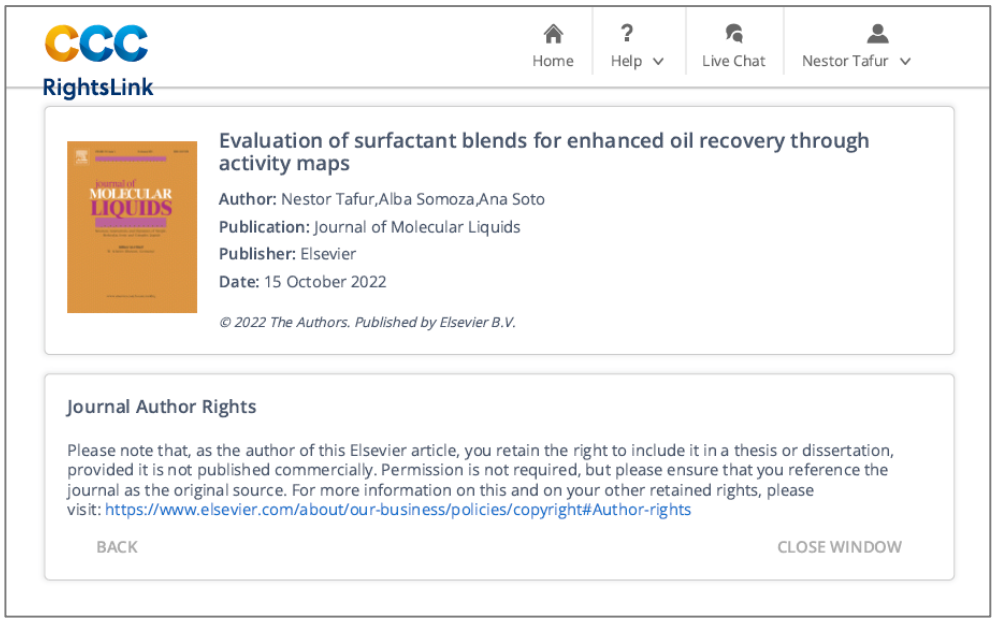
DOI: https://doi.org/10.1016/j.molliq.2022.119984

Impact factor = 6.633 (2021), ranking it 6/36 in physics, atomic, molecular & chemical (Q1).

Author contribution (CRediT taxonomy): experimental, analysis, first-draft writing.

Chapters reproducing the article content: Chapter 3

This journal allows for the use of this full article on the present thesis, both in print an electronic format without requesting further permissions, provided it is not published commercially and that it is properly referenced.



[3] Improvement of a Surfactant Blend for Enhanced Oil Recovery in Carbonate Reservoirs by Means of an Ionic Liquid

Nestor Tafur [1], Alberto P. Muñuzuri [2] and Ana Soto [1]

[1]CRETUS, Department of Chemical Engineering, Universidade de Santiago de Compostela, 15782 Santiago de Compostela, Spain

[2]Group of Nonlinear Physics, Galician Center for Mathematical Research and Technology (CITMAga), 15782 Santiago de Compostela, Spain

Journal: International Journal of Molecular Sciences (2023), MDPI. (ISSN: 1422-0067), 24, 726.

DOI: https://doi.org/10.3390/ijms24010726

Impact factor = 6.208 (2021), ranking it 50/179 in Chemistry, Multidisciplinary (Q2).

Author contribution (CRediT taxonomy): formal analysis, investigation, writing original draft.

Chapters reproducing the article content: Chapter 3

This journal allows for the use of this full article on the present thesis, both in print an electronic format without requesting further permissions, provided it is not published commercially and that it is properly referenced.



MDPI Open Access Information and Policy

All articles published by MDPI are made immediately available worldwide under an open access license. This means:

- everyone has free and unlimited access to the full-text of *all* articles published in MDPI journals;
- everyone is free to re-use the published material if proper accreditation/citation of the original publication is given;
- open access publication is supported by the authors' institutes or research funding agencies by payment of a comparatively low Article Processing Charge (APC) for accepted articles.

Permissions

No special permission is required to reuse all or part of article published by MDPI, including figures and tables. For articles published under an open access Creative Common CC BY license, any part of the article may be reused without permission provided that the original article is clearly cited. Reuse of an article does not imply endorsement by the authors or MDPI.

USC UNIVERSIDADE DE SANTIAGO DE COMPOSTELA

[4] Assessment of a surface-active ionic liquid formulation for EOR applications: Experimental and simulation studies

Nestor Tafur[a], Alba Somoza[a], Alberto P. Muñuzuri[b], Borja Rodríguez-Cabo[c], Izaskun Barrio[c], Asier Panadero[d], M. Flor García-Mayoral[d], Ana Soto[a]

[a]CRETUS, Department of Chemical Engineering, Universidade de Santiago de Compostela, E-15782, Santiago de Compostela, Spain

[b]Group of Nonlinear Physics, Dept. of Physics, Universidade de Santiago de Compostela, E-15782, Santiago de Compostela, Spain

[c] CEPSA-Química, Research Center, E-28805, Madrid, Spain

[d]CEPSA, Research Center, E-28805, Madrid, Spain

Journal: Geoenergy Science and Engineering (Former Journal of Petroleum Science and Engineering) (2023), ed. Elsevier. (ISSN: 2949-8929), 224, 211619.

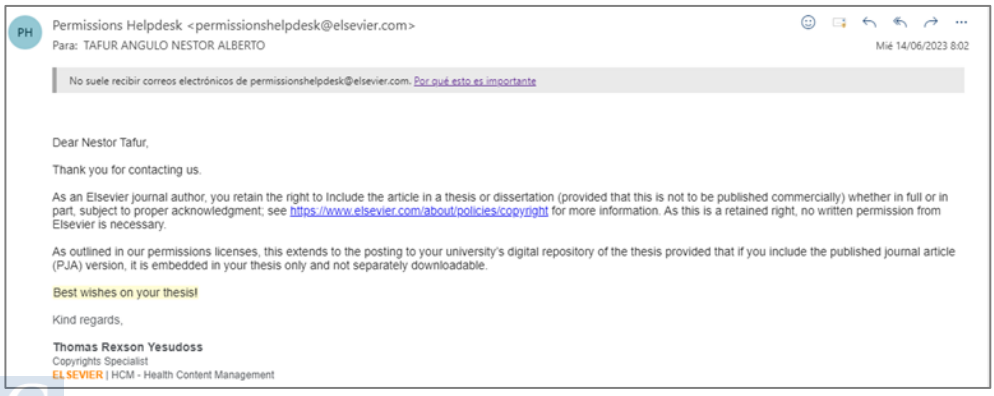
DOI: https://doi.org/10.1016/j.geoen.2023.211619

Impact factor = 5.168 (2021), ranking it 2/19 in Engineering, Petroleum (Q1). The metric data comes from the journal formerly known as the Journal of Petroleum Science and Engineering.

Author contribution (CRediT taxonomy): experimental, simulation, formal analysis, writing.

Chapters reproducing the article content: Chapter 3

This journal allows for the use of this full article on the present thesis, both in print an electronic format without requesting further permissions, provided it is not published commercially and that it is properly referenced.



Permissions Helpdesk <permissionshelpdesk@elsevier.com>
Para: TAFUR ANGULO NESTOR ALBERTO
Mié 14/06/2023 8:02

No suele recibir correos electrónicos de permissionshelpdesk@elsevier.com. Por qué esto es importante

Dear Nestor Tafur,

Thank you for contacting us.

As an Elsevier journal author, you retain the right to include the article in a thesis or dissertation (provided that this is not to be published commercially) whether in full or in part, subject to proper acknowledgment; see https://www.elsevier.com/about/policies/copyright for more information. As this is a retained right, no written permission from Elsevier is necessary.

As outlined in our permissions licenses, this extends to the posting to your university's digital repository of the thesis provided that if you include the published journal article (PJA) version, it is embedded in your thesis only and not separately downloadable.

Best wishes on your thesis!

Kind regards,

Thomas Rexson Yesudoss
Copyrights Specialist
ELSEVIER | HCM - Health Content Management

USC UNIVERSIDADE DE SANTIAGO DE COMPOSTELA

[5] Evaluation of Surface-Active Ionic Liquids in Smart Water for Enhanced Oil Recovery in Carbonate Rocks

Nestor Tafur[1], Aleksandr Mamonov[2], Md Ashraful Islam Khan[2], Ana Soto[1], Tina Puntervold[2] and Skule Strand[2]

[1]CRETUS. Department of Chemical Engineering, Universidade de Santiago de Compostela, E-15782, Santiago de Compostela, Spain.

[2]University of Stavanger, 4036 Stavanger, Norway

Journal: Energy & Fuels (2023), ACS Publications. (ISSN: 0887-0624), 37, 11730.

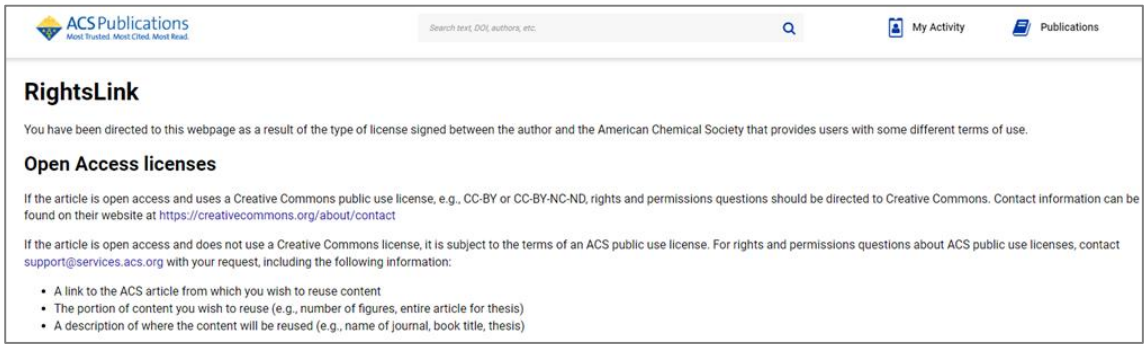
DOI: https://doi.org/10.1021/acs.energyfuels.3c01488

Impact factor = 4.654 (2021), ranking it 45/143 in Engineering, Chemical (Q2).

Author contribution (CRediT taxonomy): formal analysis, experimental, writing.

Chapters reproducing the article content: Chapter 3

This journal allows for the use of this full article on the present thesis, both in print an electronic format without requesting further permissions, provided it is not published commercially and that it is properly referenced.



USC UNIVERSIDADE DE SANTIAGO DE COMPOSTELA

USC
UNIVERSIDADE
DE SANTIAGO
DE COMPOSTELA

Appendix B:

“Resumo” (Summary, in Galician)

USC
UNIVERSIDADE
DE SANTIAGO
DE COMPOSTELA

USC
UNIVERSIDADE
DE SANTIAGO
DE COMPOSTELA

A extracción de petróleo dos xacementos é unha técnica complexa que necesitou moito tempo para ser estudada e comprendida como hoxe en día. Co paso de décadas de consumo enerxético, sendo o petróleo a principal fonte sen que outras se tivesen estudado e desenvolvido da mesma forma, as reservas de hidrocarburos obtidas de forma convencional reducíronse e os métodos secundarios (inxección de auga e gas inmiscible) comezaron a ser ineficientes. Gran parte das reservas de petróleo quédanse no subsolo sen poder ser extraídas. Isto fai necesario o desenvolvemento de novos campos petrolíferos (moitos deles costa fóra), a fractura de rocas nai, e a implementación de métodos de recuperación mellorada (EOR das súas siglas en inglés). Estes últimos implican a inxección dalgún tipo de axente no xacemento como: vapor, polímeros, surfactantes, gases miscibles... entre os máis habituais. Con estes métodos estase lonxe de extraer todo o petróleo, mais pódese estender a vida produtiva destes campos maduros. Nun momento de transición ecolóxica, ten máis sentido continuar extraendo porcións adicionais de petróleo con estas tecnoloxías dos xacementos xa explotados, que facer novas inversións en combustibles fósiles. Con iso, contribúese á seguridade da existencia de recursos mentres o mundo se encamiña á necesaria, mais lenta, obtención de fontes de materia e enerxía renovables.

O principal obxectivo desta tese e a mellora dalgunhas técnicas de EOR, mediante o deseño de novas formulacións químicas, que podan ser aplicadas en pozos que non alcanzaron aínda a súa potencialidade. Na tese pódense diferenciar tres partes. A primeira, desenvolvida no artigo 1, utiliza simulación numérica para investigar a posibilidade de mellorar o varrido areal, no desprazamento inestable de fluídos que se produce na extracción de cru, mediante unha reacción química. A segunda parte (artigos 2, 3 e 4) céntrase no deseño de formulacións acuosas baseadas en mesturas de surfactante e líquido iónico, co fin de reducir a tensión interfacial (IFT) auga-cru e así liberar o petróleo atrapado nos poros das rocas. Na terceira parte (artigo 5), investígase o potencial que teñen certos líquidos iónicos para trocar a mollabilidade por petróleo de rocas carbonatadas cara a mollabilidade por auga, o que facilita a extracción. A continuación, preséntase un resumo de cada artigo que constitúe a tese.

Desprazamento dun fluído de alta viscosidade mediante unha interface reactiva controlada quimicamente. *Chaos*, 31, 2021, 023135

Na recuperación de cru utilízanse formulacións acuosas como medio de desprazamento. Cando un fluído viscoso é desprazado por outro menos viscoso, se forman dixitacións que se propagan en cada un dos fluídos, mesturándoos e impedindo o seu normal movemento. Experimentalmente tense demostrado que é posible mellorar o desprazamento mediante unha reacción química, xerando un produto de maior viscosidade que os fluídos reaccionantes, na interface dos dous

USC UNIVERSIDADE DE SANTIAGO DE COMPOSTELA

fluídos. Este traballo centrouse en, mediante modelización e simulación numérica, optimizar as condicións deste tipo de procesos.

Na simulación considerouse un desprazamento radial e isotérmico nun reactor Hele-Shaw. Este equipo é o máis usado na investigación experimental do problema. Consiste en dúas placas planas horizontais e separadas por un pequeno espazo entre elas. A modelización fíxose a presión atmosférica e temperatura ambiente, coa inxección de fluídos no centro dunha das placas. De acordo coa configuración mencionada, o fluxo modelado é 2D radial. Os fluídos incompresibles, desprazante e desprazado, foron considerados miscibles, newtonianos e de igual densidade. A mestura dos fluídos A e B que interactúan quimicamente, fíxose mediante difusión e convección, e estableceuse un modelo de reacción química simple de A+B $\rightarrow$ C que sómente terá lugar na interface dos fluídos.

O protocolo desenvolvido consta de tres pasos. Unha primeira inxección do fluído menos viscoso no reactor previamente enchido co fluído B, un segundo paso sen inxección, e finalmente considerouse outro período de inxección cun novo caudal. En primeiro lugar, a investigación centrouse na morfoloxía da interface antes do segundo período de inxección. Atopouse que a eficacia do proceso melloraba co radio do anel interfacial e a duración do período de peche. Outro parámetro clave na eficacia do proceso foi o nivel de inestabilidade debido ao primeiro período de inxección. Os maiores caudais de inxección produciron unha maior inestabilidade (maior número e área das dixitacións) e, polo tanto, requiríronse tempos de peche máis longos para suavizalas. Isto significa que o primeiro período de inxección pode compensarse cun tempo de peche adecuado que axude a producir un anel interfacial robusto e estable.

O resto dos parámetros considerados foron a viscosidade da disolución do produto C, a segunda velocidade de inxección, e os coeficientes de difusión dos fluídos implicados. Só a viscosidade de C tivo unha gran influencia na eficacia do método, sendo a importancia dos outros dous parámetros mínima. Se a viscosidade do produto diminúe con respecto ao fluído desprazante, as súas propiedades de varrido diminúen notablemente.

O estudo demostrou que é posible desprazar un fluído de maior viscosidade (por exemplo, petróleo) con gran eficacia (en torno ao 90% de recuperación) utilizando un fluído de menor viscosidade (por exemplo, unha formulación acuosa). Aínda que a través da simulación foi posible controlar o desprazamento e mellorar a eficiencia do mesmo, a gran cantidade de variables que deben ser controladas suxiren unha baixa posibilidade de que o sistema poida ser aplicado de forma rápida e sinxela a escala de laboratorio, e aínda máis baixa a nivel de campo petrolífero.

USC
UNIVERSIDADE DE SANTIAGO DE COMPOSTELA

Avaliación de mesturas de surfactantes para a extracción mellorada de cru mediante mapas de actividade. *Journal of Molecular Liquids*, 364, 2022, 119984.

Unha das claves para mellorar a extracción de cru é acadar unha IFT auga-cru moi baixa. Isto é posible se a mestura constituída por auga, cru e surfactante forma microemulsions do tipo Winsor III (onde o surfactante é capaz de solubilizar grandes cantidades de auga e cru). Atopar este comportamento cun só surfactante é complicado, polo que habitualmente trabállase con mesturas. Non obstante, definir as condicións óptimas para a aplicación é complexo debido ao elevado número de variables implicadas. O obxectivo deste traballo foi avaliar diferentes mesturas de surfactantes para EOR usando mapas de actividade. Estas ferramentas son representacións do comportamento de fase dos surfactantes en función de diversas variables como poden ser: a proporción de surfactantes na mestura, a salinidade, e a temperatura.

Estudáronse tres mesturas cun compoñente en común, o dioctil sulfosuccinato de sodio (AOT), un surfactante aniónico altamente lipofílico. Para crear as formulacións, este surfactante foi mesturado con axentes surfactantes catiónicos e non-iónicos altamente hidrofílicos, de maneira que o AOT foi usado para engadir carácter lipofílico ás mesturas e forzar transicións do comportamento da microemulsión do tipo Winsor I-III-II. Para formular unha mestura de surfactantes aniónico/non-iónico, seleccionouse o ácido carboxílico de polioxietilen(8) octil éter (Akypo LF2®, LF2) como o compoñente non-iónico. A selección debeuse a que a súa estrutura química faino tolerante a altas salinidades e estable a altas temperaturas. Para o deseño de mesturas de tipo aniónico/catiónico, utilizáronse os líquidos iónicos con propiedades surfactantes (SAILs das súas siglas en inglés) cloruro de 1-decil-3-metilimidazolio ([C_{10}mim]Cl) e bromuro de 1-dodecil-3-metilimidazolio ([C_{12}mim]Br). Estes tres compoñentes foron escollidos pola súa capacidade para formar microemulsións Winsor tipo III, nas mesturas co AOT, sen formar precipitados.

En xeral, para a construción dos mapas de actividades realizáronse probas de comportamento de fases para as tres mesturas binarias AOT/LF2, AOT/[C_{10}mim]Cl e AOT/[C_{12}mim]Br, variando a relación de surfactantes na mestura e a salinidade da formulación. Utilizouse unha concentración total de 4% en masa do surfactante (mestura) para unha fácil identificación visual das microemulsións. A fase oleosa foi representada con *n*-octano. Analizouse a influencia da proporción de surfactantes e a salinidade no comportamento de fases (tipo de microemulsión). A avaliación foi realizada a 25, 50 e 75 °C. O obxectivo era obter una microemulsión Winsor tipo III con parámetros de solubilización (volume de auga e octano dividido polo volume de surfactante na microemulsión) iguais e de alto valor. Este parámetro óptimo de solubilización asegura un baixo valor de IFT.

USC UNIVERSIDADE DE SANTIAGO

Á temperatura de 25 °C e traballando cunha salinidade do 5% en masa de NaCl, a proporción óptima de surfactantes para a mestura AOT/LF2 foi 53/47 en masa, mentres que para as mesturas AOT/[C_{10}mim]Cl e AOT/[C_{12}mim]Br foron 44/56 e 35/65, respectivamente. O parámetro óptimo de solubilización foi maior para as mesturas cos SAILs (6,6 e 14,5 para AOT/[C_{10}mim]Cl e AOT/[C_{12}mim]Br, respectivamente), acadando un valor baixo (2,5) para a mestura AOT/LF2. Tamén observouse que a transición da microemulsión Winsor I a II no caso do LF2 foi suave, formando Winsor III nun amplo rango de concentracións e, para as mesturas cos SAILs, esta transición foi moito máis brusca. Isto demostrou a maior interacción electrostática existente entre os grupos polares das mesturas AOT/SAIL (en especial para AOT/[C_{12}mim]Br) que no caso do AOT/LF2.

A avaliación dos efectos da salinidade amosou que a mestura AOT/LF2 era moito máis sensible a este parámetro que as AOT/SAIL. O comportamento do surfactante AOT/LF2 foi similar ao que presentan os surfactantes iónicos, volvéndose mais lipofílico co aumento da salinidade. Pola contra, as mesturas AOT/SAIL foron moi estables ante a variación de sal, de xeito similar ao comportamento dos surfactantes non-iónicos que tenden a ser lixeiramente máis lipofílicos co aumento da salinidade. Co aumento da temperatura observouse un aumento na rexión trifásica nos mapas de actividade das tres mesturas pero, á vez, unha significativa redución dos parámetros óptimos de solubilización.

Os mapas de actividade construídos permitiron visualizar facilmente os cambios no comportamento de fases (tipo de microemulsión) de cada mestura, en función das variables estudadas (salinidade e temperatura). Son por tanto unha ferramenta fundamental para o entendemento das fases que poden xerar as mesturas dentro dos xacementos. Con iso, pódese mellorar a selección das mesturas en función das condicións propias dun xacemento, ter en consideración trocos na salinidade debido a diferencias entre a auga de formación e inxección, ou evitar certos comportamentos de fases indesexables para a recuperación de cru.

Mellora dunha mestura de surfactantes para a recuperación mellorada de petróleo en xacementos carbonatados mediante un líquido iónico. *International Journal of Molecular Sciences* 24, 2023, 726.

No traballo anterior demostrouse o posible interese de tres mesturas de surfactantes para EOR: AOT/LF2, AOT/[C_{10}mim]Cl, e AOT/[C_{12}mim]Br. Este novo estudo, centrouse en definir a mellor formulación para a aplicación. Tras realizar probas de tolerancia á dureza dunha auga de mar sintética, con 4,9% en masa de sólidos disoltos totais, determinouse que só a mestura AOT/LF2 era estable en presenza de ións divalentes (Ca^{2+} e Mg^{2+}). Non obstante, no estudo anterior

USC DE SANTIAGO DE COMPOSTELA

demostrouse que a mestura AOT/[C_{12}mim]Br era de maior interese porque presentaba o valor máis alto do parámetro óptimo de solubilización.

Realizáronse varios intentos para conseguir unha mestura ternaria con AOT, [C_{12}mim]Br e LF2, coa maior proporción posible de AOT/[C_{12}mim]Br para obter unha maior actividade superficial, mantendo a estabilidade en presenza de ións divalentes. De acordo aos estudos de comportamento de fases realizados con petróleo, AOT/[C_{12}mim]Br cunha proporción 45/55 en masa (en diante A-C) era a máis axeitada para mesturar con LF2. Así pois, definiuse unha formulación ternaria mediante un varrido da mestura A-C/LF2, e ensaios de estabilidade e IFT. A formulación óptima na auga de mar sintética contiña unha proporción 46/54 en masa de A-C/LF2 (a composición da mestura ternaria foi por tanto $AOT_{20,7\%}$/[C_{12}mim]$Br_{25,3\%}$/$LF2_{54\%}$).

Comparando as formulacións óptimas das mesturas AOT/LF2 e A-C/LF2, A-C/LF2 mostrou unha actividade superficial lixeiramente mellor co petróleo, alcanzando un parámetro óptimo de solubilización de 4,7 a 25 °C. Este valor foi superior a 3, valor alcanzado coa mestura binaria AOT/LF2 á mesma temperatura. Como era de esperar, as medicións de IFT tamén demostraron melloras para a mestura A-C/LF2 ($1{,}14\times10^{-2}$ mN/m) en comparación con AOT/LF2 ($1{,}50\times10^{-2}$ mN/m). Por outra banda, as mesturas mostraron un comportamento oposto ao aumentar a temperatura. A 50 °C, a microemulsión Winsor III óptima para a mestura AOT/LF2 obtívose cunha maior proporción de AOT (comportándose como unha formulación de surfactante iónico). Pola contra, á mesma temperatura, a mestura A-C/LF2 alcanzou a microemulsión óptima cunha proporción A-C máis baixa (comportándose como un surfactante non-iónico). A capacidade de solubilización de ambas mesturas diminuíu significativamente a temperaturas máis elevadas, polo que a aplicación centrouse nunha temperatura de operación de 25 °C.

Das probas de adsorción dinámica cunha fase (só fase acuosa presente no núcleo) en rocas carbonatadas, obtivéronse valores de adsorción de 0,42 mg/g_{roca} e 0,21 mg/g_{roca} para AOT/LF2 e A-C/LF2, respectivamente. Esta redución na adsorción de A-C/LF2 débese posiblemente á redución das cargas negativas libres de AOT coa formación de micelas mixtas con [C_{12}mim]Br.

As melloras de A-C/LF2 con respecto a AOT/LF2 (menor IFT e adsorción) influíron para que A-C/LF2 tivera un mellor rendemento na recuperación de petróleo nas probas de extracción. Estas realizáronse con núcleos de rocas carbonatadas a temperatura ambiente. Para AOT/LF2 acadouse unha recuperación adicional de petróleo (AOR) do 7,3 % do petróleo orixinal no lugar (OOIP), mentres que para A-C/LF2 foi do 11,5 % OOIP.

Os resultados obtidos suxiren que a adición do SAIL catiónico á formulación orixinal de surfactantes aniónico e noniónico, mellora claramente a súa eficacia en EOR.

USC DE COMPOSTELA

Avaliación dunha formulación baseada nun líquido iónico tensioactivo para aplicacións de EOR: Estudos experimentais e de simulación. *Geoenergy Science and Engineering*, 224, 2023, 211619.

O obxectivo deste traballo foi aumentar o nivel de madurez tecnolóxico dunha proposta, desenvolvida no Grupo de Investigación, baseada no uso dunha mestura de dodecilbencenosulfonato de sodio e o SAIL metilsulfato de cocosalquilpentaetoximetilamonio (IoLiLyte C1EG®, C1EG). A tal fin, adaptouse o método para a súa aplicación cun surfactante aniónico (RECOLAS103) da familia dos sulfonatos de alquilbenceno lineais (cadea C_{11}-C_{13}), sintetizado pola empresa petrolífera CEPSA. Leváronse a cabo probas de laboratorio, e estudos de simulación numérica de xacementos para ampliar o coñecemento do comportamento da mestura e optimizar os protocolos de inxección.

O comportamento de fases estudiouse variando a relación da proporción RECOLAS103/C1EG nunha formulación acuosa cunha concentración do 4 % en masa de surfactante (mestura) en SW. Utilizouse *n*-octano como modelo da fase oleosa. A proba realizouse a 25, 50 e 75 °C.

Do ensaio a 25 °C obtivéronse dúas rexións onde se observaron microemulsións Winsor III, ao 40% e ao 70% RECOLAS103. A transición da microemulsión foi do tipo Winsor I-III-II-III-I. Este comportamento particular dáse porque ambos compoñentes da mestura son hidrofílicos en estado puro, pero canto maior sexa a interacción entre os seus grupos polares, as cargas opostas redúcense coa formación de micelas mixtas. En consecuencia, a formulación en xeral será menos polar e comportarase máis lipofílica segundo as condicións de salinidade e temperatura do sistema. O sistema Winsor III cun 40% de RECOLAS103 é máis rico en surfactante catiónico. Por tanto, aínda que a carga superficial das micelas mixtas é neutralizada polas cargas opostas, a carga global da microemulsión segue sendo positiva. Isto é máis favorable para evitar a adsorción en rocas con carga positiva como os carbonatos. Por tanto, o estudo centrouse nesta proporción da mestura.

A 25 °C, a relación óptima de mestura foi estimada en 42,3/57,7 RECOLAS103/C1EG cun prometedor parámetro óptimo de solubilización de 14,37. Co aumento da temperatura a 50 e 75 °C, este parámetro diminuíu a 6,83 e 5,86, respectivamente. Das probas de estabilidade (tolerancia á dureza do SW) e medicións de IFT, definiuse unha formulación óptima para temperaturas intermedias, consistente nunha disolución acuosa cun 1% en masa de surfactante (40/60 RECOLAS103/C1EG) en SW. A IFT formulación-cru foi 2.1×10^{-2} mN/m a 25 °C e a adsorción

USC UNIVERSIDADE DE SANTIAGO DE COMPOSTELA

dinámica en núcleos de roca carbonatada estimouse en 0,60 mg/g_{roca}. Todos eles valores prometedores para EOR.

Leváronse a cabo tres probas de extracción de cru de núcleos de rocas carbonatadas, a 25 °C (CF-1 e CF-3) e a 120 °C (CF-2). Na CF-3, para aproximarse ás aplicacións reais, levouse a cabo unha etapa de inundación cunha disolución polimérica PAM 920 VHM, cunha viscosidade aparente optimizada a 6,3 mPa-s (a 10 s^{-1}), tras a inundación coa formulación de surfactante. Obtivéronse valores de AOR de 12,7%, 10,2% e 11,7%, para CF-1, CF-2 e CF-3, respectivamente.

O valor máis baixo de AOR observouse no ensaio CF-2 a 120 °C, o que podería atribuírse a unha diminución da eficiencia da mestura a temperaturas máis altas. Tras realizar varias simulacións para axustar o modelo numérico ás probas de laboratorio, atopouse como xustificación da diminución da produción de petróleo a alta temperatura, unha retención de surfactante de aproximadamente 36 mg/g_{roca}. Non obstante, as simulacións tamén confirmaron a baixa absorción obtida experimentalmente, polo que a retención do cru podería deberse á partición do surfactante cara á fase oleosa (troco da microemulsión de tipo Winsor III a microemulsión de tipo Winsor II). As simulacións nesas condicións axustáronse axeitadamente aos resultados obtidos no laboratorio.

Con novas simulacións poido optimizarse o protocolo de inxección da formulación, e mostrouse que a mestura RECOLAS103/C1EG ten potencial para alcanzar un AOR do 15 % OOIP cos mesmos parámetros de inxección usados na proba CF-3, pero usando unha disolución polimérica de viscosidade aparente igual ou superior a 20 mPa·s. En todo caso, é necesario axustar a mestura (a través da proporción de surfactantes) en función da temperatura do xacemento, para manter a microemulsión preto das condicións óptimas (Winsor III) durante todo o desprazamento.

Avaliación de líquidos iónicos surfactantes en auga intelixente para a recuperación mellorada de petróleo en rocas carbonatadas. *Energy & Fuels* (under revision).

O cambio de mollabilidade é un dos mecanismos prometedores na extracción de petróleo para xacementos nos que as rocas están preferentemente molladas polo cru, sistemas de mollabilidade intermedia, en xacementos de baixa permeabilidade, ou en sistemas moi fracturados. O obxectivo é conseguir una maior mollabilidade por auga para así favorecer a extracción de cru.

Este estudo centrouse en determinar o potencial dalgúns SAILs catiónicos para mellorar a capacidade das augas intelixentes (SmW) na modificación da mollabilidade de rocas carbonatadas. A avaliación realizouse a unha temperatura de 90 °C, debido a que tanto as SW como as SmW teñen unha alta efectividade para alterar a mollabilidade a temperaturas de 120-130 °C, pero a súa efectividade redúcese á medida que diminúe a temperatura.

USC UNIVERSIDADE

Para seleccionar os SAILs, preparáronse formulacións de once SAILs hidrófilicos ao 1 % en masa de SAIL en auga de formación, SW e SmW. A estabilidade térmica destas formulacións avaliouse a alta temperatura (ata 130 °C) para garantir que non aparecese precipitación. Tamén estudouse o comportamento de fases das formulacións con petróleo. O obxectivo desta avaliación era garantir que as formulacións con SAILs se mantivesen como microemulsións Winsor tipo I a medida que aumentaba a temperatura, evitando o cambio a Winsor II que podería dar lugar á retención do cru. Ademais, a proba utilizouse para identificar visualmente as formulacións con alta actividade superficial e, en consecuencia, alta solubilización de petróleo na fase acuosa (evidenciada pola escuridade desta fase). Tratábase dun método rápido para seleccionar as formulacións SAIL que conducían a unha baixa IFT. Por tanto, elixíronse as formulacións con fases acuosas máis escuras para as medicións de IFT con petróleo. Os SAILs seleccionados foron o bromuro de 1-dodecil-3-metilimidazolio ([C_{12}mim]Br), cloruro de 1-dodecilpiridinio ([C_{12}Py]Cl) e cloruro de 1-hexadecilpiridinio ([C_{16}Py]Cl), permitindo así analizar o efecto do anión e o tipo de anel no comportamento destas sales.

Preparáronse formulacións cun 1% en masa de SAIL en SmW, e realizáronse estudos de imbibición espontánea a 90 °C en rocas carbonatadas de mollabilidade intermedia. As AOR obtidas foron 24% OOIP para a formulación con [C_{12}mim]Br, 22% con [C_{12}Py]Cl e 5% con [C_{16}Py]Cl. Os SAILs con cadeas C_{12} melloraron a capacidade de modificación da mollabilidade da SmW (que deu lugar a unha AOR do 11%) e, pola contra, a formulación con [C_{16}Py]Cl mostrou un rendemento inferior. Dado que este último SAIL proporcionou a menor IFT, un valor moi baixo desta propiedade pode ser a causa da diminución da capacidade do SAIL para forzar a entrada da formulación na roca e iniciar o cambio de mollabilidade. Nin o tipo de anel do SAIL (imidazolio ou piridinio) nin o contra-ión pareceron ter moita influencia na recuperación.

As probas de extracción de cru de rocas carbonatadas realizáronse, a 90 °C, coa formulación de [C_{12}mim]Br en modo secundario e terciario (despois da inxección de SmW). En modo secundario, a inxección SmW levou a unha recuperación de cru do 66% e coa formulación do SAIL acadouse o 79%, o que confirmou o aumento do potencial da auga intelixente para trocar a mollabilidade coa presenza do SAIL. Doutra banda, cando a formulación do SAIL inxéctase en modo terciario despois da SmW, acádase un AOR do 4%. Do análise das presións durante as probas de desprazamento poido inferirse a formación dun banco de petróleo diante da formulación de [C_{12}mim]Br, causado pola alteración da mollabilidade e a redución da IFT. A proba de adsorción dinámica da formulación acuosa resultou nunha adsorción de 1,9 mg/g_{roca}. As causas da adsorción do SAIL catiónico na superficie da roca cargada positivamente deberán ser analizadas en profundidade,

USC UNIVERSIDADE DE SANTIAGO DE COMPOSTELA

pois disto pode depender a viabilidade económica de substituír a auga intelixente por formulacións de SAILs nos procesos de EOR.

En xeral, pode concluírse que a mellora de métodos de EOR é posible, sendo as técnicas máis prometedoras a combinación de SAILs con surfactantes tradicionais ou con auga intelixente. O coste económico do proceso será o factor clave para a súa aplicación, e debe ser obxecto de estudios futuros.

USC
UNIVERSIDADE DE SANTIAGO DE COMPOSTELA

USC
UNIVERSIDADE
DE SANTIAGO
DE COMPOSTELA

Appendix C:
Copyright

USC
UNIVERSIDADE
DE SANTIAGO
DE COMPOSTELA

USC
UNIVERSIDADE
DE SANTIAGO
DE COMPOSTELA

Figure 2.1: Forecast of total energy supply by source and CO_2 emissions by scenario.

Table: Table 2.1. World oil demand by forecast scenario.

Source: International Energy Agency (IEA), World Energy Outlook 2022, 2022. https://www.iea.org/reports/world-energy-outlook-2022.

The IEA allows the reuse of the content presented in Figure 2.1 and Table 2.1, both in print an electronic format, available under open Creative Commons Attribution 4.0 International (CC BY 4.0) license.

IEA Open Use Terms

The IEA makes much of its content available under open Creative Commons licences. Unless one of the below exceptions to the Open Use Terms applies, all text content, reports, articles, commentaries, standalone graphs, figures and infographics produced by and/or sourced to the IEA and hosted on the IEA Websites are licensed under a Creative Commons Attribution 4.0 International (CC BY 4.0) licence.

The following items are ***not*** made available under a CC BY 4.0 licence as part of the Open Use Terms:

- The *Oil Market Report*;
- Standalone datasets, data explorers and databases, including those listed at https://www.iea.org/data-and-statistics/data-sets;
- Data annexes to the World Energy Outlook or other IEA publications;
- Any content identified as a joint or collaborative work with one or more third parties; and
- The Policies and Measures Databases.

Figure 2.4: Typical capillary pressure (Pc) curves for a water-wet reservoir rock as a function of water saturation (Sw).

Source: T. Ahmed, Reservoir Engineering Handbook, Fifth edit, Gulf Professional Publishing, Cambridge, Massachusetts., 2019.

Elsevier has provided permission for reusing the content presented in Figure 2.4, both in print an electronic format.

USC UNIVERSIDADE DE SANTIAGO DE COMPOSTELA



CCC Marketplace

This is a License Agreement between Nestor Tafur / University of Santiago de Compostela ("User") and Copyright Clearance Center, Inc. ("CCC") on behalf of the Rightsholder identified in the order details below. The license consists of the order details, the Marketplace Permissions General Terms and Conditions below, and any Rightsholder Terms and Conditions which are included below.

All payments must be made in full to CCC in accordance with the Marketplace Permissions General Terms and Conditions below.

Order Date	08-Jun-2023	Type of Use	Republish in a thesis/dissertation
Order License ID	1363385-1		
ISBN-13	9780128136492	Publisher	Elsevier Science
		Portion	Image/photo/illustration

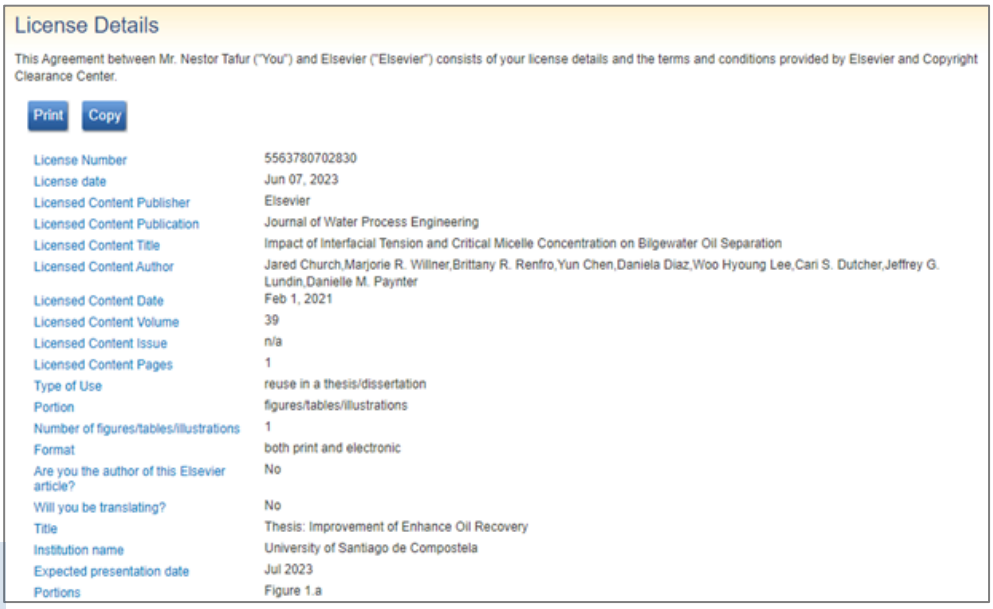
LICENSED CONTENT

Publication Title	Reservoir Engineering Handbook	Country	United States of America
		Rightsholder	Elsevier Science & Technology Journals
Author/Editor	Ahmed, Tarek		
Date	12/19/2018	Publication Type	Book
Language	English		

Figure 2.15: Typical plot for CMC estimation. IFT measurements as a function of three commercial surfactant concentration

Source: J. Church, M.R. Willner, B.R. Renfro, Y. Chen, D. Diaz, W.H. Lee, C.S. Dutcher, J.G. Lundin, D.M. Paynter, Impact of Interfacial Tension and Critical Micelle Concentration on Bilgewater Oil Separation, J. Water Process Eng. 39 (2021) 101684. https://doi.org/10.1016/j.jwpe.2020.101684.

Elsevier has provided permission for reusing the content presented in Figure 2.15, both in print an electronic format.



License Details

This Agreement between Mr. Nestor Tafur ("You") and Elsevier ("Elsevier") consists of your license details and the terms and conditions provided by Elsevier and Copyright Clearance Center.

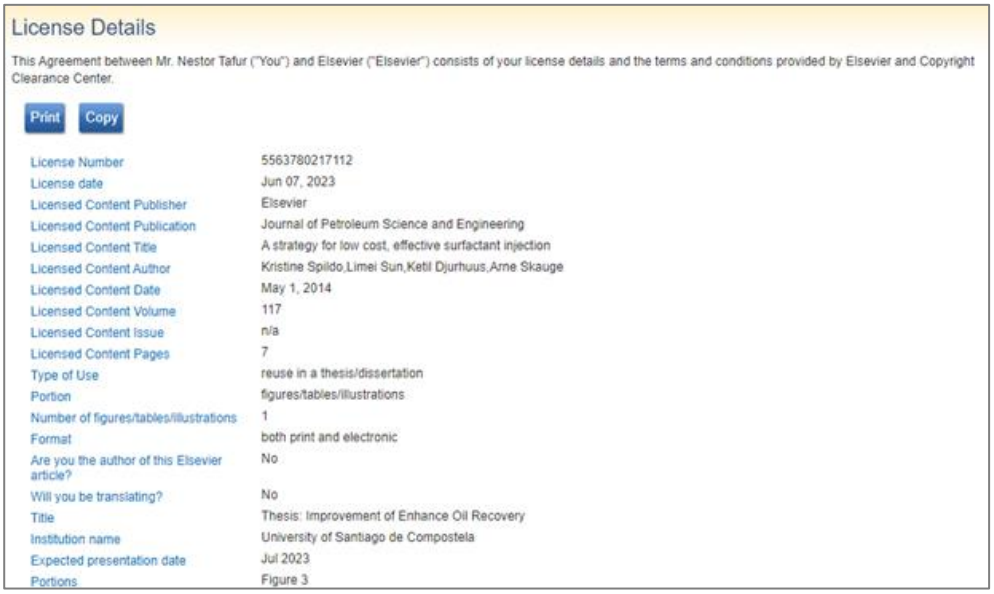
Print Copy

License Number	5563780702830
License date	Jun 07, 2023
Licensed Content Publisher	Elsevier
Licensed Content Publication	Journal of Water Process Engineering
Licensed Content Title	Impact of Interfacial Tension and Critical Micelle Concentration on Bilgewater Oil Separation
Licensed Content Author	Jared Church,Marjorie R. Willner,Brittany R. Renfro,Yun Chen,Daniela Diaz,Woo Hyoung Lee,Cari S. Dutcher,Jeffrey G. Lundin,Danielle M. Paynter
Licensed Content Date	Feb 1, 2021
Licensed Content Volume	39
Licensed Content Issue	n/a
Licensed Content Pages	1
Type of Use	reuse in a thesis/dissertation
Portion	figures/tables/illustrations
Number of figures/tables/illustrations	1
Format	both print and electronic
Are you the author of this Elsevier article?	No
Will you be translating?	No
Title	Thesis: Improvement of Enhance Oil Recovery
Institution name	University of Santiago de Compostela
Expected presentation date	Jul 2023
Portions	Figure 1.a

USC UNIVERSIDADE DE SANTIAGO DE COMPOSTELA

Figure 2.18: Correlation between the microemulsion phase behaviour and IFT.
Source: K. Spildo, L. Sun, K. Djurhuus, A. Skauge, A strategy for low cost, effective surfactant injection, J. Pet. Sci. Eng. 117 (2014) 8–14. https://doi.org/10.1016/j.petrol.2014.03.006.

Elsevier has provided permission for reusing the content presented in Figure 2.18, both in print an electronic format.



License Details

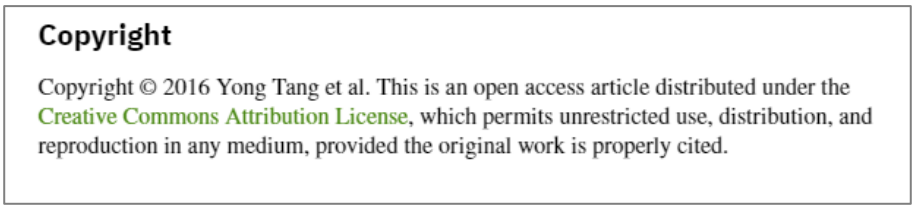
This Agreement between Mr. Nestor Tafur ("You") and Elsevier ("Elsevier") consists of your license details and the terms and conditions provided by Elsevier and Copyright Clearance Center.

Print Copy

License Number	5563780217112
License date	Jun 07, 2023
Licensed Content Publisher	Elsevier
Licensed Content Publication	Journal of Petroleum Science and Engineering
Licensed Content Title	A strategy for low cost, effective surfactant injection
Licensed Content Author	Kristine Spildo,Limei Sun,Ketil Djurhuus,Arne Skauge
Licensed Content Date	May 1, 2014
Licensed Content Volume	117
Licensed Content Issue	n/a
Licensed Content Pages	7
Type of Use	reuse in a thesis/dissertation
Portion	figures/tables/illustrations
Number of figures/tables/illustrations	1
Format	both print and electronic
Are you the author of this Elsevier article?	No
Will you be translating?	No
Title	Thesis: Improvement of Enhance Oil Recovery
Institution name	University of Santiago de Compostela
Expected presentation date	Jul 2023
Portions	Figure 3

Figure 2.23: Example of interpolated relative permeability curves
Source: Y. Tang, Z. Su, J. He, F. Yang, Numerical Simulation and Optimization of Enhanced Oil Recovery by the In Situ Generated CO2 Huff-n-Puff Process with Compound Surfactant, J. Chem. 2016 (2016). https://doi.org/10.1155/2016/6731848.

Article under open Creative Commons Attribution 4.0 International (CC BY 4.0) license.



Copyright

Copyright © 2016 Yong Tang et al. This is an open access article distributed under the Creative Commons Attribution License, which permits unrestricted use, distribution, and reproduction in any medium, provided the original work is properly cited.

USC UNIVERSIDADE DE SANTIAGO DE COMPOSTELA

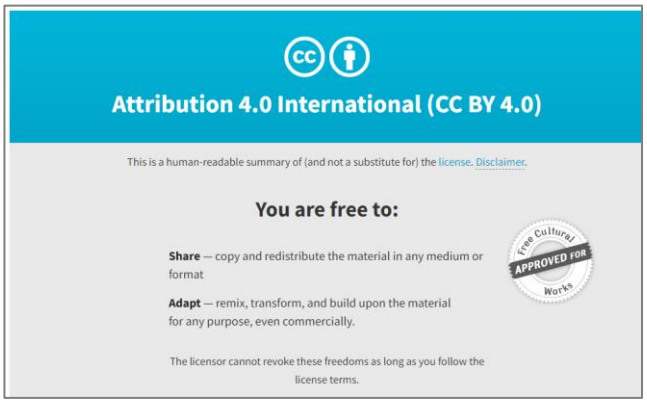
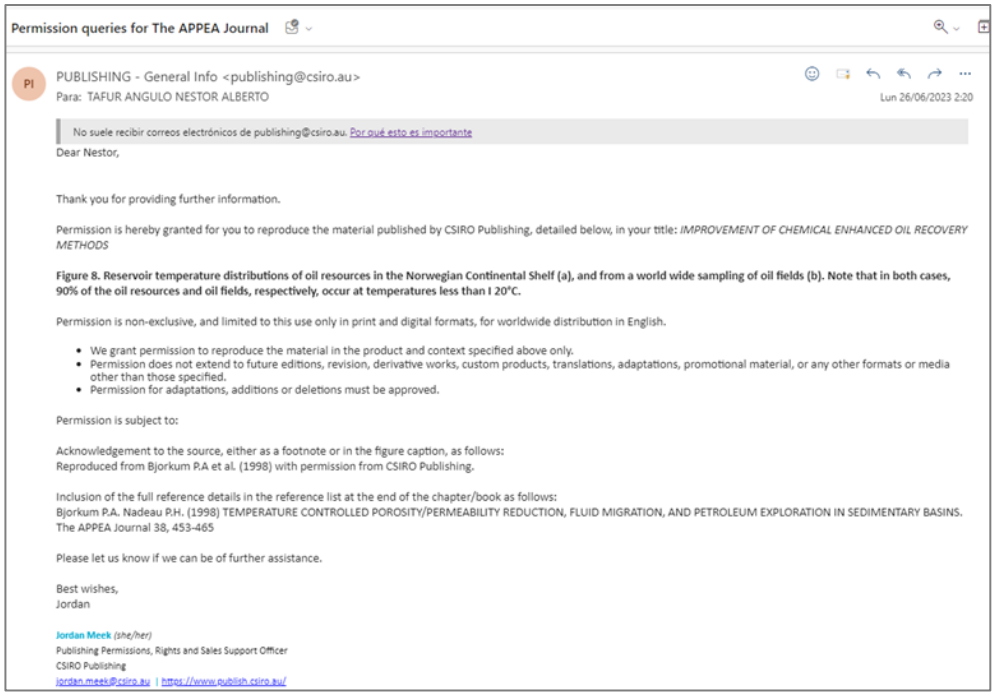


Figure 4.2: Reservoir temperature distributions of oil resources from a worldwide sampling of oil fields.

Source: P.A. Bjorkum, P.H. Nadeau, Temperature Controlled Porosity/Permeability Reduction, Fluid Migration, and Petroleum Exploration in Sedimentary Basins, APPEA J. 38 (1998) 453. https://doi.org/10.1071/aj97022.

Permission provided for reusing the content presented in Figure 4.2, both in print an electronic format.



USC UNIVERSIDADE DE SANTIAGO DE COMPOSTELA

In the midst of the imperative transition towards ecological sustainability, the role of oil as a vital energy resource is undeniable. This Thesis tackles the challenge of amplifying the oil recovery potential of Enhanced Oil Recovery (EOR) techniques applied in oil reservoirs, especially of carbonate rocks, to optimize oil extraction from existing reservoirs. The research explores three chemical EOR method approaches: the control of unstable displacement (viscous ingering), reduction of interfacial tension (IFT), and alteration of rock wettability. The study on controlling viscous ingering via chemical reactions was methodically conducted through numerical simulations. Afterward, advanced formulations employing surfactants and ionic liquid blends were examined for EOR applications by reducing IFT to low values. Several ionic liquids were evaluated to improve the rock wettability alteration properties of smart water at low temperatures. The results obtained in this work show promising techniques to move beyond known oil recovery methods, balancing today's demands with the imperatives of tomorrow.